

AD-A168 267

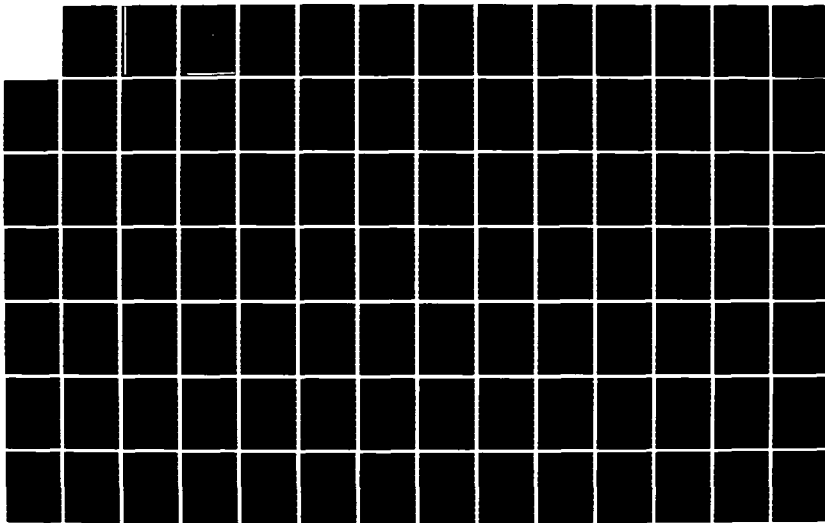
FRACTURE IN STABILIZED SOILS VOLUME 1(U) TEXAS  
TRANSPORTATION INST COLLEGE STATION D M LITTLE ET AL.  
31 DEC 85 AFOSR-TR-86-0242-VOL-1 F49620-82-K-0027

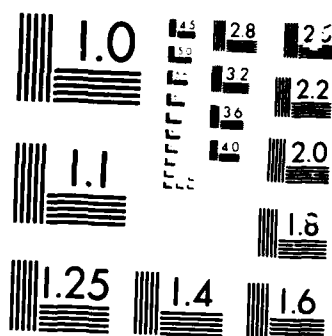
1/4

UNCLASSIFIED

F/G 8/13

NL





MICROCOPY

11131

AD-A168 267

**FRACTURE IN STABILIZED  
SOILS**

**VOLUME I**

**FINAL TECHNICAL REPORT**

**DECEMBER 31, 1985**



**Prepared by  
The Texas Transportation Institute**

*Approved for public release;  
distribution unlimited.*

**The Texas A&M University System  
College Station, Texas**



**B**

**86 4 28 174**  
**4**

# REPORT DOCUMENTATION PAGE

1. REPORT SECURITY CLASSIFICATION Unclassified		1b. RESTRICTIVE MARKINGS	
2. SECURITY CLASSIFICATION AUTHORITY		3. DISTRIBUTION/AVAILABILITY OF REPORT Approved for public release; distribution unlimited.	
4. DECLASSIFICATION/DOWNGRADING SCHEDULE		5. MONITORING ORGANIZATION REPORT NUMBER(S) AFOSR-TR- 86-0242	
6. PERFORMING ORGANIZATION REPORT NUMBER(S)		7a. NAME OF MONITORING ORGANIZATION Air Force Office of Scientific Research	
7. NAME OF PERFORMING ORGANIZATION Texas A&M University Texas Transportation Institute ADDRESS (City, State and ZIP Code) College Station, Texas 77843		7b. ADDRESS (City, State and ZIP Code) Bolling AFB, DC 20332	
8. NAME OF FUNDING/SPONSORING ORGANIZATION Office of Scientific Research ADDRESS (City, State and ZIP Code) Bolling AFB DC 20332-6448		8b. OFFICE SYMBOL (If applicable) NA	
9. PROCUREMENT INSTRUMENT IDENTIFICATION NUMBER F49620-82-K-0027		10. SOURCE OF FUNDING NOS.	
11. TITLE (Include Security Classification) Fracture in Stabilized Soils - Vol 1 & 2		PROGRAM ELEMENT NO. 61102F PROJECT NO. 2302 TASK NO. C2 WORK UNIT NO.	
12. PERSONAL AUTHOR(S) R. H. Little, W. W. Crockford, and Y. Kim			
13a. TYPE OF REPORT Final Technical		13b. TIME COVERED FROM 820401 TO 851231	
14. DATE OF REPORT (Yr., Mo., Day) 851231		15. PAGE COUNT 390	
16. SUPPLEMENTARY NOTATION			

COSATI CODES			18. SUBJECT TERMS (Continue on reverse if necessary and identify by block number)  Fracture Mechanics
FIELD	GROUP	SUB. GR.	

19. ABSTRACT (Continue on reverse if necessary and identify by block number)  
 Conventionally the thickness design of stabilized soil layers has been based upon the tensile strength of the stabilized soil layer and/or the appearance of the first crack. The design literature does not allow one to consider the true development of cracking in the stabilized soil layer. Knowledge of the mode of such cracking could drastically alter the philosophy behind thickness design of layers.  
 In this research the principles of theoretical fracture mechanics are used to explain the mode and mechanism of fracture in fine grained media stabilized with portland cement. Experimental fracture mechanics is used to validate or verify and in some cases to investigate more fully the hypothesized mechanisms of fracture. The influence of osmotic and matrix soil section, temperature, binder content, thermal and kinetic energy, from sources outside the crack, are considered in the study.  
 Linear elastic fracture mechanics is proven to be a highly acceptable analytical tool for these materials.

20. DISTRIBUTION/AVAILABILITY OF ABSTRACT UNCLASSIFIED UNLIMITED <input type="checkbox"/> SAME AS RPT. <input type="checkbox"/> DTIC USERS <input type="checkbox"/>		21. ABSTRACT SECURITY CLASSIFICATION Unclassified	
22a. NAME OF RESPONSIBLE INDIVIDUAL LAWRENCE D. HOKANSON		22b. TELEPHONE NUMBER (Include Area Code) (202) 767-4935	
		22c. OFFICE SYMBOL NA	

AIR FORCE OFFICE OF SCIENTIFIC RESEARCH (AFSC)  
 NOTICE OF TECHNICAL RESEARCH  
 This technical report is approved and is  
 distributed as such. AFOSR-10-12.  
 MATTHEW J. ROSEN  
 Chief, Technical Information Division

TABLE OF CONTENTS . . . . . ii

LIST OF TABLES . . . . . vi

LIST OF FIGURES . . . . . vii

TABLE OF CONTENTS

	Page
CHAPTER I: INTRODUCTION . . . . .	1
Problem Definition . . . . .	1
Approach to Solution . . . . .	3
Organization of the Report . . . . .	4
Volume 1 . . . . .	4
Volume 2 . . . . .	4
Coordinate Systems . . . . .	5
CHAPTER II: FRACTURE UNDER MONOTONIC LOADING . . . . .	6
Literature Review and Theory . . . . .	6
Stress Intensity Factor . . . . .	6
Strain Energy Density . . . . .	13
Strain Energy Density Factor . . . . .	16
Stress Intensity and Strain Energy . . . . .	19
"Ideal" Fracture Strength . . . . .	20
Experimental Considerations . . . . .	26
New Developments . . . . .	31
Experimental Procedure . . . . .	32
Experimental Results . . . . .	37

## Table of Contents (Continued)

	Page
Test Results (28 Day) . . . . .	37
Curing Date Study . . . . .	46
Statistical Inferences . . . . .	47
Conclusions . . . . .	56
Future Work . . . . .	58
CHAPTER III: CRACK GROWTH DURING CYCLIC LOADING . . . . .	61
Literature Review and Theory . . . . .	61
New Developments . . . . .	65
Experimental Procedure . . . . .	69
Data Analysis . . . . .	70
Experimental Results . . . . .	72
Statistical Inference . . . . .	85
Comparison with Other Materials . . . . .	86
Conclusions . . . . .	92
Future Work . . . . .	92
CHAPTER IV: APPLICATIONS . . . . .	94
Literature Review and Theory . . . . .	94
New Developments . . . . .	95
Line Load on a Boundary . . . . .	96
Point Load on a Boundary . . . . .	98
Disk with Opposing Line Load . . . . .	99
Circularly Distributed Uniform Load Over Part of a Boundary . . . . .	100
Design Example . . . . .	101

## Table of Contents (Continued)

	Page
Conclusions . . . . .	105
CHAPTER V: RELATIONSHIP BETWEEN TENSILE CREEP AND FATIGUE CRACKING . . . . .	106
General . . . . .	106
Literature review . . . . .	108
The Origin of Microcracks . . . . .	108
Creep and Fatigue . . . . .	110
Shift Variables . . . . .	112
Preparation of Specimens and Laboratory Testing . . . . .	116
Material . . . . .	116
Preparation of Specimens . . . . .	116
Testing Program . . . . .	120
Governing Equations and Method of Analysis . . . . .	127
Governing Equations . . . . .	127
Method of Analysis . . . . .	133
Determination of Material Properties . . . . .	134
Creep Index and Crack Speed Index . . . . .	140
Discussion of Results . . . . .	144
Cement Content . . . . .	144
Curing Age . . . . .	157
Relative Humidity . . . . .	165
Temperature . . . . .	170
CHAPTER VI: SUMMARY . . . . .	174

## TABLE OF CONTENTS (Continued)

	Page
APPENDIX I.-REFERENCES . . . . .	179
APPENDIX II.-NOTATION AND CONVERSION FACTORS . . . . .	192
APPENDIX III.-DATA . . . . .	196
APPENDIX IV.-CALCULATOR AND COMPUTER ANALYSIS OF DATA . . . . .	247
APPENDIX V.-SCANNING ELECTRON MICROSCOPY . . . . .	278
APPENDIX VI.-INDIVIDUAL CREEP TEST RESULTS . . . . .	282

## LIST OF TABLES

TABLE	Page
1 Specimen Constitution. . . . .	32
2 Specimen History. . . . .	33
3 Summary of initial crack extension data (28 day). . . . .	38
4 Summary of results of fracture tests (28 day, monotonic loading). . . . .	39
5 Summary of results of fracture tests (curing study, monotonic loading). . . . .	48
6 Regression analyses using $K_{IC}$ as the dependent variable. . .	52
7 Regression analyses using $J_{IC}$ as the dependent variable. . .	53
8 Regression relationships between CSI and Stress Intensity. . . . .	84
9 Characteristics of the material. . . . .	117
10 Compactive effort calculation. . . . .	122
11 Creep test program. . . . .	126
12 Creep and indirect tensile test results and predicted fatigue parameters at different cement contents. . . . .	145
13 Creep and indirect tensile test results and predicted fatigue parameters at different curing ages. . . . .	146
14 Creep and indirect tensile test results and predicted fatigue parameters at different relative humidities. . . .	147
15 Creep and indirect tensile test results and predicted fatigue parameters at different temperatures. . . . .	148
16 Comparison of the experimental and the predicted fatigue parameters at different cement contents. . . . .	153
17 Comparison of the experimental and the predicted fatigue parameters at different curing ages. . . . .	163

## LIST OF FIGURES

FIGURE		Page
1	Fracture in layered pavement systems. . . . .	2
2	Modes of cracking and specimen dimensions. . . . .	3
3	Coordinate system used for the study. . . . .	5
4	Stress distribution ( $1/\sqrt{r}$ ) ahead of the crack. . . . .	12
5	The crack tip plastic zone (redrawn from Broek [15]) . . .	13
6	The path independent line integral. . . . .	14
7	The Barenblatt [8] crack tip model (a) versus an elliptical shape (b). . . . .	16
8	The Lennard-Jones Potential (Redrawn from Porterfield [79]). . . . .	21
9	Plane strain versus plane stress. (Redrawn from Broek [15]) . . . . .	27
10	Load-displacement record: cement stabilized soil . . . . .	29
11	Applicability of Linear Elastic Fracture Mechanics. . . . .	41
12	Source of toughness. . . . .	45
13	Possible stress-strain behaviors. . . . .	46
14	Visualization of changes in a Lennard-Jones type potential. . . . .	47
15	Experimental results using $K_{IC}$ in equation (49). . . . .	55
16	Residual error plot for the model of Figure (15) . . . . .	56
17	Experimental results using $J_{IC}$ in equation (49). . . . .	57
18	Residual error plot for the model of Figure (17) . . . . .	58
19	Factorial Analysis for Future Studies . . . . .	59
20	Schematic of the regions of crack growth behavior	

## List of Figures (Continued)

FIGURE	Page
(redrawn from [85]) . . . . .	62
21 Comparison of $K_{IC}$ with $K_{max}$ at fatigue failure. . . . .	68
22 Schematic of crack length versus cycle number. (a) Ideal, (b) Soil cement. . . . .	70
23 $\log_{10}A$ versus $n$ for modified compaction specimens(28 day). . . . .	73
24 $\log_{10}A$ versus $n$ for standard compaction specimens(28 day). . . . .	74
25 $\log_{10}A$ versus $n$ for the curing day study. . . . .	75
26 $\log_{10}A$ versus $n$ using the three point running average technique. . . . .	76
27 $\log_{10}A$ versus $n$ for different methods of fitting the crack growth curve. . . . .	77
28 Residual error plot from $N$ versus $a$ (quadratic regression specimen 020C). . . . .	78
29 Comparison of crack speed indices (Quadratic method). . . . .	80
30 Comparison of crack speed indices (Secant method). . . . .	81
31 Comparison of crack speed indices. . . . .	83
32 Prediction of failure cycle from static test. . . . .	85
33 Prediction of crack length at fatigue failure from static test. . . . .	86
34 Comparison of $\log_{10}A$ versus $n$ for various materials. . . . .	88
35 Comparison of $\log_{10}A$ versus $n$ using materials tested in displacement control. . . . .	89
36 Comparison of dissimilar materials by CSI. . . . .	91
37 Superposition (redrawn from Sih [97]). . . . .	94
38 Boundary conditions for (a)Flamant, (b) IDT, (c) Boussinesq (point), (d) Distributed, and (e) Burmister solutions. . . . .	96

## List of Figures (Continued)

FIGURE	Page
39 Boundary conditions for cracked bodies (a) arbitrary load, (b) interface, (c) penny-shaped. . . . .	97
40 Variation of CSI with percentage of $\Delta K_{IC}$ . . . . .	103
41 Schematic presentation of the fatigue curve. . . . .	111
42 The moisture-density curve for 5% cement content. . . . .	118
43 The moisture-density curve for 15% cement content. . . . .	119
44 Grips developed for the direct tensile creep test. . . . .	121
45 Schematic presentation of the humidity chamber. . . . .	123
46 Barenblatt's crack tip model. . . . .	128
47 Predicted fatigue curve from Schapery's theory. . . . .	135
48 Possible stress-strain behavior of soil-cement. . . . .	141
49 $K_{IC}$ vs. $\sigma_m$ at different cement contents and curing ages. . . . .	142
50 Creep curves at different cement contents. . . . .	150
51 $\log (D(t)-D_0)$ vs. $\log t$ at different cement contents. . . . .	151
52 $\log A$ vs. $n$ of the predicted and the experimental results at different cement contents. . . . .	156
53 Creep curves at different curing ages. . . . .	160
54 $\log (D(t)-D_0)$ vs. $\log t$ at different curing ages. . . . .	162
55 $\log A$ vs. $n$ of the predicted and the experimental results at different curing ages. . . . .	164
56 Shrinkage-moisture loss relationships in pure cement pastes during drying (After Mindess and Young [67]). . . . .	166
57 Creep curves at different relative humidities. . . . .	168
58 $\log (D(t)-D_0)$ vs. $\log t$ at different relative humidities. . . . .	169
59 Creep curves at different temperatures. . . . .	171
60 $\log (D(t)-D_0)$ vs. $\log t$ at different temperatures. . . . .	172

## CHAPTER I: INTRODUCTION

### *Problem Definition*

In this report, the failure of Portland cement stabilized fine grained base courses is investigated. The mode of failure has been clearly established to be tensile; however, the nature of tensile failure has not been clearly defined. For example:

(1) What is the physical nature of crack propagation within the heterogeneous, composite soil cement material? Specifically, what is the nature of the process zone at the crack tip?

(2) Can linear elastic fracture mechanics principles be used to characterize the rate of crack growth within these materials?

(3) Can failure criteria for soil cement in terms of both monotonic and cyclic, or fatigue, loading be developed and incorporated in the pavement design and analysis schemes?

(4) Can fracture parameters be predicted for soil cement based on the viscous response of these materials?

(5) Can economical finite element models be developed to describe crack growth in pavement systems which utilize Portland cement stabilized soil as part of the design?

The objectives of this report are to answer the above questions. As shown in Figure 1, pavement systems are generally composed of several layers (at least a surface layer, base course, and subgrade). The layer of particular interest is any course composed of portland cement stabilized fine grained soil (usually the base course). In this study, primary emphasis is placed on the problem of crack

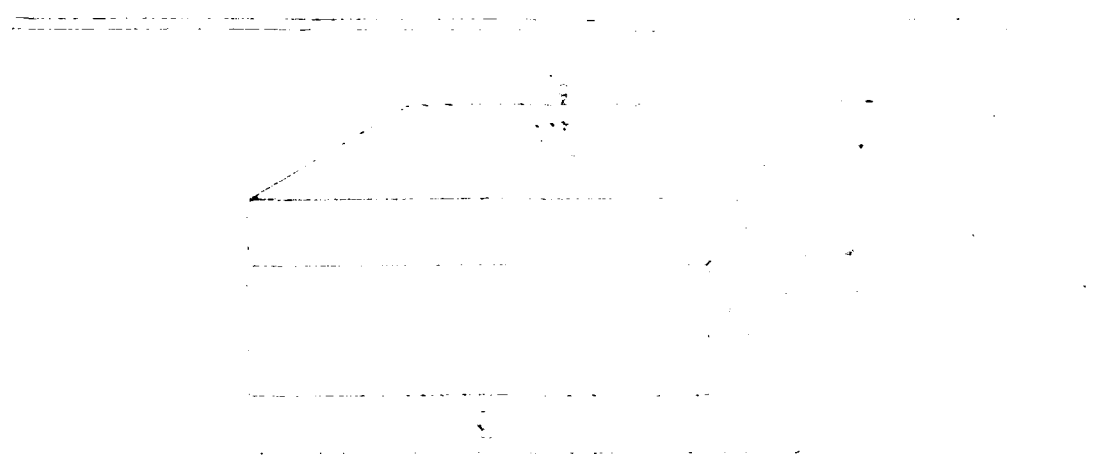


Figure 1. Cracking in layered pavement systems.

The diagram illustrates the cracking in layered pavement systems. It shows a cross-section of a pavement structure with three distinct layers. The top layer is the thickest, followed by a middle layer, and a bottom layer. A horizontal line represents the interface between the top and middle layers. A vertical line represents the interface between the middle and bottom layers. A diagonal line represents the interface between the top and bottom layers. The diagram is labeled with 'S' and 'Z'.

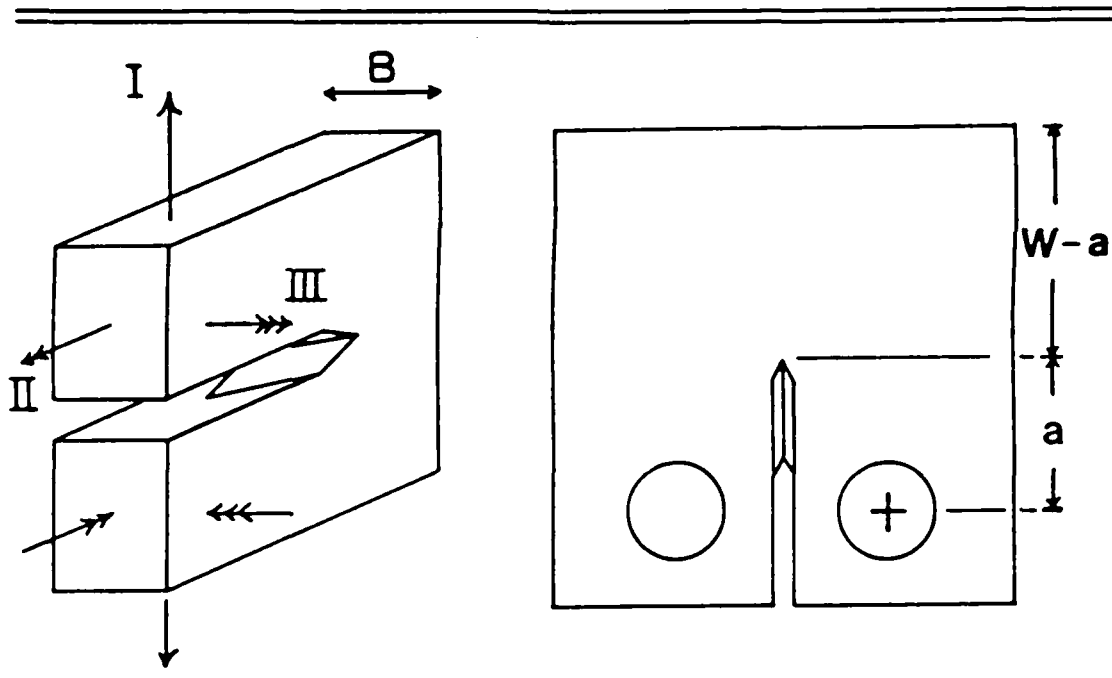


Figure 2. Modes of cracking and specimen dimensions.

#### *Approach to Solution*

The problems discussed above are addressed using the theories of linear elastic fracture mechanics (LEFM). In general, two dimensional stress fields are considered in the analysis. However, some discussion of three dimensional crack problems is included in the study. Fracture toughnesses calculated from "static" (monotonic loading) tests [5, 7] will be combined with scanning electron micrograph (SEM) data in order to assess the nature of crack developement and the applicability of linear elastic fracture mechanics. Cyclic load fatigue testing was performed in order to address question 3. The fourth question is addressed in Chapter V

4

using a method based on linear viscoelastic theory. An economical finite element program was developed and is presented in Volume 2 of this report in response to question 5.

#### *Organization of the Report*

The report is composed of two volumes:

Volume 1. Chapters II and III contain the results of fracture studies on cement stabilized soil under monotonic and cyclic loading conditions, respectively. These results are used to verify hypothesized behavior presented in those chapters. Chapter IV presents approximate solutions for stress intensity factors in cracked bodies based on existing exact solutions from the theory of elasticity for cracked and uncracked bodies. In addition, Chapter IV contains an example problem which ties together the results of Chapters II through IV. Chapter V of Volume 1 illustrates how creep and viscoelastic theory can be used to generate parameters for models of cyclic crack growth similar to those used in Chapter III. The effects of temperature and humidity on creep are also discussed in Chapter V.

Volume 2. The second volume of the report concerns the application of the finite element method to the solution of pavement system problems. Chapter II of this volume discusses the basic approach to the problem and the choice of the element used to model the crack. Chapter III considers the superposition of solutions necessary to solve for the stress intensity factor in the cracked body problem. Chapter IV extends the static solution to the case of cyclic loading.

# Coordinate Systems

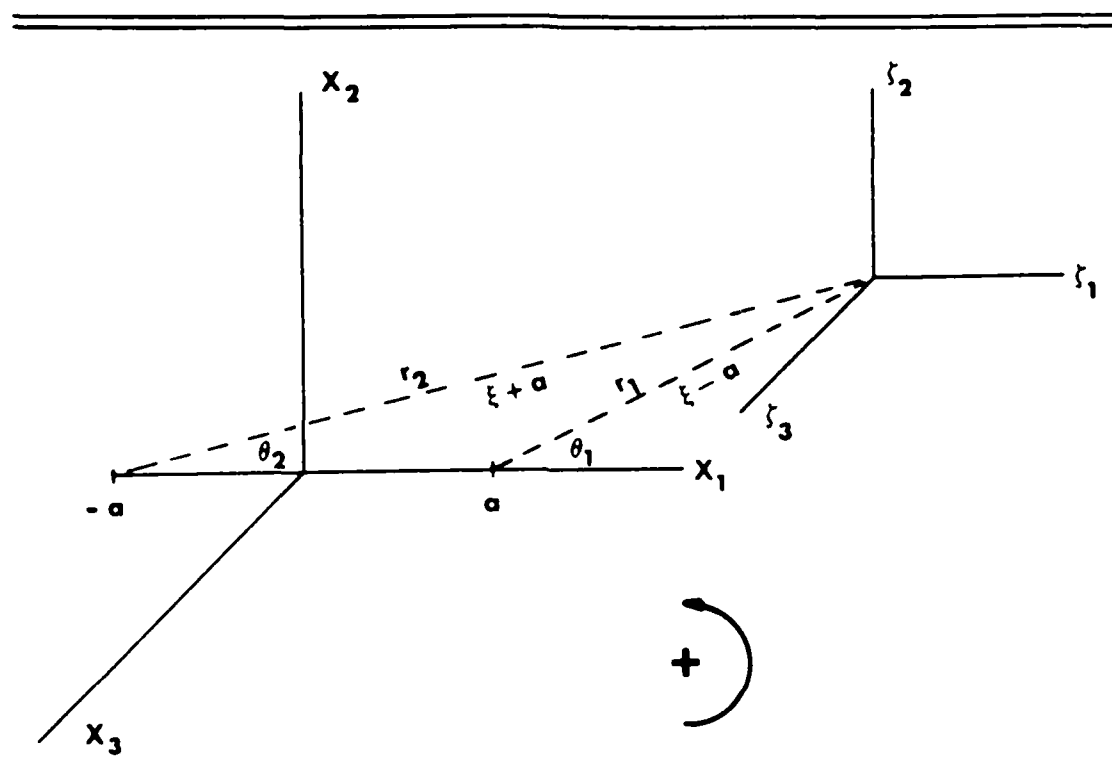


Figure 3. Coordinate system used for the study.

Unless otherwise noted, the Cartesian coordinate system shown in Figure 3 will be used. "Local" ( $\zeta_1, \zeta_2, \zeta_3$ ) and "Global" ( $X_1, X_2, X_3$ ) coordinate systems are presented in the figure. The global system alone is used for the majority of the report, while the two systems together are used in the discussion of the stress intensity factor in the following section.

## CHAPTER II: FRACTURE UNDER MONOTONIC LOADING

### *Literature Review and Theory*

There are two basic approaches to LEFM. Both the continuum mechanics stress field and the strain energy density approaches are based on elastic theory.

Stress Intensity Factor. This brief review of the field equations of elasticity is primarily synthesized from references [57, 58, 54, 103, and 104]. In the discussion, index notation is used to indicate differentiation and the values of the subscripts may be related to the three orthogonal axes by 1=X, 2=Y, 3=Z. Five basic categories of equations are necessary for the solution of problems in elasticity. The first category includes the equations of equilibrium:

$$\sigma_{ij,j} + F_i = 0 \quad (1)$$

Normally, the body force,  $F$ , is taken to be zero with the consequence that the equation is reduced to only the stress term.

Included in the second category are the compatibility or constraint equations:

$$\epsilon_{ij,kl} + \epsilon_{kl,ij} = \epsilon_{ik,jl} + \epsilon_{jl,ik} \quad (2)$$

This set of equations invokes a requirement for a unique, continuous displacement field.

The third category of equations is kinematic:

$$\epsilon_{ij} = (u_{i,j} + u_{j,i})/2 \quad (3)$$

These equations require small displacement gradients which results in the requirement for small strains. Compliance with these requirements allows the elimination of a nonlinear term,  $(u_{i,j}u_{i,k})/2$  which would have appeared in equation (3).

Material specific parameters enter into the analysis in the fourth set of equations. The stress and strain tensors are second order tensors. When the analysis is limited to linear elastic materials, the stress and strain tensors must be related by a fourth order tensor of elastic moduli,  $E$ :

$$\sigma_{ij} = E_{ijkl}\epsilon_{kl} \quad (4)$$

Due to symmetry, there are 36 possible moduli. In the usual case, a continuous potential function exists from which the stresses can be derived. The existence of this function implies additional symmetry so that  $E_{ijkl} = E_{klij}$ . Therefore, for the anisotropic case, 21 elastic constants exist. Further reductions in the number of constants are possible even when dealing with particulate composites such as this fine grained stabilized soil when the material is considered on the macroscale. A transversely isotropic material possesses an axis of symmetry (vertical or Z axis in this case). This axis of symmetry reduces the number of constants to five. The plane of symmetry is perpendicular to the axis of symmetry. The five constants include Young's moduli and Poisson's ratio in the plane of isotropy and perpendicular to the plane of isotropy (i.e. transverse). The fifth constant involves the shear modulus in the transverse direction. The number of independent constants is reduced

to two (involving Young's modulus and Poisson's ratio) in the isotropic case. It is expected, due to the layered "sheet" structures of many soils, that many cement stabilized soils are transversely isotropic. Isotropic analyses are useful when the axis of symmetry is oriented properly and for soil structures composed of randomly oriented particles. In the isotropic case, the fourth set of equations (constitutive equations) become:

$$\sigma_{ij} = \frac{E}{1+\nu} [\epsilon_{ij} + \frac{\nu}{1-2\nu} \epsilon_{kk} \delta_{ij}] \quad (5)$$

The last set of equations is determined by boundary conditions. Either displacements or tractions must be specified along the boundary. For the two dimensional case, the statically indeterminate equilibrium and compatibility equations can be satisfied by a biharmonic Airy stress function. The stress function which has the potential to solve the systems of equations must also result in the satisfaction of the boundary conditions. The stress function can be stated equivalently in terms of either real or complex variables by means of mapping techniques. In the analysis of cracked bodies, complex stress functions are used. For the case of uniform biaxial tension,  $\sigma_0$ , in an infinite sheet, the boundaries are the two crack faces and the boundary at infinity. The stress function is chosen so that its value is real in the material and imaginary at the crack. The stress function,  $\phi$ , is chosen so as to satisfy the biharmonic equation,  $\nabla^4 \phi = 0$ . The chosen stress function can then be used to determine the boundary conditions:

$$\phi = \operatorname{Re} \int \phi d\xi + X_2 \operatorname{Im} \int \phi d\xi \quad (6)$$

If the stress function satisfies the biharmonic equation,

$$\begin{aligned} \sigma_{22} &= \operatorname{Re} \phi + X_2 \operatorname{Im} \phi, \xi \\ \sigma_{11} &= \operatorname{Re} \phi - X_2 \operatorname{Im} \phi, \xi \\ \sigma_{12} &= -X_2 \operatorname{Im} \phi, \xi \end{aligned} \quad (7)$$

A candidate function is:

$$\phi = \sigma_0 \xi (\xi+a)^{-1/2} (\xi-a)^{-1/2} \quad (8)$$

The function is designed to be analytic in the material but not analytic along the crack. Therefore, branch cuts are taken along  $X_2=0$  in order to exclude the region  $X_2=0$ ,  $-a < X_1 < a$ . Arbitrarily setting  $a=1$ , it can be shown that  $\xi-1 = r_1 e^{i\theta_1}$  and  $\xi+1 = r_2 e^{i\theta_2}$ . Allowing the range of  $\theta$  to be defined as  $0 \leq \theta_1 < 2\pi$ ,  $0 \leq \theta_2 < 2\pi$  results in the existence of a function  $g(\xi) = (r_1 e^{i\theta_1})^{1/2} (r_2 e^{i\theta_2})^{1/2}$  which is analytic everywhere. If point  $Q$  is between  $-a$  and  $+a$ ,  $Q^+$  is defined as the value of interest at  $Q$  when approaching  $Q$  from the positive (counter clockwise) direction (origin at  $+a$ ).

$$\therefore \text{ at } Q^+ \theta_1 = \pi, \theta_2 = 0 \text{ and } g(\xi) = (r_1 r_2 e^{i\pi})^{1/2}$$

$$\text{ at } Q^-, \theta_1 = \pm\pi, \theta_2 = 2\pi \text{ and } g(\xi) = (r_1 r_2 e^{i3\pi})^{1/2}$$

Note that there is no discontinuity here because of the cyclic nature of the trigonometric functions with odd multiples of  $\pi$ .

Changing the range of  $\theta$  so that  $-\pi < \theta_3 < \pi$ ,  $-\pi < \theta_4 < \pi$  results in a new function  $g_1(\xi) = (r_1 e^{i\theta_3})^{1/2} (r_2 e^{i\theta_4})^{1/2}$  which has two branch cuts originating at  $a$  and  $-a$  respectively and overlapping along a portion of the negative  $X_1$  axis. If it can be shown that  $g_1 = g$  for  $Q_+ \geq a$  and

$Q \leq -a$ , it can be concluded that the function  $g_1$  does not require branch cuts in those regions and may be considered analytic there. For  $g_1$ , the subscripted sign on  $Q$  means the same as the superscripted sign for  $Q$  when using  $g$ .

At point  $Q_+^+$ ,  $\theta_3=0$ ,  $\theta_4=0$  and  $g_1=(r_1r_2)^{1/2}$

$\theta_1=0$ ,  $\theta_2=0$  and  $g=(r_1r_2)^{1/2}$

At point  $Q_+^-$ ,  $\theta_3=0$ ,  $\theta_4=0$  and  $g_1=(r_1r_2)^{1/2}$

$\theta_1=2\pi$ ,  $\theta_2=2\pi$  and  $g=(r_1r_2)^{1/2}e^{i\pi}e^{i\pi}=(r_1r_2)^{1/2} \therefore g_1=g$

for  $Q_+ \geq a$ .

At point  $Q_-^+$ ,  $\theta_3=\pi$ ,  $\theta_4=\pi$  and  $g_1=(r_1r_2)^{1/2}e^{i\pi}=-(r_1r_2)^{1/2}$

$\theta_1=\pi$ ,  $\theta_2=\pi$  and  $g=(r_1r_2)^{1/2}e^{i\pi}=-(r_1r_2)^{1/2}$

At point  $Q_-^-$ ,  $\theta_3=-\pi$ ,  $\theta_4=-\pi$  and  $g_1=(r_1r_2)^{1/2}e^{-i\pi}=-(r_1r_2)^{1/2}$

$\theta_1=-\pi$ ,  $\theta_2=-\pi$  and  $g=(r_1r_2)^{1/2}e^{-i\pi}=-(r_1r_2)^{1/2} \therefore g_1=g$

for  $Q_- \leq -a$ .

At point  $Q^+$ ,  $\theta_3=\pi$ ,  $\theta_4=0$  and  $g_1=(r_1r_2)^{1/2}e^{i\pi/2}$

$\theta_1=\pi$ ,  $\theta_2=0$  and  $g=(r_1r_2)^{1/2}e^{i\pi/2}$

At point  $Q^-$ ,  $\theta_3=-\pi$ ,  $\theta_4=0$  and  $g_1=(r_1r_2)^{1/2}e^{-i\pi/2}=-i(r_1r_2)^{1/2}$

$\theta_1=-\pi$ ,  $\theta_2=2\pi$  and  $g=(r_1r_2)^{1/2}e^{i\pi/2}=i(r_1r_2)^{1/2} \therefore g_1 \neq g$

for  $-a < Q < a$ .

This also implies that the chosen stress function, equation (6), is analytic everywhere except along the crack. The above discussion illustrates that the use of a stress function which is analytic everywhere is incorrect for a cracked body. In qualitative terms, the use of a stress function which is analytic everywhere does not allow a traction free boundary (i.e. a crack) in the interior of the body. In contrast to real material behavior, this method assumes no

separation of the crack faces. This assumption is the cause of concern over crack tip radii. To describe material behavior with LEFM, a small crack tip radius and parallel crack faces are desired.

Two modifications must be made to obtain the Mode I, plane strain stress intensity factor,  $K_I$ . First, the solution for a stress applied at infinity equal and opposite to the uniform tensile stress parallel to  $X_1$  must be superimposed on the uniform solution. Secondly, the origin of the global coordinate system must be moved to point a. The stresses at the origin of the local coordinate system (located at a distance  $r_1$  from the global system) are:

$$\begin{aligned}\sigma_{22} &= \sigma_0 \left(\frac{a}{2r_1}\right)^{1/2} \left[ \cos\frac{\theta_1}{2} \left(1 + \sin\frac{\theta_1}{2} \sin\frac{3\theta_1}{2}\right) \right] + \text{H.O.T.} \\ \sigma_{11} &= \sigma_0 \left(\frac{a}{2r_1}\right)^{1/2} \left[ \cos\frac{\theta_1}{2} \left(1 - \sin\frac{\theta_1}{2} \sin\frac{3\theta_1}{2}\right) \right] + \text{H.O.T.} \\ \sigma_{12} &= \sigma_0 \left(\frac{a}{2r_1}\right)^{1/2} \left[ \sin\frac{\theta_1}{2} \cos\frac{\theta_1}{2} \cos\frac{3\theta_1}{2} \right] + \text{H.O.T.}\end{aligned}\quad (9)$$

The higher order terms (H.O.T.) in equations (9) are small in comparison to the first terms only when the local coordinate system is "near" the crack tip. When  $(\xi - a) \ll a$  (i.e. "near" the crack tip), it can be shown that equation (8) reduces to

$$\phi = \frac{\sigma_0 a}{[2a(\xi - a)]^{1/2}} \quad (10)$$

The Mode I stress intensity factor,  $K_I$ , is now defined as

$$K_I = \lim_{(\xi - a) \rightarrow 0} [2\pi(\xi - a)]^{1/2} \phi = \sigma_0 \sqrt{\pi a} \quad (11)$$

It can easily be seen that the stresses of equations (9) now reduce to a set of equations of the form:

$$\sigma_{\alpha\beta} = \frac{K_I}{\sqrt{2\pi r}} f_{\alpha\beta}(\theta)$$

indicating, of course, the widely accepted fact that once  $K_I$  is known, the whole stress field in the vicinity of the crack is known. In fact, if the higher order terms of equations (9) are known, the whole field is known exactly. It should be noted that  $\sigma_{33}=0$  for plane stress and that  $\sigma_{33}=\nu(\sigma_{11}+\sigma_{22})$  for the plane strain case. It should also be noted that early literature (e.g. 44, 29) did not include the constant  $\pi$  in the limit of equation (11) which results in the requirement to multiply the earlier results by  $\sqrt{\pi}$  before a comparison may be made with the more recent literature. The shape of the stress distribution is shown in Figure 4.

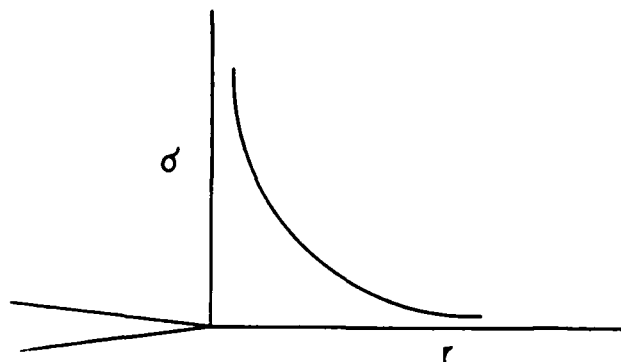


Figure 4. Stress distribution ( $1/\sqrt{r}$ ) ahead of the crack.

Conceptually, the problem of infinite stress at the crack tip was addressed by Irwin [15, 45]. The stress was essentially cut off at the yield strength of the material causing a "plastic" zone ahead of the crack tip as illustrated in Figure 5.

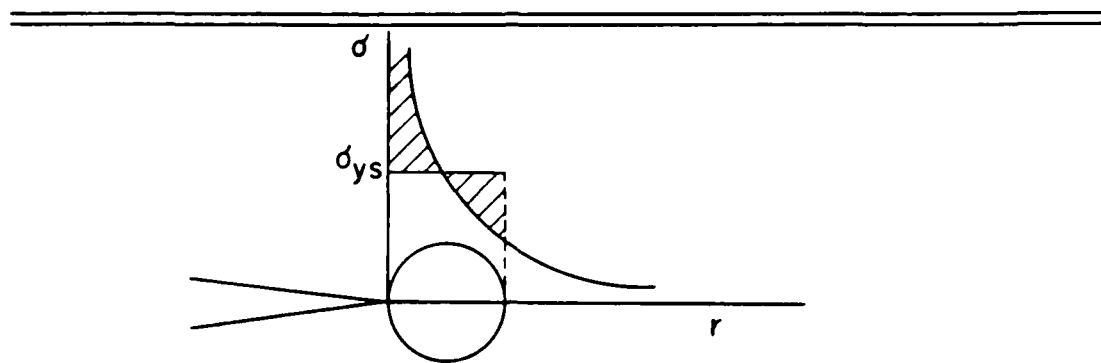


Figure 5. The crack tip plastic zone (redrawn from Broek [15])

It is obvious that a large plastic zone could distort the  $1/\sqrt{r}$  stress dependence due to the redistribution of stress to such an extent that LEFM would no longer apply.

Strain Energy Density. Rice [83] developed an approximate analysis of strain concentration by identifying a path independent line integral. A discussion of a portion of that paper follows. The strain energy density,  $W$ , is defined as

$$W = \int_0^{\epsilon} \sigma_{ij} d\epsilon_{ij}$$

A path independent integral is defined as

$$J = \int_C (W dy - T_i \cdot \frac{\partial u}{\partial x} ds) \quad (13)$$

where  $T_i = \sigma_{ij} \vec{n}_j$ . The coordinate system and appropriate parameters are shown below in Figure 6.

A potential energy parameter (per unit thickness),  $P_e$ , was defined as follows:

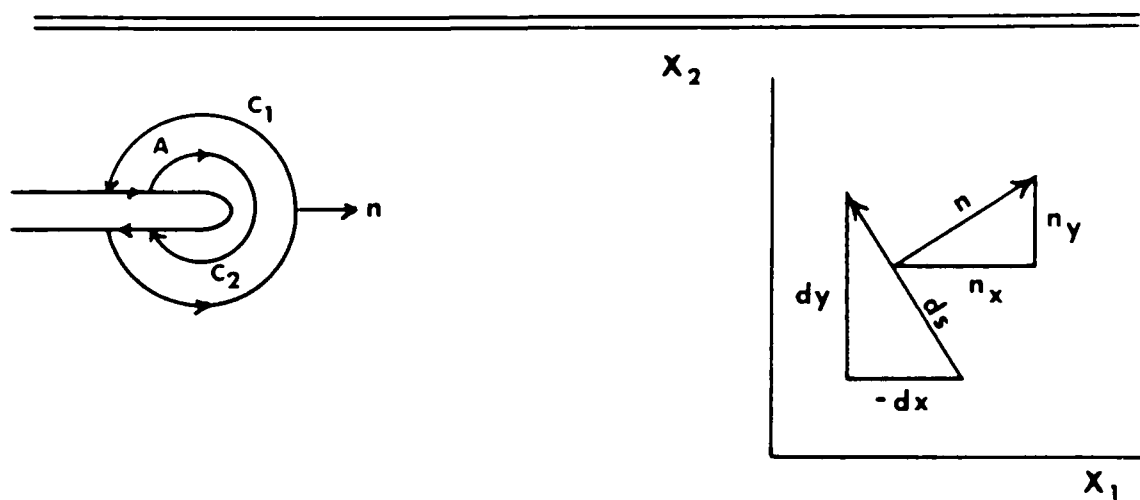


Figure 6. The path independent line integral.

$$P_e = \iint_A W dx dy - \int_{C'} T \cdot u ds \quad (14)$$

where  $A$  is the area bounded by  $C_1$ ,  $C_2$  and the crack faces and  $C'$  is that portion of  $C$  over which the tractions are prescribed. Body forces are assumed to be zero which implies that  $\sigma_{ij,j} = 0$  and that  $\sigma_{ij} = \sigma_{ji}$  is a constant. It can now be seen that

$$\begin{aligned} \int_{C_1} (W dy - T_i u_{i,1} ds) &= \int_{C_1} W dy - \int_{C_1} T_i u_{i,1} ds \\ &= \int_{C_1} (0 + W dy) - \int_{C_1} \sigma_{ij} n_j u_{i,1} ds \end{aligned}$$

and that

$$n_x = |n| \cos \theta = \cos \theta$$

$$n_y = \sin \theta$$

$$-dx = ds \sin \theta$$

$$dy = ds \cos \theta$$

$$\Rightarrow n_x ds = n_1 ds = \cos \theta ds = dy = dx_2$$

$$n_y ds = n_2 ds = \sin \theta ds = -dx = -dx_1$$

$$\Rightarrow \sigma_{i1} u_{i,1} n_1 ds = \sigma_{i1} u_{i,1} dy$$

$$\sigma_{i2} u_{i,1} n_2 ds = -\sigma_{i2} u_{i,1} dx$$

$$\therefore \int_{C_1} (W dy - T_i u_{i,1} ds) = \int_{C_1} (0 + W dy) - \int_{C_1} (-\sigma_{i2} u_{i,1} dx + \sigma_{i1} u_{i,1} dy)$$

Applying Green's theorem for simply connected domains (see [53]):

$$\begin{aligned} &\Rightarrow \iint_A W_{,1} dx dy - \iint_A [(\sigma_{i1} u_{i,1})_{,1} + (\sigma_{i2} u_{i,1})_{,2}] dx dy \\ &= \iint_A [W_{,1} - (\sigma_{ij} u_{i,1})_{,j}] dx dy = 0 \end{aligned} \quad (15)$$

which can be verified by noting that

$$\begin{aligned} W_{,1} &= (\partial W / \partial \epsilon_{ij}) (\partial \epsilon_{ij} / \partial x) = \sigma_{ij} \epsilon_{ij,1} \\ &= (1/2) \sigma_{ij} [(u_{i,j})_{,1} + (u_{j,i})_{,1}] = \sigma_{ij} [(u_{i,1})_{,j}] \\ &= [\sigma_{ij} u_{i,1}]_{,j} \end{aligned}$$

Since  $T=0$  and  $dy=0$  along the portion of  $C$  which is on the crack surfaces, the integral has the same value regardless of the path chosen. If  $C_2$  is chosen so that  $dy \neq 0$ , and  $T=0$  (i.e. the leading edge of the crack tip), then

$$J = \int_{C_2} W dy \quad (16)$$

and  $J$  is seen to be an integrated measure of the strain at the tip

which can be seen in Figure 7. The crack tip model (a) has a singularity. It should be noted that the elliptical crack tip model (see Figure 7) would not allow for a singularity near the tip.

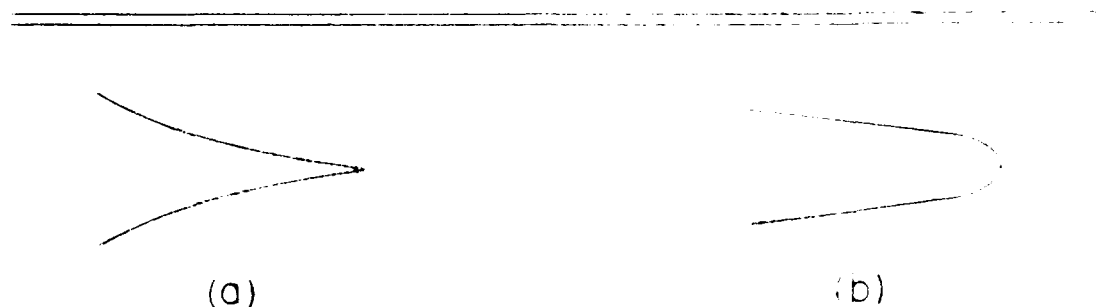


Figure 7. The Barenblatt [8] crack tip model (a) versus an elliptical shape (b).

It should also be noted that the derivation relies on a simply connected domain which requires no mathematical holes between  $C_1$  and  $C_2$ . If holes exist between  $C_2$  and the crack tip (e.g. microcracks exist which are of a more influential nature than those outside  $C_2$ ), a multiply connected domain exists and

$$\int_{C_1} (Wdy - T_{ij}u_{i,j}ds) = - \int_{C_2} Wdy - T_{ij}u_{i,j}ds$$

implying that equation (15) would no longer be valid. Nevertheless,  $J$  is a useful approximation of toughness in many materials including cement stabilized soil.

Strain Energy Density Factor. The possibility of a multiply connected domain is handled in a qualitative fashion by the concept of a crack tip process zone. A three dimensional "core" region is

used by Sih [97, 54, 98, 27] in his extension of the strain energy density idea to a strain energy density factor,  $S$ , where

$$S = r_0 \frac{dW}{dV} \quad (17)$$

and  $r_0$  is the radius of a three dimensional spherical core region not unlike the Irwin [15, 45, 46] plastic zone for two dimensional analysis, and  $dW/dV$  is the strain energy per unit volume of an element located in the material ahead of the core (i.e. ahead of  $r_0$ ). For a through crack of length  $2a$  in a uniformly stressed plate, Sih [54] assumes failure occurs when

$$\sigma_c \sqrt{a} = \left[ \frac{2ES_c}{(1+\nu)(1-2\nu)} \right]^{1/2} = \text{constant} \quad (18)$$

which, in some respects, is similar to the original Griffith [36, 37] criterion but is of a different origin. The form of equation (18) changes when the load is not applied perpendicular to the plane of the crack. In the case of the crack inclined at an angle  $\beta$  with the load, equation (18) becomes

$$\sigma_c \sqrt{a} = \left[ \frac{S_c}{F(\beta, \theta_0)} \right]^{1/2} = \text{constant} \quad (19)$$

where

$$F(\beta, \theta_0) = (a_{11} \sin^2 \beta + 2a_{12} \sin \beta \cos \beta + a_{22} \cos^2 \beta) \sin^2 \theta_0 \quad (20a)$$

$$16\mu a_{11} = (3-4\nu - \cos \theta_0)(1 + \cos \theta_0) \quad (20b)$$

$$8\mu a_{12} = \sin \theta_0 (\cos \theta_0 - (1-2\nu)) \quad (20c)$$

$$16\mu a_{22} = 4(1-\nu)(1 - \cos \theta_0) + (1 + \cos \theta_0)(3 \cos \theta_0 - 1) \quad (20d)$$

where  $a_{ii}$  is a constant, not crack length, for equation (20) only and

$\theta_0$  is the direction of crack growth for a given  $\beta$ . The crack grows toward the point near the crack tip where  $S$  is a minimum. Multiple mode fracture (the analysis of which is, presumably, the primary purpose of Sih's theory) allows the possibility of all three modes of cracking to exist simultaneously. Fracture would then occur at some critical combination of the three modes. The strain energy density factor can be divided into two components. The volume element can store strain energy by dilatation (volume change,  $v$ ) or by distortion (shape change,  $s$ ). Therefore,  $S = S_v + S_s$ , where

$$S_v = b_{11}K_I^2 + 2b_{12}K_I K_{II} + b_{22}K_{II}^2 + b_{33}K_{III}^2$$

and

$$S_s = c_{11}K_I^2 + 2c_{12}K_I K_{II} + c_{22}K_{II}^2 + c_{33}K_{III}^2$$

the coefficients  $b_{ij}$ ,  $c_{ij}$  are defined in reference [54] and are not necessary for utilization of solutions presented in that work. An alternative representation of the partitioning of  $S$  is given by Gdoutos [27] in terms of  $dW/dV$ :

$$dW_s/dV = \frac{1+\nu}{6E} [(\sigma_{11}-\sigma_{22})^2 + (\sigma_{22}-\sigma_{33})^2 + (\sigma_{33}-\sigma_{11})^2 + 6(\tau_{12}^2 + \tau_{23}^2 + \tau_{31}^2)]$$

and

$$dW_v/dV = \frac{1-2\nu}{6E} (\sigma_{11} + \sigma_{22} + \sigma_{33})^2$$

In terms of principal stresses for the plane strain condition

$$\sigma_3 = \nu(\sigma_1 + \sigma_2)$$

$$\frac{dW_v/dV}{dW_s/dV} = \frac{(1-2\nu)(1+\nu)[(\sigma_1/\sigma_2)+1]^2}{[(\sigma_1/\sigma_2)-1]^2 + [(1-\nu)-\nu(\sigma_1/\sigma_2)]^2 + [(1-\nu)(\sigma_1/\sigma_2)-\nu]^2}$$

The hypotheses which apply to this theory are [54]:

1. Given any point (surrounded by a sphere) along the crack front, the direction of crack propagation is toward the direction of the minimum value of  $S$ ,  $S_{\min}$ , anywhere on the sphere.
2. Crack extension occurs when  $S_{\min} = S_c$ .
3.  $S_{\min}/r_0$  is constant along the new crack front.

This theory has the following implications for the current pavement problem:

1. Some specific three dimensional problems may be studied analytically [54].
  2. The inclined crack will tend to propagate in such a manner as to orient itself toward the Mode I orientation [27].
  3. In most cases (e.g.  $\beta > 60^\circ$ ), crack extension initiates at the ends of the minor axis of an embedded elliptical flaw [27].
- Therefore, the elliptical flaw will often evolve to an embedded circular flaw.

Stress Intensity and Strain Energy. It has been established (e.g. 15, 44, 76) that

$$G = \frac{1-\nu^2}{E} \left[ K_I^2 + K_{II}^2 + \frac{K_{III}^2}{1-\nu} \right] \quad (21)$$

which becomes, for the plane strain Mode I case

$$G = \left( \frac{1-\nu^2}{E} \right) K_I^2 \quad (22)$$

In the linear elastic case,  $J=G$  [15, 60, 83]. This is also

apparently correct for small-scale yielding [60]. Therefore, equation (22) now becomes:

$$K^2 = \frac{JE}{1-\nu^2} \quad (23)$$

This equation can be rearranged so as to facilitate evaluation of compliance with the linear elastic assumption in experimental work:

$$c(K^2)^b = \frac{JE}{1-\nu^2}$$

$$\rightarrow \ln(c) + b \ln(K^2) = \ln \frac{JE}{(1-\nu^2)} \quad (24)$$

where  $c=1$ ,  $b=1$  for the linear elastic case

"Ideal" Fracture Strength. The Lennard-Jones 6-12 potential is used to illustrate the calculation of "ideal" material parameters. This potential is a model which describes the balance of attraction and repulsion tendencies of particles in terms of potential energy. This model is primarily used for Van der Waals crystals [59]. A general form of the equation is (see [26, 79])

$$U = U_0[(x_0/x)^{12} - 2(x_0/x)^6], \quad x > 0 \quad (25)$$

where the exponents 12 and 6 are actually dependent on the type of bonding, and the parameters are as shown in Figure 8. The parameter  $D$  in Figure 8 corresponds to particle separation distance, or  $x$ , and the potential energy corresponds to  $U$ .

Reversing the sign in order to associate attraction with the positive  $Y$  axis, and differentiating with respect to  $x$  yields a force representation of this potential:

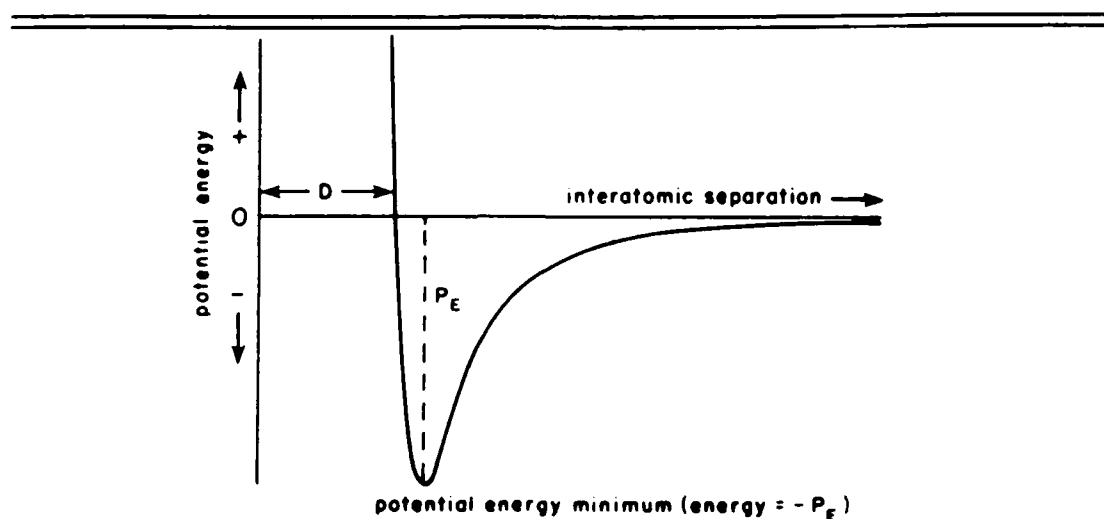


Figure 8. The Lennard-Jones Potential (Redrawn from Porterfield [79]).

$$\begin{aligned}
 F &= dU/dx = U_0[-12x_0^{12}/x^{13} + 12x_0^6/x^7] \\
 &= \frac{12U_0}{x_0} [(x_0/x)^7 - (x_0/x)^{13}]
 \end{aligned}
 \tag{26}$$

As discussed in reference [58],  $x_0$  is taken to be the length of one side of a cube which is the building block of a material having a lattice plane made up of squares. It should be noted here that the use of this potential for stabilized soil is somewhat qualitative due to the assumed lattice structure, bonding type, and size scale of the particles at the nodes of the lattice. For a clay material, a tetrahedron ( $\text{SiO}_4$ ), octahedron ( $\text{Al}(\text{OH})_6$ ), hexagon (unit cell or ring), or some shape based on arrangement of adsorbed water may be more appropriate than the cube as a lattice arrangement. Nevertheless, the cubical arrangement is acceptable for this

discussion concerning a silty sand with low plasticity. The choice of a model which describes Van der Waals type forces is appropriate due to the fact that the cement-soil bond is partly due to Van der Waals forces [67] and so is the balance of forces in the diffuse double layer of a dispersed clay [99]. The size scale used in the discussion is the particle size (as opposed to atomic or molecular scale). Using the lattice spacing to define the area over which the force in equation (26) acts, it is noted that

$$F/x_0^2 = \frac{12U_0}{x_0^3} [(x_0/x)^7 - (x_0/x)^{13}] \quad (27)$$

where

$$\sigma = F/x_0^2$$

In the pursuit of a theoretically based model which can describe the variation in fracture toughness with changes in cement content and compaction effort, the following assumptions are necessary.

- (1) LEFM is applicable.
- (2) Whole planes of particles separate at fracture.
- (3) Displacement at peak load (as corrected for crack length) is approximately constant for all values of toughness (i.e. all specimens), and strain to failure is approximately constant.
- (4) The bond type which is most responsible for failure is of a Van der Waals type.
- (5) The lattice plane is essentially square (i.e. cubic).
- (6) Fracture essentially occurs at the particle spacing which results in the maximum attractive force in the Lennard-Jones model.
- (7) Reduction of the three dimensional tensor integration necessary for strain energy density approaches to a single element stress-strain combination is permissible.
- (8) Two conveniently measureable parameters exist (e.g. nominal compaction energy and binder content for the material used in this study) which will be likely to model, in a linear fashion, the particle spacing and the maximum attractive force at failure, respectively.

Utilizing the assumptions discussed above, the behavior of toughness as a function of particle spacing and bond strength is presented below. An indication of strain is

$$\epsilon = \frac{\Delta x}{x_0} = (x - x_0)/x_0 = (x/x_0) - 1 \quad (28a)$$

$$\therefore E = (d\sigma/d\epsilon)|_{x=x_0} = d(F/x_0^2)/d(\Delta x/x_0) \quad (28b)$$

and

$$x = \epsilon x_0 + x_0$$

Note that  $2\gamma = G = J = \int_{C_2} [\int_0^\epsilon \sigma_{ij} d\epsilon_{ij}] dy$  for the linear elastic case. For the linear elastic case in certain specific configurations [83],  $J$  is the strain energy times some constant, i.e.  $J = cW$ .

$$\begin{aligned} \therefore J &= c \int_0^{\epsilon_f} \sigma d\epsilon = \\ c \int_0^\epsilon \frac{12U_0}{x_0^3} \left[ \left( \frac{x_0}{\epsilon x_0 + x_0} \right)^7 - \left( \frac{x_0}{\epsilon x_0 + x_0} \right)^{13} \right] d\epsilon \\ &= \frac{12cU_0}{x_0^3} \left[ x_0^7 \int_0^\epsilon \frac{d\epsilon}{(\epsilon x_0 + x_0)^7} - x_0^{13} \int_0^\epsilon \frac{d\epsilon}{(\epsilon x_0 + x_0)^{13}} \right] \\ &= \frac{12cU_0}{x_0^3} \left[ x_0^7 \frac{(\epsilon x_0 + x_0)^{-6}}{-6x_0} - x_0^{13} \frac{(\epsilon x_0 + x_0)^{-12}}{-12x_0} \right] \\ &= 12cU_0 \left[ x_0^3 \frac{(\epsilon x_0 + x_0)^{-6}}{-6} - x_0^9 \frac{(\epsilon x_0 + x_0)^{-12}}{-12} \right] \\ &= \frac{12cU_0}{6} \left[ \frac{x_0^9}{2} (\epsilon x_0 + x_0)^{-12} - x_0^3 (\epsilon x_0 + x_0)^{-6} \right] \quad (29) \end{aligned}$$

From equations (28b and 27):

$$\begin{aligned}
 \sigma &= (12U_0/x_0^3) [(x/x_0)^{-7} - (x/x_0)^{-13}] \\
 &= \frac{12U_0}{x_0^3} \left[ \left( \frac{x}{x_0} \right)^{-1+1}^{-7} - \left( \frac{x}{x_0} \right)^{-1+1}^{-13} \right] \\
 &= \frac{12U_0}{x_0^3} [(\epsilon+1)^{-7} - (\epsilon+1)^{-13}] \quad (30a)
 \end{aligned}$$

$$\therefore \left. \frac{d\sigma}{d\epsilon} \right|_{\epsilon=0} = E = \frac{12U_0}{x_0^3} [-7(\epsilon+1)^{-8} + 13(\epsilon+1)^{-14}] \Big|_{\epsilon=0} = 72U_0/x_0^3 \quad (30b)$$

which is dimensionally correct. Noting that  $\sigma = \sigma_{\max}$  where  $d\sigma/d\epsilon = 0$  and using equation (30b) results in

$$13(\epsilon+1)^{-14} = 7(\epsilon+1)^{-8}$$

$$\Rightarrow (\epsilon+1)^{-6} = 7/13$$

$$\Rightarrow (x_0/x_m)^6 = 7/13$$

$$\therefore x_m = (13/7)^{1/6} x_0 \approx 1.10868 x_0 \quad (31)$$

where  $x_m$  is the value of  $x$  at  $\sigma_{\max}$ . Using  $x_m$  as the value for  $x$  at failure,  $x_f$ , in equations (28a and 29), it is seen that

$$\begin{aligned}
 J_c &\approx \frac{2cU_0}{x_0^3} \left[ \frac{x_0^{12}}{2} (x_f)^{-12} - x_0^6 (x_f)^{-6} \right] \\
 &= \frac{cE}{36} \left[ \frac{1}{2} \left( \frac{x_0}{x_f} \right)^{12} - \left( \frac{x_0}{x_f} \right)^6 \right] \quad (32)
 \end{aligned}$$

where it is seen that  $c$  must have a dimension of length to make the equation (32) dimensionally correct. In the case cited by Rice [83],

c does indeed have the dimension of length. It can now be seen that

$$\sigma = \sigma_{\max} \text{ at } x=x_f=(13/7)^{1/6}x_o$$

$$\approx 2.6899(U_o/x_o^3)$$

which is dimensionally correct (this equation results from the substitution of the expression for  $\sigma_{\max}$  into equation (27)).

Finally, the primary results of this derivation are seen to be

$$J \approx 0.744c\sigma_{\max} \left[ \frac{1}{2} \left( \frac{x_o}{x_f} \right)^{12} - \left( \frac{x_o}{x_f} \right)^6 \right]$$

$$\partial J / \partial \sigma_{\max} \approx 0.744c \left[ \frac{1}{2} (x_o/x_f)^{12} - (x_o/x_f)^6 \right] \quad (33a)$$

and

$$\partial J / \partial x_o \approx -1.11c\sigma_{\max}/x_o \quad (33b)$$

which are also dimensionally correct. From equations (33) it is seen that if one could separate the components which determine toughness into those which control  $\sigma_{\max}$  and those which affect equilibrium spacing, the value of the slopes of the regression equations which relate the toughness to these two parameters could be compared with equations (33). Alternatively, knowledge of the parameters in equations (33) may allow detection of which compositional factors affect J by changing  $\sigma_{\max}$  versus those which affect J by changing  $x_o$ . This, of course, would only be possible if  $x_f$  were constant. It will be shown later in this report that the displacement to failure of the cement stabilized soil studied is approximately constant, lending credence to the  $x_f=\text{constant}$  assumption. For this qualitative

discussion, it is sufficient to note that, under the assumed conditions,  $\partial J / \partial \sigma_{\max}$  is constant while  $\partial J / \partial x_0$  varies inversely with  $x_0$ .

Experimental Considerations. The treatment of fracture to this point has generally assumed a plane strain stress state, Mode I orientation, and the topic of resistance to crack growth has not been addressed. As discussed by Broek in reference [15], especially in plane stress, the resistance to crack extension varies with crack growth. In plane strain, the resistance to crack extension is approximately constant and equal to the energy release rate ( $G$  or  $J$ ). When crack growth is stable, an increase in stress is required to maintain that growth to reach instability. Equations (11, and 23) with the term  $(1-\nu^2)$  for plane strain omitted for the case of plane stress results in

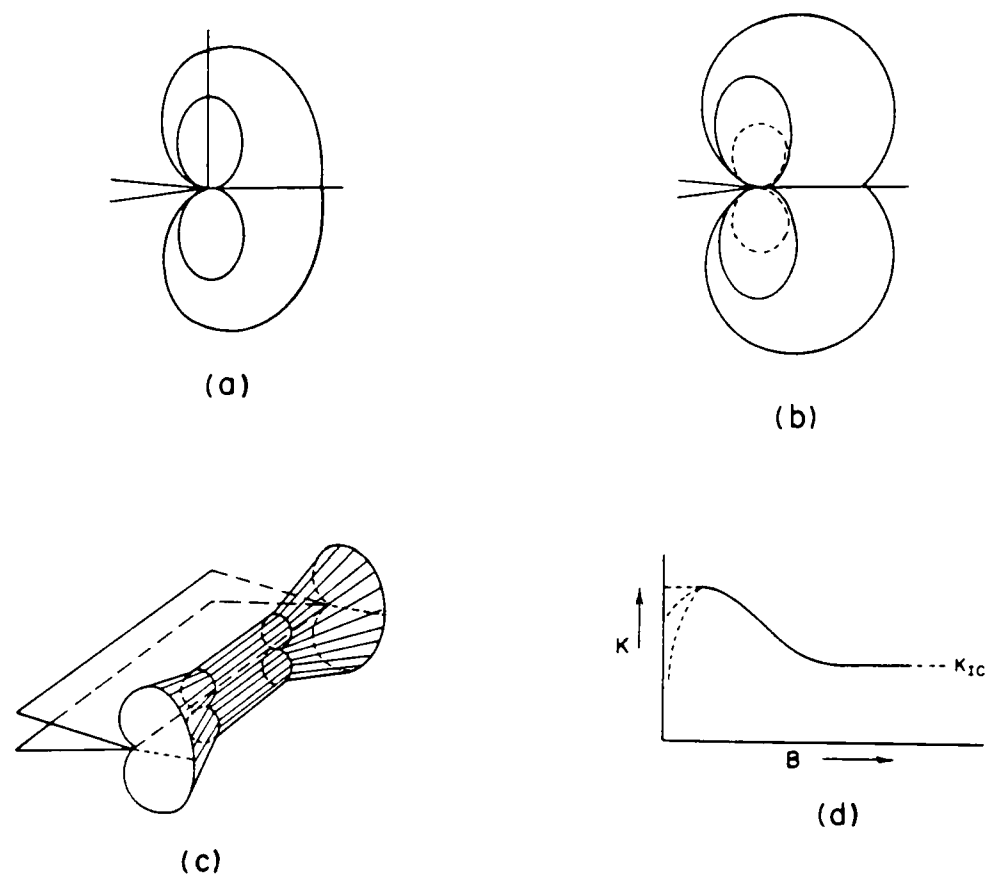
$$J = \frac{\pi \sigma_0^2 a}{E}$$

$$\Rightarrow dJ/da = \frac{\pi \sigma_0^2}{E} \quad (34)$$

which indicates that the R-curve is non-linear when the stress state is plane stress. Instability occurs when [15]

$$J \geq J_R \quad \text{and} \quad \frac{dJ}{da} \geq \frac{dJ_R}{da} \quad (35)$$

The important concepts to note here for the material being studied are that as  $dJ/da$  approaches zero, the predominance of plane strain through the sample thickness becomes more complete. The predominance of plane strain is important because the material constant,  $K_{IC}$ , is only constant when plane strain prevails as illustrated in Figure 9.



(a) Von Mises (b) Tresca (c) In three dimensions  
(d) Toughness as a function of thickness

Figure 9. Plane strain versus plane stress. (Redrawn from Broek [15])

Part (a) of the figure shows a plastic zone shape around the crack tip generated by using the Von Mises yield criterion. Part (b) shows the Tresca yield shape. Part (c) shows the decrease in the size of the plastic zone with increasing constraint (i.e. plane stress at the free surfaces, plane strain in the interior). Part (d) illustrates that  $K$  only reaches the value of  $K_{IC}$ , a material constant, if the thickness of the material,  $B$ , is sufficient to cause the plane strain stress state to be predominant.

The value of  $K_{IC}$  is calculated in the ASTM standard [5] by using an equation of the form:

$$K = \frac{P}{B\sqrt{W}} f(a/W)$$

which corresponds to equation (11) when applied to different boundary conditions. The load versus displacement record which results from a displacement controlled test on cement stabilized soil with periodic partial unloading is as shown in Figure (10).

The unload-reload cycles appearing as elongated loops on the record require adoption of a technique other than the compliance method mentioned in reference [5]. The choice of how to standardize the measurement of compliance was considered to be too arbitrary. Therefore, crack length was measured directly.

A 5% secant offset procedure applied to the load-displacement record is specified in the ASTM standard [5] and is based on, among other factors, a limit of two percent crack extension prior to this point on the load-displacement record. The position (displacement coordinate) of the point where the 5% offset intersects the load-

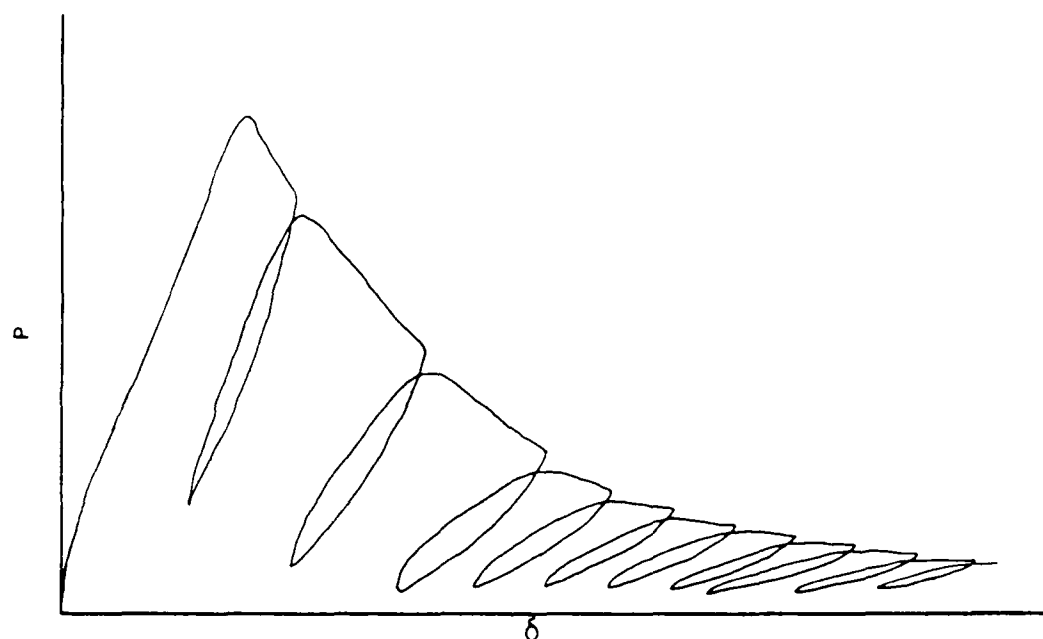


Figure 10. Load-displacement record: cement stabilized soil

displacement ( $\delta_{5\%}$ ) record in relation to the displacement coordinate of the peak load ( $\delta_{mxp}$ ) determines which category of the three possible load-displacement record categories is appropriate. In terms of the standard [5], the material studied often exhibits a "Type III" load-displacement record (i.e.  $\delta_{mxp} < \delta_{5\%}$ ).

The following discussion of the offset procedure is based on the work of Knott in reference [58]. Assume that a nonlinear load-displacement record is to be analyzed. The difference between the recorded displacement at maximum load and the displacement at maximum

load on a linear  $P-\delta$  curve having the same initial slope as the recorded curve is a finite quantity,  $\Delta\delta$ . If this difference is due to a change in crack length,  $\Delta a$ , which is assumed to be smaller than or equal to the size of the plane strain plastic zone,  $r$ , where

$$r = \frac{K_{IC}^2}{6\pi\sigma_Y^2} \leq 0.02a_0 \quad (37)$$

then

$$\Delta a/a_0 \leq 0.02 \quad (38)$$

The factor  $1/6$  in equation (37) comes from multiplying the expression generated by yield theories in plane stress by  $1/3$  which originates in the "constraint factor" (2.57 for the Tresca yield criterion, 2.96 for the Mises criterion - see equation 5.10.2 in reference [58] or equation 4.26 in reference [15]) which raises the plane strain yield strength to a value approaching three times the plane stress value. Expressions relating  $\delta$ ,  $P$ , and  $a$  have the form [88, 89]

$$\frac{BE\delta}{P} = f(a/W) \quad (39)$$

At constant load

$$\Delta\delta/\delta = [f(a_0/W + \Delta a/W) - f(a_0/W)]/f(a_0/W) \quad (40)$$

noting that  $\Delta a \ll a_0$ , Knott finds

$$\Delta\delta/\delta = \frac{1}{f(a_0/W)} \left[ \frac{df(a_0/W)}{d(a_0/W)} \right] (\Delta a/W)(a_0/a_0) = c_{11}\Delta a/a_0 \quad (41)$$

$$\Rightarrow \Delta a/a_0 = (\Delta\delta/\delta)/c_{11} \quad (42)$$

but  $\Delta a/a_0 \leq 0.02$

$$\therefore (\Delta\delta/\delta)/c_{11} \leq 0.02 \quad (43)$$

$$\Rightarrow \Delta\delta/\delta \leq 0.02c_{11}$$

$$\Rightarrow \Delta\delta \leq 0.02c_{11}\delta \quad (44)$$

At load  $P_{\max}$ , and displacement  $\delta+\Delta\delta$ , calculation of compliance gives

$$(\delta+\Delta\delta)/P \leq (0.02c_{11}\delta+\delta)/P = (\delta/P)(1+0.02c_{11}) \quad (45)$$

For  $0.45 \leq (a_0/W) \leq 0.55$ ,  $0.02c_{11}$  takes an average value of approximately 0.05, which leads to the requirement that

$$(\delta+\Delta\delta)/P \leq 1.05(\delta/P) \quad (46)$$

being based on a maximum of 2% apparent crack extension, equation (38). As will be shown later in this report, the average crack extension before peak load for the material studied was 1.67% with the peak of the distribution located at an even smaller value. The important consideration here is that this load-displacement record type and the small extension before peak load confirms the existence of linear behavior for the material studied.

#### *New Developments*

As will be shown later in the report, the form of a regression equation based on the derivation of equations (33) was successful in modelling toughness as a function of the cement content and compaction effort.

### Experimental Procedure

The soil used was obtained near Vicksburg, Mississippi, and was light brown to tan in color. The natural soil and the soil as prepared for testing are described further in Table 1.

**Table 1. Specimen Constitution.**

NATURAL SOIL	
Natural Soil:	Silty sand (SM, A-4)
Sieve Analysis:	100% passing U.S. number 40 47.5% passing U.S. number 200
Liquid Limit:	27.8%
Plastic Limit:	18.9%
Plasticity Index:	8.9%
Stabilizer:	Portland Cement, Type I
Stabilizer Content:	10%
Compaction:	AASHTO T180 [2]
Optimum Moisture:	16.8% (distilled water)
COMPACT TENSION SPECIMEN	
Sieve Analysis:	100% passing U.S. number 100
Stabilizer Contents:	5, 10, and 15 percent
Mold:	4 inch (10.16 cm) diameter cylinder 4.6 inches (11.68 cm) high
Compaction:	M = 5 layers, 25 blows per layer [2] 10 lb (44.48 N) hammer, 1.5 ft (45.72 cm) drop S = 3 layers, 25 blows per layer [1] 5.5 lb (24.46 N) hammer, 1.0 ft (30.48 cm) drop
Moisture Content:	16.8% (distilled water) (i.e. not necessarily optimum moisture content)

The soil was stored at 140°F(60°C), 10% relative humidity. The time schedule for fabricating and curing the specimens is shown in Table 2.

Table 2. Specimen History.

DAY	ACTION
1	Sieve natural soil through number 100 sieve Sieve Portland cement through number 100 sieve Mix and compact Place in environmental room: 73 degrees Fahrenheit (22.8°C) 95 percent relative humidity
2-6	Turn samples over each day
7	Place in environmental room: 73 degrees Fahrenheit (22.8°C) 50 percent relative humidity
21-34	Begin cutting, milling, and instrumenting the samples
35	Conduct tests (28 days since removal from 95% room): ASTM E399 [5] ASTM E813 [7] ASTM E647 [6]

In this report, references to the curing date in this experimental work refer to the number of days **after** moist curing is complete (i.e. 35 days since molding is referred to as a 28 day specimen). Each molded cylinder was cut into three cylinders approximately 1.5 inches (3.81cm) high and 4 inches (10.16cm) in diameter using a masonry saw with the blade dry or very lightly lubricated with water. The three small cylinders were then milled on a vertical milling machine to the specifications of the compact tension specimen utilizing the chevron notch shape described in reference [5] and illustrated in the right hand portion of Figure 2. The notch was cut using a specially ground carbide tipped saw blade, the holes were drilled with a carbide tipped masonry drill bit, and the outer dimensions were obtained using either a center cutting carbide tipped end mill or a mounted

grinding wheel. The outer dimensions were cut first, the notch was cut next, and the holes were drilled last. To avoid breaking large pieces out of the specimen at the free surface ahead of the drill bit, it was necessary to back the specimen with a block of wood while drilling. All cutting operations, after the initial masonry saw cuts mentioned previously, were performed using dry cutters only on the milling machine for two reasons:

- (1) Dry cutters were used to avoid changing the characteristics of the sample by lubricants.
- (2) The mill was used at all times to insure accuracy of the cuts.

The distance from the load line (center of the hole) to the point of the chevron notch,  $a$ , at the free surface was measured to the nearest 0.001 inch (0.00254cm). A cast epoxy backed Krak-gage® was mounted on one side of the specimen using cyanoacrylate. The distance from the load line to the point of the notch in the Krak-gage® was measured to the nearest 0.001 inch (0.00254cm). Electrical leads were attached to the gage and a linear variable differential transformer (LVDT) was glued to the front face of the specimen to measure displacement. Applied load was measured by a load cell on an MTS (810 Material Test System).

The static tests were conducted using the ASTM standards [5, 7] for fracture toughness in terms of the stress intensity factor and in terms of the J-integral, respectively. A correction to the displacement measurement was required because the measurement was not taken at the load line. The correction to the load line was

determined from Saxena et. al. [88, 89]. Displacement control was used for the static test and both  $J_{IC}$  and  $K_{IC}$  were determined from the same load-displacement record. The rate of loading in terms of LVDT displacement was 0.008 in/min (0.002cm/min).

Two deviations from the ASTM standards [5, 7] for fracture toughness were required. However, results which will be discussed later in the report justify the use of the subscript "Ic", indicating the critical value for plane strain toughness (Mode I). The first deviation was that the nature of the material did not allow measurement of the crack front curvature or its angle of intersection with the free surface. The chevron notch was used to initiate the crack in the center of the specimen thickness and to establish the desired crack plane, thereby minimizing the possibility of asymmetric crack growth. Therefore, the Krak-gage® which was mounted on one side of the specimen was assumed to give an accurate representation of the crack length across the width of the specimen. The second deviation from the standard was that precracking of the specimens was conducted using monotonic loading in displacement control. This would be a serious deviation for a tough metal, but is not significant for this material for a combination of reasons. First, metals require fatigue precracking to keep the crack tip sharp (i.e. to avoid creating a large plastic zone at the crack tip which is surrounded by elastic material putting the crack tip process zone in compression). Second, cement stabilized soil has a Poisson's ratio,  $\nu$ , of 0.1 to 0.15 [100], a fracture toughness near two to three orders of magnitude less than metals, and a slope of the R-curve

generally between 0.44 psi (0.3 kPa) to 1.36 psi (9.4 kPa) (essentially zero in comparison to metals). The cumulative effect of these factors points toward a small crack tip process zone and little blunting of the type seen in ductile alloys. Assuming  $\nu \approx 0.3$ , and using the data in reference [15] for reactor steel, it can be seen that the ratio of the plastic zone sizes is:

$$r_{p(\text{soil})}/r_{p(\text{reactor steel})} \approx 0.04/0.69 = 0.058$$

It must also be noted that when using the plain strain plastic zone size based on the Tresca or Mises criteria, many steels and metals have smaller zone radii than cement stabilized soil. Noting that the minimum thickness requirement of [7] is

$$25 \cdot J_{IC} / \sigma_{ys}$$

and using the values in reference [39] for Al 2014-T6 and Steel 18Ni (200), it can be easily shown that the minimum thickness required for cement stabilized soil is approximately one order of magnitude smaller than that of the two alloys. It is possible that the three dimensional plastic zone is smaller in plane strain for cement stabilized soil than for metals. It is also possible that a maximum displacement or maximum strain failure criterion may better describe the plastic zone in this cement stabilized soil. Fatigue precracking in load control was attempted but unsuccessful due to sample variability coupled with the very small load difference between no crack growth and catastrophic failure. This difficulty associated with precracking ceramic type materials has been documented [24]. Although precracking philosophy is quite varied, the consensus seems to be that high load levels are tolerable for

some materials (up to  $0.8K_{IC}$  for aluminum alloy - see Kaufman and Schilling in reference [55] pages 312-319; up to 90% of breaking load for westerly granite - see Schmidt and Lutz in reference [24] pages 166-182). No precracking is done in some cases (see the discussion of short rod testing in reference [39]). Monotonic loading to precrack in displacement control was the chosen solution to the problem in light of the process zone considerations involved and in light of existing literature.

The data were analyzed using the equations and methods defined in references [5, 7, 88, 89] and Appendix IV of this report.

### *Experimental Results*

Test Results (28 Day). The magnitude of fracture parameters is an important but secondary result of this research. Of primary interest are the applicability of the fracture mechanics approach to failure of this material and the explanation of more basic physical concepts of failure.

In Appendix V, the intergranular nature of the fracture process from the static and fatigue tests is illustrated. The preferred fracture path indicates that the "weakest link" is either in the matrix or at the bond between the matrix and the soil particles. Although there is some crack branching, microcracking appears to be confined to a very small region around the macroscale crack. The mean value for crack extension,  $\Delta a/a_0$ , prior to the peak load as measured with the Krak-gage® was less than two percent, as shown in Table 3. Since this is the extension prior to the peak load, not an

arbitrary offset, the mean crack extension statistic lends credence to a claim of linear elastic behavior.

**Table 3. Summary of initial crack extension data (28 day).**

All Specimens N=38			
Parameter	Mean	Std Dev	Skewness
$\Delta a/a_0$	0.0167	0.0132	1.122
$dJ/da$	0.5742 psi (3.959 kPa)	0.3580 psi (2.468 kPa)	0.557

Statistics on the crack extension parameter,  $\Delta a/a_0$ , are tabulated in Table 3. Statistics on the values of  $K_{IC}$  for the various cement/compaction effort combinations are shown in Table 4 in order of decreasing toughness. The parameter N in the tables is the number of samples included in the appropriate statistic. All statistics are calculated as discussed in reference [87]. The parameter  $\sigma_{IDT}$  is the indirect tensile strength of the material (see [104, 111]).

The average slope of the resistance curve for J for all the specimens is given in Table 3. Statistics for toughness in the form of the J-Integral are given in Table 4. The parameter, J, does not require linear behavior. The equation used to calculate J is

$$J = \frac{A}{B(W-a)} f(a/W) \quad (47)$$

where the parameters are as defined in reference [7] and are shown in Figure 2. The parameter A is the area under the load-displacement curve. The K and J values reported herein may be compared to the

**Table 4. Summary of results of fracture tests (28 day, monotonic loading).**

15%, Modified ( $\sigma_{IDT} \approx 186$ psi (1.283 MPa)) N=6				
Parameter	Mean	Std Dev	Units	
$K_{IC}$	209.3(230.0)	30.7(33.7)	psi/in(kPa/m)	
$J_{IC}$	0.0712(0.0125)	0.0174(0.0030)	in-lb/in <sup>2</sup> (N/mm)	
$E_{JK}$	626.3(4319.3)	155.5(1072.4)	ksi(MPa)	
$E_{west}$	597.6(4121.4)	108.5(748.3)	ksi(MPa)	
15%, Standard ( $\sigma_{IDT} \approx 145$ psi (1.0 MPa)) N=6				
Parameter	Mean	Std Dev	Units	
$K_{IC}$	149.1(163.9)	28.8(31.7)	psi/in(kPa/m)	
$J_{IC}$	0.0529(0.0093)	0.0163(0.0029)	in-lb/in <sup>2</sup> (N/mm)	
$E_{JK}$	420.3(2898.6)	59.6(411.0)	ksi(MPa)	
$E_{west}$	390.1(2690.3)	103.3(712.4)	ksi(MPa)	
10%, Modified ( $\sigma_{IDT} \approx 155$ psi (1.069 MPa)) N=8				
Parameter	Mean	Std Dev	Units	
$K_{IC}$	138.6(152.3)	22.2(24.4)	psi/in(kPa/m)	
$J_{IC}$	0.0486(0.0085)	0.0056(0.0010)	in-lb/in <sup>2</sup> (N/mm)	
$E_{JK}$	394.3(2719.3)	118.4(816.6)	ksi(MPa)	
$E_{west}$	355.6(2452.4)	95.2(656.6)	ksi(MPa)	
10%, Standard ( $\sigma_{IDT} \approx 117$ psi (0.807 MPa)) N=5				
Parameter	Mean	Std Dev	Units	
$K_{IC}$	95.8(105.3)	6.2(6.8)	psi/in(kPa/m)	
$J_{IC}$	0.0423(0.0074)	0.0067(0.0012)	in-lb/in <sup>2</sup> (N/mm)	
$E_{JK}$	216.3(1491.7)	37.7(260.0)	ksi(MPa)	
$E_{west}$	205.4(1416.6)	30.6(211.0)	ksi(MPa)	
5%, Modified ( $\sigma_{IDT} \approx 75$ psi (0.517 MPa)) N=7				
Parameter	Mean	Std Dev	Units	
$K_{IC}$	83.8(92.1)	20.7(22.7)	psi/in(kPa/m)	
$J_{IC}$	0.0313(0.0055)	0.0131(0.0023)	in-lb/in <sup>2</sup> (N/mm)	
$E_{JK}$	260.0(1793.1)	156.6(1080.0)	ksi(MPa)	
$E_{west}$	176.0(1213.8)	41.0(282.8)	ksi(MPa)	
5%, Standard ( $\sigma_{IDT} \approx 40$ psi (0.276 MPa)) N=6				
Parameter	Mean	Std Dev	Units	
$K_{IC}$	68.6(75.4)	11.6(12.7)	psi/in(kPa/m)	
$J_{IC}$	0.0303(0.0053)	0.0071(0.0012)	in-lb/in <sup>2</sup> (N/mm)	
$E_{JK}$	154.3(1064.1)	28.1(193.8)	ksi(MPa)	
$E_{west}$	142.5(982.8)	25.3(174.5)	ksi(MPa)	

values of K and G reported in [29] and [110] with the realization that equation (11) is used in the recent literature. The J and G values may be directly compared in the linearly elastic case.

In the linear elastic case,

$$K^2 = JE/(1-\nu^2) \quad (23)$$

Since measurements of both K and J were made on each specimen, a simple evaluation of the applicability of linear elastic theory may be accomplished by performing a linear regression as mentioned in equation (24). Such a regression plot is shown in Figure 11. The solid line in this figure represents equation (23). The line with long dashes represents the regression model, and the lines composed of shorter dashes represent the 95 percent confidence limits for individual predicted values. Forcing c to 1, we find  $b=0.9889$ . It is apparent that LEFM is applicable to this material.

The small difference in b from the value of 1.0 can be attributed to two possible sources: nonlinearity of the material or simply the difference in the crack extension at the point of measurement of the applicable fracture parameter. The J-integral is calculated at zero crack extension ( $\Delta a=0.0$ ), while K is measured, in this case, at 1.67% crack extension (maximum 2% in the ASTM standard). For a discussion of this concept, see reference [7 or 39].

Based on standard statistical analyses, the effects of cement content on fracture toughness were more pronounced than the effects of compactive effort. The effect of the interaction of these two variables on toughness was generally weak.

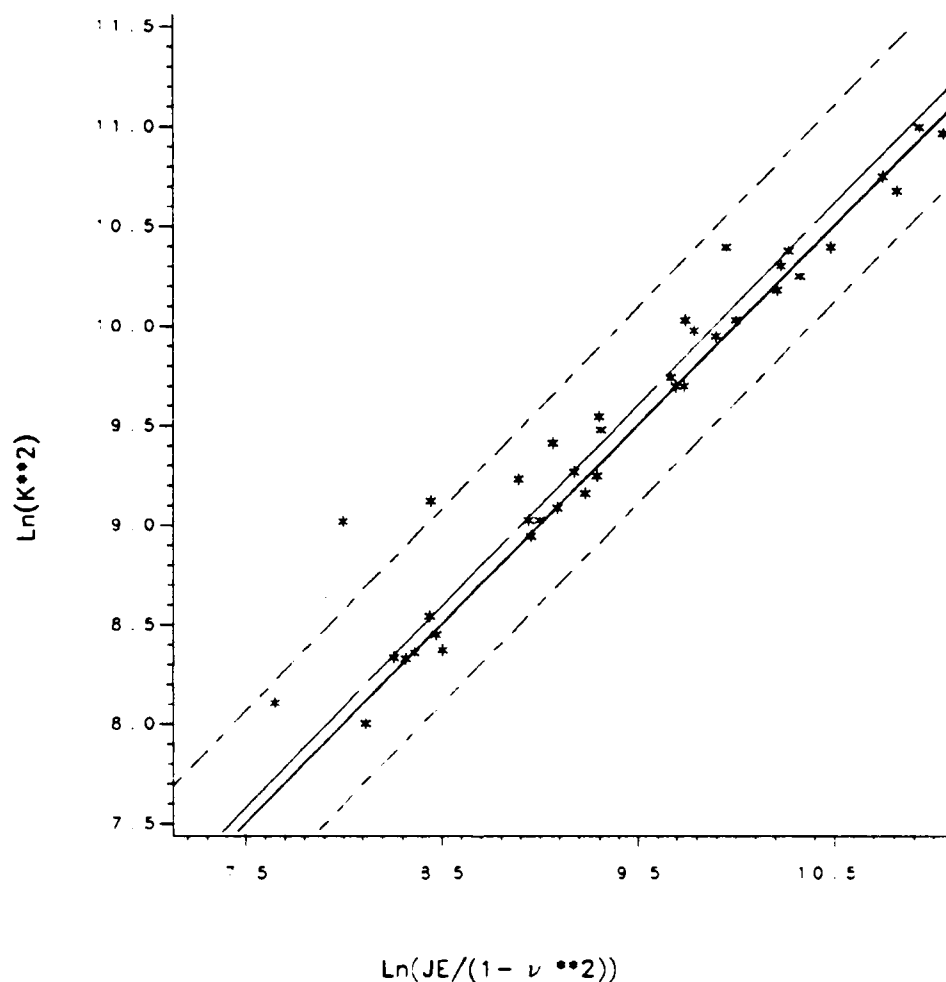


**Figure 11. Applicability of Linear Elastic Fracture Mechanics.**

It is interesting to compare the results of this study with those of George in reference [29]. As was noted earlier,  $G$  and  $J$  should be equal in the linear elastic case. Although the material studied by George was not the same as the material studied in this report, two of his soils (M30-2 and IK34) had somewhat similar densities, optimum moisture, plasticity, and clay contents. In George's work, the

cement content was 6%, the curing was apparently seven days moist cure (equivalent to zero days in the terminology of the present report), the compaction was apparently standard Proctor [1], and the specimen was a beam. Apparently, no precracking was performed in George's study, which would cause higher toughness values if this were a metal, but may not be significant for this material. Although George's paper reports  $K_C$  in units of lb/in, the equation he used indicates that this is simply a typographical error and that the reported values actually have the correct units of psi/in. The values in George's paper averaged for all notch depths are:

SOIL	E(ksi)	G(lb/in)	$K_C$ (psi/in)	$K_{IC}$ (psi/in)
IK34-6	768.6	0.0353	98.3	174.2
M30-6	302.3	0.0604	79.8	141.4

where the last column of  $K_{IC}$  values are simply the values from George's paper multiplied by  $\sqrt{\pi}$  to enable direct comparison with the values from the current study. Comparison of the IK34 soil  $G_C$  value with the 5% standard compaction soil in Table 4 and with the seven day cure (modified compaction, 10% cement) values in Table 5 show remarkable agreement. The seven day specimens were cured seven days longer than George's beams, the cement content was 4% higher, the density was higher, and the compactive effort was greater than George's which would imply that the observed higher toughness might be expected for the present material. The 5% standard material was cured 28 days longer than George's material. The slightly lower

observed value of toughness for the present material may be due simply to statistical variation, the method of precracking used in this study, or some other factor (e.g. shrinkage cracking). The value of  $K_{IC}$  is much higher for George's material than for the material used in this study. George stated that the modulus of elasticity could not be precisely determined. This lack of confidence in the value of  $E$  leads to an important conclusion. The values of  $G$  in reference [29] appear to be correct and in general agreement with the present work, but the  $K$  values should only be used with caution due to the lack of confidence in the modulus. A valuable by-product of fracture testing performed in this research is the ability to measure  $E$ ,  $J_{IC}$ , and  $K_{IC}$  independently.

In metals, a decrease in fracture toughness is often observed with an increase in yield strength. In stabilized soil, an increase in fracture toughness accompanies an increase in the indirect tensile strength. It has been shown [83] that fracture toughness in the form of the J-Integral is controlled by both the strain,  $\epsilon$ , and stress,  $\sigma$ , to fracture:

$$J \propto \int_0^{\epsilon} \sigma_{ij} d\epsilon_{ij} \quad (48)$$

In addition, equation (47) is valid for the compact tension specimen (7). It was observed that the  $J$  value for the area under the load-displacement record,  $A$ , corresponding to the point of the maximum load was approximately equal to the final value of  $J_{IC}$ . If load is considered to be related to stress and displacement related to strain (see [55, 60, 83]), the right side of equation (47) can be broken

into two multiplicative parts: the displacement at maximum load,  $\delta_{mxp}$ , and a constant (involving the original crack length, specimen width, and specimen thickness) times the maximum load,  $P_{mxf}$ . A plot of  $P_{mxf}$  versus  $\delta_{mxp}$  is shown in Figure 12.

The slope of the linear regression is  $-17478 \text{ pci}$  ( $-4744 \text{ N/cc}$ ). This slope suggests that the source of changes in toughness may be in the stress to failure (the integrand) rather than in the strain to failure (the limits of integration in equation 12). Thus, the stress-strain diagram changes with toughness for this material may be as shown in Figure 13.

Of course, the steep negative slope of the linear regression mentioned above is related to the slope of the failure envelope curve (dashed line in Figure 13). The stabilized soil used is expected to exhibit the behavior shown in part (a) of Figure 13. That is, the area under the stress-strain curve (which is related to toughness) for the 5% cement content would be less than the area under the curve for 15% cement content primarily because the lower failure stress is accompanied by a relatively small change in the failure strain. This trend is supported by test results on similar materials which apparently actually exhibit simultaneous increases in tensile strength and modulus [35]. For some materials (e.g. ductile alloys versus high yield strength steel), a drop in the yield strength would be accompanied by an increase in toughness due to the large increase in strain to failure as shown in part (b) of Figure 13.

It has been shown that the cement content greatly affects the toughness of this material and that it apparently accomplishes these

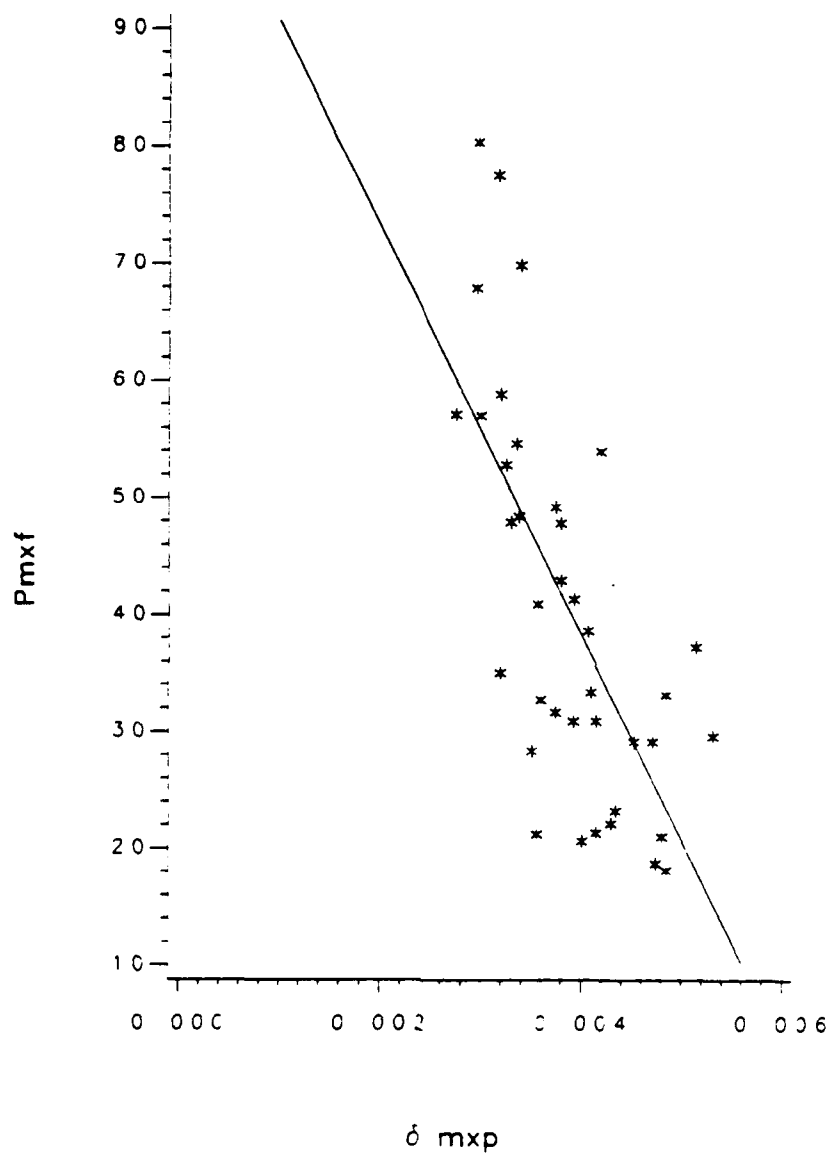


Figure 12. Source of toughness.

changes by increasing the load to failure without substantially changing the strain to failure. Therefore, in terms of a force representation of the Lennard-Jones potential, it is postulated that

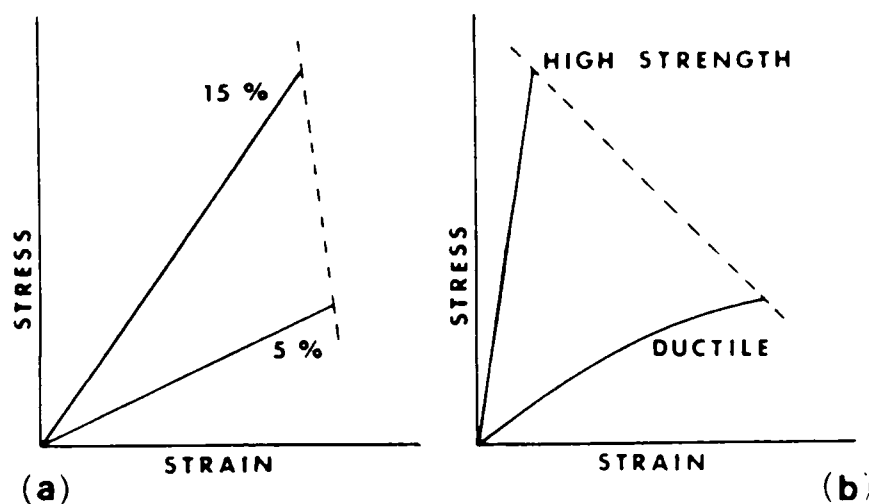


Figure 13. Possible stress-strain behaviors.

an ideal curve (the solid line in Figure 14) exists for the closest (theoretically) possible particle spacing ( $S_T$ ). The curve for a selected compaction energy may be as shown by the dashed line ( $S_1$ ). Increasing compaction tends to move the initial spacing from  $S_1$  toward  $S_T$  allowing the material to more closely approach a theoretical maximum cohesive strength.

Curing Date Study. The same tests were performed on modified Proctor [2] samples with a single stabilizer content (10%) which had been cured for a shorter period of time than that indicated in Table 2. The results are shown in Table 5.

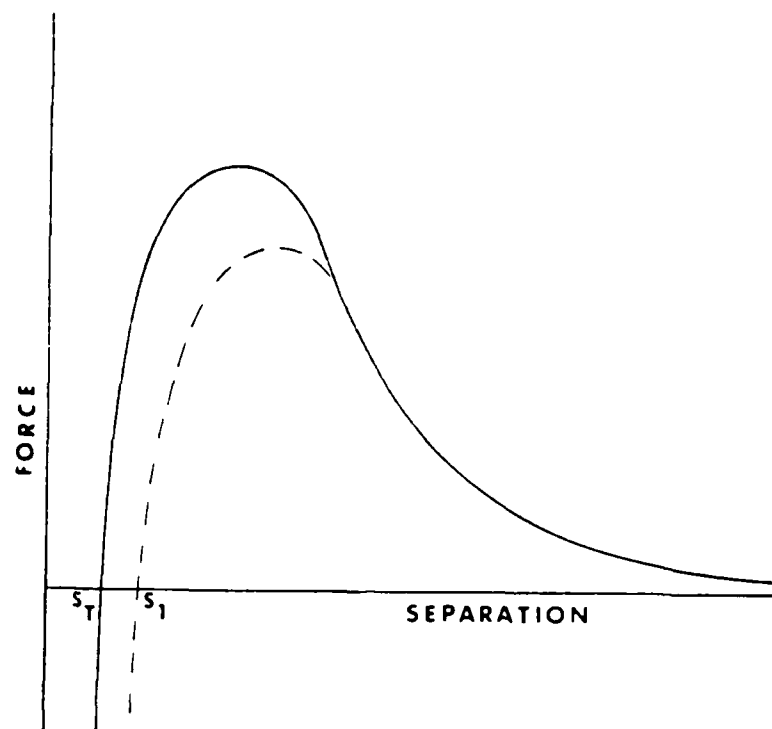


Figure 14. Visualization of changes in a Lennard-Jones type potential.

Statistical Inferences. It should be noted that the method of compaction was slightly different for the curing date study than for the two factor study. Table 4 documents the results obtained when a manually operated rammer was used by a single operator. Table 5 gives the results for specimens molded using an automatic rammer operated by a single operator. The operators of the two different types of rammers were not the same individual.

In Table 4, two values of modulus are presented.  $E_{JK}$  was back calculated from equation (23), while  $E_{west}$  was back calculated from

Table 5. Summary of results of fracture tests (curing study, monotonic loading).

7 Day ( $\sigma_{IDT} \approx 128$ psi (0.883 MPa)) N=5				
Parameter	Mean	Std Dev	Units	
$K_{IC}$	88.0(96.7)	13.0(14.3)	psi/in(kPa/m)	
$J_{IC}$	0.0375(0.0066)	0.0072(0.0013)	in-lb/in <sup>2</sup> (N/mm)	
$E_{west}$	206.1(1421.1)	34.2(235.8)	ksi(MPa)	
14 Day ( $\sigma_{IDT} \approx 149$ psi (1.027 MPa)) N=5				
Parameter	Mean	Std Dev	Units	
$K_{IC}$	126.2(138.7)	37.5(41.2)	psi/in(kPa/m)	
$J_{IC}$	0.0527(0.0092)	0.0136(0.0024)	in-lb/in <sup>2</sup> (N/mm)	
$E_{west}$	270.1(1862.3)	99.9(688.8)	ksi(MPa)	
28 Day ( $\sigma_{IDT} \approx 155$ psi (1.069 MPa)) N=3				
Parameter	Mean	Std Dev	Units	
$K_{IC}$	152.4(167.5)	79.2(87.0)	psi/in(kPa/m)	
$J_{IC}$	0.0657(0.0115)	0.0301(0.0053)	in-lb/in <sup>2</sup> (N/mm)	
$E_{west}$	325.5(2244.3)	204.0(1406.6)	ksi(MPa)	

the equations in reference [88].  $E_{west}$  was used for generating Figure 11 because it could be calculated for each specimen without using any information other than load, displacement, geometry, and crack length.

Pairwise comparisons of the means of  $K_{IC}$  using Fisher's least significant difference (LSD) method were accomplished. The value of mean square error (MSE) from the analysis of variance (ANOVA) was 477.14. The model used included percent cement, compaction effort, an interaction between the two, and the location of the specimen (top, center, or bottom) in the original large cylinder which was nested within the compaction/cement. The Shapiro-Wilk statistic indicated that the assumption of normal population was satisfied.

The Hartley test for equal variances showed that the variances were not equal due to the low variance in the 10% modified specimens. The LSD analysis showed that the standard and modified compaction samples at 5% cement content were not significantly different. The 5% modified and 10% standard were not different, and the 10% modified was not different from the 15% standard specimens. All other pairwise comparisons showed that the means of  $K_{IC}$  were significantly different. The same pairwise comparison procedure was performed on the results ( $MSE=915.83$ ) of the curing study. The model used included day, location within day. The 7 day  $K_{IC}$  was not significantly different from the 14 day. The 14 day was not significantly different from the 28 day. However, the 7 day was significantly different from the 28 day.

The value of  $R^2$  for the regression in Figure 11, as redefined by SAS [87] for the case where the intercept is forced to zero was 0.9994. The slope of the line was 0.9889 for the model

$$\ln[JE/(1-\nu^2)] = \beta_1 \ln K^2$$

Testing the null hypothesis that  $\beta_1=1.0$  against the alternative that  $\beta_1>1.0$  using the t-test does not result in rejection of the null hypothesis. If the alternative  $\beta_1\neq 1.0$  is used, the probability of wrongly rejecting the null hypothesis (Type I error rate) would have to be reduced to approximately 0.01 in order for the same conclusion to be reached (i.e. do not reject the null hypothesis). Since it has been shown that  $\beta_1$  may be expected to be less than 1.0 simply due to the difference in how much crack extension occurs prior to the

measurement of  $J_{IC}$  and  $K_{IC}$ , the author feels justified in accepting the smaller Type I error rate and declaring  $\beta_1=1.0$ , indicating statistical verification of linear elastic behavior.

As noted earlier in equation (33),  $\partial J/\partial x_0$  varies inversely with  $x_0$  and  $\partial J/\partial \sigma_{max}$  is constant. It was also noted earlier that compaction effort is probably associated with  $x_0$  and cement content may control  $\sigma_{max}$ . Therefore, a regression equation relating  $J$  to cement content and compaction effort might take the form:

$$J = \beta_0 + \beta_1(CMT \cdot \ln(1/CE)) \quad (49)$$

where the  $\beta$ 's are regression parameter estimates, CMT is the percent cement content (i.e. 10% cement  $\rightarrow$  CMT=10), and  $\ln(1/CE)$ =natural logarithm of the inverse of the compaction effort in lb-in/in<sup>3</sup>.

The rationale for the form of the model shown in equation (49) begins with the desire for a simple linear model which would model toughness satisfactorily and would yield first partial derivatives which would be similar to equations (33). The independent variable, CMT, was assumed directly proportional to  $\sigma_{max}$  and could have values ranging from zero to infinity but with a practical range from zero to some value less than 100 percent cement content by weight of the soil. The variable CE (nominal compaction effort) was assumed inversely proportional to  $x_0$ . In order to arrive at the expected form of the equation and its first partial derivatives, CE should be limited to a range of between one and infinity. That is, at zero cement content,  $J$  is not necessarily zero; at zero CE,  $J$  is not necessarily undefined (or infinite); at infinite CMT,  $J$  is not

necessarily infinite; and at infinite CE, J is not necessarily undefined. In more concise terminology; it is deduced that physical, mathematical, and economical factors limit the range of the independent variables to:

$$0 < CMT < \infty$$

$$1 < CE < \infty$$

Note that the end points of the acceptable range are not included in the range. A subset of the available range near the lower boundary of the range is the more realistic scenario for the variables and will result in the proper combinations of signs for the model and its first partial derivatives. At least for the range of values occurring in this study, the simple linear model discussed above is quite satisfactory.

The results for various regression models used to model toughness are shown in Tables 6 and 7. The column labelled "t-TEST" indicates which of the model parameters were found to be different from zero in an individual t-test. The column labelled "SSR" is the residual sum of squares.

Several inferences can be made concerning the regressions presented. First,  $R^2$  is higher for the models which use  $K_{IC}$  as the dependent variable. The author suspects that the manual analysis of the area under the load-displacement curve necessary for the J integral but not for  $K_{IC}$  may have been one source of variability. Automated data acquisition may improve the  $R^2$  for the models involving  $J_{IC}$ . Secondly, it can be seen that in all models (which use the same independent variables) involving cement directly, the

Table 6. Regression analyses using  $K_{IC}$  as the dependent variable.

MODEL	F VALUE	MSE	SSR	$R^2$	t-TEST
$K_{IC} = -3056.466 + 10.663CMT + 27.889DEN + 6.84CE - 0.062SYNDC$					
42.8	482.4	15917.8	0.84		CMT
$K_{IC} = -755.993 + 8.756CMT + 7.080DEN - 0.875 \cdot 10^{-2}CE$					
57.8	474.8	16143.1	0.84		INTERCEPT, CMT, DEN
$K_{IC} = -7.830 + 10.246CMT + 0.107 \cdot 10^{-2}SYNDC$					
71.5	553.4	19369.4	0.80		CMT, SYNDC
$K_{IC} = -716.308 + 8.844CMT + 6.699DEN$					
89.2	461.6	16155.8	0.84		INTERCEPT, CMT, DEN
$K_{IC} = -9.253 + 10.359CMT + 0.124CE$					
70.0	563.2	19713.6	0.80		CMT, CE
$K_{IC} = 16.890 + 1.091LCS$					
124.6	613.5	22085.6	0.78		LCS
$K_{IC} = 23.112 + 2.177LCD$					
74.8	889.3	32015.6	0.68		LCD
$K_{IC} = 17.741 - 2.049CLIC$					
166.7	486.0	17496.7	0.82		CLIC
$K_{IC} = 26.906 + 24.649SDAY$					
4.6	1751.5	19266.6	0.29		--
$K_{Opt} = 291.6 \sin(1.303M_1)$					
N/A	1025.3	N/A	N/A		N/A

Table 7. Regression analyses using  $J_{IC}$  as the dependent variable.

MODEL	F VALUE	MSE	SSR	$R^2$	t-TEST
$J_{IC}=0.400+0.202*10^{-2}CMT-0.342*10^{-2}DEN-0.199*10^{-2}CE+0.178*10^{-4}SYNDC$	13.1	$0.137*10^{-3}$	$0.453*10^{-2}$	0.61	--
$J_{IC}=-0.262+0.256*10^{-2}CMT+0.256*10^{-2}DEN-0.213*10^{-4}CE$	17.9	$0.134*10^{-3}$	$0.454*10^{-2}$	0.61	CMT
$J_{IC}=0.832*10^{-2}+0.312*10^{-2}CMT+0.234*10^{-6}SYNDC$	23.6	$0.142*10^{-3}$	$0.498*10^{-2}$	0.57	CMT, SYNDC
$J_{IC}=-0.166+0.278*10^{-2}CMT+0.164*10^{-2}DEN$	26.8	$0.132*10^{-3}$	$0.462*10^{-2}$	0.61	INTERCEPT, CMT, DEN
$J_{IC}=0.808*10^{-2}+0.314*10^{-2}CMT+0.267*10^{-4}CE$	23.4	$0.143*10^{-3}$	$0.501*10^{-2}$	0.57	CMT, CE
$J_{IC}=0.137*10^{-1}+0.326*10^{-3}LCS$	50.5	$0.135*10^{-3}$	$0.487*10^{-2}$	0.58	INTERCEPT, LCS
$J_{IC}=0.151*10^{-1}+0.622*10^{-3}LCD$	40.0	$0.154*10^{-3}$	$0.554*10^{-2}$	0.53	INTERCEPT, LCD
$J_{IC}=0.144*10^{-1}-0.604*10^{-3}CLIC$	54.4	$0.129*10^{-3}$	$0.466*10^{-2}$	0.60	INTERCEPT, CLIC
$J_{IC}=0.104*10^{-1}+0.107*10^{-1}SDAY$	6.0	$0.254*10^{-3}$	$0.280*10^{-2}$	0.35	SDAY

---

The parameters in Tables 6 and 7 have the following meanings:

MEANINGS	RANGE OF VALUES
CMT=cement content (%)	(5-15)
DEN=density (lb/in <sup>3</sup> )	(108.9-118.1)
CE=nominal compaction energy (lb-in/in <sup>3</sup> )	(86.1-393.1)
SYNDC=DEN*CE	
LCS=CMT*ln(SYNDC)	
LCD=CMT*ln(DEN)	
CLC=CMT*ln(CE)	
CLIC=CMT*ln(1/CE)	
SDAY= $\sqrt{\text{Day}}$	( $\sqrt{7}$ - $\sqrt{28}$ )
M <sub>1</sub> =molding moisture content (%)	(11.79-16.8)

---

parameter estimates for that variable are generally of the same magnitude and are very often larger than any other estimates (with the exception of the intercept). This indicates a consistent and dominant effect of cement content on toughness. In general, density and/or compaction energy have a secondary effect which is occasionally almost as significant as the effect of the cement. It is significant that the expected form of the model from equations (33) worked well in this case yielding an  $R^2$  within about 2% of the maximum  $R^2$  of any of the models and obtained this  $R^2$  with fewer parameter estimates. Plots of the regression models (equation (49) and an equation of the same form but with K replacing J) and residual error plots are included in Figures 15, 16, 17, and 18. The abscissa on the residual plots is the predicted value of  $K_{IC}$  or  $J_{IC}$ , as applicable.

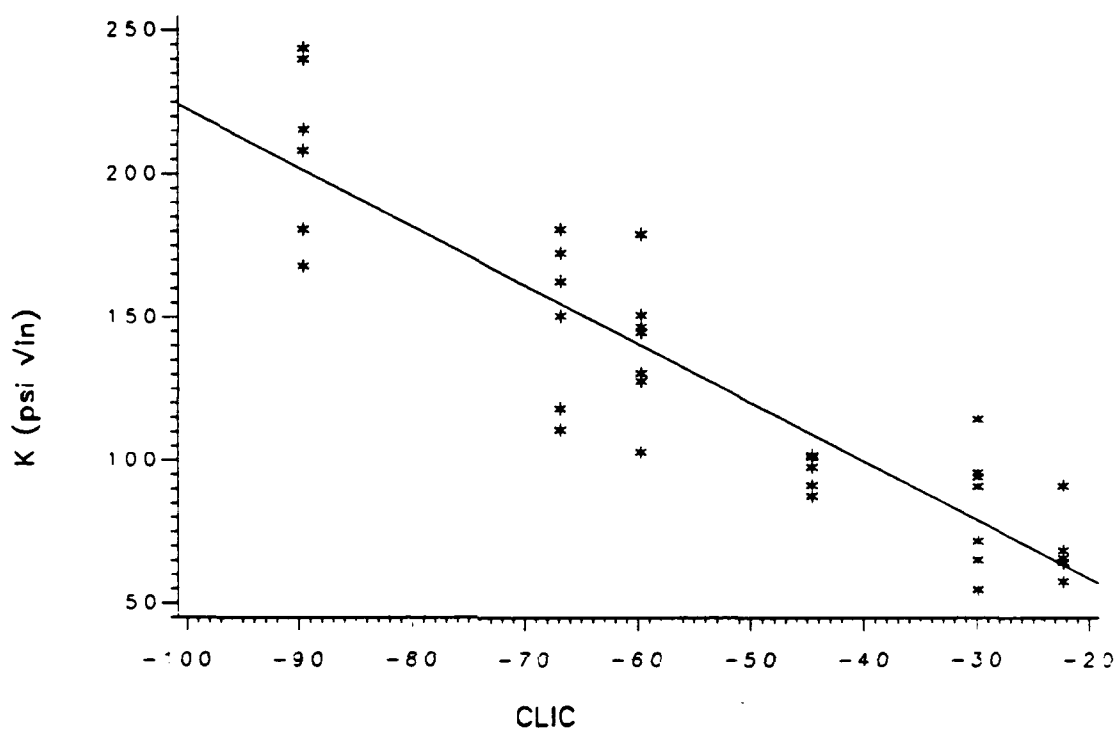


Figure 15. Experimental results using  $K_{IC}$  in equation (49).

The models pertaining to curing date studies and optimum moisture studies are felt by the author to be unacceptable for design use due to the poor statistics caused by lack of sufficient data, variability, or incorrect models. Further research into possible forms of the models and more experimentation is in order for these studies. The models are presented only for completeness.

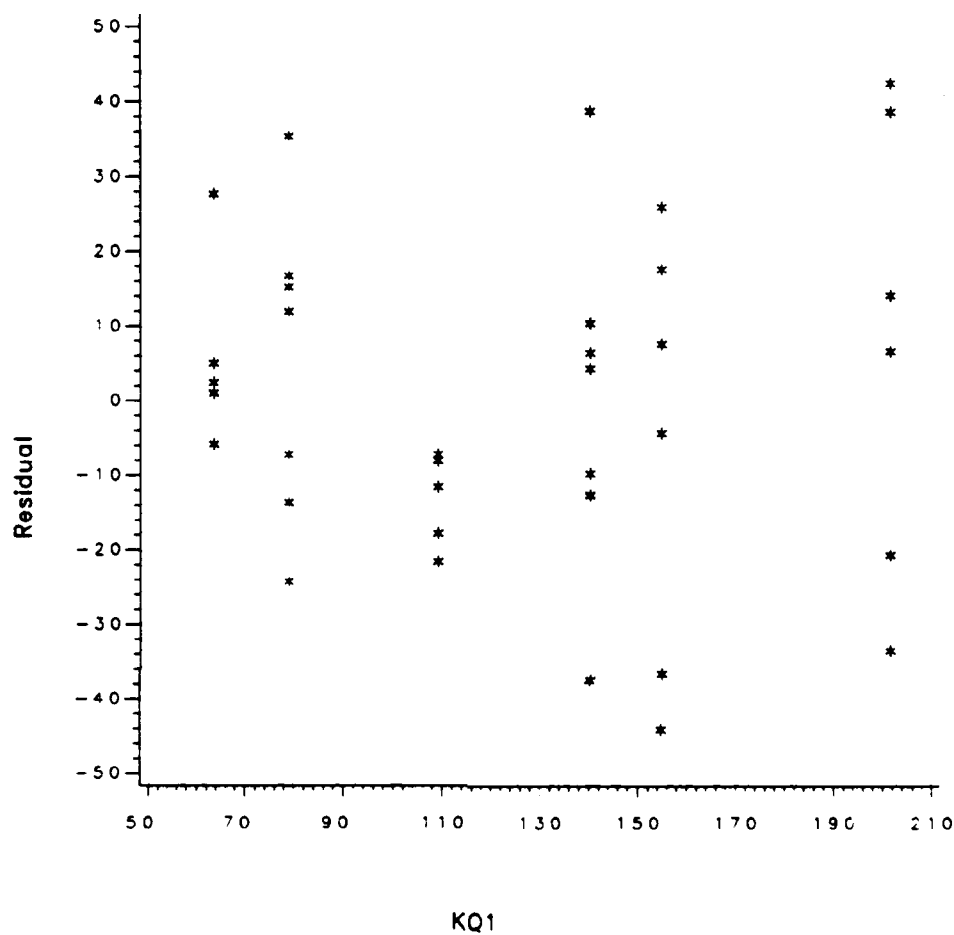


Figure 16. Residual error plot for the model of Figure (15)

### Conclusions

The portland cement stabilized fine grained soil used in this study behaves according to LEFM theory. Plane strain prevailed in the specimens as illustrated by the shallow slope of the R-curve ( $dJ/da$ ) and by the large value of specimen thickness (in relation to

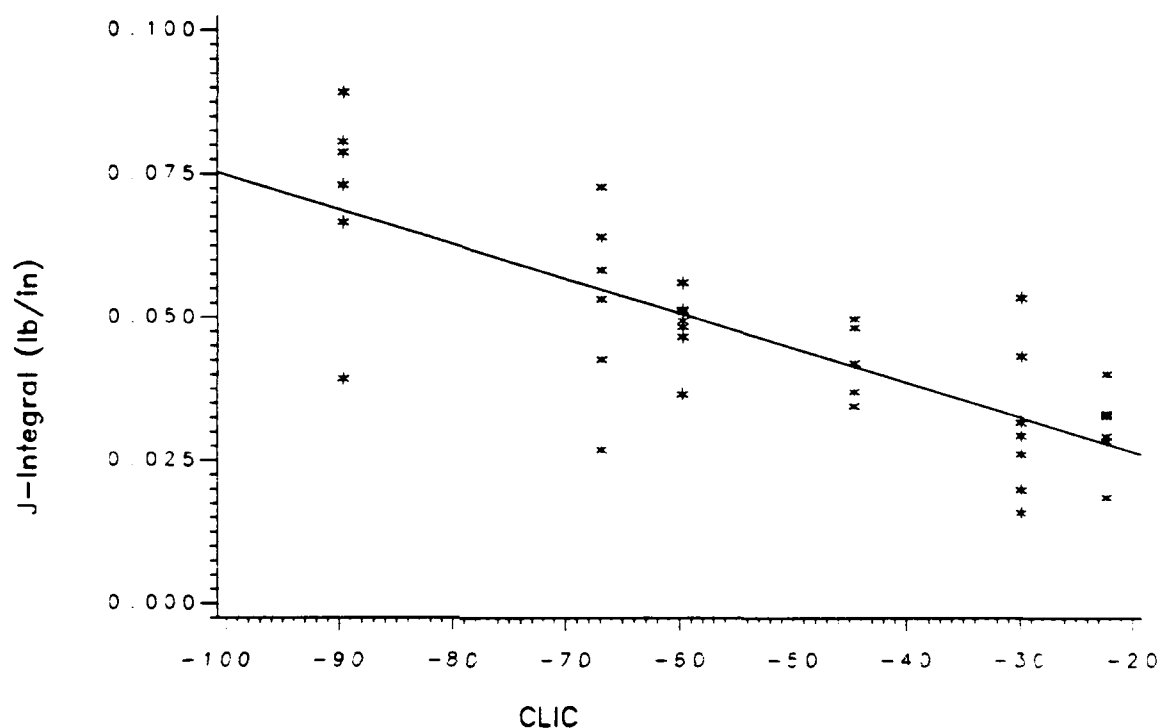


Figure 17. Experimental results using  $J_{IC}$  in equation (49).

that required by reference [7]). A strain or displacement failure criterion is most appropriate for this material as is evident in Figure 12 where it is noted that the displacement at failure (actually at peak load) is approximately constant. Cement content apparently controls the magnitude of the peak attractive force, and compaction controls the initial particle spacing in a Lennard-Jones type model. A regression model shows the relative influence of the compositional factors of interest on the toughness of the finished materials. It is hoped that the model will prove useful not only for

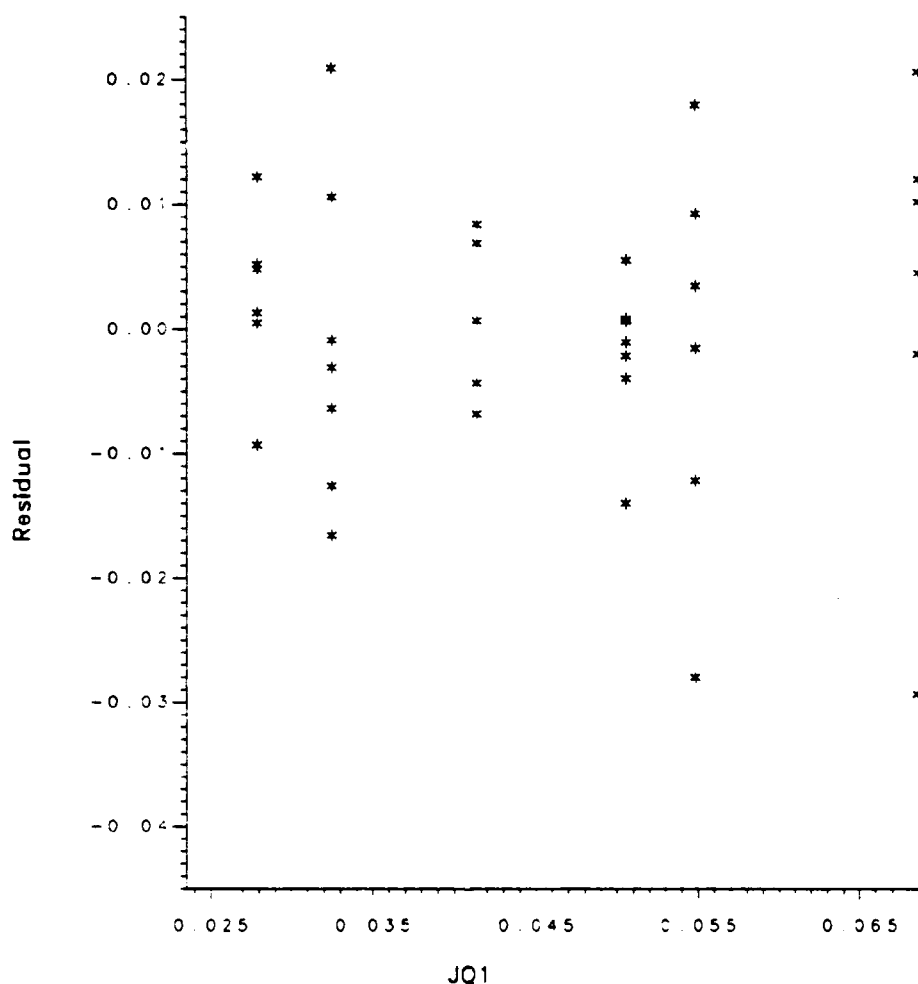
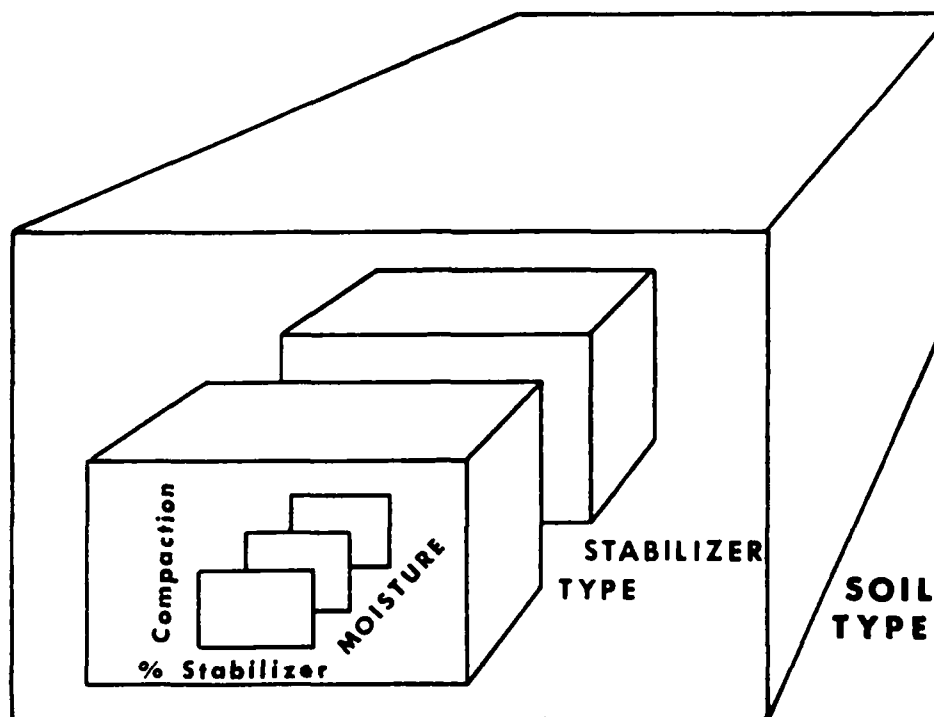


Figure 18. Residual error plot for the model of Figure (17)

foundation materials but also for other cementitious composites (e.g. autoclaved concrete, compressed fiber-reinforced composites, ceramics).

Future Work. A relatively comprehensive factorial analysis suggested for future studies is depicted in Figure 19. Several combinations of compactive effort and stabilizer contents



**Figure 19. Factorial Analysis for Future Studies**

could be studied for each stabilizer type of interest, at several different molding moisture contents for each combination. Many levels of these factors would have to be used in order to fully investigate the impact of equations (33). This process could be repeated for different classes of soils which have different reactivity, texture, gradation, etc. to optimize the stabilization process. Of course, other studies such as the curing date study could also be placed in the experimentation process. One study which may prove valuable is a study of how thermal gradient induced

stresses might affect failure. If the thermal gradient is known, and the fracture toughness is known, the stress field caused by a wheel load might be superimposed on the thermally generated stress field to calculate variations in damage to the stabilized layer due to applications of load at different times of the year or day.

### CHAPTER III: CRACK GROWTH DURING CYCLIC LOADING

#### *Literature Review and Theory*

It has been experimentally observed that crack growth occurs at very low loads when many engineering materials are loaded in a cyclic fashion. Paris [74] described this behavior by modeling the crack growth per cycle as a function of the change in stress intensity factor during each cycle:

$$da/dN = A\Delta K^n \quad (50)$$

This model is only applicable for the region of stable crack growth labeled Region II in Figure 20. Region I is an area in which crack growth essentially does not occur while Region III illustrates the region of unstable crack propagation.

It should be noted here that this behavior is most often studied using metals. There is a tendency in the literature to compare materials by comparing exponents of the Paris equation (e.g. 85). Although the exponent may be useful for comparing some materials in that it may indicate how sensitive crack growth is to differences in  $\Delta K$ , there existed early evidence that the exponent may not be invariant. Miller [65] found exponents which varied by a factor of two. It should be noted that Miller precracked the specimens prior to heat treatment and the results therefore are contingent on the adherence to strict procedures for the treatment. In the same paper, Miller claims that the exponent appears to be inversely related to the material constant  $K_{IC}$ . On the other hand, Hertzberg [39] claims

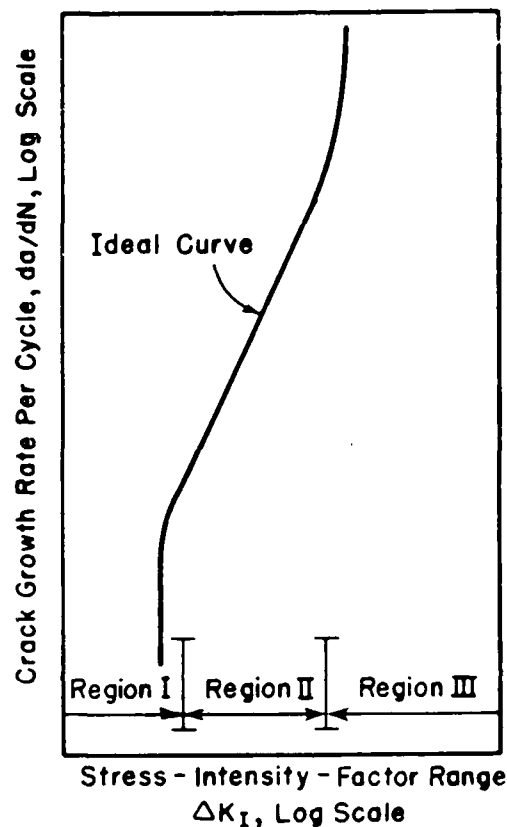


Figure 20. Schematic of the regions of crack growth behavior (redrawn from [85])

that fatigue crack propagation is not related to monotonic properties. Still another approach is offered by Schapery [91, 92, 93] where it can be seen that  $n$  is inversely proportional to the exponent of time in a creep compliance model. Obviously, some controversy exists as to whether or not the exponent in the equation (50) is a material constant and as to whether or not fatigue behavior is related to monotonic loading behavior. It will be shown

later in this report that, for the tests conducted on this material, a relationship exists between monotonic test results and fatigue testing. In addition, it was experimentally observed that  $n$  was apparently not constant, for which observation a discussion of the role of variability and regression methods is included. It has been shown that material variability is not the only source of variability. The type of analysis used is also a source of variability ( $\approx$  a factor of 3 on  $da/dN$  as shown in reference [19]). Two papers which document the existence of variability in fatigue research are found in references [19 and 107]. Reference [107] showed that the first forward difference (or secant) method and parabolic curve fitting procedures introduced less bias but more scatter than the incremental polynomial method. In the present research, the same trend for scatter (as evidenced by changes in  $R^2$ ) was observed from a modified secant method versus a total (quadratic) polynomial method. However, the changes in the exponent of equation (50) were much greater than and of opposite trend to the changes documented in reference [107]. Residual error plots confirmed the existence of systematic lack of fit for which a physical explanation is given later in this paper.

Two other methods of describing fatigue crack growth which are related to equation (50) are mentioned here for completeness. These models are found in references [23, and 73]. The Forman model [23] is of the form:

$$da/dN = \frac{c\Delta K^n}{(1-K_{min}/K_{max})K_{IC}-\Delta K} \quad (51)$$

where  $K_{min}$  and  $K_{max}$  correspond to the minimum and maximum values of  $K$  in a single cycle. It is easily seen that this model presumeably allows extension of the model into Region III of Figure 20. Owen, et. al. [73] has used a nondimensional form of equation (51) for the case when  $K_{min}=0$  (or the case  $K_{max} \gg K_{min}$ ). The Forman approach was applied to this study but was eliminated from presentation due to the very poor  $R^2$  values from the regression analyses. Owen's approach was not used in this study.

Therefore, equation (50) was the general form of the model used and presented in this study. In addition, a method of calculating the number of cycles to failure is presented which makes use of monotonic loading behavior. Kim [56] has used the results of this study to relate his tensile creep study to fatigue by means of Schapery's theory.

The topic of random spectral cyclic loading history is addressed in Chang et. al. [18]. The basic conclusion seems to be that overloads reduce subsequent crack growth while compressive loads tend to accelerate (or to decrease the tensile overload effect on) crack growth. This phenomenon has been explained in basically the same way by several individuals [14, 39, 57). A tensile overload causes a plastic deformation (and blunting of the crack tip) but the material outside the zone is elastic. Therefore, when the overload is released, the elastic material puts a portion of the plastic zone into compression resulting in reduced crack growth rate. On the

other hand, an applied compressive stress, in effect, resharps the crack tip and leads to acceleration of the crack growth. A low toughness material with a very small plastic zone, or a process zone made only of microcracks, would not be expected to exhibit this phenomenon to the extent observed in tough materials because of the lack of residual strains at zero load (i.e. all elastic energy might be released by microcracking).

#### *New Developments*

As will be discussed in future sections, the existence of positive serial correlation (or systematic lack of fit) between the succeeding values of the independent variable in conventional regression models for  $a$  versus  $N$ ,  $N$  versus  $a$ , and  $da/dN$  versus  $\Delta K$  was verified by residual plots and the Durbin-Watson test statistic. Some simple methods of interpreting results in spite of the correlation were employed. More sophisticated time series analyses [87] may be necessary in some cases.

A new technique was developed for prediction of the number of cycles to failure using the monotonic test results. This technique is very simplistic and empirical in nature. A more rigorous method for a slightly different, but nonetheless similar, problem is often used in studying ceramics and can be found in references [130, 64].

It was assumed that the crack growth rate would be approximately constant at the same percentage of  $K_{IC}$  in both the monotonic and cyclic loading case. That is, the change in crack length with the change in load at  $0.75K_{IC}$  in the monotonic test was assumed to be

equal to the change at  $\Delta K=0.75K_c$  in the cyclic test. Therefore a function which related  $a$  to  $P$  in the monotonic test was desired. The monotonic test was conducted in displacement control while the fatigue test was conducted in load control. Load control is often the better approximation to actual runway loading conditions, but it has been shown (see 15) that the critical values of fracture toughness parameters are essentially the same regardless of the method of control of the test (e.g. load or displacement control). However, the method of loading is important when considering how  $J$ , for example, varies with crack extension. In displacement control, crack extension causes a load drop with a consequent drop in  $J$ . However, in load control, crack extension is accompanied by an increase in  $J$  which causes catastrophic failure. Therefore, the function which related  $a$  to  $P$  was chosen so that its slope would be zero at  $P=0$  and infinite at  $P=P_{\max}$ . The function chosen was of the form

$$a = \beta_0 + \beta_1 \left[ \cos\left(\frac{\pi P}{2P_{\max}}\right) \right]^{-1/2} \quad (52)$$

It can be seen that

$$\left. \frac{da}{dP} \right|_{P=0} = \frac{\pi\beta_1}{4P_{\max}} \left[ \cos\left(\frac{\pi P}{2P_{\max}}\right) \right]^{-3/2} \left[ \sin\left(\frac{\pi P}{2P_{\max}}\right) \right] = 0$$

and

$$\left. \frac{da}{dP} \right|_{P=P_{\max}} = \infty$$

The value of  $P_{\max}$  is the maximum load reached during the displacement controlled monotonic test while  $\beta_1$  is a regression constant. The SAS

program ("STATFAT") which does the regression is included in Appendix IV. Once the coefficient  $\beta_1$  is obtained, the number of cycles to failure is calculated by a FORTRAN program ("NTOF"). NTOF essentially allows the crack to grow in cyclic loading by an amount the crack grew during monotonic loading between corresponding percentages of  $K_{IC}$  and  $\Delta K_{IC}$ . That is, if the crack grew by the amount, say  $\Delta a_1$ , between zero and  $0.7K_{IC}$  in the static test, it was allowed to grow the same amount between zero and  $0.7\Delta K_{IC}$  during any single cycle in which the combination of load and crack length reached  $0.7\Delta K_{IC}$ . The cyclic test was conducted so that  $K_{min} \approx 0$  ( $K_{max} \gg K_{min}$ ). However, a very slight load ( $P < 1$  lb (453.6 gm)) was present at  $K_{min}$  due to the need to keep the testing machine from "bottoming out" on each cycle.  $\Delta K_{IC}$  was the last value of  $K_{max}$  observed at fatigue failure and was used in the development of this approach because  $K_{IC}$  and  $\Delta K_{IC}$  were close to, but not exactly equal to each other in many cases. For the method to be useful,  $K_{IC}$  would have to be used in practice (instead of  $\Delta K_{IC}$ ). A plot of  $\Delta K_{IC} = K_{max}$  versus  $K_{IC}$  is included for comparison of the values of  $K$  in the monotonic and cyclic loading cases. In Figure 21, the solid line is the line  $K_q = K_{IC}$ . The parameter  $K_q$  is one of two values of  $K$ . The short dashed linear regression line with asterisks as symbols is a representation of  $K_{max}$  versus  $K_{IC}$ . The regression line with alternating long and short dashes and the circled plus symbols presents the value of  $K$  from the static test using the value of crack length at maximum load (instead of the crack length at the beginning of monotonic loading in the static test,  $a_0$ ) versus  $K_{IC}$ .

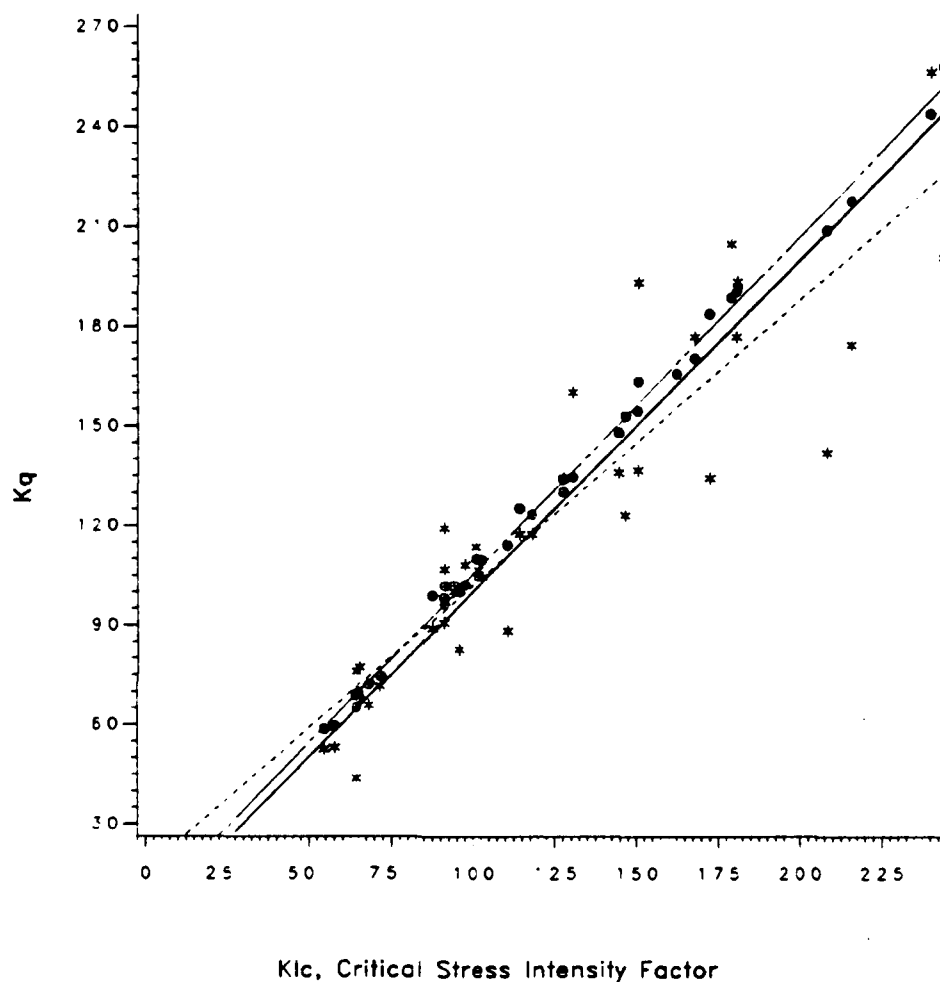


Figure 21. Comparison of  $K_{IC}$  with  $K_{max}$  at fatigue failure.

Program NTOF uses the peak load in each cycle (i.e. the loading function must be known),  $\Delta K_{IC}$ , and the crack length at the start of the cycle to calculate two parameters: the value of  $P$  which would result in  $\Delta K_{IC}$  at the current value of  $a$  (function "PKA" in the program), and the growth of the crack which would occur during loading to the percentage of  $\Delta K_{IC}$  due to the magnitude of the actual

applied load. The growth in the cycle was added to the crack length which existed at the start of the cycle and this new crack length was used for the starting crack length for the next cycle. The crack growth was evaluated as follows:

$$\int_{a_0}^{a_1} da = \frac{\pi \beta_1}{4 P_{\max}} \int_{P_0}^{P_1} \left[ \cos\left(\frac{\pi P}{2 P_{\max}}\right) \right]^{-3/2} \left[ \sin\left(\frac{\pi P}{2 P_{\max}}\right) \right] dP$$

$$= a_0 + \beta_1 \left[ \left( \cos\left(\frac{\pi P_1}{2 P_{\max}}\right) \right)^{-1/2} - \left( \cos\left(\frac{\pi P_0}{2 P_{\max}}\right) \right)^{-1/2} \right] \quad (53)$$

which is evaluated in function "PHINT" of program NTOF.

#### *Experimental Procedure*

The cyclic testing was accomplished on the same specimen after the monotonic test had been completed. The basic procedure used is presented in references [6 and 25]. Unless otherwise noted in the text, all results are from tests conducted in load control using a positive offset sine wave ( $P_{\min} \approx 0$ ) with a period of one cycle per second and an amplitude determined as a percentage of the load required to give  $K_{IC}$  at the starting crack length. The crack length was continuously monitored by the Krak-gage® and plotted on a time base strip chart recorder. The time base was converted to cycles by using the period of the waveform. The amplitude of the waveform was periodically sampled to insure that only small variations in amplitude and/or drift of  $P_{\min}$  occurred during the test. The test was allowed to run until complete failure of the specimen occurred (with the exception of a few samples used for SEM pictures and display purposes which are not included in the numerical results given here).

Data Analysis. The ideal crack length versus cycle number curve is shown in Figure 22(a), while a typical curve for the material used in this study is shown in part (b) of the same figure.

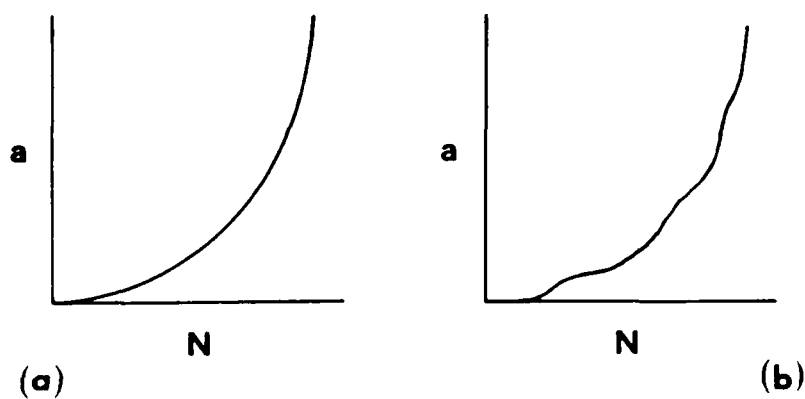


Figure 22. Schematic of crack length versus cycle number. (a) Ideal, (b) Soil cement.

It is obvious that any smooth, monotonically increasing curve fitted to the data will result in a systematic lack of fit or positive serial correlation. It is, of course, possible that the  $a$  versus  $N$  curve has the appearance shown in the figure simply because of small cyclic fluctuations in the base line of the waveform which generated the cyclic load. The possibility of base line fluctuations was

essentially ruled out by observing that the fluctuations in maximum and minimum voltages with time appeared to be random and not related to crack length. Nevertheless, since the methods of determining  $da/dN$  suggested in reference [6] are not compulsory, the curve fits were conducted in two ways with interesting results. The SAS program which does the curve fitting is documented in Appendix IV under the name "FATIGUE". The first method of fitting the  $a$  versus  $N$  curve was a quadratic fit using all the data and crack length as the independent variable in an attempt to model the expected increase in curvature near failure. Then,  $da/dN$  was calculated by taking the derivative of the quadratic formula.  $R^2$  was typically acceptable ( $\approx 0.9$ ) using this method of curve fitting. However, residual plots indicated positive serial correlation. The second method was similar to the first difference (secant) method described in reference [6]. The difference method used for this report used a three point running average technique:

$$(da/dN)_i = (1/2) \left[ \left( \frac{a_i - a_{i-1}}{N_i - N_{i-1}} \right) + \left( \frac{a_{i+1} - a_i}{N_{i+1} - N_i} \right) \right]$$

The curve fit for equation (50) was then performed using

$$\log_{10}(da/dN)_i = \log_{10}A + n \log_{10}(\Delta K)_i$$

where the estimates were  $\beta_0 = \log_{10}A$ ,  $\beta_1 = n$ . Although the differencing technique often eliminated patterns in the residual plots, which were only available from the regression equation (50) because no regression is needed in this method to fit  $a$  to  $N$ , occasional occurrences of the patterns still appeared.

### *Experimental Results*

The first method of fitting  $a$  versus  $N$  using a quadratic is similar to the method discussed in reference [25] and is somewhat similar to the incremental polynomial method in reference [6] with all the data points used for a single regression (i.e. more smoothing occurs in this method, which is essentially the same as the total polynomial method discussed in reference [19], than in the ASTM method). Plots of the resulting values of  $\log_{10}A$  and  $n$  are included in Figures 23 and 24.

As expected [39, 56, 91, 92, 93],  $\log_{10}A$  and  $n$  are linearly related. There appears to be a trend with changing cement content in the linear relationship in Figure 23. However, a trend could not be identified in Figure 24 due either to the lack of data points or to some other factor (e.g. lack of significant differences in  $K_{IC}$  or simple variability in the data). In Figure 25, results for the curing date study are presented ( $A=7$  day,  $B=14$  day,  $C=28$  day).

The results of the fit using the three point running average method are shown in Figure 26 where  $M$  denotes modified compaction,  $S$  denotes standard compaction, and  $C$  denotes curing date study. It was found that the values of  $\log_{10}A$  and  $n$  for the three point ( $T$ ) method and for the quadratic curve fitting method ( $Q$ ) lie on the same line as shown in Figure 27 which is for the 14 day cured specimens.

As mentioned previously, positive serial correlation was noted when fitting the  $a$  versus  $N$  curves. A typical residual plot (from the quadratic curve fitting method) is included as illustration (Figure 28). The reader should be aware that  $R^2$  for the curve fit

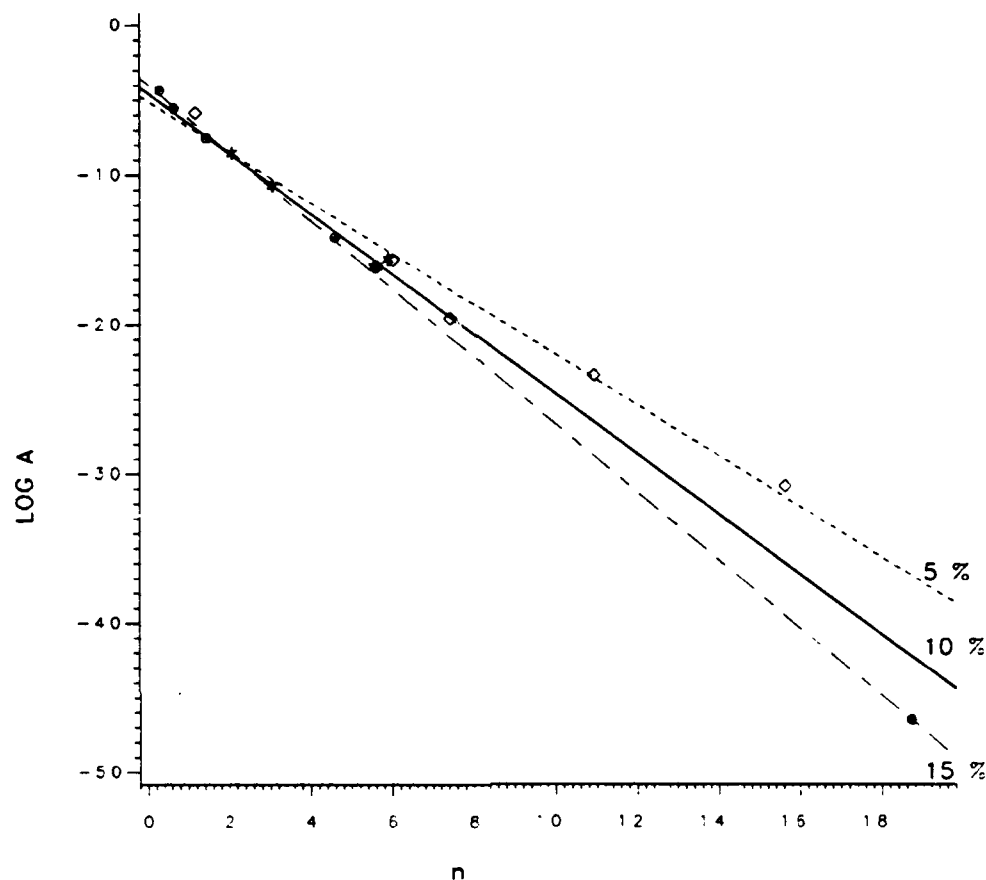


Figure 23.  $\text{Log}_{10}A$  versus  $n$  for modified compaction specimens (28 day).

which generated these residuals was 0.996 and the overall  $F$  value was 2757.342 with two degrees of freedom (model), and 20 degrees of freedom (error). Obviously, an excellent  $R^2$  does not necessarily imply that serial correlation does not exist (the Durbin-Watson statistic for this specimen was 0.73).

As further illustration, it is noted that, for the nine specimens in the curing date study (for fatigue), the average Durbin-Watson

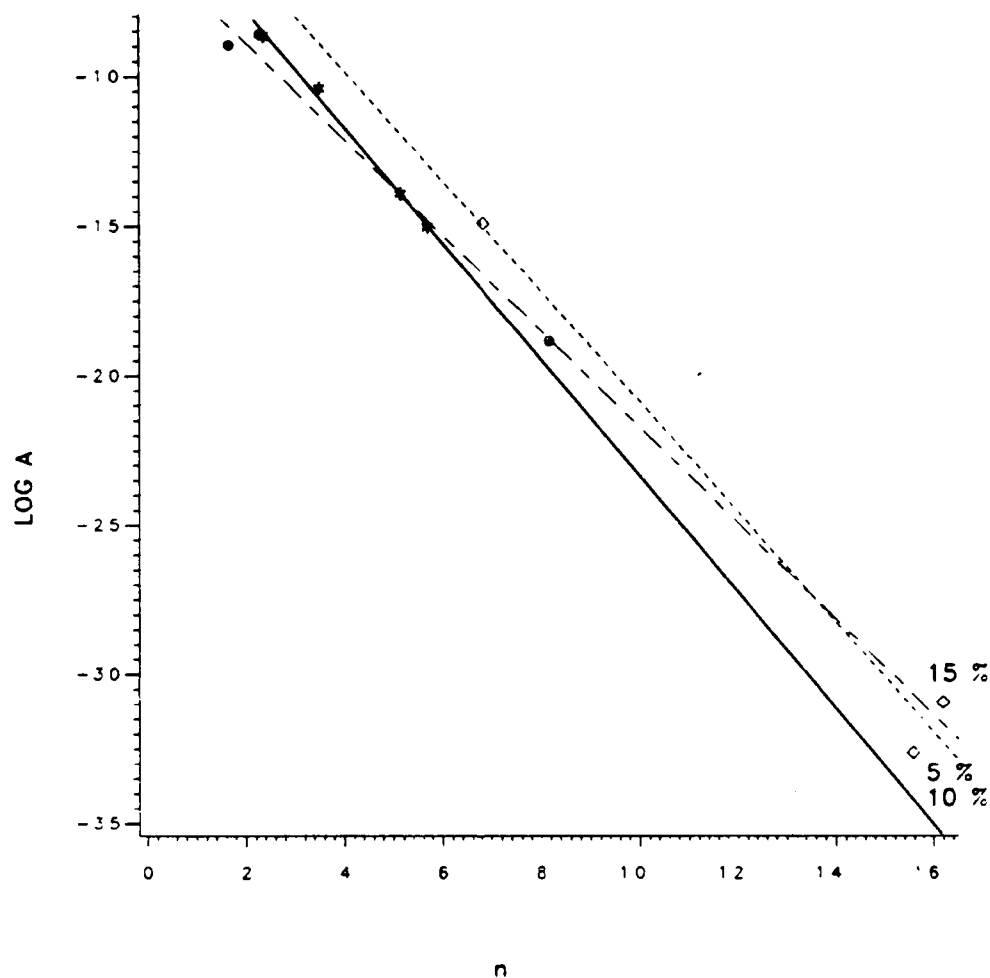


Figure 24.  $\log_{10}A$  versus  $n$  for standard compaction specimens (28 day).

statistic was 0.605 with a standard deviation of 0.489 and skewness 1.632, kurtosis 4.978. The average change (20 observations on nine specimens) in crack length between adjacent positive and negative maxima (minima) was approximately 0.047 in (0.121 cm) with a standard deviation of 0.032 in (0.081 cm) and skewness 0.32, kurtosis 1.56.

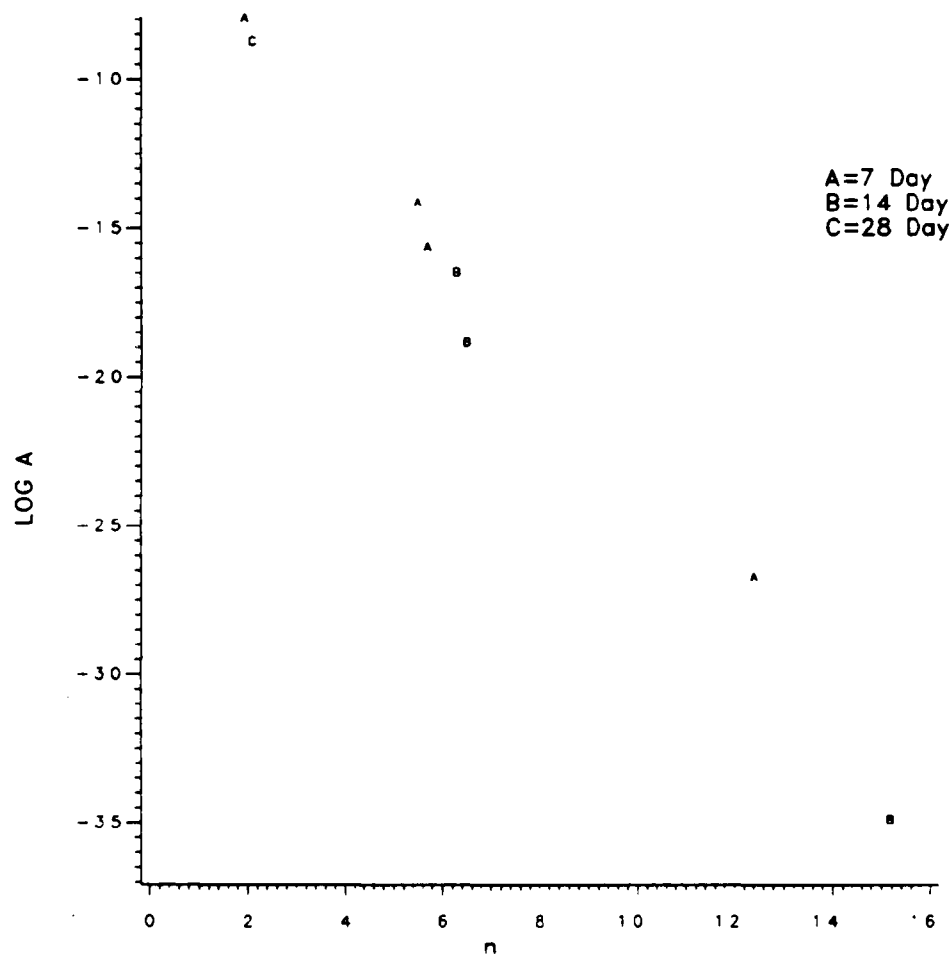


Figure 25.  $\log_{10} A$  versus  $n$  for the curing day study.

The following explanations are offered as possible reasons for the "stick-slip" type behavior of the crack growth curve.

(1) A crack tip process zone (microcracked region or some sort of plastic zone) forms which has a radius  $\approx 0.05\text{in}(0.127\text{cm})$  through which the macrocrack travels at a decreasing speed. As the

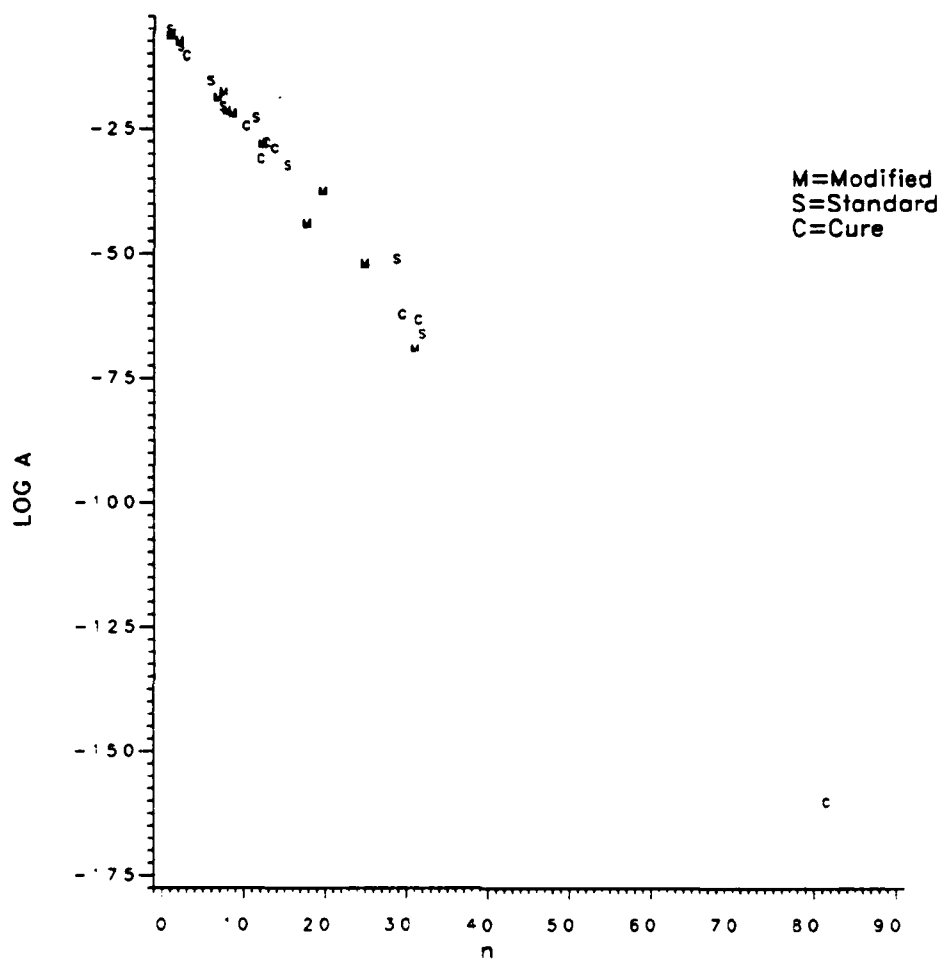


Figure 26.  $\log_{10} A$  versus  $n$  using the three point running average technique.

macrocrack approaches the diffuse "boundary" of the process zone it begins to accelerate until a new process zone begins to be established at which time the macrocrack begins to decelerate again. The process then begins all over until the process zone can not stop unstable crack extension at  $\Delta K_{IC}$ . The average value of the radius,

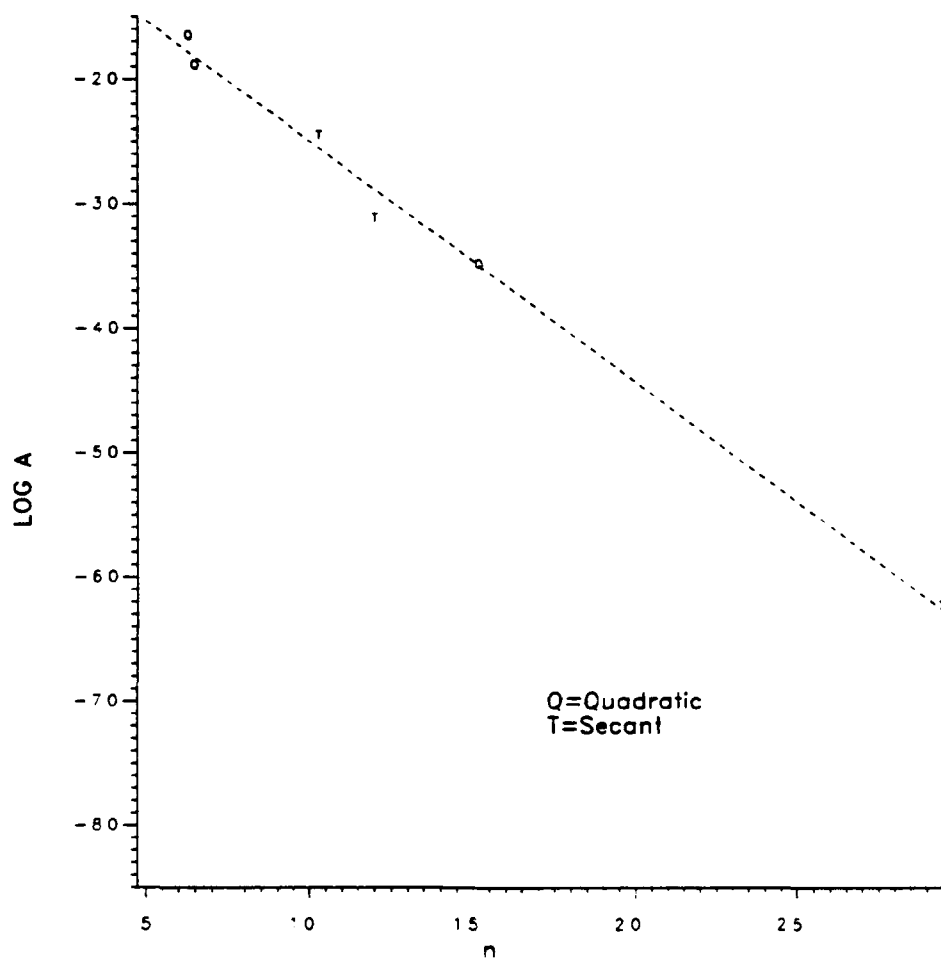


Figure 27.  $\text{Log}_{10}A$  versus  $n$  for different methods of fitting the crack growth curve.

$r$ , of the process zone ( $\bar{r}=0.035$ , standard deviation=0.019,  $N=9$ ) calculated using equation (37) is very close to the average value of the change in crack length between residual error maxima and minima in the analysis of systematic lack of fit.

(2) Flocculation is known to occur in essentially all fine-

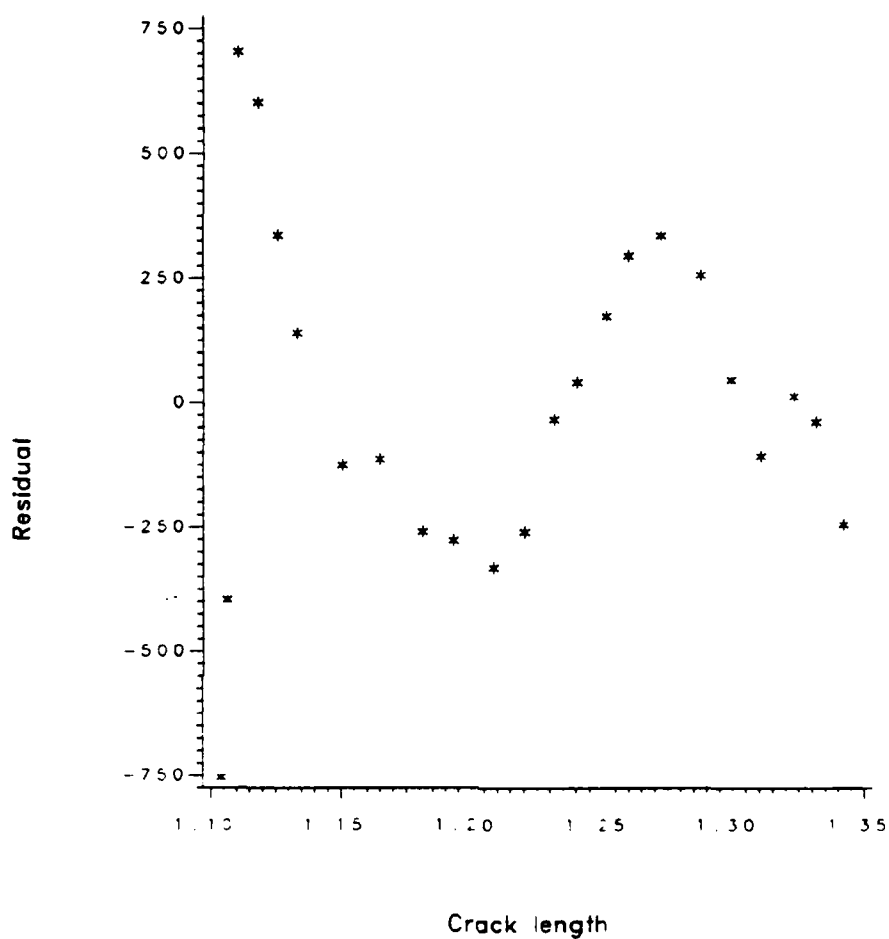


Figure 28. Residual error plot from N versus a (quadratic regression specimen 020C).

grained soils upon the addition of cement. Perhaps this flocculation occurs in such a manner as to produce relatively uniform ( $\approx 0.05\text{in}(0.127\text{cm})$ ) spacing between flocculated and/or cemented regions, and high void regions. This material heterogeneity may affect acceleration or deceleration of the macrocrack.

(3) Small regions exist where the macrocrack branches (thus decreasing the observed crack growth rate) temporarily and later rejoins into the main macrocrack (causing acceleration back to the previously observed growth rate). The possibility of this behavior can be seen in the SEM pictures in Appendix V.

(4) A sinusoidal shaped R-curve exists in which resistance to crack extension fluctuates.

The total polynomial (quadratic) method results for  $\log_{10}A$  and  $n$  were used in conjunction with  $\Delta K_{IC}$  and  $K_{IC}$  to produce a plot of the "crack speed index" (CSI) (see [77], [61]) where

$$CSI_1 = \log_{10}A + 2n$$

$$CSI_2 = \log_{10}A + n \log_{10}(0.75 \Delta K_{IC})$$

Note that the above equations were used to calculate the ordinal value for each of the points indicated in Figure 29. Once the values of CSI were calculated for each specimen, the abscissa (effectively  $\Delta K_{IC}$  for the specimen) was paired with the CSI to produce the plot. The regression line on the plot (the equation of which is presented in Table 8) is the regression of the ordinal value (the CSI of interest) as a function of the abscissa (KQD).

It can be seen from Figure 29 that  $CSI_2$  is approximately constant while  $CSI_1$  shows a variation (with higher values of CSI associated with lower toughness values). This indicates that the crack growth rate per cycle at a given percentage of  $\Delta K_{IC}$  does not change much with material composition changes which increase  $K_{IC}$ . Therefore, the beneficial effect of adding more cement to the material is primarily

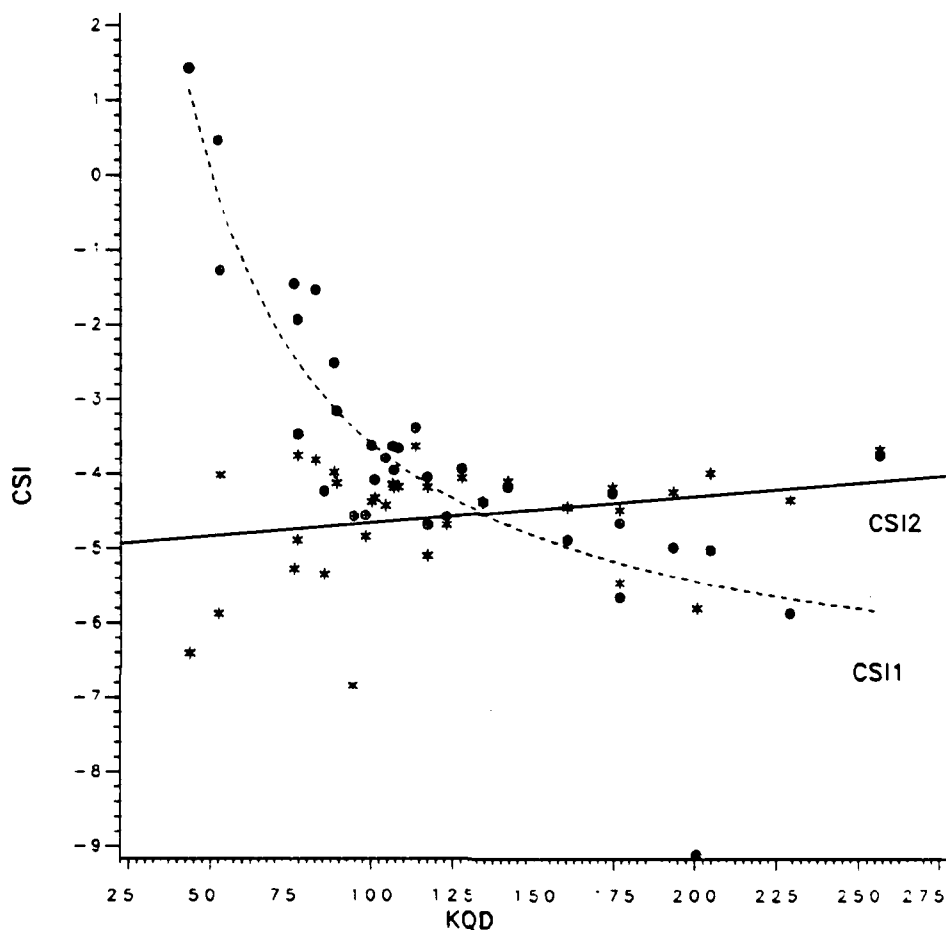


Figure 29. Comparison of crack speed indices (Quadratic method).

in the increase in  $K_{IC}$  which, in turn, increases the load (or number of cycles) required to reach a given percentage of  $\Delta K_{IC}$  thus increasing fatigue life. The same type plot is shown in Figure 30 for the CSI calculated from the three point secant method (instead of from the total polynomial method used for Figure 29).

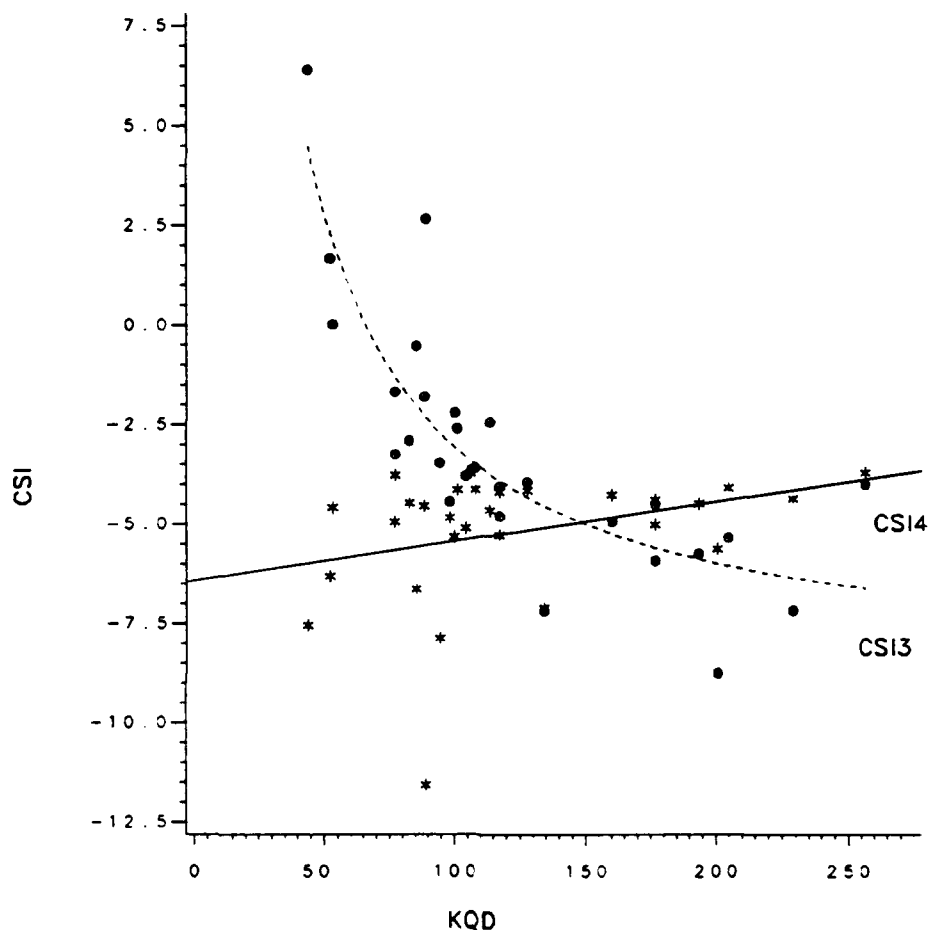


Figure 30. Comparison of crack speed indices (Secant method).

The same conclusions are reached as before and statistical verification that  $CSI_2$  and  $CSI_4$  are independent of KQD is given in Table 8. Notice that  $R^2$  is essentially zero for both models involving  $CSI_2$  and  $CSI_4$ . In addition, the t-test for the slope regression parameter,  $\beta_1$ , indicated that  $\beta_1$  was not statistically

different from zero. Comparisons of the two methods of curve fitting (quadratic and secant) were made using models involving similar CSI's for the two different methods. The first model,  $CSI_4 = \beta_0 + \beta_1 CSI_2$ , showed that  $\beta_0 = 0.90$  was not significantly different from zero and  $\beta_1 = 1.25$  was not significantly different from 1.0 ( $R^2 = 0.83$ ). The second model,  $CSI_3 = \beta_0 + \beta_1 CSI_1$ , showed that  $\beta_0 = 2.83$  was significantly different from zero, and  $\beta_1 = 1.58$  was significantly different from 1.0 ( $R^2 = 0.86$ ). Of course, it can be seen that CSI is aptly named an "index" because a value of  $\Delta K = 100$  psi/in (109.9 kPa/m) for a material which has a  $K_{IC} < 100$  psi/in (109.9 kPa/m) is essentially unattainable. Therefore, a more realistic scenario might be as in Figure 31 where the line labeled CSI35 is obtained using ordinal values generated by the equation:

$$CSI_{35} = \log_{10} A + n \log_{10} (50)$$

using the secant method. The value of  $\Delta K = 50$  psi/in (54.95 kPa/m) is near the minimum value of  $K_{IC}$  observed in the test results. Also plotted in Figure 31 is the line determined by the ordinal values given by

$$CSI_{49} = \log_{10} A + n \log_{10} (0.90 \Delta K_{IC})$$

Even though  $CSI_{35}$  is more realistic than  $CSI_1$  or  $CSI_3$ ,  $\Delta K = 50$  psi/in (54.95 kPa/m) was not always within the range of values used in the regression models and therefore must still be treated as an "index".

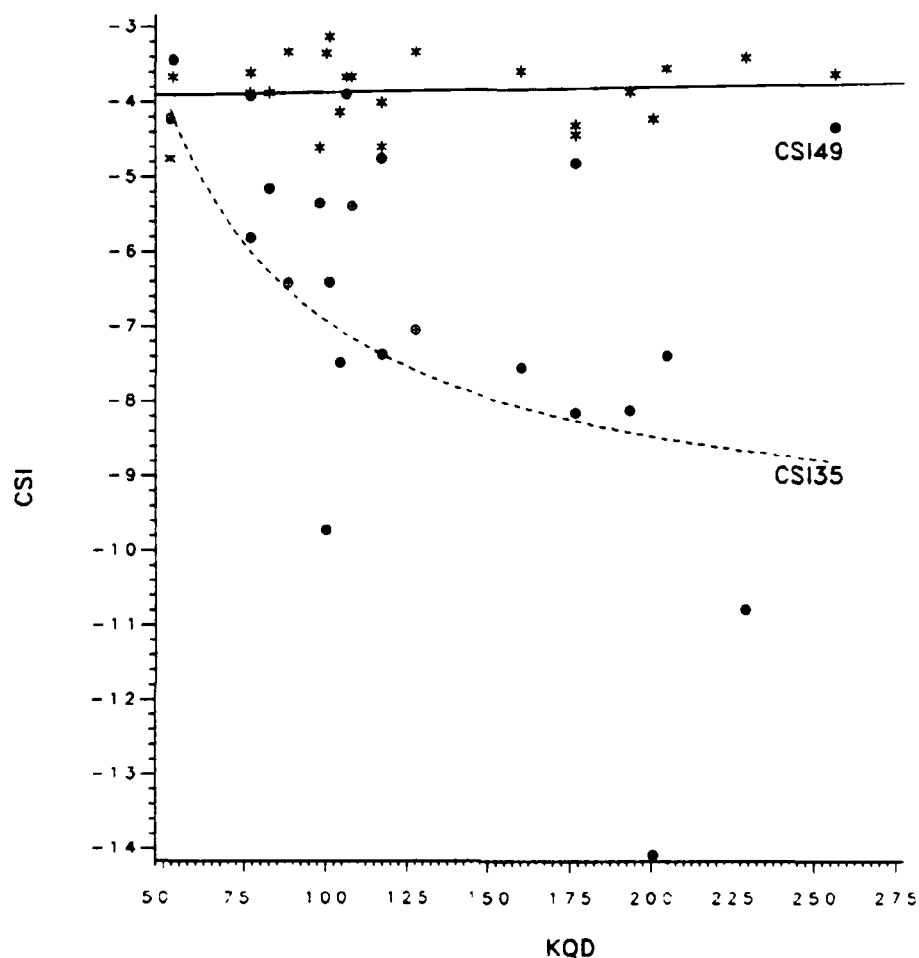


Figure 31. Comparison of crack speed indices.

The results of the method of using static data to model fatigue behavior mentioned in the section on new developments are shown in Figure 32.  $R^2$  for the regression in this plot was approximately 0.84.

Table 8. Regression relationships between CSI and Stress Intensity.

Arbitrary $\Delta K$		
$\Delta K=100$ psi/in		
$CSI_1 = -7.279 + (367.828/KQD)$		$R^2=0.73$
$CSI_3 = -8.913 + (585.139/KQD)$		$R^2=0.73$
$\Delta K=50$ psi/in		
$CSI_{35} = -10.016 + (309.063/KQD)$		$R^2=0.24$
Percentage of $\Delta K_{IC}$		
At $0.60\Delta K_{IC}$		
$CSI_2 = -5.889 + 0.00595KQD$		$R^2=0.05$
$CSI_4 = -8.979 + 0.01853KQD$		$R^2=0.10$
At $0.75\Delta K_{IC}$		
$CSI_2 = -5.017 + 0.00358KQD$		$R^2=0.06$
$CSI_4 = -6.425 + 0.00992KQD$		$R^2=0.11$
At $0.85\Delta K_{IC}$		
$CSI_2 = -4.385 + 0.000842KQD$		$R^2=0.00$
$CSI_4 = -4.993 + 0.00508KQD$		$R^2=0.09$
At $0.90\Delta K_{IC}$		
$CSI_2 = -4.138 + 0.00000389KQD$		$R^2=0.00$
$CSI_{49} = -4.338 + 0.00288KQD$		$R^2=0.05$
At $1.00\Delta K_{IC}$		
$CSI_2 = -3.683 - 0.00154KQD$		$R^2=0.01$
$CSI_4 = -3.133 - 0.00119KQD$		$R^2=0.01$

It should be noted that the model did not perform well for

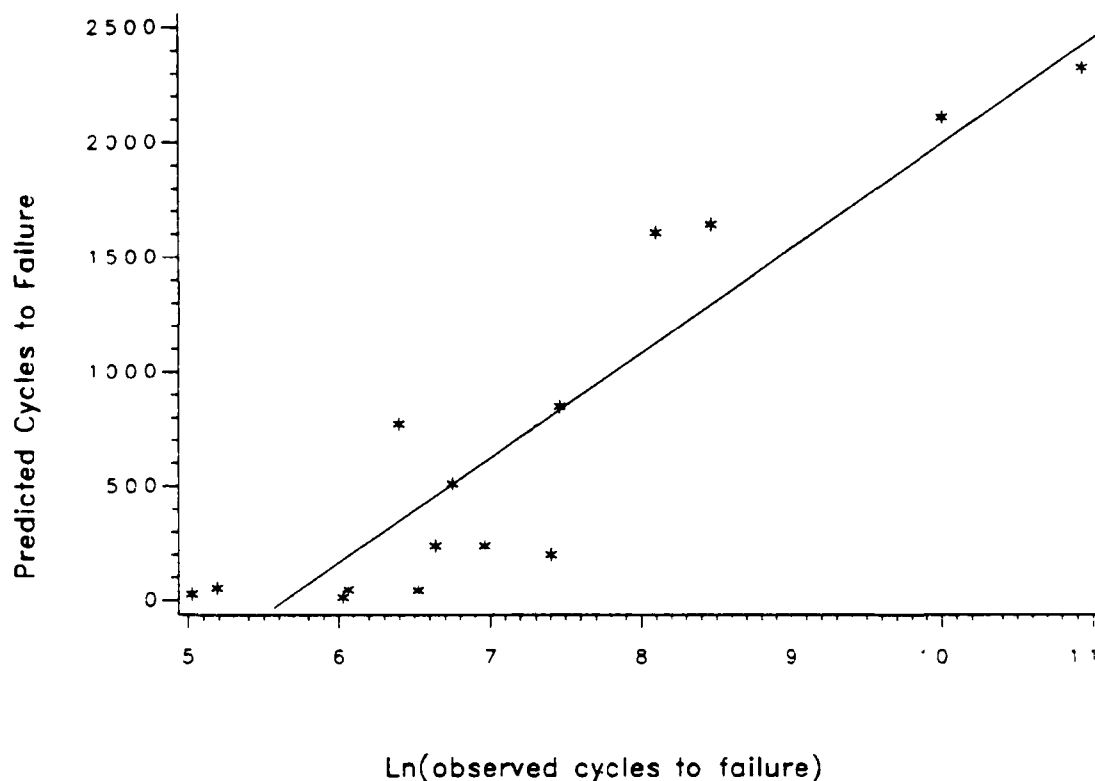


**Figure 32. Prediction of failure cycle from static test.**

specimens which had very few cycles to failure due to the close proximity to unstable crack extension. If the model did not correctly predict the crack length at failure, the data point was eliminated from the plot. A plot of the predicted versus observed crack lengths for the data presented in Figure 32 is shown in Figure 33.

Statistical Inference. The slopes of the lines in Figure 23 (-1.70, -2.01, -2.27 for 5, 10, and 15% cement content respectively) are statistically different. The intercepts are statistically the

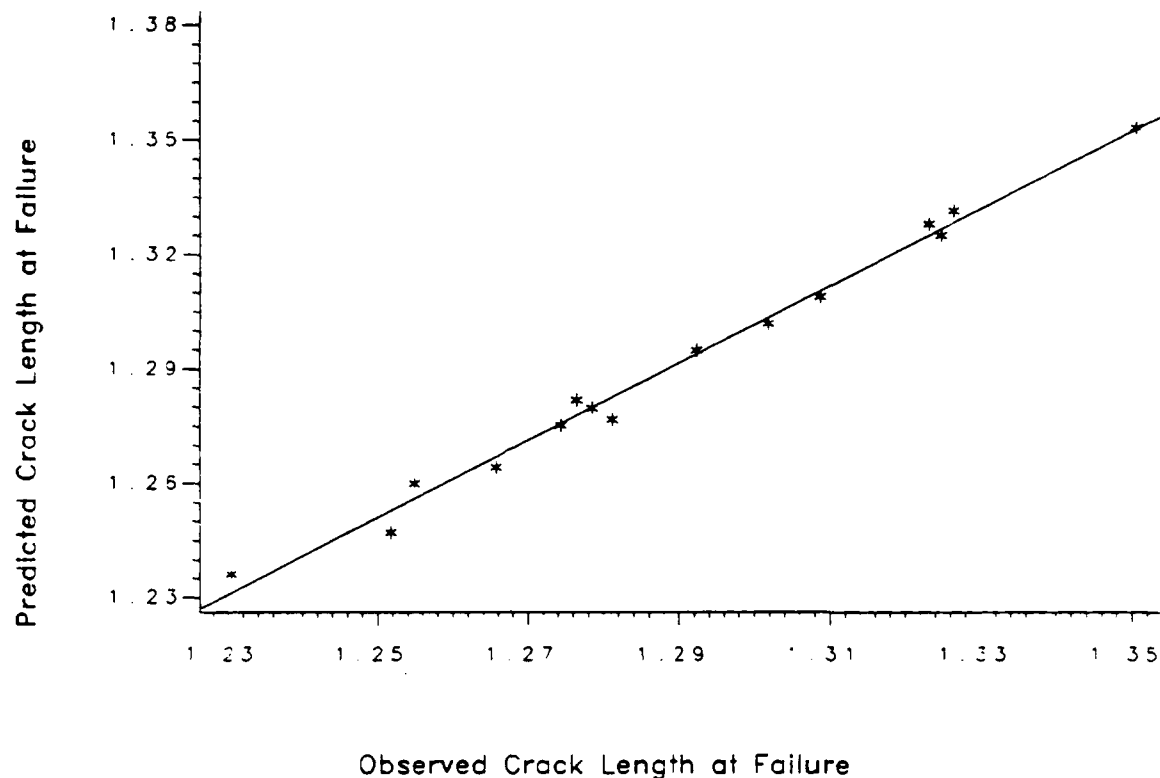


**Figure 33. Prediction of crack length at fatigue failure from static test.**

same ( $-5.08, -4.47, -3.95 \Rightarrow \bar{\beta}_0 = -4.497$ ). In Figure 24, the slopes ( $-1.84, -1.95, -1.61$ ) are statistically the same as are the intercepts ( $-2.44, -3.89, -5.67 \Rightarrow \bar{\beta}_0 = -3.997$ ). Therefore, the intercept was also larger for the lower toughness materials.

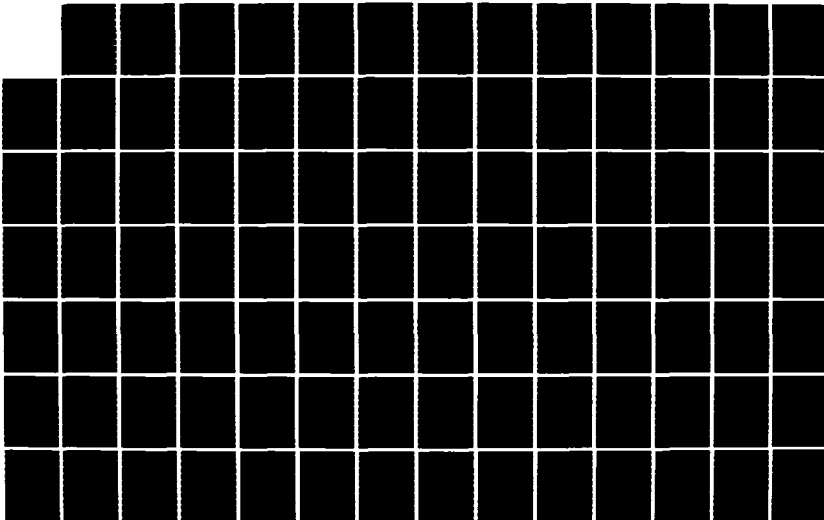
Comparison with Other Materials. An interesting comparison of soil cement with other engineering materials may be made by using  $\log_{10} A$  versus  $n$  plots. Data on various materials was obtained from different authors and an equivalent  $\log_{10} A$  calculated using the

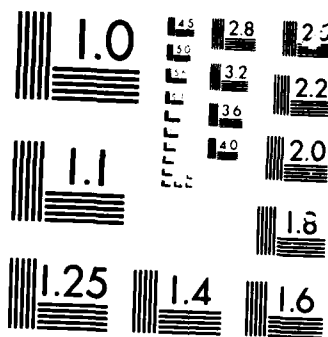
FRACTURE IN STABILIZED SOILS VOLUME 1(U) TEXAS  
TRANSPORTATION INST COLLEGE STATION D N LITTLE ET AL.  
31 DEC 85 AFOSR-TR-86-0242-VOL-1 F49620-82-K-0027

31 DEC 85 AFOSR-TR-86-0242-VOL-1 F49620-82-K-0027

F/G 8/13

ML





MICROCOPY

10000

method outlined in Appendix II. Some of the values were computed graphically from figures in the literature which often did not report the specific values which generated the plots. Appendix III contains the values and sources of the  $\log_{10}A$  and  $n$  values used in this document. It is emphasized that the following plots are for  $da/dN$  in units of inches/cycle and for  $\Delta K$  in units of psi/in. Hertzberg [39] has noted that the method of test control (e.g. stress versus strain control) may have a pronounced effect on the parameters  $A$  and  $n$ . A time dependent material (e.g. polymer at an appropriate temperature) may be particularly sensitive to the mode of control. Therefore, two plots are presented.

Figure 34 contains  $\log_{10}A$  versus  $n$  data for materials which are known (or suspected) to have been tested in load control. Figure 35 contains data known to have been conducted in displacement control. In both cases, the solid line represents a regression line for the data in Figure 26 for cement stabilized soil tested in load control. One possible way of interpreting Figures 34 and 35 is to limit the comparison to materials and specimens which have similar sensitivity to  $\Delta K$ , i.e. those which have equal values of  $n$ . For example, choosing  $n=5$  and imagining a regression line drawn through the points which are determined by basically similar materials, it can be seen that metals have the lowest  $\log_{10}A$  (equivalently, the lowest CSI or  $da/dN$ ), and composites follow the metals very closely. Plastics and asphaltic concrete materials fall fairly close together at the third lowest CSI. Cement stabilized soil has a faster crack growth rate than plastic in this region. Finally, Figure 35 seems to indicate

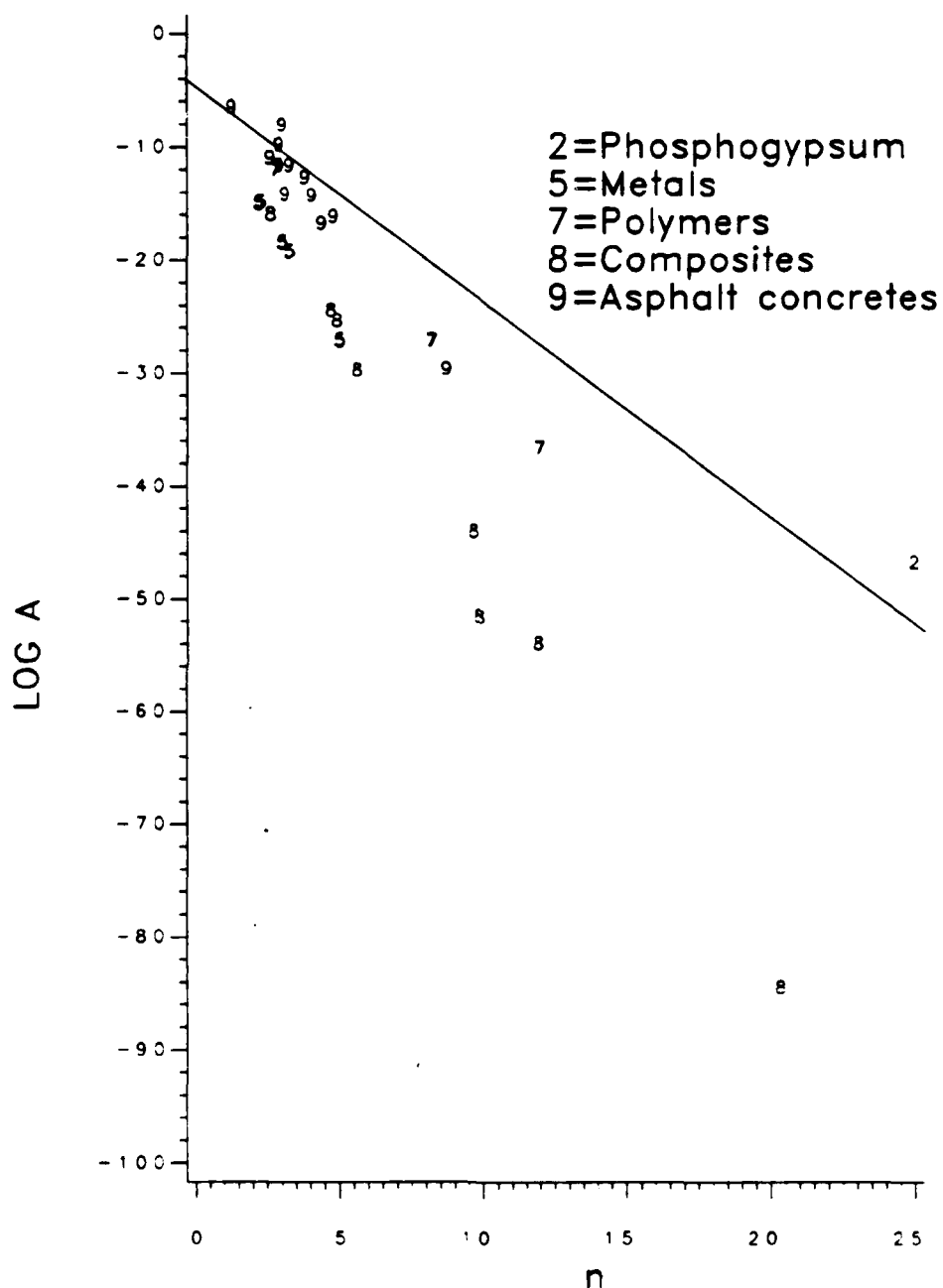


Figure 34. Comparison of  $\log_{10} A$  versus  $n$  for various materials.

that the fabric reinforced asphalt concrete material [77, 31], and

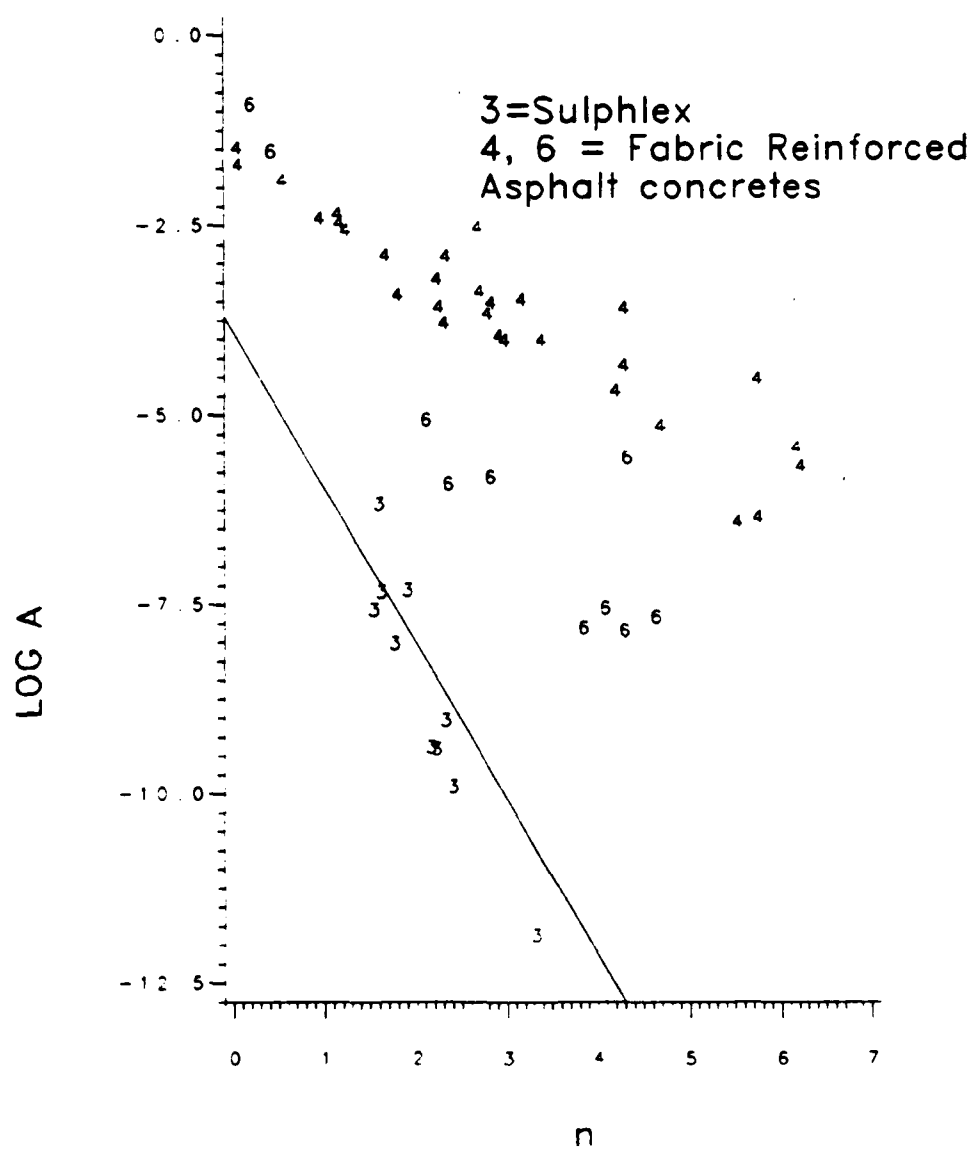


Figure 35. Comparison of  $\text{Log}_{10} A$  versus  $n$  using materials tested in displacement control.

sulphlex material [61] tested in displacement control have the largest CSI. This trend seems anomalous but may be due to the testing method, the type of binder, the test temperature, or the use of some parameters which are based on linear elasticity to approximately describe a somewhat nonlinear material.

At the present level of understanding, no reasonable explanation is offered for the observation that an individual cement stabilized soil specimen which happens to have a very high exponent ( $n$  value) will have a lower  $\text{Log}_{10}A$  than, for instance Ti, which has an exponent of five. Therefore, an alternative and slightly more consistent method of comparing dissimilar materials is presented using CSI in Figure 36.

For selected materials, the threes in the plot are equivalent to  $\text{CSI}_{35}$  while the fours are equivalent to  $\text{CSI}_4$ . The asterisks and zeros at the left side of the plot are values of  $\text{CSI}_{35}$  and  $\text{CSI}_4$  for cement stabilized soil, respectively. Note that the other materials (metals and composites), in general, have lower CSI's (indicated by the threes) than cement stabilized soil (indicated by asterisks). The lowest metal or composite CSI in the plot at  $\Delta K=50 \text{ psi/in}(54.95\text{kPa}\sqrt{\text{m}})$  was a glass reinforced plastic, the next lowest was a B-Al metal matrix composite, and the highest was a martensitic steel. As expected, stabilized soil displays a rather high CSI in relation to other materials. Note, once again, that the values in the plot must be considered indices because a value of  $\Delta K=50 \text{ psi/in}(54.95\text{kPa}\sqrt{\text{m}})$  is generally below the threshold  $\Delta K$  for these materials (see reference [85] p.224).

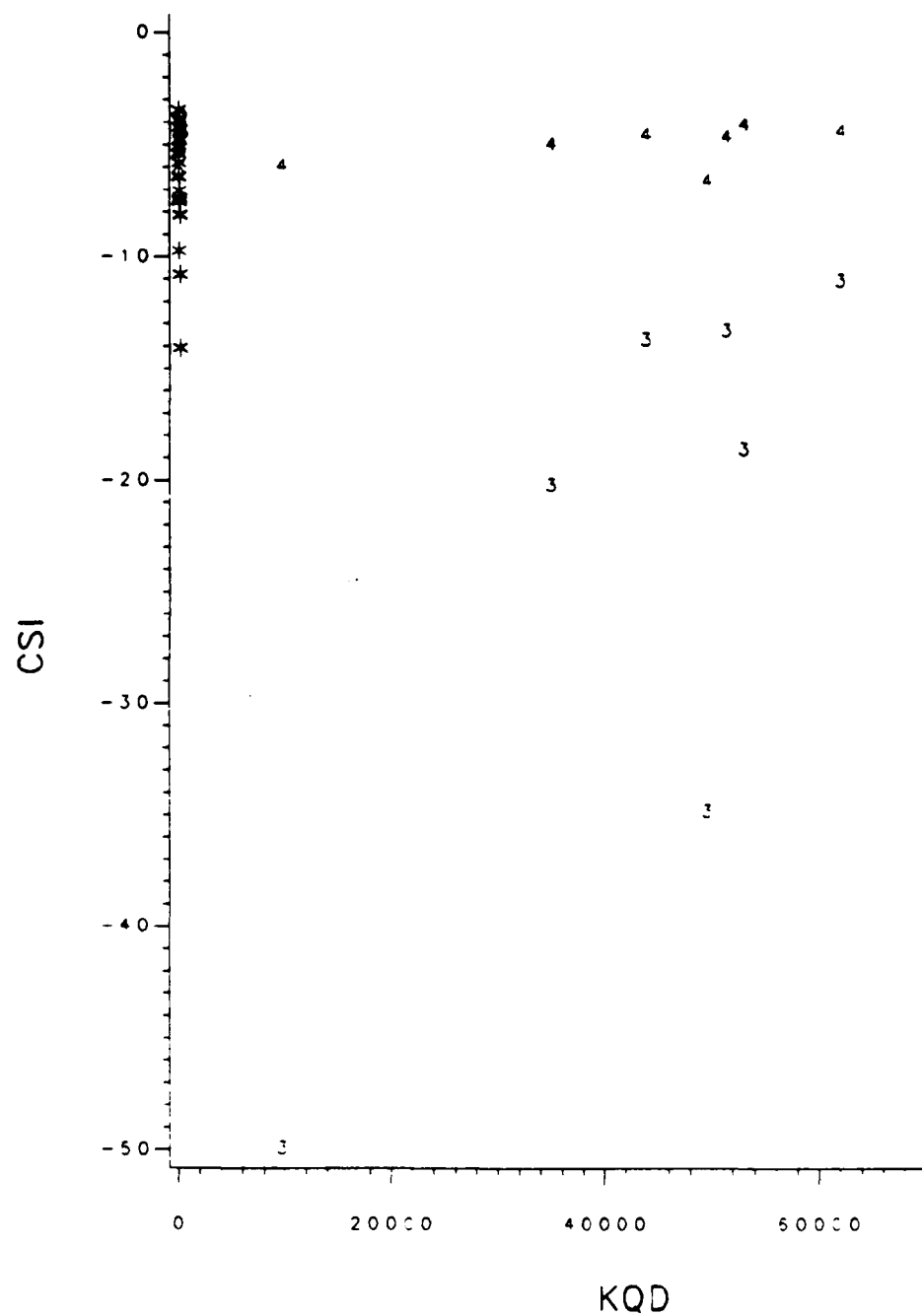


Figure 36. Comparison of dissimilar materials by CSI.

### Conclusions

The "stick-slip" behavior of the  $a$  versus  $N$  curve is most likely a result of crack branching followed by a rejoining with the main branch or by the secondary branch simply stopping. The crack speed is slower through the higher toughness material. At least for this material, comparison of materials using fatigue parameters should be based on a parameter which includes both  $A$  and  $n$ . In addition, the method of determining  $A$  and  $n$  should be noted as well as the presence or absence of serial correlation. The presence of serial correlation may prove (if observed in other materials) useful in modelling an estimate of the size of a crack tip process zone based on fatigue measurements. Serial correlation or systematic lack of fit should be considered using the methods described herein or by more sophisticated time series analyses [87]. It is suspected that  $CSI_2$  and  $CSI_4$  are material properties that can be detected even in the presence of systematic lack of fit. Comparison of  $CSI_2$  and/or  $CSI_4$  with  $CSI_1$  and/or  $CSI_3$  can be used to determine the source of increased fatigue life. Portland cement stabilized soil apparently has a faster crack growth rate (at a given sensitivity to  $\Delta K$ ) than many engineering materials.

Future Work. Much research needs to be done into the fatigue behavior of cement stabilized soil. The effect of loading wave shape and frequency, the effect of the method of test control, and the method of obtaining crack length are certainly worthy of further study. However, some more immediate needs are:

- (1) Identification of what controls the process zone, the zone

volume, and the crack tip process zone behavior during cyclic loading.

(2) Determination of the utility of a model which uses thermal fluctuations over time as the definitive stress for  $K_{min}$ , and which uses traffic loading to define  $K_{max}$ . This type model would result in a  $da/dN$  versus  $\Delta K$  plot which would simultaneously reflect the effects of thermal stress, wheel load, and crack length.

(3) Determination of the impact of stress corrosion cracking. In this case, water may carry the "corroding" element in one of two ways. Water may carry a deleterious chemical which weakens the binder (e.g. sulfate attack of Portland cement). Secondly, an approach similar to item (2) above may be taken to assess how freeze-thaw cycling of water in an existing crack may cause crack extension due to a "wedge opening load" caused by expansion against the crack faces during the transition to the solid phase.

## CHAPTER IV: APPLICATIONS

*Literature Review and Theory*

Considerable recent effort has been devoted to the use of finite element analysis in two dimensional fracture mechanics problems. This effort has been fueled perhaps by the ability to handle complex boundary conditions more readily than in an analytical approach. Nevertheless, some analytical solutions exist for boundary conditions which can be used as limiting cases. The principle of superposition [15, 97] is applied in crack problems as shown in Figure 37.

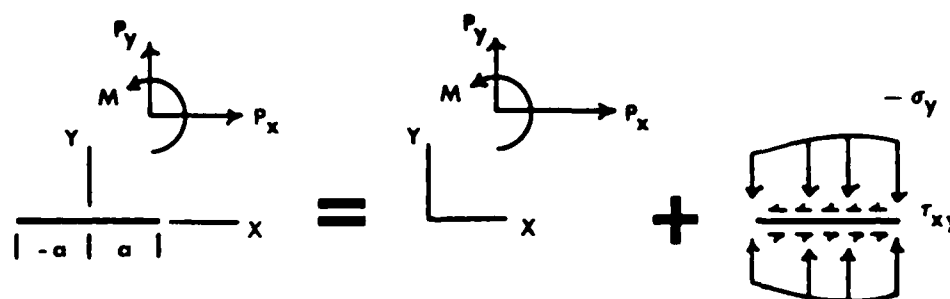


Figure 37. Superposition (redrawn from Sih [97]).

There are four analytical solutions for stresses in uncracked bodies that are of interest in this report. The treatment is limited basically to a general study of the Mode I component generated by

indirect tensile stresses resulting from compressive applied loads at a free surface. The four solutions are the Flamant solution for a uniform line load on the boundary of a semi-infinite body (see [104]), the solution (extended from the Flamant solution) for opposing line loads on a circular disk (see [111], the indirect tension test), the solution for a distributed load over a portion of a semi-infinite body (which is an extension of the three dimensional solution for a point load on the boundary due to Boussinesq, see reference [104]), and the modification of the Boussinesq theory by Burmister [16, 17, 48]. The geometries are shown in Figure 38.

There are three solutions for crack problems of interest in this report. These solutions include the case of arbitrary tractions applied to the crack surface (see [97]), the solution for a crack at any angle to an interface between two dissimilar materials [4], and the three dimensional solution for the imbedded penny-shaped crack normal to a boundary [54]. These geometries are shown in Figure 39.

#### *New Developments*

Only approximate analyses for solutions to very specific problems are included in this section. However, the problems and analyses are directly applicable to pavement and foundation problems. The two dimensional problems are formulated so that the crack plane lies in the plane of the load and the crack is remote from the boundary. The three dimensional problems are also formulated with the plane of the crack perpendicular to the boundary and passing through the center of the area over which the load is distributed.

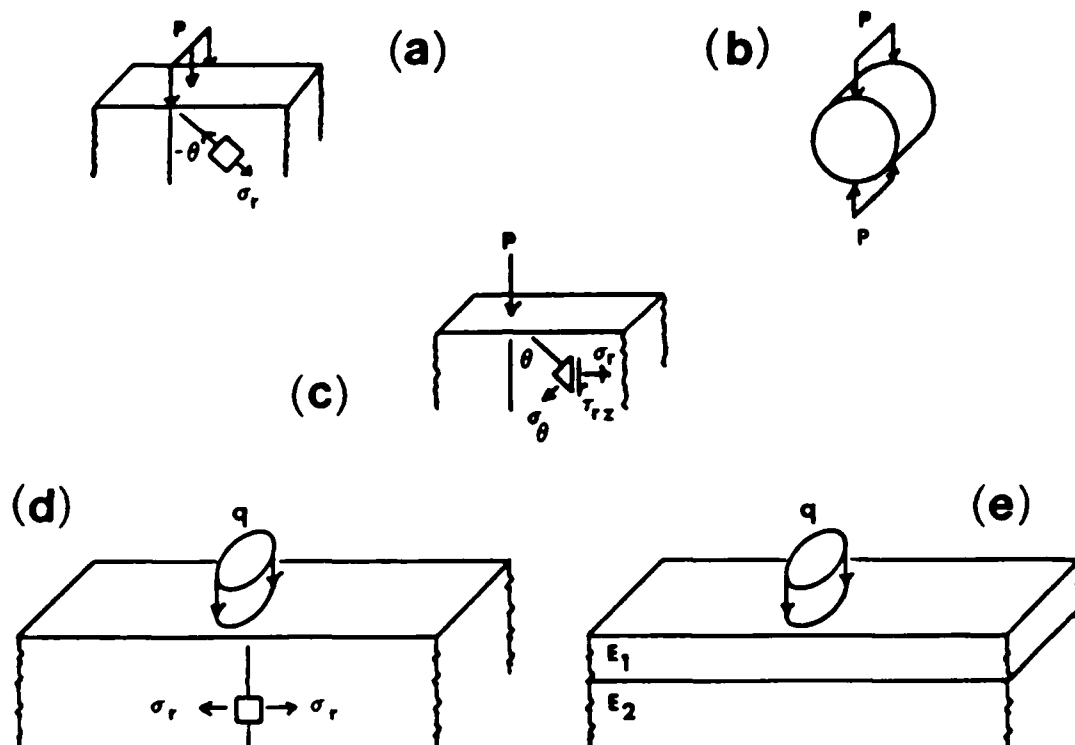


Figure 38. Boundary conditions for (a) Flamant, (b) IDT, (c) Boussinesq (point), (d) Distributed, and (e) Burmister solutions.

Line Load on a Boundary. The stress field solution for the uncracked body is (see [104]):

$$\sigma_r = -(2P/\pi r) \cos \theta \quad (54a)$$

$$\sigma_\theta = \tau_{r\theta} = 0 \quad (54b)$$

This solution implies that  $K_I = K_{II} = 0$  along the line where  $\theta = 0$ . It is useful to find the value of  $\theta$  at which the value of  $J$  is a maximum on a vertical plane which is located a horizontal distance,  $c$ , from the plane of the load. Note that the equation for  $J$  in the case of

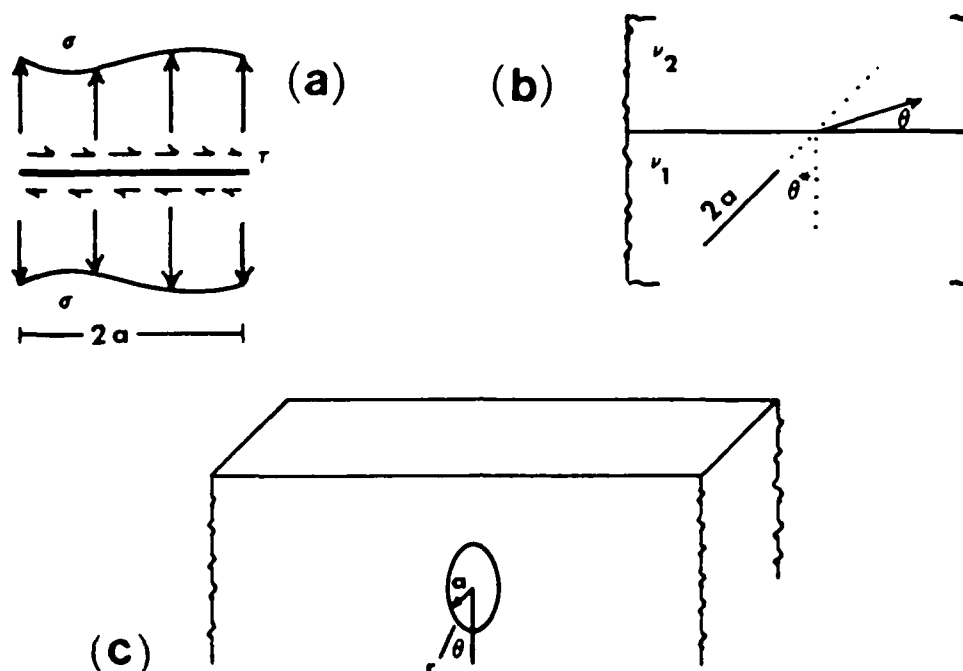


Figure 39. Boundary conditions for cracked bodies (a) arbitrary load, (b) interface, (c) penny-shaped.

combined mode I and II loading is similar to equation (21)

$$J_{\max} = [(1-\nu^2)/E](K_I^2 + K_{II}^2) \quad (55)$$

where (see [97])

$$K_I = (\pi/a)^{-1} \int_{-a}^a \sigma_r \left(\frac{a+z}{a-z}\right)^{1/2} dz \quad (56a)$$

which, for this problem becomes

$$K_I = [(-2P \cos^2 \theta \sin^2 \theta) / (\pi/a)] \\ [\sin^{-1}(z/a) - (1 - (z^2/a^2))^{1/2} + (2/a^2)(1 - a^2)^{1/2} + (2/a) \sin^{-1} a] \quad (56b)$$

$$K_{II} = (\pi/a)^{-1} \int_{-a}^a r_{rz} \left(\frac{a+z}{a-z}\right)^{1/2} dz = 0 \quad (56c)$$

and for this problem

$$K_{II} = K_I / \tan \theta \quad (56d)$$

It can easily be seen by setting  $\partial J_{\max} / \partial \theta$  equal to zero that the maximum  $J$  value is reached at  $\cos \theta = 2/\sqrt{6}$ . Therefore,  $J_{\max}$  occurs at a  $\theta$  of approximately  $35.3^\circ$ . It can be concluded that two peaks in  $J$  will occur as a moving load approaches the plane of interest, one as the load approaches the plane and one as the load moves away from the plane. Of course, the depth must also be known to determine the actual magnitude of  $J$ .

Point Load on a Boundary. The stresses given in reference [104] are

$$\sigma_r = \frac{P}{2\pi} [(1-2\nu) \left[ \frac{1}{r^2} - \frac{z}{r^2} (r^2+z^2)^{-1/2} \right] - 3r^2 z (r^2+z^2)^{-5/2}] \quad (57a)$$

$$\sigma_z = - \frac{3P}{2\pi} z^3 (r^2+z^2)^{-5/2} \quad (57b)$$

$$\sigma_\theta = \frac{P}{2\pi} [(1-2\nu) \left[ - \frac{1}{r^2} + \frac{z}{r^2} (r^2+z^2)^{-1/2} \right] + (r^2+z^2)^{-3/2}] \quad (57c)$$

$$\tau_{rz} = - \frac{3P}{2\pi} r z^2 (r^2+z^2)^{-5/2} \quad (57d)$$

At  $r=0$  (i.e. directly under the line load):

$$\sigma_z = -\frac{3P}{2\pi z^2} \rightarrow d\sigma_z/dz = 3P/(\pi z^3) \quad (58a)$$

$$\tau_{rz} = 0 \quad (58b)$$

$$\lim_{r \rightarrow 0} \sigma_r = P(1-2\nu)/(4\pi z^2) = \lim_{r \rightarrow 0} \sigma_\theta \quad (58c)$$

As shown in reference [97], the solutions for  $K_I$  and  $K_{II}$  in the case of arbitrary tractions applied to this case for  $\sigma_r$  and  $\tau_{rz}$  are:

$$\begin{aligned} K_I &= (\pi/a)^{-1} \int_{-a}^a \sigma_r \left(\frac{a+z}{a-z}\right)^{1/2} dz \\ &= \frac{P(1-2\nu)\sqrt{a}}{4\pi^2 z^2} [\arcsin(z^2/a^2) - (1 - (z^2/a^2))^{1/2}] \end{aligned} \quad (59a)$$

$$K_{II} = (\pi/a)^{-1} \int_{-a}^a \tau_{rz} \left(\frac{a+z}{a-z}\right)^{1/2} dz = 0 \quad (59b)$$

Of course, this solution is conservative at best because this is the solution only at the axis through the point load. Therefore,  $\sigma$  would decrease in the plane of a crack which extended infinitely in the third direction (as the distance from the axis of the load is increased). In other words, a three dimensional stress solution to a two dimensional crack solution is not really correct. In the section on the circularly distributed load, a more conceptually correct but still approximate solution is discussed.

Disk with Opposing Line Load. This problem is the basis for the indirect tension test (IDT). The solution for the stresses along the plane of the load line are (see [111]):

$$\sigma_z = -6P/(\pi B d) \quad (60a)$$

$$\tau_{\theta z} = 0 \quad (60b)$$

$$\sigma_\theta = 2P/(\pi B d) \quad (60c)$$

The form of the stress intensity factor solution is the same form as in equation (59).

$$K_I = (\pi/a)^{-1} \int_{-a}^a \sigma_{\theta} \left( \frac{a+z}{a-z} \right)^{1/2} dz$$

$$= (2P/a)/(\pi B d) \quad (61a)$$

$$K_{II} = 0 \quad (61b)$$

Circularly Distributed Uniform Load Over Part of a Boundary. The equation for the stress of interest is (see [104]):

$$\sigma_r = (q/2) [-(1+2\nu) + 2z(1+\nu)/(r^2+z^2)^{1/2} - z^3/(r^2+z^2)^{3/2}] \quad (62)$$

where  $q$  is the distributed load and  $r$  is the radius of the area over which the load is applied. In pavement analyses, this uniform distribution is a convenient approximation to reality since it is known that the distribution is not uniform for many tire and pavement interactions. However, the approximation becomes more reasonable as depth increases. A solution to the problem of a penny shaped crack in a half space is presented graphically in reference [54]. The crack solution requires a linearly varying load of the form  $P=P_1(1+r_z \cos \theta)$  where  $P_1$  is a constant,  $r_z$  is the radius from a point on the  $z$  axis, and  $\theta$  is the angle between the positive  $z$  axis (vertical downward) and the point of interest on the crack boundary. It can be shown from equation (62) that

$$\begin{aligned} \partial\sigma_r/\partial z = (q/2) & \left[ -(1+2\nu) \right. \\ & + [(r^2+z^2)^{-1} [2(1+\nu)(r^2+z^2)^{1/2} - [(5+2\nu)z^2(r^2+z^2)^{1/2}]^{1/3} \\ & \left. + (3z^4(r^2+z^2)^{1/2})^{1/5} ] \right] \end{aligned} \quad (63)$$

and that

$$\lim_{z \rightarrow 0} \partial\sigma_r/\partial z = (q/2) [-(1+2\nu) + (2(1+\nu)/a)] \quad (64a)$$

$$\lim_{z \rightarrow \infty} \partial\sigma_r/\partial z = (q/2) [-(1+2\nu)] \quad (64b)$$

From this analysis, it can be seen that the stress varies linearly with depth only in the limiting cases. However, the limiting case as  $z \rightarrow \infty$  may be a useful approximation for very thick base courses. If the approximation is allowed and further extended to the boundary of the crack, an approximately linearly varying load of the form required by the solution in reference [54] is generated by using equations (64b and 62).

Design Example. A contrived example using fracture mechanics is presented to illustrate the general procedure and the utility of the concepts discussed in this report. For simplicity, the disk with opposing line load is used. Thus, this example is more applicable to laboratory work than field application. However, the basic procedure illustrated may be applied to the solutions which are more applicable to the field. Any contribution to the solution from  $K_{II}$  is ignored and only  $K_I$  for the plane coincident with the vertical line load is considered. The  $K_{IC}$  is 100 psi/in (109.9 kPa/m) which corresponds to approximately 7% cement content and modified compaction effort (calculated from a rearrangement of the regression equation (49) as

presented in Table 6).

A one inch (2.54cm) through crack (in a 4 inch (10.16cm) thick, 4 inch (10.16cm) diameter cylinder) is located in the plane of the load and oriented such that the crack is at the center of the disk. For this problem,  $a=0.5$  inch (1.27cm) and  $P$  is a cyclic load of 2666 lb (11858.4N) applied at 1 hertz in a sinusoidal waveform.

Noting that  $CSI_4$  was almost constant in many cases, a plot of  $CSI_4$  versus  $\Delta K_{Applied}/\Delta K_{IC}$  (where  $\Delta K_{IC}=100$  psi/in (109.9kPa/m)) was found to be useful for solving this problem. Figure 40 presents the results of the computation of  $CSI_4$  at the various percentages of  $\Delta K_{IC}$  using  $K_{QD}=\Delta K_{IC}=100$  psi/in (109.9kPa/m) in the five applicable equations which are presented in Table 8.

The equation of the regression line in the plot is:

$$CSI_4 = -16.595 + 19.367(\Delta K_{Applied}/\Delta K_{IC}) - 6.06444(\Delta K_{Applied}/\Delta K_{IC})^2 \quad (65)$$

which has an  $R^2=1.0$ . A simple iterative technique is used to calculate the crack length after cycle number three of the loading.

Cycle 1:

$$a_0 = 0.5 \text{ in (1.27cm)}$$

From equation (61a),  $K_I=75.0076$  psi/in (82.43kPa/m)

$$\Delta K_{Applied}/\Delta K_{IC}=75.0076/100=0.750076$$

for which value  $CSI_4$  is calculated using equation (65).

$$\therefore CSI_4=-5.44472 \Rightarrow da/dN=3.59156 \times 10^{-6} \text{ in (} 9.1 \times 10^{-6} \text{cm)}$$

Cycle 2:

$$a_0=0.5+3.59156 \times 10^{-6} \text{ in}$$

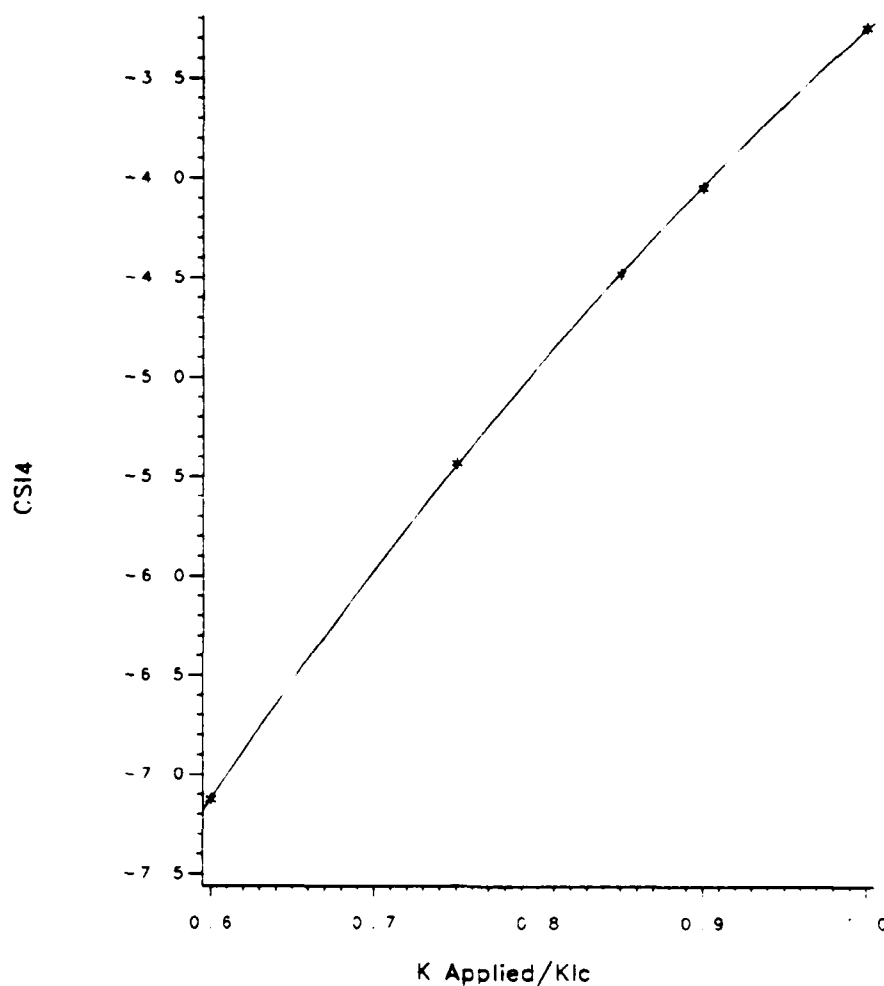


Figure 40. Variation of CSI with percentage of  $\Delta K_{Ic}$ .

$$K_I = 75.0079 \text{ psi}/\text{in} \text{ (82.43 kPa}/\text{m)} \Rightarrow \Delta K_{\text{Applied}}/\Delta = 0.750079$$

$$\therefore da/dN = 3.59179 \times 10^{-6} \text{ in} \text{ (9.1} \times 10^{-6} \text{ cm)}$$

Cycle 3:

$$a_0 = 0.5 + 3.59156 \times 10^{-6} + 3.59179 \times 10^{-6} \text{ in}$$

$$\Delta K_{\text{Applied}}/\Delta K_{Ic} = 0.750081$$

$$\therefore da/dN = 3.59202 \times 10^{-6} \text{ in } (9.1 \times 10^{-6} \text{ cm})$$

$$* a = 0.50001078 \text{ in } (1.27003 \text{ cm})$$

The iterative process of calculating the crack length could be carried out until some failure criterion is met. The number of cycles to reach the failure criterion is obviously the parameter of interest. The failure criterion would most probably be either based on a maximum allowable crack length or on  $K_I$  as it approaches  $K_{IC}$ . The iterative process would be a simple matter to program on a programmable calculator. In some cases, a larger computer may be necessary because a very small crack extension on a single cycle added to a comparatively large initial crack length may be represented in a form essentially truncated (actually rounded in most cases) to the original length in the calculator. That is, the calculator may not be capable of carrying enough significant digits (precision) to correctly calculate crack lengths at very small crack growth rates. It is easily seen that a 5% cement content (modified compaction) specimen would have a shorter fatigue life than the 6.72% specimen in the example. For example, for the 5% material,  $K_{IC} = 83.8 \text{ psi}\sqrt{\text{in}} (92.1 \text{ kPa}\sqrt{\text{m}})$ . For cycle number 1,  $\Delta K_{\text{Applied}} / \Delta K_{IC} = 0.895079$  which would give a crack extension of  $73.6873 \times 10^{-6} \text{ in } (1.87166 \times 10^{-3} \text{ mm})$ . This extension is more than one order of magnitude larger than that of the first example. At the end of the third cycle,  $a = 0.500221 \text{ in } (1.27056 \text{ cm})$ , which is a larger crack length than after three cycles on the 6.72% material. It should be noted that a new equation of the form (65) was required because of the difference in  $\Delta K_{IC}$  in the two examples.

### *Conclusions*

Several approximate solutions to crack problems are presented based on analytical approaches. Future research should involve refining the solutions, attempting to superpose the Ashbaugh (or some other layered crack) solution for cracked bodies on the Boussinesq solution as modified by Burmister, and applying the  $da/dN$  results from this study to the cracked body problem. Incorporation of crack growth modeling into existing layered elastic programs and/or finite element programs would be a long term goal of continued research.

Volume 2 of this report discusses a more detailed finite element solution to the problem of crack propagation in layered pavements.

## CHAPTER V: RELATIONSHIP BETWEEN TENSILE CREEP AND FATIGUE CRACKING

### *General*

It has been found that cement-stabilized soil shows a time-dependent deformation characteristic [28]. In order to evaluate the time-dependent characteristic of a material, the creep test is the most simple and convenient test method. Creep compliance can be calculated from

$$D(t) = \frac{\epsilon(t)}{\sigma_0}$$

where  $D(t)$  = creep compliance at time  $t$ ,

$\epsilon(t)$  = measured strain at time  $t$  and

$\sigma_0$  = constant stress applied.

Considerable compressive creep testing has been done on cement-stabilized soil and concrete. However, the bimodular property of cement-stabilized soil has caused researchers to doubt the validity of applying compressive creep data to the pavement design criteria. Several authors performed tensile creep tests and concluded that the time-dependent deformation characteristics of cement-stabilized soil, under applied tensile loadings, could not be estimated from specimens stressed in compression [13,20,43]. The bending test was performed on asphalt concrete and strains were measured on both sides of the specimen [94]. The result of this test was that the amount and the increasing rate of strain became considerably larger at a distance from the tensile surface. To

answer the need for the direct measurement of the tensile properties of cement-stabilized soil, the uniaxial tensile creep test was performed and analyzed in this study.

There are both differences and similarities in the creep of soil-cement and polymers. Creep in polymeric materials is usually governed by molecular chain rotation, unkinking and disentanglement. As a contrast, it has been proved by many researchers that creep in concrete is mainly controlled by the microcracking phenomenon, i.e., under tension, small preexisting flaws start to grow and coalesce to form microcracks and, eventually, macrocracks. Since most of the factors that influence creep in concrete will undoubtedly also affect the creep response of cement-treated soil, it is prudent for soil-cement researchers to ask the following questions:

- (1) What is the origin of microcracks in cement-stabilized soil?
- (2) Since microcrack propagation as well as fatigue cracking can be explained by local yielding where stresses are highly concentrated, does the creep strain rate have a unique relationship with the crack propagation rate from a fatigue test?
- (3) What kinds of compositional factors or environmental conditions influence creep results, and why do they do so?

To investigate the origin of microcracks in soil-cement, literature on soil-cement and concrete were cited, and the Scanning Electron Microscope (SEM) was used to observe the fracture surface of a soil-cement sample.

Fracture and cyclic fatigue tests were performed under a separate phase of this study. All testing was performed on the same material types. To answer the second question, a comparison of the fatigue data with the predicted crack growth from the creep test by virtue of Schapery's crack growth theory in linear viscoelastic media was made.

From the literature review, it was decided to investigate four compositional or environmental factors: cement content, curing age, relative humidity, and temperature. The effects of each factor were compared in terms of creep parameters and crack growth parameters, and the mechanism of creep under different conditions was explained separately.

#### *Literature review*

The Origin of Microcracks. The presence of microscopic cracks and the progression of internal splitting of concrete specimens in compression was first suspected by Brandtzaeg in 1929 [84]. He observed the volumetric changes of plain concrete under compression to be between 77 and 85% of the maximum load, and concluded that failure progressed by internal splitting in microscopic regions distributed throughout the material. After Brandtzaeg, many researchers developed different methods to infer the presence and development of microcracks in concrete [7 - 20]. In a remarkable study, Rusch [86] showed the interdependence of creep and cracking by means of the intensity of internal noises developed during creep loading at different percentages of ultimate strength.

Shrinkage cracking of soil-cement bases has been observed by George [30]. In his report, he claimed to have advanced a theory of cracking that states that the microcracks were initiated in the vicinity of pre-existing flaws; with increasing shrinkage stress the microcracks coalesced to form macrocracks. Under the tensile creep condition, the concentrated stress at the microcrack tip will cause the microcracks to propagate and interconnect with each other.

In 1964 Bofinger [12] disproved a widely accepted hypothesis, which was founded on the assumption that the strength of soil-cement was only dependent on the cementing action of the hydration products of the cement. He claimed that a continuous skeleton existed throughout soil-cement, and the skeleton strength depended not only on the strength of the hydrated cement particles, but also on the strength of the secondary products formed from the reaction between the lime of hydration and reactive soil silica. In the Proceedings of the International Conference on the Structure of Concrete in 1965, many researchers reported that bonds between paste or mortar and aggregate were much weaker than any of the constituents alone. These weak links might act as pre-existing stress risers [96,51,34].

Alhashimi and Chaplin [3] concluded that soil-cement consisted of:

- (1) a continuous non-rigid matrix in which sand particles and aggregated clay domains are embedded and
- (2) randomly distributed rigid inclusions of sand.

The authors reported that in the clay-sand-cement and sand-cement the sand matrix contact zones and cavities within the matrix acted as potential sources of microcracks.

Fracture surfaces of soil-cement samples were observed by means of the Scanning Electron Microscope (SEM) as a part of this study. It was concluded from the observations that

- (1) the fracture occurred in a very brittle and intergranular manner, and
- (2) fracture was due to the weak bonds between the matrix and sand particles.

Creep and Fatigue. It has been shown that Linear Elastic Fracture Mechanics (LEFM) is applicable to the investigation and determination of realistic failure criteria of fine-grained soils stabilized with Portland cement. This is due to the fact that the radius of curvature at the tip of a microcrack is small enough for the cohesive strength to be much smaller than the energy-limited strength. As long as linear elastic fracture is considered as the failure mechanism, prediction of the service life of the stabilized soil is dependent on the prediction of the crack propagation rate.

Paris and Erdogan [75] have empirically shown that an S-shaped curve on log-log paper typically represents fatigue data presented in terms of crack growth rate per cycle of loading,  $\frac{da}{dN}$ , and the fluctuation of the opening stress intensity factor,  $\Delta K_I$ . This curve has been divided into three regions and is shown in Figure 41.

Region I tells us that there is a  $\Delta K_{Ic}$  value under which no significant crack growth occurs. This  $\Delta K_{Ic}$  value is called the threshold stress intensity factor. In region III, the crack growth is catastrophic over a certain stress intensity factor which is called the critical stress intensity factor. Stable crack growth

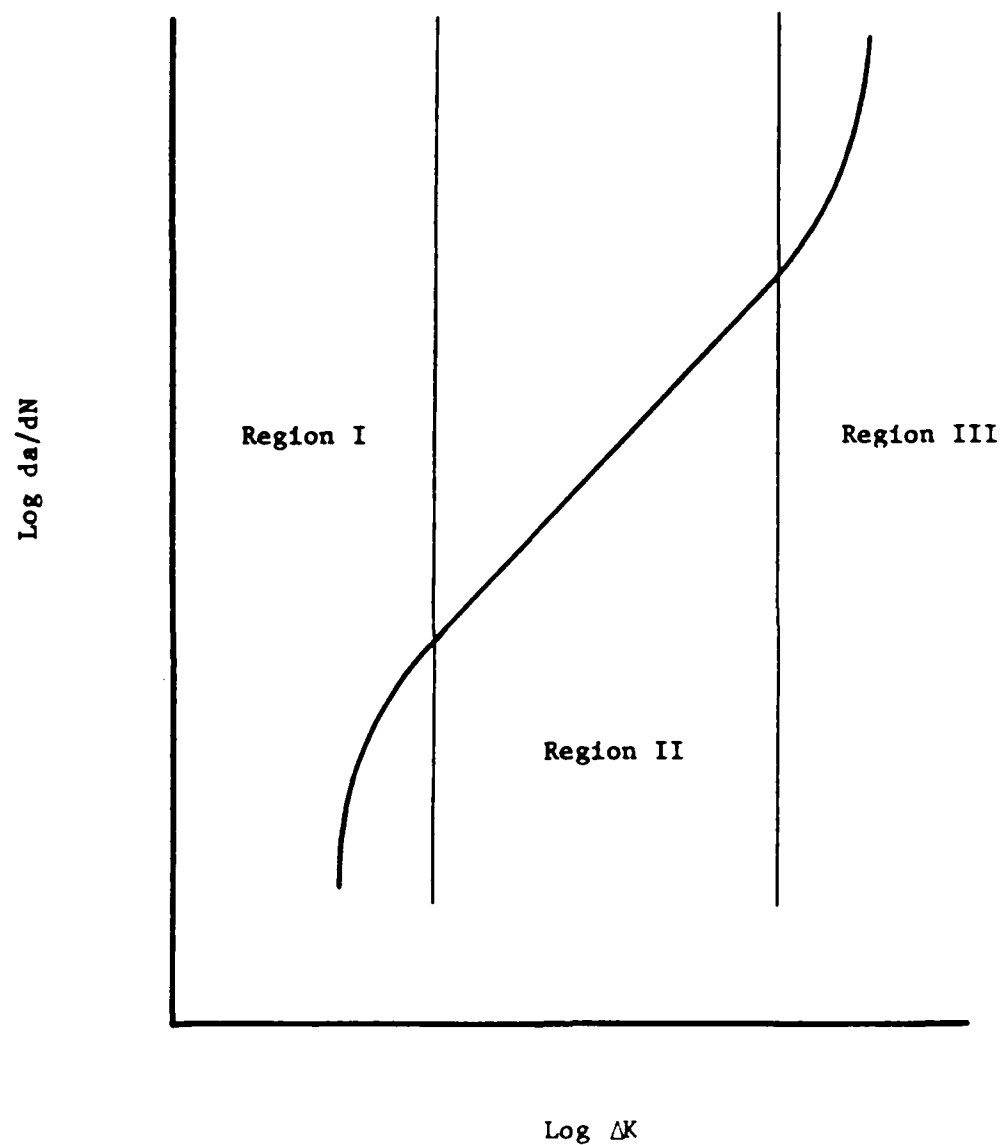


Figure 41. Schematic presentation of the fatigue curve.

occurs in region II. The straight line in this region is represented by Paris and Erdogan's power law (usually called Paris' law),

$$\frac{da}{dN} = A (\Delta K_{\max})^n$$

where A and n are regression coefficients under a certain environmental condition and a fixed load cycle shape, and  $\Delta K_{\max}$  is the amplitude of the oscillating stress intensity factor.

While this law was developed and has been proved by many researchers empirically, Schapery, in 1973, theoretically showed the relationship among the power law constants A and n and the creep parameters and material properties of viscoelastic media [90]. He started from linear elastic stress and displacement distributions and generalized to viscoelastic solutions by means of the classical correspondence principle plus Laplace transform inversion. During his derivation, he introduced two empirical power forms to represent the creep compliance as a function of time. One is the power law,  $D(t) = D_1 \times t^m$ , and the other is the generalized power law,  $D(t) = D_0 + D_2 \times t^m$ . As a result, he was able to express the crack velocity explicitly and show the crack growth parameters, A and n in Paris' law, in terms of the creep parameters and material properties. A more detailed review of his theory is presented in a later section.

Shift Variables. It has been well established that environmental conditions as well as material properties strongly influence creep in concrete and soil-cement. The wet-dry and freeze-thaw criteria have been considered especially important in deciding the proper cement content. Wang and Lee [105] investigated the effects of both

compositional and environmental factors under compressive creep conditions. The authors concluded that the creep strain was nonlinearly proportional to the creep stress and that the creep strain decreased with increasing cement content but was nearly independent of a variation in molding moisture content. In addition, they concluded that the creep strain increased with increasing clay content, and that sodium-montmorillonite exhibited the greatest creep strain. Both the tensile and compressive creep tests on concrete at different temperatures were performed by McDonald [63]. He reported that at higher temperatures creep strain was larger for both compressive and tensile loading, and the tensile creep was comparatively larger than the compressive creep. Raad and Monismith have interpreted the fatigue in soil-cement bases by using a fatigue model based on Griffith's failure criteria and a finite element program [81]. They claimed that the crack propagation rate should be considered in pavement thickness design and permitting crack propagation to the surface rather than designing only for crack initiation would yield considerably thinner design base courses. As a result, the rate of crack propagation decreased by increasing curing age and by reducing the applied load magnitude.

Recently, Mindess [68] has accomplished a comprehensive and detailed review of the application of fracture mechanics to cement and concrete. He reported from the literature review that the presence of water appeared to enhance subcritical crack growth and confirmed it experimentally [66]. In addition, it was noted that the fracture surface energy (estimated from the area under the  $\sigma$ - $\epsilon$  curve)

was less for wet than for dry specimens, and that the critical strain energy release rate,  $G_c$ , also decreased considerably as specimens were dried, particularly below 20% relative humidity. This behavior was explained in various ways, such as stress corrosion, thermodynamic approach, and so forth.

Wittmann [109] described the heterogeneous structure of concrete in terms of three different levels: micro-level, meso-level and macro-level. The structure of hardened cement paste and the interaction of the xerogel with water were considered in the micro-level. The Munich model was recommended. The Munich model introduces two terms which can be related to strength and failure of concrete:

- (1) interfacial energy of the xerogel and
- (2) disjoining pressure of adsorbed water films.

Big pores, pre-existing cracks and inclusions were introduced as the main characteristic features of the meso-level. On the macro-level the actual macroscopically observed behavior was described by means of fracture mechanics parameters.

Based on the work of Mindess and Wittmann, it is evident that the movement of water and the size and distribution of pores or cracks were the most important parameters to explain the creep or fracture behavior of cement-treated material. Wittmann [108] performed creep tests with hardened cement paste at different relative humidities. He reported that at higher humidities interlayer water and crystal water of some of the hydration products which had been lost during the drying process could be fixed again in the structure and this

process led to an increased creep deformation. Pihlajavaara [78] studied the effects of the drying rate of concrete at different relative humidities. He concluded that moisture conductivity, or the drying rate of non-carbonating concrete, increased when the ambient humidity decreased. Gillen [32] prepared two concrete specimens with either 100% or 0% initial internal moisture condition and concluded that the magnitude of creep strains of dried specimens was smaller than the strains of moist concrete at each test temperature. Ishai and Glucklich [47] subjected torsionally-loaded cylindrical specimens to cycles of drying and wetting under constant load. Any environmental transition, from dry to wet or vice versa, resulted in an increase in creep. The authors explained that cracking under drying was attributed to oriented restrained shrinkage, and cracking under wetting to the decrease in surface tension of the cement gel due to the adsorption of water.

Pretorius [80] reviewed the effects of testing conditions after extensive research on the creep behavior of concrete. He concluded from his research that the magnitude and rate of creep increased with a decrease in the relative humidity. George [28] performed a compression creep test on a soil-cement sample and concluded that, for a given soil-cement mixture, the creep was higher as relative humidity decreased. As shown above, the observations of creep at different relative humidities are somewhat contradictory.

### *Preparation of Specimens and Laboratory Testing*

Material. The material selected for this study was a silty sand. Only the portion which was finer than the No. 100 sieve was used in order to minimize heterogeneity due to large particle effects. Characteristics of the original material are listed in Table 9. The sieved soil was stored at 140° F for enough time to be completely dried before the test.

Type I portland cement passing the No. 100 sieve was used as the stabilizer. The optimum cement content was computed based on the procedures recently developed for the Air Force (Draft Manual AFM 87-6, Chapter 4-1982). Three cement contents of 5, 10 (the optimum cement content) and 15% by weight of dry soil were selected, and the optimum moisture contents were calculated from the moisture-density tests for 5% and 15% cement contents [147]. The test results are shown in Figure 42 and 43. To avoid the moisture content effect, however, 16.8% water by weight of dry soil was used for all cement contents. The densities of the different cement content samples at this moisture content were all above 95% of maximum density which is a typical specification requirement.

Preparation of Specimens. The dry soil and the correct weight of cement were pulverized thoroughly. Then the water was added to the soil-cement and mixed quickly. The addition and mixing procedure took less than two minutes, and the mixture was compacted into the mold immediately upon completion of the mixing process.

The tensile creep molds were modified from the asphalt force-ductility test specified in the American Society for Testing

Table 9. Characteristics of the material.

---

Sieve Analysis	:	100% passing U.S. #40
		47.5% passing U.S. #200
Liquid Limit	:	27.8%
Plastic Limit	:	18.9%
Plasticity Index	:	8.9%
Unified Soil Classification	:	SM

---

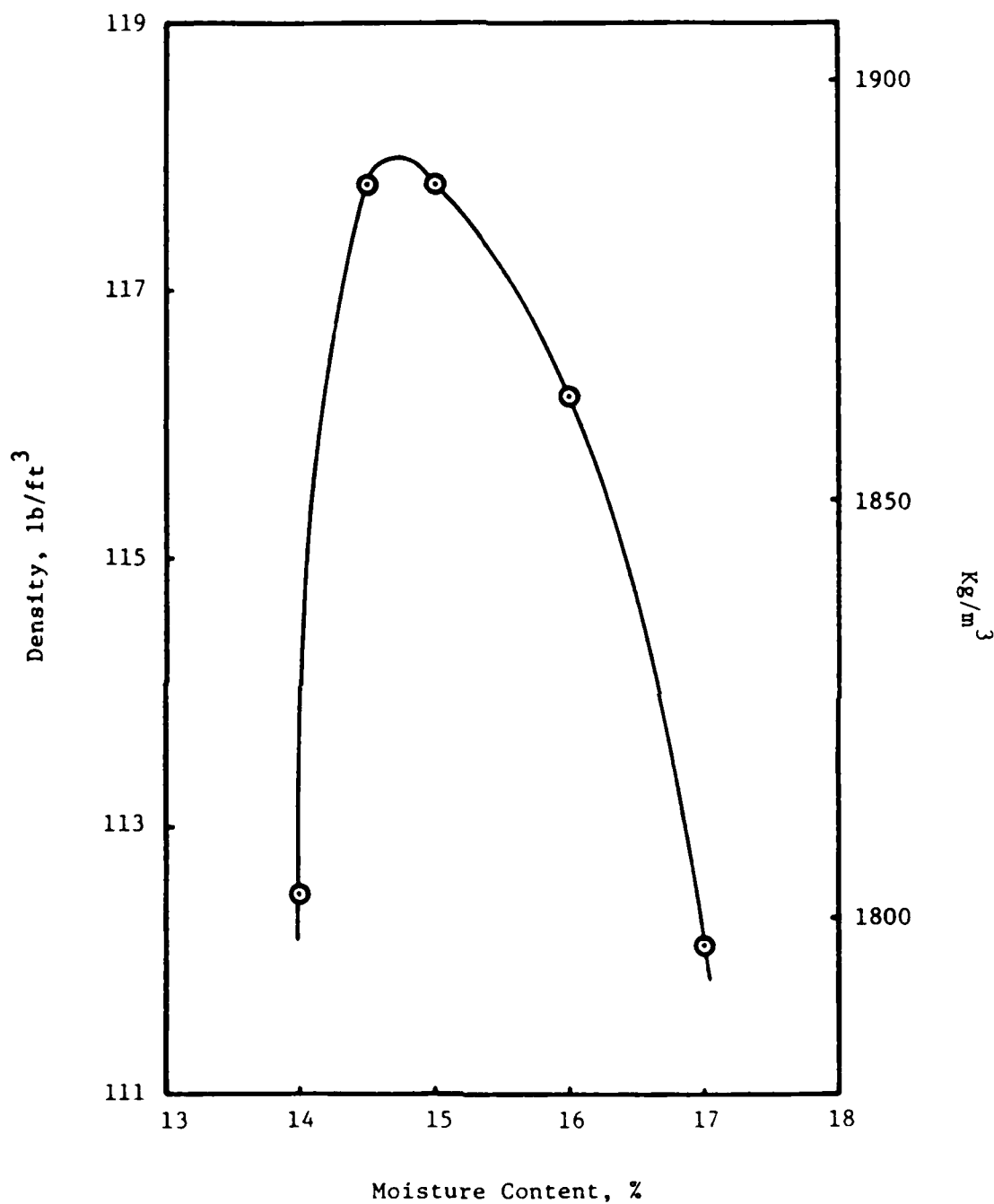


Figure 42. The moisture-density curve for 5% cement content.

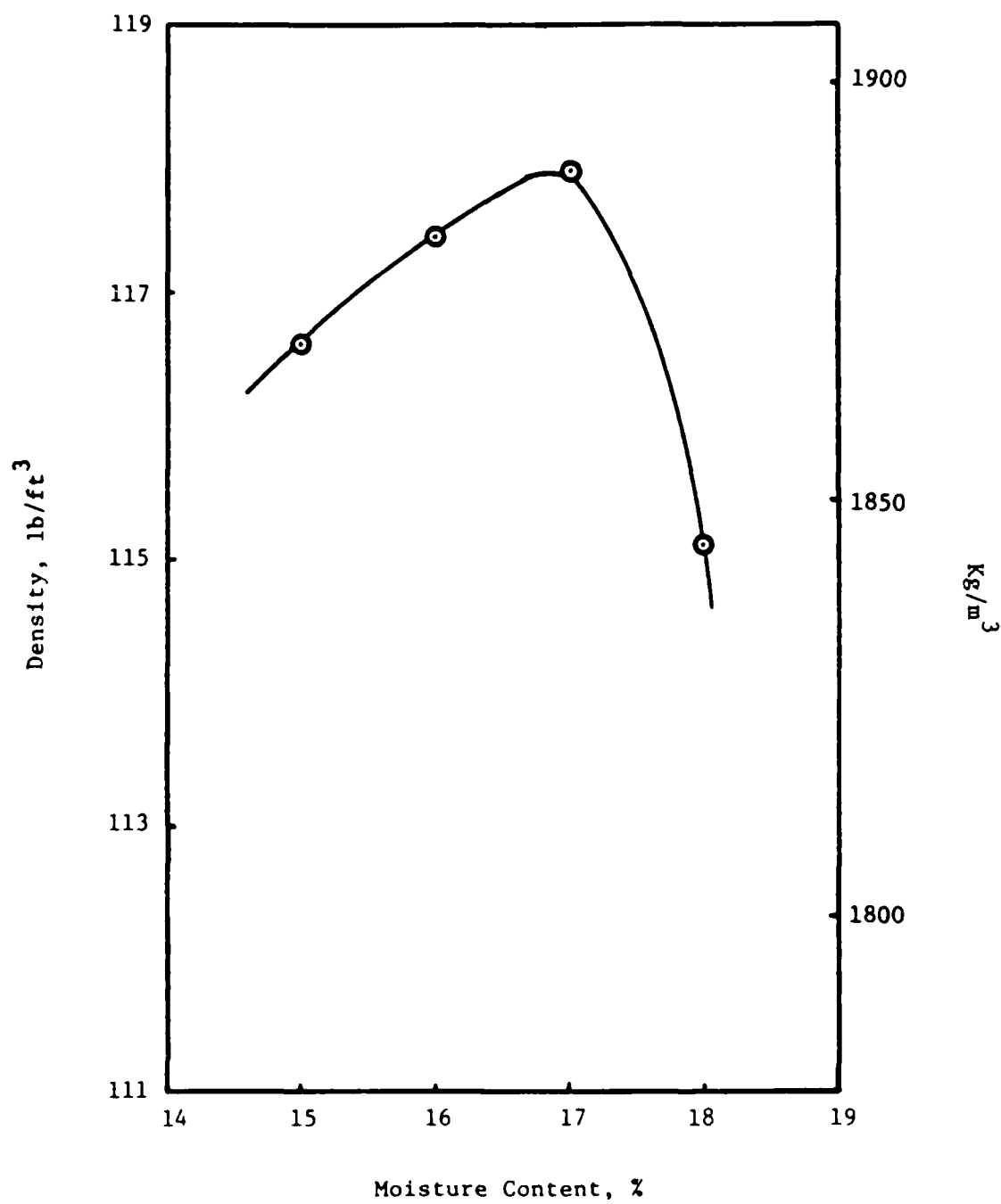


Figure 43. The moisture-density curve for 15% cement content.

and Materials (ASTM) D113. Special grips were designed to reduce the stress concentration that normally occurs in tensile samples. The size and shape of the mold are shown in Figure 44. The samples were compacted in the mold with a compactive energy equivalent to the Modified Proctor Compaction Method in the American Association of State Highway and Transportation Officials (AASHTO) T-180.

Another type of specimen was prepared, a Proctor sample 4.6 in. high and 4 in. in diameter which was used in the splitting tensile test under various conditions. The data and results for compaction of both samples are shown in Table 10.

Each sample was cured in the moist curing room (95%) for seven days to give enough hydration and minimize the carbonation effect on the sample. After this, the samples were moved to a dry curing room at 73° F and 55% relative humidity.

Testing Program. After a certain number of days of dry curing, the direct tensile creep tests were performed under a steady load at 50% of the ultimate strength for a duration of at least 30 hours.

Linear Variable Differential Transformers (LVDT) and a strip chart recorder were used to measure and record the displacement of the creep sample.

Usually, the soil-cement layer in the pavement system is not loaded critically until 7 days after compaction. After 28 days, there is no additional significant strengthening effect in the soil-cement. Therefore, curing ages of 7, 14 and 28 days were selected to simulate field conditions.



Table 10. Compactive effort calculation.

	Proctor Sample (4.6 in.×4 in. dia.)	Creep Sample
No. of Layers	5	1
No. of Blows/Layer	25	14
Weight of Hammer, Kg ( lb )	4.54 ( 10 )	4.54 ( 10 )
Drop, m ( ft )	0.46 ( 1.5 )	0.46 ( 1.5 )
Measured Volume of the Specimen, cm <sup>3</sup> ( in. <sup>3</sup> )	947.34 ( 57.81 )	105.37 ( 6.43 )
Compaction Energy per Unit Volume, Kg·m/m <sup>3</sup> ( ft·lb/ft <sup>3</sup> )	275,561 ( 56,050 )	277,476 ( 56,435 )

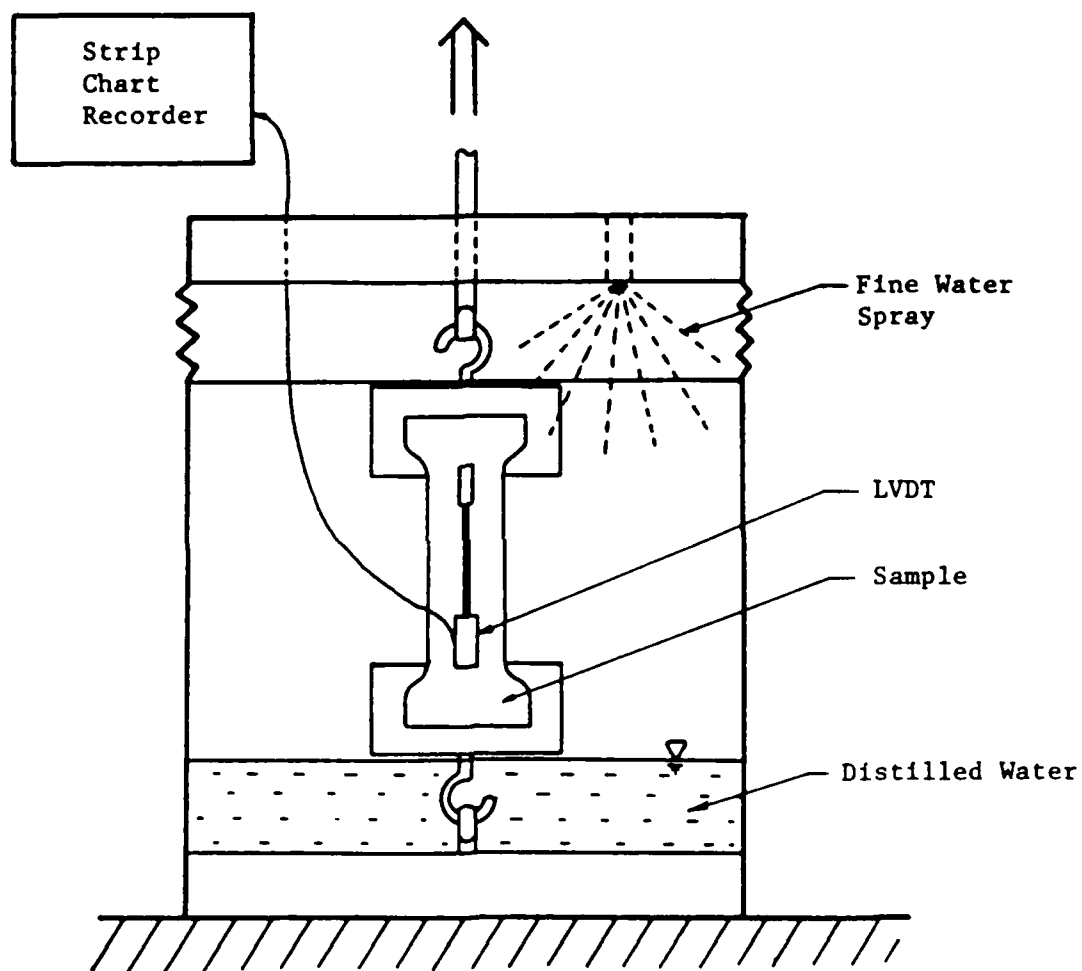


Figure 45. Schematic presentation of the humidity chamber.

Environmental conditions, temperature and relative humidity, have been isolated from each other. Since the humidity changed along with the temperature, it was very difficult to perform the test without any interaction between two variables, especially at high temperatures. Hence, the humidity chamber was designed to run the tests with various temperatures at 100% relative humidity. As shown in Figure 45, the chamber is a cylinder which has two small holes (one for the LVDT connection and the other for spraying the water) and a door. This chamber contained water at its bottom when the specimen was introduced. Then the system was sealed except for one hole through which water was sprayed for about 30 seconds to make the relative humidity inside the chamber 100%. The hole was sealed immediately after spraying. The idea was based on the definition of relative humidity. That is, assuming the chamber was perfectly sealed, the air inside the chamber would try to keep the equilibrium (100% relative humidity). Therefore, if the humidity in the chamber dropped below 100%, the water at the bottom of the chamber would evaporate and satisfy the equilibrium state. To be sure of perfect sealing, the water level was checked before and after the test. There was no significant change in the water levels, while the same amount of water set outside the chamber evaporated completely during the test period.

The environmental rooms with 100% RH were also used to perform the creep tests at 33° F and 73° F. The data from the humidity chamber and the environmental rooms were very close.

After it was concluded that the temperature per se did not make a big difference above the freezing point, the low humidity tests were performed in a 104° F environmental room. Measured humidity was 35%. The data from these tests were compared with those from a 73° F room with a dehumidifier. Again, the results were close enough to neglect the temperature effects on the creep. The relative humidity of the 73° F environmental room was 55%. Therefore, three levels of relative humidities were observed in this study, 35%, 55% and 100%.

The effects of temperature and humidity were evaluated by performing creep tests on specimens which were subjected to a specific temperature and humidity condition. This condition was maintained throughout the test and was begun six hours before testing. The detailed test schedule is shown in Table 11.

The indirect tensile test was performed on the samples which had been kept at the same conditions as the creep samples. The tensile strengths of the soil-cement samples at different conditions were determined using the indirect tensile test. This test employs an indirect method of measuring mixture strength. A cylindrical specimen is loaded diametrically at a constant rate of deformation until complete failure occurs. Diametral deformation perpendicular to the loaded plane is usually monitored in order to quantify mixture stiffness. The tests were conducted with a deformation rate of 0.05 inch per minute.



### *Governing Equations and Method of Analysis*

The ability to predict the fatigue life of a pavement layer is greatly dependent upon an ability to measure the crack velocity under a certain condition. As a means of accomplishing this goal, Schapery's crack growth theory of linear viscoelastic material [90] was studied. This section introduces the pertinent equations of Schapery's crack velocity model and the method of analyzing the creep data by means of this model.

Governing Equations. Schapery assumed Barenblatt's crack tip model and divided the material in a small neighborhood surrounding the crack tip into two regions as shown in Figure 46: (i) a failure zone where disintegration and eventual failure occur and (ii) a linearly viscoelastic, macroscopically homogeneous and isotropic continuum with inertial effects excluded.

With the elastic solutions of stress and displacement near the crack tip, he explained the failure zone size,  $a$ , as

$$a = \frac{\pi K_I^2}{2 \sigma_m^2 I_1^2} \quad (66)$$

where  $K_I$  is the stress intensity factor for the opening mode,  $\sigma_m$  is the maximum tensile stress inside the failure zone, and  $I_1$  is the dimensionless integral,

$$I_1 = \int_0^1 \left[ f(a\eta)/\eta^{\frac{1}{2}} \right] d\eta$$

( $\eta$  and  $f$  are a normalized coordinate and normalized failure stress distribution in the failure zone, respectively).

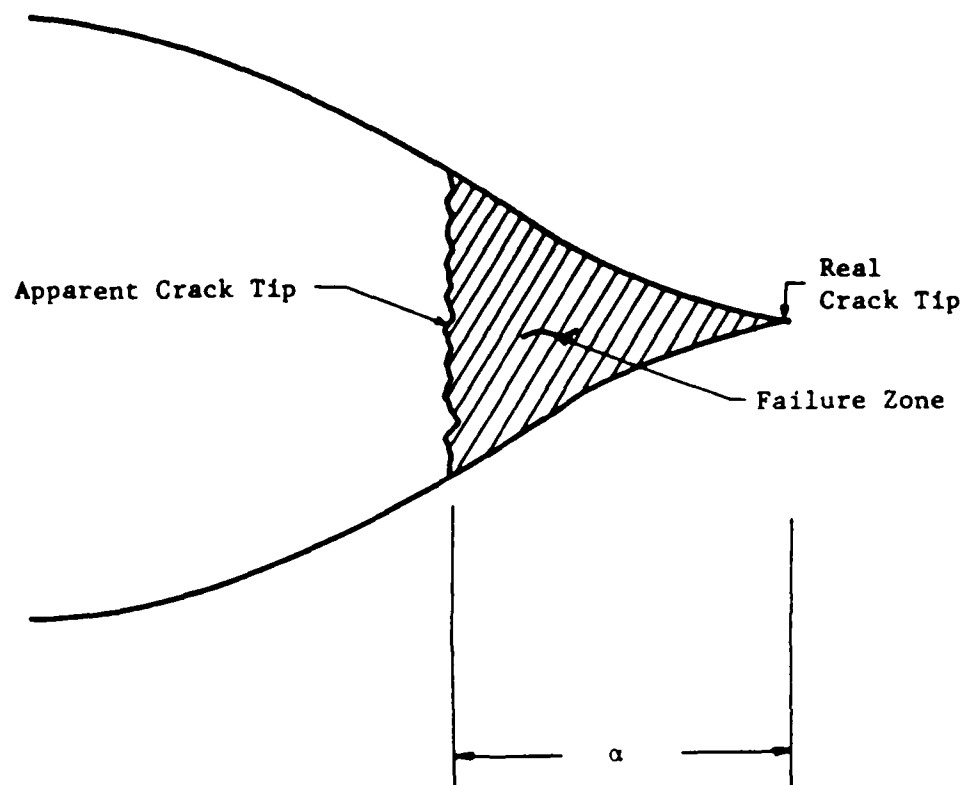


Figure 46. Barenblatt's crack tip model.

Then he applied the classical correspondence principle and Laplace transform inversion to the elastic stress and displacement distributions to achieve the viscoelastic solutions. He defined the function  $C_v(t)$  in the solution as a plane-strain creep compliance denoted as

$$C_v(t) = 4(1 - \nu^2)D(t) \quad (67)$$

where  $\nu$  is Poisson's ratio and  $D(t)$  is the uniaxial tensile creep compliance.

He claimed that a log-log plot of creep compliance has small curvature over most, if not all, of its range of variation. The power law was adopted to represent creep compliance;

$$C_v(t) = C_1 t^m \quad (68)$$

where  $m$  is the log-log slope of the creep compliance and  $C_1$  is the value of the compliance where the tangent line intercepts the  $\log t = 0$  axis.

In order to substitute the viscoelastic compliance into the elastic solution, he introduced the effective time parameter,  $\tilde{t}$ , which represented an equivalent time to give the same compliance for time-dependent rather than immediate behavior of the material. The correction factor,  $\lambda_m^{\frac{1}{m}}$ , was used to express the effective time of viscoelastic crack growth. Recognizing that the time taken for the elastic crack tip to move a distance  $a$  (failure zone size) was equal to  $a/\dot{a}$ , the effective time for the viscoelastic case could be

obtained from:

$$\tilde{t}_a = \lambda_m \frac{1}{a} \frac{a}{\dot{a}} \quad (69)$$

where  $\dot{a}$  is the crack velocity,  $m$  is the log-log slope of the creep compliance curve and

$$\lambda_m = \frac{3\pi \Gamma(m+1)}{4(m+1.5) \Gamma(m+1.5)}$$

where  $\Gamma(m)$  is the Gamma function:

$$\Gamma(m) = \int_0^\infty t^{m-1} e^{-t} dt.$$

He also evaluated the fracture energy,  $\Gamma$ , which is the work done on a material to increase the surface area of the material a unit area, and concluded that

$$C_v(\tilde{t}_a) = \frac{8 \Gamma}{K_1^2} \quad (70)$$

By combining the equations (66) - (70), he expressed the crack tip velocity,

$$\frac{da}{dt} = \left\{ \frac{(1 - \nu^2) D_1 \lambda_m}{2 \Gamma} \right\}^{\frac{1}{m}} \frac{\pi K_I^{2(1+1/m)}}{2 \sigma_m^2 I_1^2} \quad (71)$$

To prove that this equation was consistent with Paris' law, Schapery introduced the weighting function  $W(t)$  which defines the wave shape of the stress intensity factor,

$$W(t) = \frac{K_I}{\Delta K_{max}} \quad (72)$$

where the maximum value of stress intensity factor during a cycle,  $\Delta K_{\max}$ , may vary from cycle-to-cycle.

The shape of the stress intensity factor was a haversine which could be expressed as

$$W(t) = \sin \frac{2\pi t}{T} \quad (73)$$

where  $T$  is one cycle of the sine wave.

If equation (72) is substituted into equation (71) and separation of variables is completed, then the following equation results:

$$\begin{aligned} \int_a^{a+\Delta a} da &= \Delta a = \frac{da}{dN} \\ &= \frac{\pi}{2 \sigma_m^2 I_1^2} \left\{ \frac{(1 - \nu^2) D_1 \lambda_m}{2 \Gamma} \right\}^{\frac{1}{m}} \int_0^{\Delta t} W(t)^{2(1+1/m)} dt \times (\Delta K_{\max})^{2(1+1/m)} \end{aligned} \quad (74)$$

where  $\Delta t$  is half of  $T$ .

Now, the crack growth parameters,  $A$  and  $n$ , can be expressed as:

$$A = \frac{\pi}{2 \sigma_m^2 I_1^2} \left\{ \frac{(1 - \nu^2) D_1 \lambda_m}{2 \Gamma} \right\}^{\frac{1}{m}} \int_0^{\Delta t} W(t)^{2(1+1/m)} dt \quad (75)$$

$$\text{and } n = 2(1 + \frac{1}{m}). \quad (76)$$

However, equation (74) has adopted the power law which is good for materials with very small elastic strain. If the elastic strain is relatively large, the generalized power law,  $D(t) = D_0 + D_2 t^m$ , fits the creep compliance data much better. The crack velocity equation (74) was modified by means of the generalized power law. That is, the generalized power law,

$$C_v(t) = C_0 + C_2 t^m \quad (77)$$

replaced

$$C_v(t) = C_1 t^m$$

and another crack velocity equation was developed in terms of equations (66), (67), (69), (70) and (77). During his derivation, Schapery introduced the glassy critical stress intensity factor,  $K_{Ig}$ , which was represented as

$$K_{Ig} \approx \frac{8 \Gamma}{C_v(0)} \quad (78)$$

where  $C_v(0) \equiv C_0$ .

Then the crack velocity was rewritten as

$$\frac{da}{dt} = \frac{\pi}{2} \left[ \frac{(1 - \nu^2) D_2 \lambda_m}{2\Gamma \{1 - (K_I/K_{Ig})^2\}} \right]^{\frac{1}{m}} \times \frac{K_I^{2(1+1/m)}}{\sigma_m^2 I_1^2} \quad (79)$$

The above equation can be modified by the aid of equations (72) and (73) as :

$$\frac{da}{dN} = \int_0^{\Delta t} \frac{\pi}{2} \left[ \frac{(1 - \nu^2) D_2 \lambda_m}{2\Gamma \left\{1 - \left(\frac{\Delta K_{max} \sin(2\pi t/T)}{K_{Ig}}\right)^2\right\}} \right]^{\frac{1}{m}} \times \frac{\{\Delta K_{max} \sin(2\pi t/T)\}^{2(1+1/m)}}{\sigma_m^2 I_1^2} dt \quad (80)$$

To simplify this equation, determination of the parameters was needed. The parameter  $\lambda_m^{\frac{1}{m}}$  is dependent only on  $m$  and  $\lambda_m^{\frac{1}{m}} \approx 1/3$  for  $0 \leq m \leq 1$ .  $I_1$  is the integral measure of the shape of the stress distribution in the failing material, and the value is dependent on the shape of stress-strain curve. Usually,  $I_1$  falls between 1 and 2,

and 1.5 will be used throughout this analysis.

The term  $K_{I\Gamma}$  was introduced earlier in terms of the elastic compliance,  $C_0$ , and the fracture energy,  $\Gamma$ . The glassy critical stress intensity factor is normally larger than the critical stress intensity factor; however, for brittle materials like soil-cement, we can approximate the  $K_{I\Gamma}$  by  $K_{IC}$ . This is more desirable than using the definition of  $K_{I\Gamma}$  in this analysis, since the initial movement at the interface between the sample and the mold might result in larger immediate displacement.

For the purpose of this study,  $\nu$  is equal to 0.15,  $T$  is equal to 2 seconds, and  $\Delta t$  is 1 second. This is because the cyclic fatigue test was performed at 1 second/cycle.

Now equation (80) can be simplified as

$$\frac{da}{dN} = \Delta a = \int_0^1 \frac{\pi}{13.5} \left[ \frac{0.9775 D_2}{2\Gamma \left\{ 1 - \left( \frac{\Delta K_{\max} \sin \pi t}{K_{IC}} \right)^2 \right\}} \right]^{\frac{1}{m}} \times \frac{(\Delta K_{\max} \sin \pi t)^{2(1+1/m)}}{\sigma_m^2} dt \quad (81)$$

which is the principal equation in this study to predict the crack growth based on the generalized power law.

Method of Analysis. Assuming that the creep compliance parameters ( $D_2$  and  $m$ ),  $\Gamma$  and  $\sigma_m$  are constant, or at least a very weak function of time, one may be mathematically able to integrate equation (81) by means of the partial fraction integration technique. However, this exact solution will be very cumbersome. Instead of using the mathematical integration technique, a numerical integration program based on Simpson's rule was used to obtain the  $\frac{da}{dN}$  values corresponding to a series of  $\Delta K_{\max}$  values. That is, obtaining  $D_2$ ,  $m$ ,

$\Gamma$ ,  $K_{IC}$  and  $\sigma_m$  at a certain condition, one can insert an arbitrary  $\Delta K_{max}$  value into the equation, integrate the equation over  $t$ , and evaluate the crack velocity corresponding to that specific  $\Delta K_{max}$ . By repeating this step in the reasonable region of  $\Delta K_{max}$ , one can achieve a series of  $\frac{da}{dN}$  at different  $\Delta K_{max}$  values. The typical shape of  $\log \frac{da}{dN}$  vs.  $\log \Delta K_{max}$  curve from this method is shown in Figure 47. This plot is generated in the region of  $0.5K_{IC} \leq \Delta K_{max} \leq K_{IC}$ . Notice that, from equation (79) and Figure 47, the crack velocity goes to infinity as  $\Delta K_{max}$  approaches  $K_{IC}$ , which simulates the fracture behavior in region III of the fatigue curve. However, Paris' law is only valid in region II.

Therefore, the range of  $\Delta K_{max}$  should be determined to fit the linear regression between  $\log \frac{da}{dN}$  and  $\log \Delta K_{max}$ . From the cyclic fracture test, it has been found that under 45-50% of  $K_{IC}$  there is no significant crack growth observed in the soil-cement. Also, above 80-90% of  $K_{IC}$ , the crack growth is unstable. Therefore, only the points between  $0.5K_{IC}$  and  $0.75K_{IC}$  were considered in the development of the linear regression model.

Determination of Material Properties. In order to use the numerical integration method, several material properties should be quantified. These parameters are  $D_2$ ,  $m$ ,  $\Gamma$ ,  $K_{IC}$  and  $\sigma_m$ .  $D_2$  and  $m$  are determined from the creep test. If it is assumed that the failure stress distribution is constant,  $\sigma_m$  can be obtained from equation (1) by knowing  $K_I$  and  $a$ . However, the measurement of the failure zone size,  $a$ , is very difficult. In this study, the tensile strength from the indirect tensile test was used as an approximate estimation of

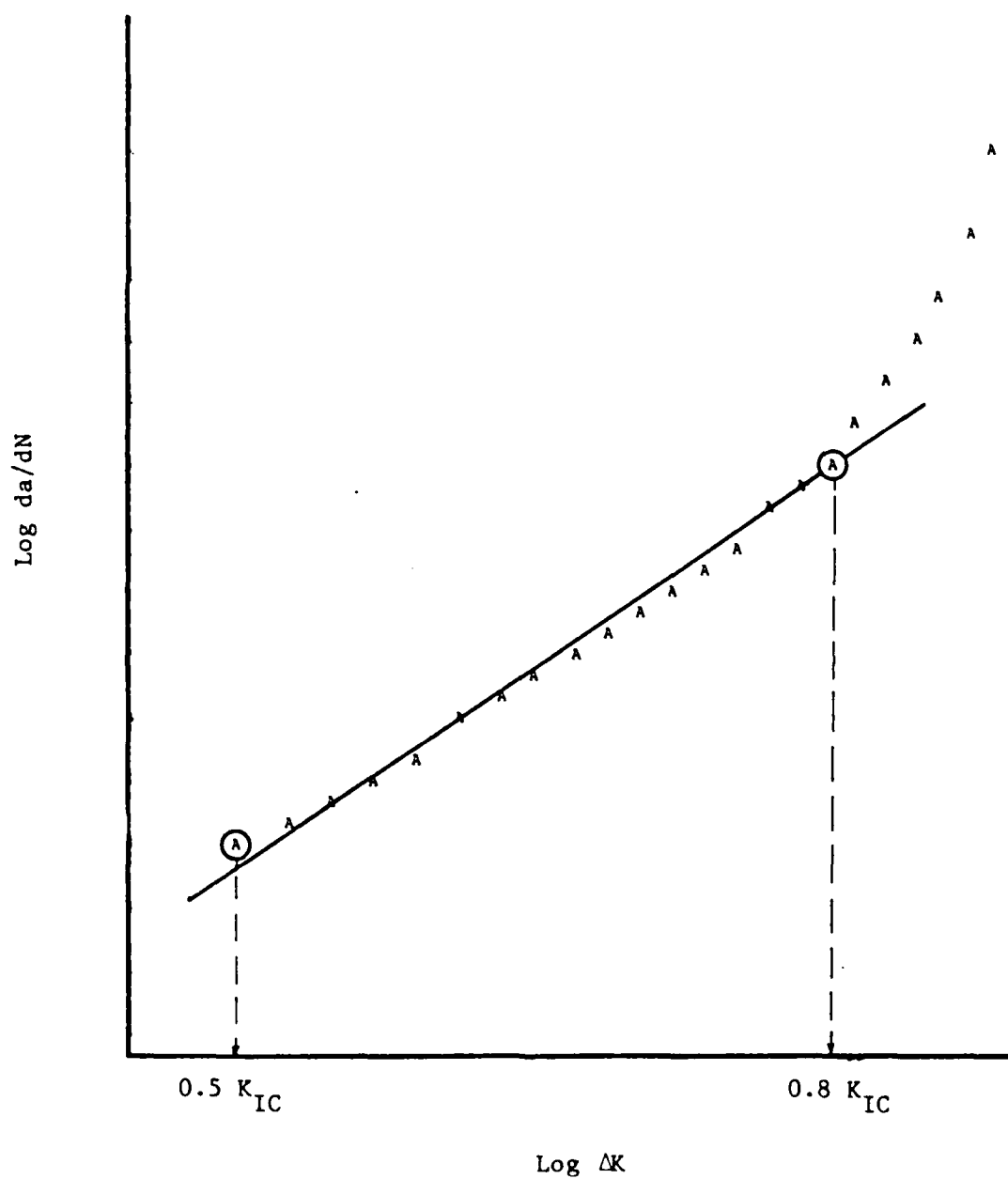


Figure 47. Predicted fatigue curve from Schapery's theory.

$\sigma_m$ .

Fracture energy ( $\Gamma$ ) and the critical stress intensity factor ( $K_{IC}$ ) can be obtained from the static fracture test. Previous chapters have reported the fracture properties of the material used in this research at different cement contents and curing ages. The stress intensity factor,  $K_{IC}$ ; energy per unit area of crack extension, the J-integral,  $J_{IC}$ ; and the fatigue parameters were reported in those chapters. Since the fracture energy was defined as the work done on a material to increase the surface area of the material per unit area, and after a unit crack extension, two crack surfaces are created, the  $\Gamma$  value at each cement content was obtained by dividing  $J_{IC}$  by two.

However, the direct measurement of the fracture parameters at various temperatures and humidities is very tedious and expensive, so the ability to predict these parameters over a range of humidity and temperature conditions is highly desirable.

#### ( 1 ) Fracture Energy, $\Gamma$

Setzer [95] used the "thermodynamic approach" and interpreted his sorption data by means of the Griffith energy equation. He proposed that strength changes could be related to changes in the surface free energy by

$$(\sigma/\sigma_0)^2 = 1 - (\Delta\Gamma/\Gamma_0) = \Gamma/\Gamma_0$$

where  $\sigma_0$  = strength at saturation,

$\Gamma_0$  = surface free energy at saturation,

$\sigma$  = the strength at a given relative humidity,

$\Delta\Gamma$  = the corresponding change in surface free energy, and

$\Gamma$  = the surface free energy at a given relative humidity.

Applying the above relation at relative humidities of 35% and 55% results in:

$$\left( \frac{\sigma_{35\%}}{\sigma_0} \right)^2 = \frac{\Gamma_{35\%}}{\Gamma_0} \quad (82)$$

$$\left( \frac{\sigma_{55\%}}{\sigma_0} \right)^2 = \frac{\Gamma_{55\%}}{\Gamma_0} \quad (83)$$

where  $\sigma_{35\%}$  and  $\Gamma_{35\%}$  are the strength and the fracture energy at 35% relative humidity, and  $\sigma_{55\%}$  and  $\Gamma_{55\%}$  are the respective values at 55% relative humidity.

Dividing the equation (82) by the equation (83) yields

$$\left( \frac{\sigma_{35\%}}{\sigma_{55\%}} \right)^2 = \frac{\Gamma_{35\%}}{\Gamma_{55\%}}$$

Since it is easy to measure the strengths at 35% and 55% relative humidity, and the fracture energy at 55% relative humidity has already been measured from the fracture test, the fracture energy at 35% relative humidity can be predicted from this equation. For the high relative humidity, however, Wittmann [109] claimed that this equation was not valid because the action of disjoining pressure could not be neglected and therefore additional weakening of the structure had to be anticipated.

Another way of evaluating the fracture energy was reported by Molenaar [69]. He tried to express the fracture energy in terms of the material properties which could be obtained more easily, such as the elastic modulus, tensile strength and a fatigue exponent. Having studied several equations, he decided that best estimates for  $\Gamma$  could be obtained from

$$\log \Gamma = \text{linear function of } \log (E \cdot \sigma_m \cdot n)$$

where  $n$  = exponent of the crack growth law,

$\sigma_m$  = tensile strength of the material at a certain condition and

$E$  = stiffness modulus of the material at a certain condition.

This linear relationship between  $\log \Gamma$  and  $\log E \cdot \sigma_m \cdot n$  could be checked at different cement contents and curing ages. The tensile strength,  $\sigma_m$ , can be measured by the indirect tensile test. The fatigue exponent,  $n$ , was calculated by means of Schapery's equation. The elastic modulus,  $E$ , was obtained from the relationship between the fracture parameters,  $K_{IC}$  and  $J_{IC}$ . Assuming the linear elastic case,  $J_{IC}$  is identical to  $G_{IC}$  and can be calculated from

$$G_{IC}^2 = \frac{K_{IC}^2}{E} (1 - \nu^2).$$

Measuring  $K_{IC}$  and  $J_{IC}$  from the fracture test, the elastic modulus was calculated. Then, linear regression techniques were used to achieve  $\log \Gamma$  and  $\log E \cdot \sigma_m \cdot n$ . The resulting equation was

$$\log \Gamma = - 3.932 + 0.259 \times \log E \cdot \sigma_m \cdot n$$

with  $R^2 = 0.969$ .

In order to use the Molenaar's equation to predict the fracture energy at different temperatures and humidities, the determination of  $\sigma_m$ ,  $n$ , and  $E$  was required. While  $\sigma_m$  could be measured at different conditions satisfactorily through the indirect tensile test, the determination of  $E$  was a different matter. Although  $E$  can be measured by the indirect tensile test, the heterogeneity of the material, the inaccuracy of measurement of deformation, and the irregular development of shrinkage cracks during curing period result in the inconsistent measurement of the failure strain and consequently, the elastic modulus.

In this research, Molenaar's equation was modified; that is, the inverse of the creep recovery compliance from the immediate unloading,  $\frac{1}{D_r}$ , and the inverse of the creep exponent,  $\frac{1}{m}$ , replaced  $E$  and  $n$ , respectively. As a result, a relationship between  $\log \Gamma$  and the parameters  $D_r$ ,  $m$  and  $\sigma_m$  of the form

$$\log \Gamma = -4.689 + 0.369 \log \left( \frac{1}{D_r} \cdot \frac{1}{m} \cdot \sigma_m \right)$$

was obtained with  $R^2 = 0.906$ . The fracture energy varied only from 0.018 - 0.025 in.lb./in.<sup>2</sup> for 10% cement content samples at various curing ages. Due to the insensitivity of the fracture energy on equation (81), this approximation was satisfactory enough for different temperature and humidity conditions.

( 2 ) Critical Stress Intensity Factor,  $K_{IC}$

It has been shown in Chapter II that the source of toughness of soil-cement is in the stress to failure rather than in the strain to failure. The possible stress-strain behavior of soil-cement was shown in Figure 48.

Based on this observation,  $K_{IC}$  vs.  $\sigma_m$  was plotted at different cement contents and curing ages (see Figure 49). The tensile strengths at different temperatures and humidities were measured, and  $K_{IC}$ 's at those conditions are predicted based on the curve from Figure 49.

Creep Index and Crack Speed Index. In order to compare the creep data and predicted fatigue results for different conditions, two indices are introduced: creep index and crack speed index.

#### (1) Creep Index

The generalized power law,  $D(t) = D_0 + D_2 t^m$ , can be divided into time-independent term,  $D_0$ , and time-dependent term,  $D_2 t^m$ . The "normalized compliance" which is defined as  $(D(t) - D_0)$  is used to obtain the regression coefficients,  $D_2$  and  $m$ .

It should be noted that the important factor determining the increasing rate of creep compliance is not only  $m$  but also  $D_2$ . Both terms,  $D_2$  and  $m$ , should be compared at the same time in order to analyze the creep data at different conditions. The creep index was introduced for this purpose and is defined as the slope of the creep compliance curve at  $t = 20000$  seconds. Therefore, the creep index can be determined from

$$D'(20000) = (D_0 + D_2 t^m)'_{t=20000} = D_2 \cdot m (20000)^{m-1}$$

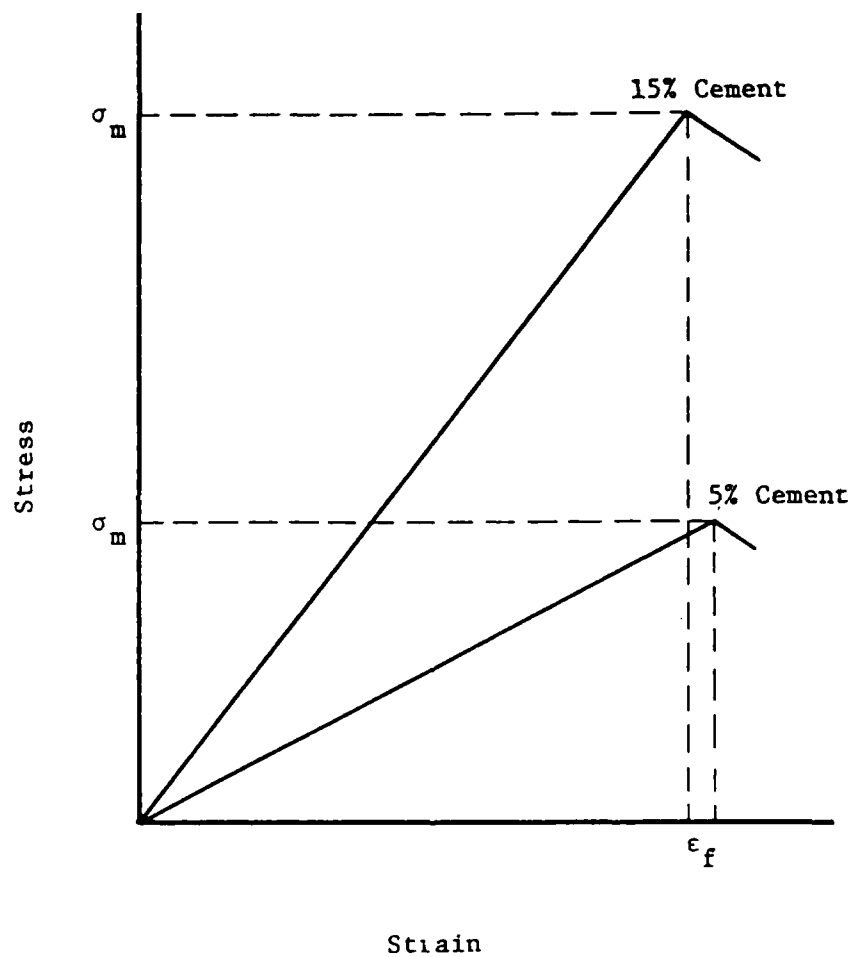


Figure 48. Possible stress-strain behavior of soil-cement.

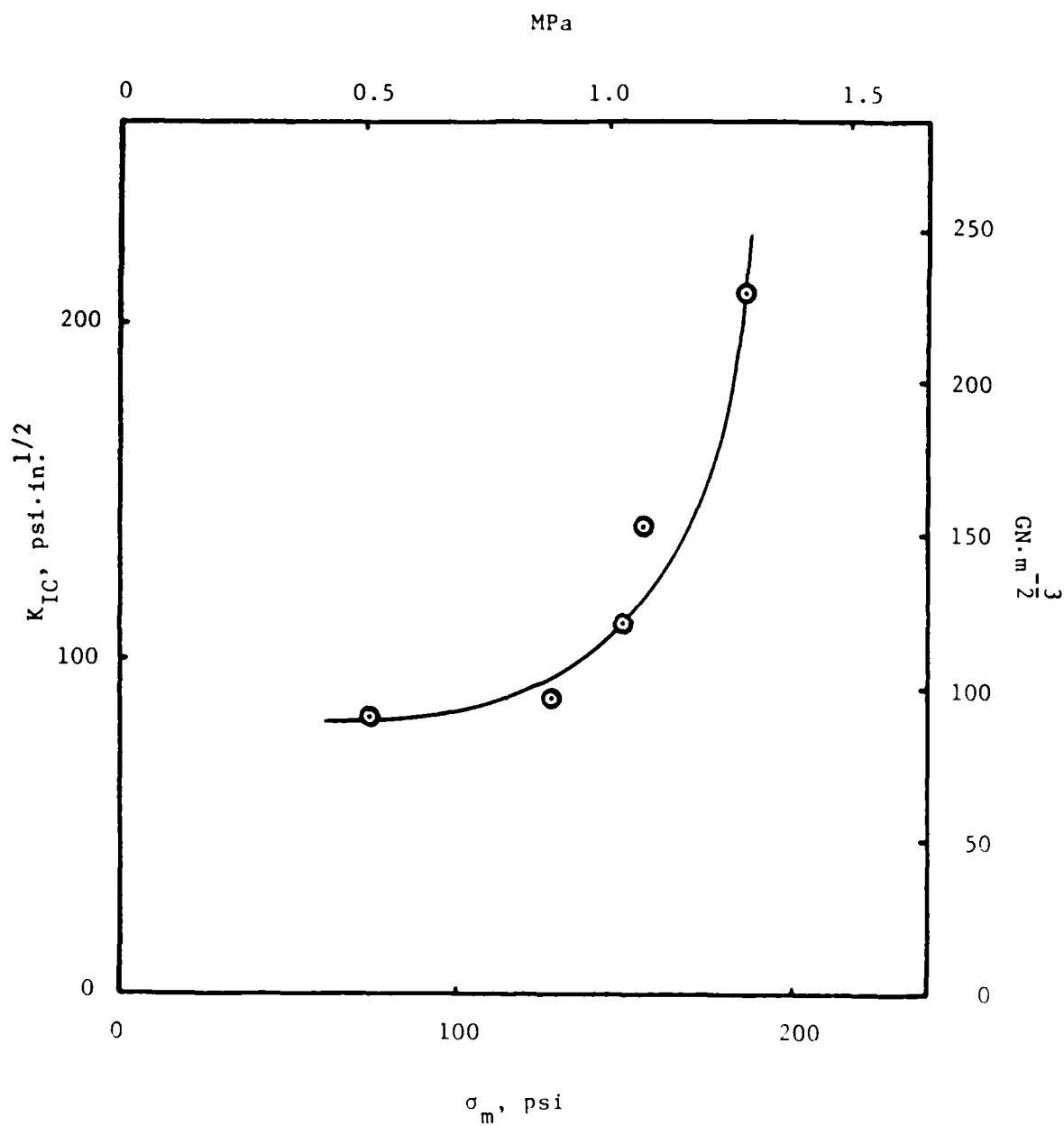


Figure 49.  $K_{IC}$  vs.  $\sigma_m$  at different cement contents and curing ages.

## (2) Crack Speed Index

In order to evaluate the fatigue life of a material by virtue of Paris' power law, one should consider two regression coefficients, A and n. If  $\Delta K_{\max}$  in equation (81) is much smaller than  $K_{IC}$ , equation (81) is essentially identical to equation (74) based on the power law. Therefore, it was expected that the calculated A and n from the numerical integration and regression analysis would have forms similar to equation (75) and (76), but different coefficients. Indeed, the regression analysis between the predicted n from equation (81) and measured  $\frac{1}{m}$  shows that  $n = 1.727 + 3.375 \times \frac{1}{m}$  with  $R^2 = 0.998$ . From the observation of equation (75), since the term  $\left\{ \frac{(1 - \nu^2) D_1 \lambda_m}{2 \Gamma} \right\}$  is much smaller than 1, an increase in the exponent,  $1/m$ , results in the decrease of the A value. Meanwhile, from equation (76), n increases as  $\frac{1}{m}$  increases. Consequently, as A gets smaller, n becomes larger, which makes it hard to compare the crack growth rates by evaluating only one parameter. Here, the crack speed index is introduced. Taking the logarithm from both sides of Paris' law yields

$$\log \frac{da}{dN} = \log A + n \log (\Delta K_{\max}).$$

By selecting a reasonable number of  $\log (\Delta K_{\max})$  during crack propagation, the crack growth rates in terms of  $\log A$  and n can be evaluated. From the observation of the  $K_{IC}$  values at different conditions, 2 was selected as the value of  $\log (\Delta K_{\max})$ . Now the crack speed index,  $CSI_1$ , is determined from

$$CSI_1 = \log A + 2.0 \cdot n.$$

### *Discussion of Results*

The creep under different environmental or compositional factors is discussed in this section. The creep behavior of soil-cement can be explained in terms of:

- (1) density and strength of cementitious interparticle bonds,
- (2) development of pores and cracks in the structure, e.g. shrinkage cracks and
- (3) movement of the moisture in the system.

Primarily, long term time-dependent deformation was analyzed by the effects of different levels of water in the system on the intrinsic microcrack propagation.

The creep data and the material properties were used to predict the fatigue parameters,  $A$  and  $n$ . The fatigue behavior at different conditions were compared in terms of these parameters and explained by means of moisture effects and interparticle bond effects on the preexisting crack propagation.

The average values of the creep parameters, the material properties, the predicted fatigue parameters, creep index, and crack speed index are listed in Tables 12, 13, 14 and 15, and the individual test values are presented in Appendix VI.

Cement Content. The effects of varying the cement content can be explained by the stiffness modulus change due to the density of cementitious interparticle bonding. That is, a larger amount of cement will give more interparticle bonds, higher stiffness and higher strength. It has been observed visually from the fracture test specimens that the fracture occurs in a brittle, intergranular

Table 12. Creep and indirect tensile test results and predicted fatigue parameters at different cement contents.

	5 %	10 %	15 %
$D_2 ( \times 10^{-7} )$	8.94	3.91	2.10
$m$	0.177	0.143	0.177
Creep Index ( $\times 10^{-11}$ )	4.57	1.15	1.07
$\sigma_m$ , MPa ( psi )	0.517 ( 75 )	1.069 ( 155 )	1.283 ( 186 )
$\Gamma$ , J/m <sup>2</sup> ( in.lb/in. <sup>2</sup> )	2.749 ( 0.01567 )	4.260 ( 0.02428 )	6.244 ( 0.03559 )
$K_{IC}$ , MN·m <sup>-3/2</sup> ( psi·in. <sup>1/2</sup> )	92,088 ( 83.8 )	152,308 ( 138.6 )	230,000 ( 209.3 )
$A$	$5.42 \times 10^{-43}$	$8.12 \times 10^{-59}$	$1.45 \times 10^{-53}$
$n$	20.67	25.28	21.24
Crack Speed Index	-0.93	-7.53	-10.36

NOTE : Tests are performed on the 28 days cured samples at 73°F and 55% relative humidity.

Table 13. Creep and indirect tensile test results and predicted fatigue parameters at different curing ages.

	7 days	14 days	28 days
$D_2 ( \times 10^{-7} )$	3.00	3.47	3.91
$m$	0.294	0.206	0.143
Creep Index ( $\times 10^{-11}$ )	8.11	2.75	1.15
$\sigma_m$ , MPa ( psi )	0.883 ( 128 )	1.028 ( 149 )	1.069 ( 155 )
$\Gamma$ , J/m <sup>2</sup> ( in.lb/in. <sup>2</sup> )	3.289 ( 0.01875 )	4.246 ( 0.02420 )	4.260 ( 0.02428 )
$K_{IC}$ , MN·m <sup>-3/2</sup> ( psi·in. <sup>1/2</sup> )	96,593 ( 87.9 )	121,868 ( 110.9 )	152,308 ( 138.6 )
$A$	$1.10 \times 10^{-30}$	$7.26 \times 10^{-43}$	$8.12 \times 10^{-59}$
$n$	13.30	18.41	25.28
Crack Speed Index	-3.35	-5.32	-7.53

NOTE : Tests are performed on the samples with 10% cement at 73°F and 55% relative humidity.

Table 14. Creep and indirect tensile test results and predicted fatigue parameters at different relative humidities.

	35 %	55 %	100 %
$D_2 ( \times 10^{-7} )$	3.87	3.00	4.04
m	0.313	0.294	0.307
Creep Index ( $\times 10^{-11}$ )	13.44	8.11	12.97
$\sigma_m$ , MPa ( psi )	0.986 ( 143 )	0.883 ( 128 )	0.773 ( 112 )
$\Gamma$ , $J/m^2$ ( in.lb/in. <sup>2</sup> )	3.686 ( 0.02101 )	3.289 ( 0.01875 )	3.163 ( 0.01803 )
$K_{IC}$ , $MN \cdot m^{-3/2}$ ( psi $\cdot$ in. <sup>1/2</sup> )	114,286 ( 104.0 )	96,593 ( 87.9 )	89,011 ( 81.0 )
A	$3.48 \times 10^{-29}$	$1.10 \times 10^{-30}$	$8.25 \times 10^{-29}$
n	12.51	13.30	12.76
Crack Speed Index	-3.45	-3.35	-2.57

NOTE : Tests are performed on 7 days cured samples with 10% cement at 73°F.

Table 15. Creep and indirect tensile test results and predicted fatigue parameters at different temperatures.

	-10° F	33° F	73° F	104° F
$D_2 ( \times 10^{-7} )$	3.81	4.85	4.04	0.93
m	0.243	0.278	0.307	0.369
Creep Index ( $\times 10^{-11}$ )	5.14	10.58	12.97	6.63
$\sigma_m$ , MPa ( psi )	2.290 ( 332 )	0.773 ( 112 )	0.773 ( 112 )	0.773 ( 112 )
$\Gamma$ , J/m <sup>2</sup> ( in.lb/in. <sup>2</sup> )	3.289 ( 0.01875 )	3.163 ( 0.01803 )	3.163 ( 0.01803 )	3.163 ( 0.01803 )
$K_{IC}$ , MN·m <sup>-3/2</sup> ( psi·in. <sup>1/2</sup> )	96,593 ( 87.9 )	89,011 ( 81.0 )	89,011 ( 81.0 )	89,011 ( 81.0 )
A	$6.96 \times 10^{-36}$	$9.77 \times 10^{-31}$	$8.25 \times 10^{-29}$	$9.84 \times 10^{-27}$
n	15.49	13.83	12.76	10.96
Crack Speed Index	-4.18	-2.34	-2.57	-4.09

NOTE : Tests are performed on the 7 days cured samples with 10% cement at 55% relative humidity.

manner. Therefore, weaker bonded soil particles provide more chances to nucleate the microcracks or macrocracks when the load is applied. Once the crack is initiated, its propagation rate is mainly dependent on the matrix strength. Certainly, less cement gives a weaker matrix strength and results in the larger creep and creep index as shown in Figure 50 and Table 12.  $\log(D(t)-D_0)$  vs.  $\log t$  has been plotted in Figure 51. As a result, the slope  $m$  did not change while the intercept term,  $D_2$ , varied in direct response to the cement content.

For the 28-day-cured samples, regardless of the cement content, the time-dependent strain was smaller than the immediate strain. Since the pure power law is valid only when the immediate strain can be neglected, the generalized power law should be used to describe the time-dependent behavior of the soil-cement.

Based on the creep tests of 15% cement content samples, a constant strain level was often achieved after several hours of loading. This is explained by the crack arrest phenomena. When the crack meets the strong cementitious matrix or strongly bonded sand particle, the crack is arrested due to the much higher strength of the matrix or of the particle.

After the creep was observed as a basic characteristic of the soil-cement, the creep data were used to predict the fatigue life of soil-cement at different cement contents by virtue of Schapery's crack growth theory. Based on the material properties and creep data in Table 12, equation (81) was integrated for different  $\Delta K_{\max}$  values by means of the numerical integration program shown in Appendix IV. Then the  $\Delta K_{\max}$  values and the resultant  $\frac{da}{dN}$  values were input into a

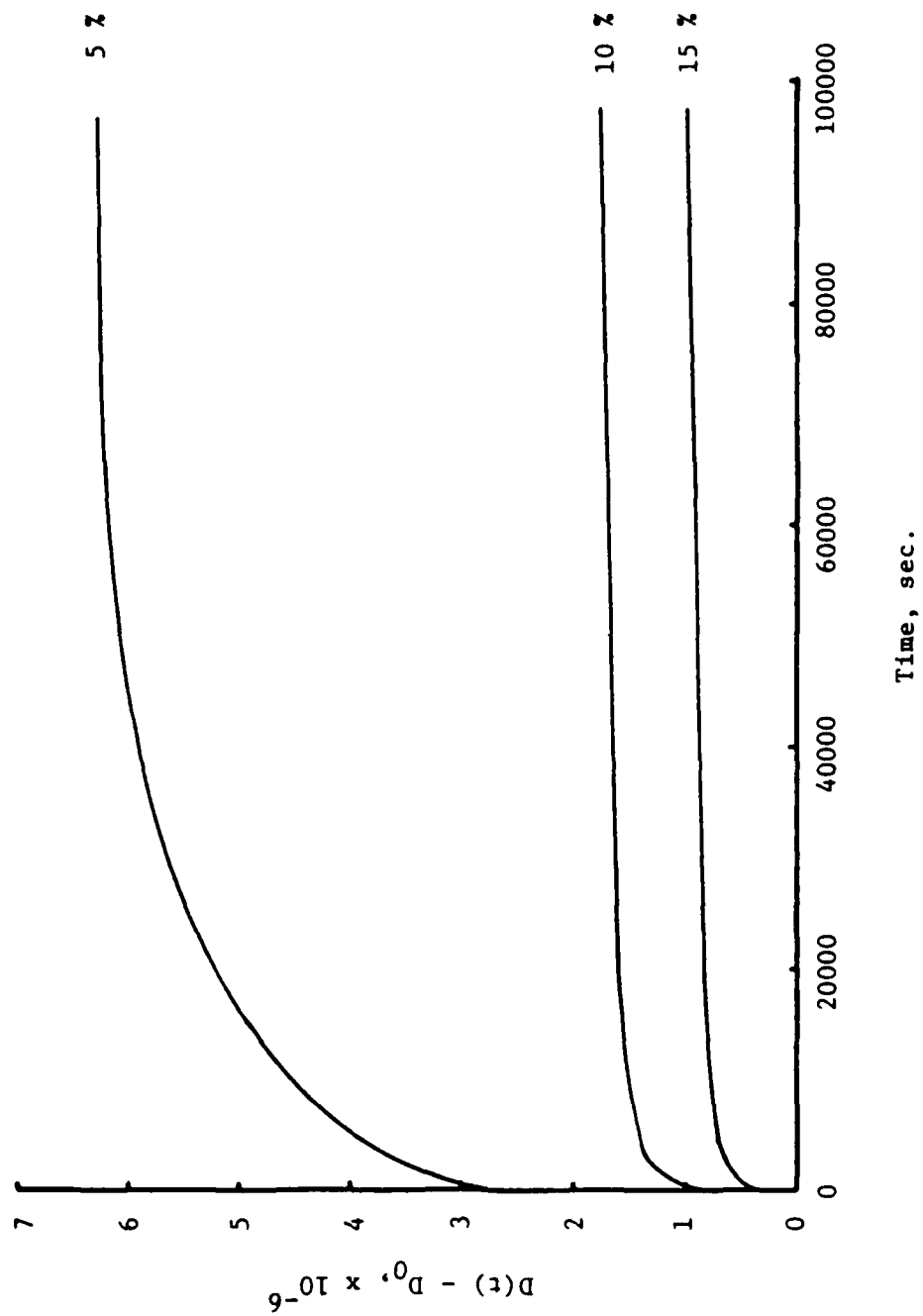


Figure 50. Creep curves at different cement contents.

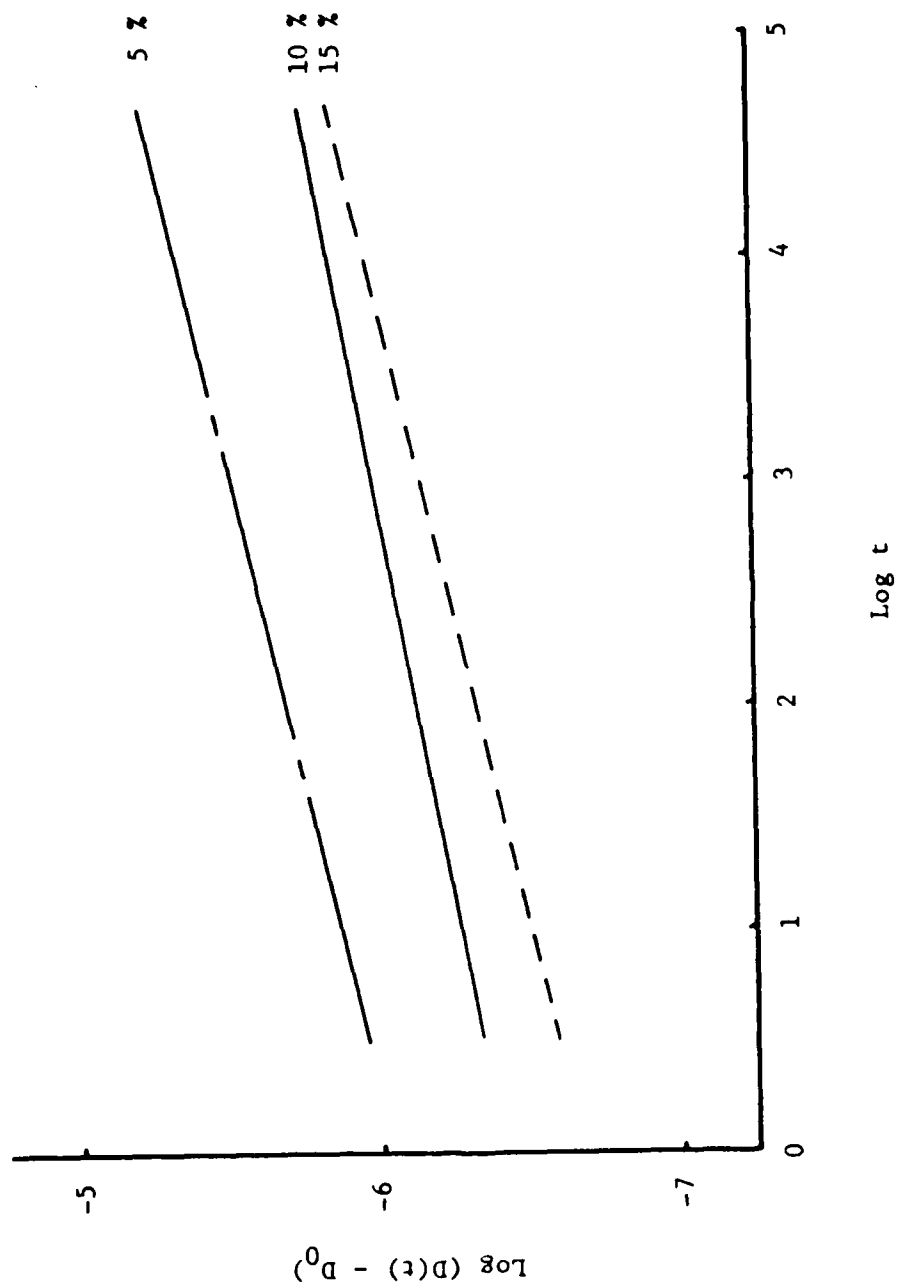


Figure 51.  $\text{Log } (D(t) - D_0)$  vs.  $\text{Log } t$  at different cement contents.

regression analysis in order to obtain the crack growth parameters,  $A$  and  $n$ . These regression coefficients and crack speed indices are listed for different cement contents and compared with the experimental fatigue data of Chapter III in Table 16. The crack speed index,  $\log A + 2 \cdot n$ , was used to evaluate the tendency of the crack growth as affected by cement content. However, in order to show the trend between the experimental and the predicted fatigue crack growths, the modified crack speed index,  $\log A + C \cdot n$ , where  $C = \log(0.75K_{IC})$  for each cement content, was used.

The following trends were noted: (1) It was proven both experimentally and theoretically that 5% cement content gives the largest crack speed index and the 15% the smallest. (2) The experimental crack growth rates were larger than the predicted ones. This may be explained by the interconnection of the microcracks which was not taken into account in Schapery's theory. (3) The experimental exponent,  $n$ , was smaller than the predicted  $n$ . Assuming that the fatigue exponent,  $n$ , is inversely proportional to the creep exponent,  $m$ , there is more viscoelastic response at the crack tip than was measured using the creep test. In the creep test, the bulk viscoelastic response of a material was measured. The viscoelastic response at the crack tip may be greatly different from that in bulk. This may be a result of the local heat generation at the crack tip which cannot be measured in the creep test.

Another possible reason of the larger  $n$  from the experiments is due to the difficulty of determining the immediate strain. Even though the load was applied immediately, it was somewhat hard to

Table 16. Comparison of the experimental and the predicted fatigue parameters at different cement contents.

		5 %		10 %		15 %	
		Pred. <sup>a</sup>	Exper. <sup>b</sup>	Pred.	Exper.	Pred.	Exper.
A		$5.42 \times 10^{-43}$	$3.98 \times 10^{-28}$	$8.12 \times 10^{-59}$	$1.55 \times 10^{-30}$	$1.45 \times 10^{-53}$	$2.60 \times 10^{-20}$
n		20.67	12.55	25.28	12.33	21.24	6.91
Crack Speed Index ( $\log A + 2 \cdot n$ )		-0.93	-2.31	-7.53	-5.15	-10.36	-6.90
Modified Crack Speed Index ( $\log A + C \cdot n$ )		-4.85	-5.03	-6.27	-5.08	-6.32	-4.56

a Predicted values from Schapery's theory.

b Experimental results from the cyclic fatigue tests.

c  $C = 1.81$  for 5% cement content,  
 $= 2.05$  for 10% cement content, and  
 $= 2.19$  for 15% cement content.

distinguish the immediate deformation from the viscoelastic deformation. In order to obtain the unique trends among the different conditions, a straight portion of the creep curve was drawn by a straight edge. The method used to determine the immediate response of the material was somewhat arbitrary, may not measure the elastic compliance precisely, and may result in a smaller creep exponent and a larger fatigue exponent.

The parameters A and n, based on the generalized power law, are expected to have the similar forms to the A and n shown in equations (75) and (76), which are based on the power law. Taking the logarithm to both sides of equation (75) yields

$$\log A = \log \left( \frac{\pi}{2 \sigma_m^2 I_1^2} \right) + \log \left\{ \int_0^1 W(t)^{2(1+1/m)} dt \right\} + \frac{1}{m} \log \left\{ \frac{(1 - \nu^2) D_1 \lambda_m}{2 \Gamma} \right\} \quad (84)$$

Molenaar [69] has approximated that

$$\log \int_0^1 W(t)^{2(1+1/m)} dt = -0.2696 - 0.1825 \cdot \log \left\{ 2 \left( 1 + \frac{1}{m} \right) \right\}.$$

For the same material and conditions,  $\nu$ ,  $\Gamma$ ,  $\sigma_m$  and  $I_1$  are constants and the right side of the approximation does not vary much in the range of  $0 \leq m \leq 0.5$ . In addition,  $D_1$  is usually in the same order of magnitude irrespective of the testing conditions. Consequently, all the log terms on the right side of the equation (84) can be regarded as constants. Then,  $\log A$  can be expressed as a linear function of  $\frac{1}{m}$  as n is. Based on this observation, both predicted  $\log A$  vs. n and experimental  $\log A$  vs. n relationships were plotted and compared. As can be seen from Figure 52, the theoretical points

(from Schapery's equation) and the experimental points (from cyclic fatigue testing) fell onto approximately the same line at each cement content. This illustrates several important aspects. First of all, even though the material behaves nonlinearly viscoelastically, Schapery's crack velocity equation, which was derived from linear viscoelasticity, gives great promise for predicting the fatigue life of soil-cement, at least with respect to changing cement content and for purposes of comparison. Second, the assumptions made in Schapery's report to develop the crack velocity equation are acceptable for soil-cement. They are summarized by Germann and Lytton [32] in the following statements;

1. Stresses and displacements very close to the crack tip can be represented by Barenblatt's crack tip model.
2. The second derivative of the logarithm of creep compliance with respect to the logarithm of time is small for linear viscoelastic materials.
3. Failure can be defined by the work done to fail all strands in a region of small cross-sectional area known as the "failure zone" in Barenblatt's crack tip model.

Barenblatt [8], in 1962, assumed a cusp-shaped crack tip model and gave a stress solution at the crack tip. He assumed the stress at the crack tip approached a limiting value, while Irwin assumed the stress went to infinity. In his report, he also assumed a small plastic zone size. This assumption is satisfactory for soil-cement, since it is a fairly brittle material. The second assumption that the slope of the log compliance versus log time plot does not vary

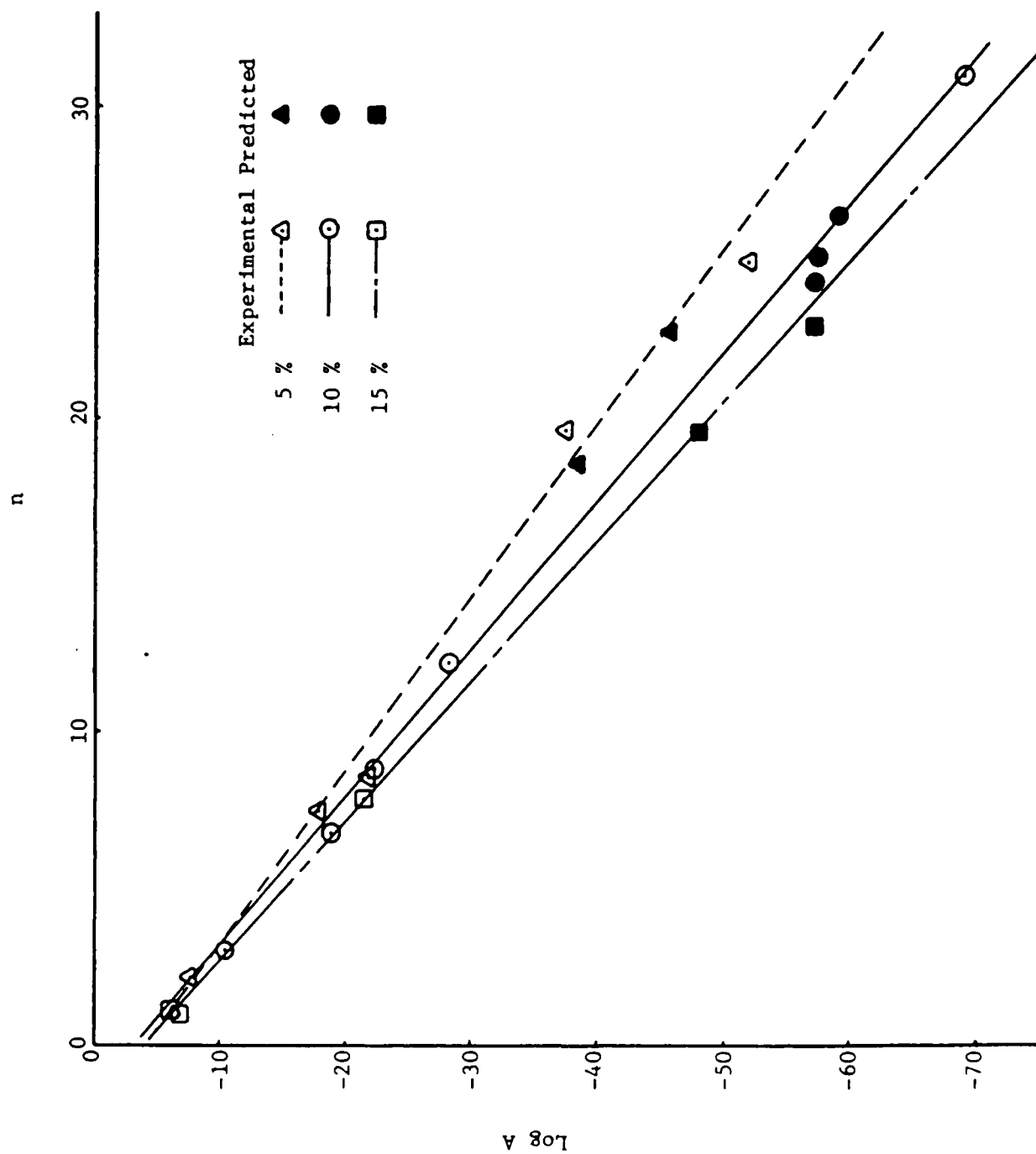


Figure 52.  $\log A$  vs.  $n$  of the predicted and the experimental results at different cement contents.

much can be proven by observing seven-day creep tests. From his third assumption, Schapery defined the fracture energy,  $\Gamma$ , as the work done in this failure zone to create a unit area of crack surface.

In addition to these assumptions, the time independence of  $\nu$ ,  $\Gamma$ , and  $\sigma_m$  is implicitly assumed when equation (81) is integrated with respect to  $t$ . In a brittle material with small strain, the Poisson's ratio is usually a very weak function of time. For verification of the time independence of the fracture energy,  $\frac{dJ}{da}$  from the fracture test was observed. The term  $\frac{dJ}{da}$ , the change in work done for the unit area of crack extension per crack length, was approximately zero for the soil-cement. Since  $\Gamma$  is half of the  $J$  value and  $a$  is a function of time (very slow parabolic function from  $a$  vs.  $N$  plot of the fatigue test), we can easily observe the time independence of the fracture energy from  $\frac{dJ}{da} \approx 0$ .

Curing Age. To describe the effect of curing age on the creep in cement-stabilized soil, the chemical reactions and the properties of their products should be considered first. Portland cement is an energy-rich anhydrous tricalcium silicate with excess lime. The basic reaction of cement with soil consists of cation exchange, flocculation and agglomeration, and pozzolanic reaction. In addition to these reactions, a cementitious reaction occurs in the portland cement itself. The first two reactions are immediate, while the pozzolanic and the cementitious reactions are time-dependent.

The pozzolanic reaction is the reaction between silicates and aluminates from the soil and free lime from portland cement. Calcium

silicate hydrate (CSH) is the product of this reaction. The cementitious reaction in portland cement is due to the hydration effect of the pure cement compounds. That is, when calcium silicates or tricalcium aluminates meet water, chemical reactions occur and produce the cementitious hydration products with time. The hydration products are calcium silicate hydrate, calcium hydroxide, ettringite and monosulfoaluminate. The most predominant product from these reactions is the calcium silicate hydrate. This material is characterized by a poor degree of crystallinity, compositional variability and very large surface area. In order to describe the behavior of cement-stabilized material with time and effects of moisture, a complete and accurate explanation of the effect of calcium silicate hydrate is critical.

It has been found that calcium silicate hydrate is formed during curing and, after 28 days, there is no significant amount of additional formation. At early days of curing, the calcium silicate grains are covered with a coating of CSH, which gives them a spiny appearance like a burr. These spines grow more and more and, finally, mesh with each other. As this bond develops with continued hydration, the spines appear to transform to the underlying CSH. Since CSH is dominant in the hydrated cement paste, the area and number of these points of contact determine the strength of the cement paste [67]. Furthermore, the drying effect of the adsorbed water on CSH particles produces a stronger system due to an increase in van der Waal's bonding.

From Figure 53 and Table 13, we can see the smallest creep and creep index from the 28-day-cured sample. To explain the smaller creep and creep index of longer-cured samples, three investigations are proposed:

- (1) the effect of amount of evaporable water in the system,
- (2) the effect of the porosity and
- (3) the effect of weaker bond strength between CSH particles.

There are three types of water in the cement paste: the water in the large capillary pores, the adsorbed water at the surfaces of CSH particles, and the structural water of CSH. Above 40% relative humidity, the capillary water in the pores is the main evaporable water [67]. (Note that the creep tests of different curing ages were performed at 55% relative humidity). The amount of water lost and the evaporation rate of this water will be the greatest for 7-day-cured specimens. Meanwhile, 28-day-cured specimens have little evaporable water, and the evaporation effect will be almost negligible. When the sample is loaded, the net stress at the crack tip can be obtained by subtracting the hydrostatic tension of capillary water from the total stress concentrated at the crack tip. Therefore, as the evaporation rate increases, the decrease in the surface tension is faster and results in a higher rate of increase in the net stress and higher slope of the creep curve of the 7-day-cured sample.

Another effect of curing age is the porosity. It has been found that as curing age increases, the mean effective pore diameter decreases [67]. Since it is thought in this study that the creep is

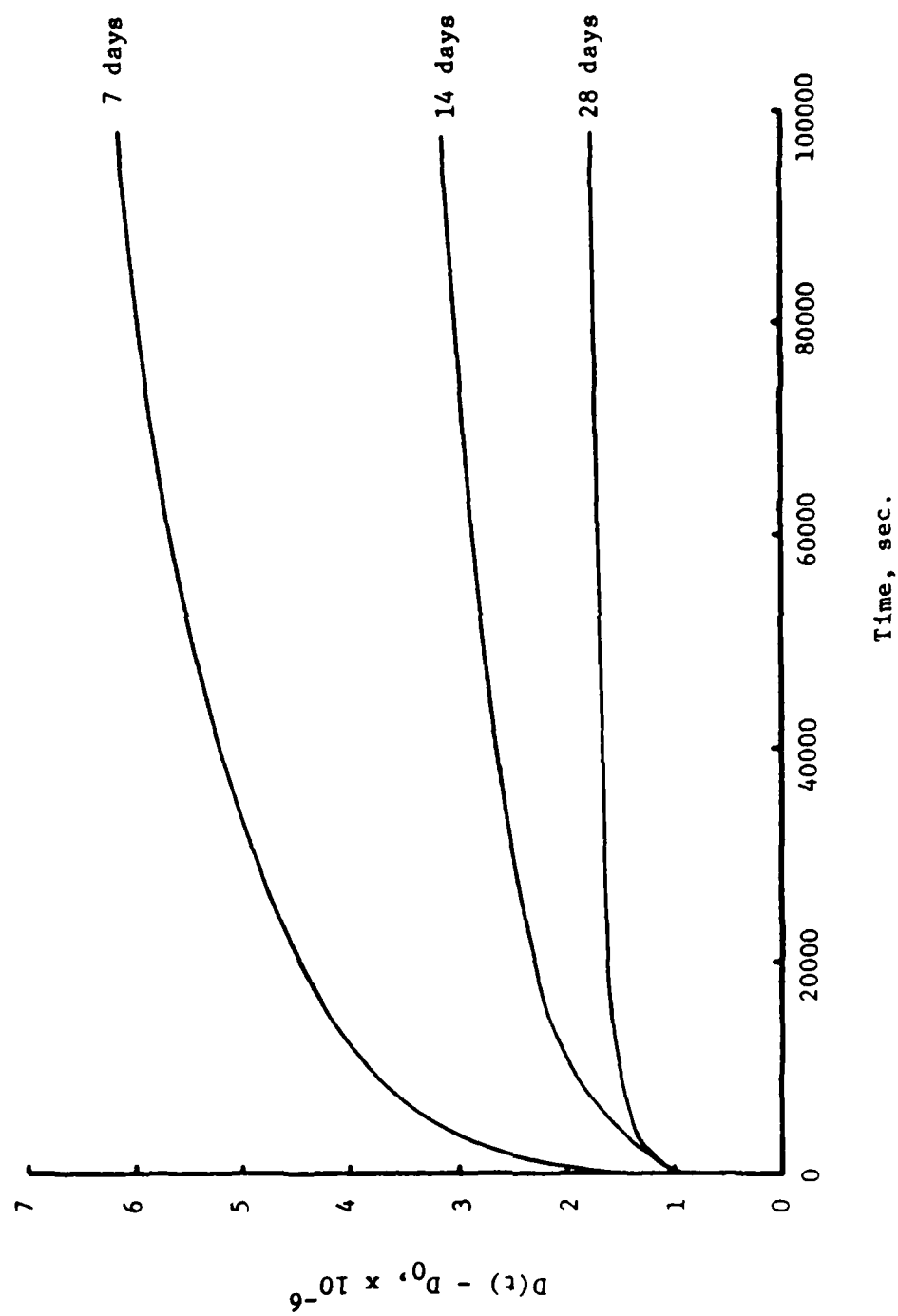


Figure 53. Creep curves at different curing ages.

a result of microcrack propagation, the pore size itself is considered important from the fracture mechanics point of view. The stress intensity factor, which is the most important factor in determining the crack growth, is determined by the size of the crack and the applied stress. Therefore, it is apparent that the smaller pores in 28-day-cured samples result in smaller stress intensity factors and smaller crack growth. Furthermore, thinner and weaker bonds between CSH particles in the 7-day-cured specimen may make the amount of creep larger.  $\log (D(t)-D_0)$  vs.  $\log t$  was plotted for each curing age in Figure 54. It was found that, as curing age increases,  $D_2$  increases and  $m$  decreases.

The creep parameters and the predicted  $\log A$  and  $n$  are summarized in Table 13. As shown, the 7-day-cured specimen shows the fastest crack growth with 14-day- and 28-day-cured specimens showing progressively slower crack growth rates.

The predicted and the experimental crack growth parameters are compared in Table 17 and  $\log A$  is plotted versus  $n$  in Figure 55. It is noticed here that the shorter curing age data gives better accuracy in predicting the parameters. That is, the larger amount of evaporable water in the system results in larger time-dependent strain and makes the viscoelastic approach to predicting the crack growth more precise. As shown in Figure 55, the predicted values (from Schapery's equation) and the experimental values (from the cyclic loading tests) once again fall onto approximately the same line at each curing age.

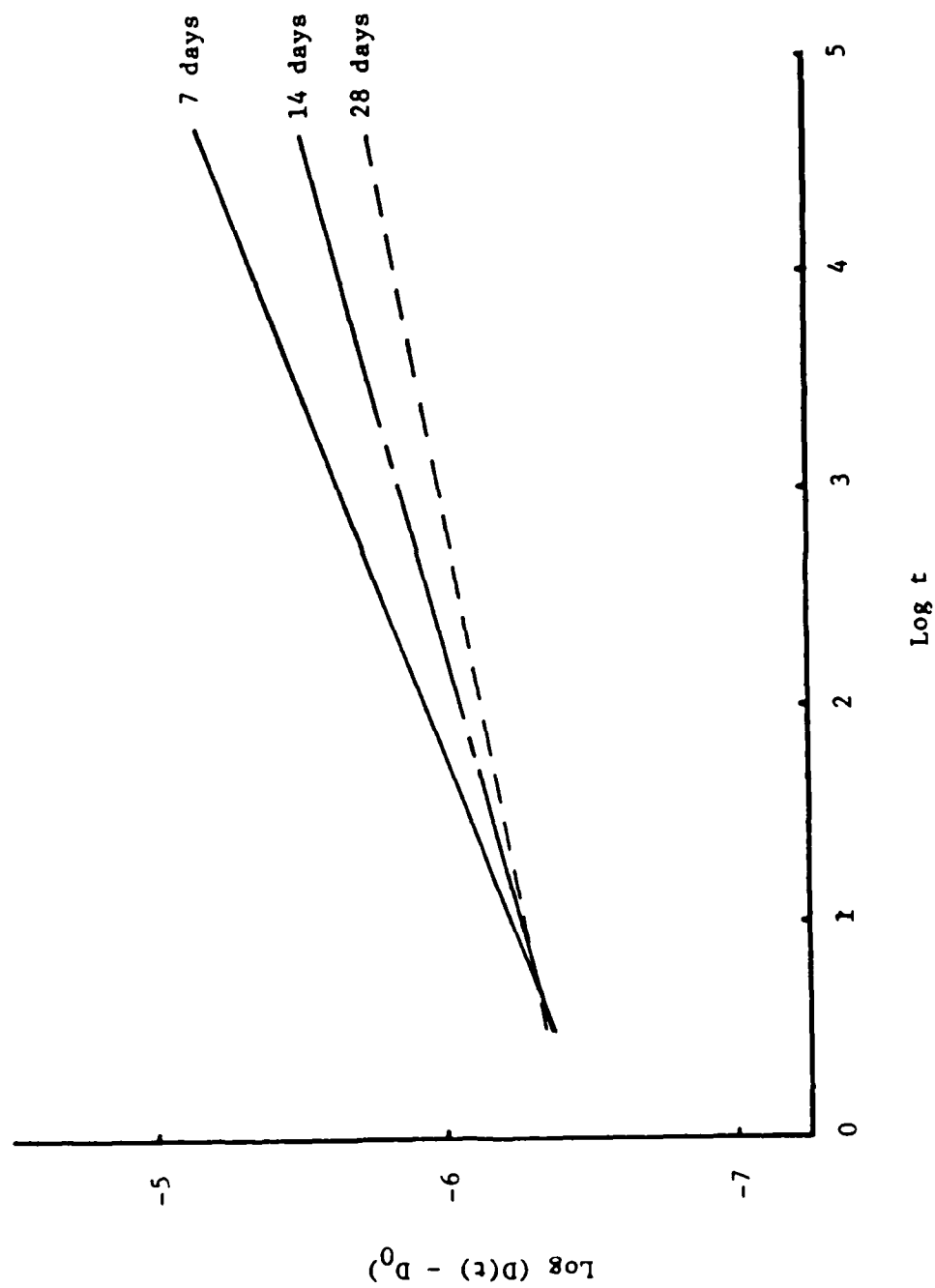


Figure 54.  $\text{Log } (D(t) - D_0)$  vs.  $\text{Log } t$  at different curing ages.

Table 17. Comparison of the experimental and the predicted fatigue parameters at different curing ages.

	7 days				14 days				28 days			
	Pred. <sup>a</sup>	Exper. <sup>b</sup>	Pred.	Exper.	Pred.	Exper.	Pred.	Exper.	Pred.	Exper.	Pred.	Exper.
A	$1.10 \times 10^{-30}$	$3.45 \times 10^{-29}$	$7.26 \times 10^{-43}$	$4.42 \times 10^{-40}$	$8.12 \times 10^{-59}$	$1.55 \times 10^{-30}$						
n	13.30	13.15	18.41	17.24	25.28	12.33						
Crack Speed Index ( $\log A + 2 \cdot n$ )	-3.35	-2.16	-5.32	-4.87	-7.53	-5.15						
Modified Crack Speed Index ( $\log A + C^C \cdot n$ )	-5.76	-4.55	-4.36	-5.46	-6.17	-5.08						

<sup>a</sup> Predicted values from Schapery's theory.

<sup>b</sup> Experimental results from the cyclic fatigue tests.

<sup>c</sup> C = 1.82 for 5% cement content,  
 = 2.05 for 10% cement content, and  
 = 2.05 for 15% cement content.

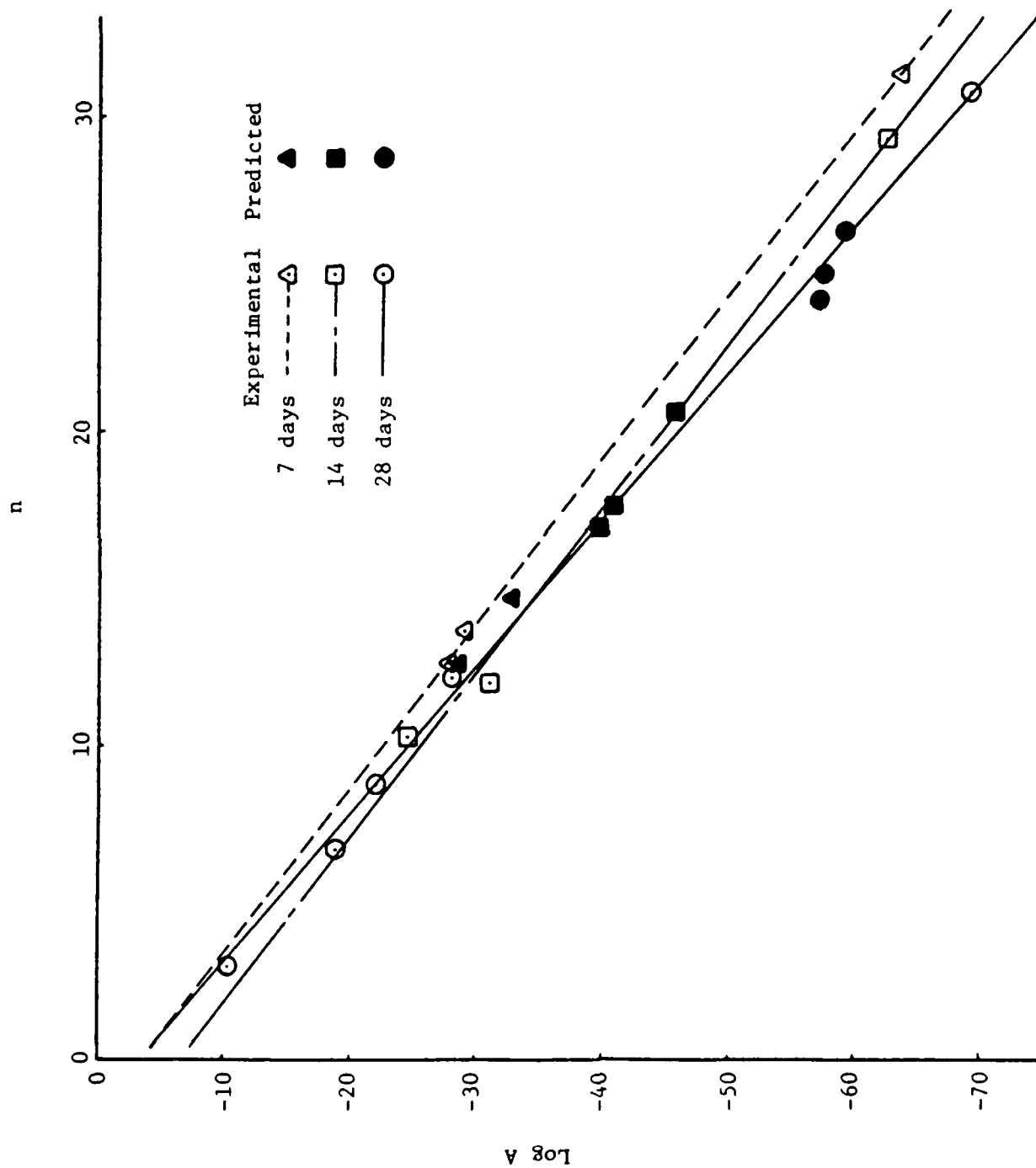


Figure 55.  $\log A$  vs.  $n$  of the predicted and the experimental results at different curing ages.

Relative Humidity. Since the moisture movement of cement-stabilized soil is one of the most important factors affecting creep phenomena, the effects of relative humidity are very significant. Creep behavior under three levels of the relative humidity (100%, 55% and 35%) was investigated in this study. In order to illustrate the effect of relative humidity, again three different levels of water in the system should be considered: the capillary water, the adsorbed water and the structural water. While the first two types of water can be evaporated at relative humidities typically occurring in nature, the structural water is held so strongly that it cannot be dried above 10% relative humidity [67]. Therefore, the role of the structural water on creep will be neglected through this study.

Two important stresses due to water in the system are the hydrostatic tension of the capillary water and the disjoining pressure of adsorbed water. The relation between the shrinkage and the relative humidity has been illustrated by Mindess and Young [67] in Figure 56. Domains (1) and (2) have been attributed to loss of water from capillary pores, domain (3) represents loss of adsorbed water from the surfaces of CSH particles, domain (4) results from the loss of water that contributes to the structure of CSH, and domain (5) is due to the decomposition of CSH.

At 100% RH, rather small capillary stresses are developed due to a relatively large volume-to-surface ratio. Meanwhile, large amounts of adsorbed water on the CSH surfaces create a disjoining pressure which decreases with the decrease in relative humidity. When the

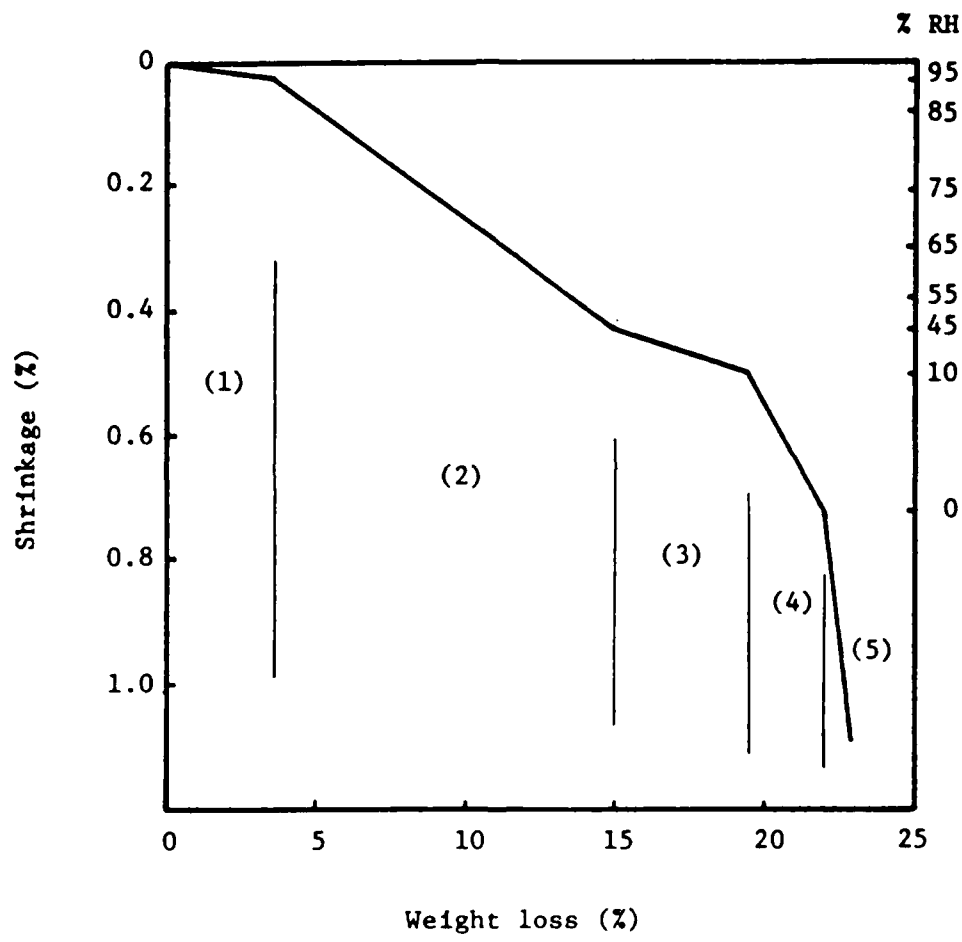


Figure 56. Shrinkage-moisture loss relationships in pure cement pastes during drying (After Mindess and Young [67]).

disjoining pressure exceeds the van der Waal's attractions between the CSH particles, the particles will be forced apart. Disjoining pressure disappears below 50% RH. In addition to these physical effects of moisture, probably the corrosion phenomena of the moisture on the bonds between CSH particles at the crack tip also weakens the structure of cement-stabilized soil.

At 55% RH, the capillary stresses are relatively large, because the capillary stress is an inverse function of the radius of the meniscus (i.e., an inverse function of relative humidity). Meanwhile, the disjoining pressure will not be very effective below this relative humidity.

At 35% RH, capillary stresses cannot exist since the menisci are no longer stable. The disjoining pressure, also disappears at this humidity. However, due to preconditioning the sample for six hours before the creep test, additional shrinkage cracks were developed. Also, due to the low external humidity, the drying rate of the sample was faster than at 55% RH.

Finally, 100% RH yields rather small capillary stresses and large disjoining pressure, relatively. A relative humidity of 55% results in relatively large capillary stresses and small disjoining pressure. At 35% RH, the size and density of shrinkage cracks and the drying rate of the water in the system determine the creep behavior.

The results from the three different relative humidities are shown in Table 14 and Figures 57 and 58. The data show similar results to what was expected. The samples at 35% RH and 100% RH showed larger creep and creep indices than the sample at 55% RH. From the creep

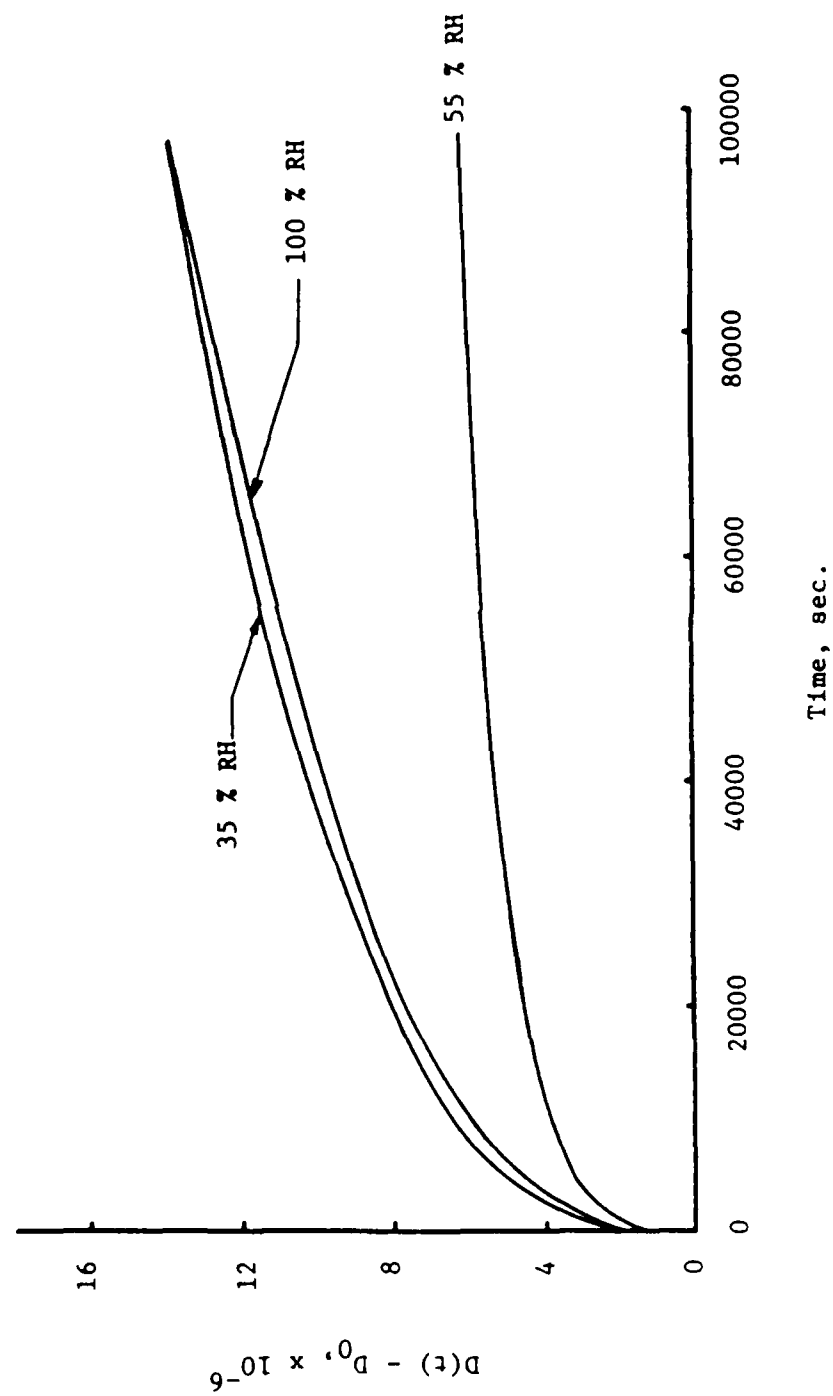


Figure 57. Creep curves at different relative humidities.

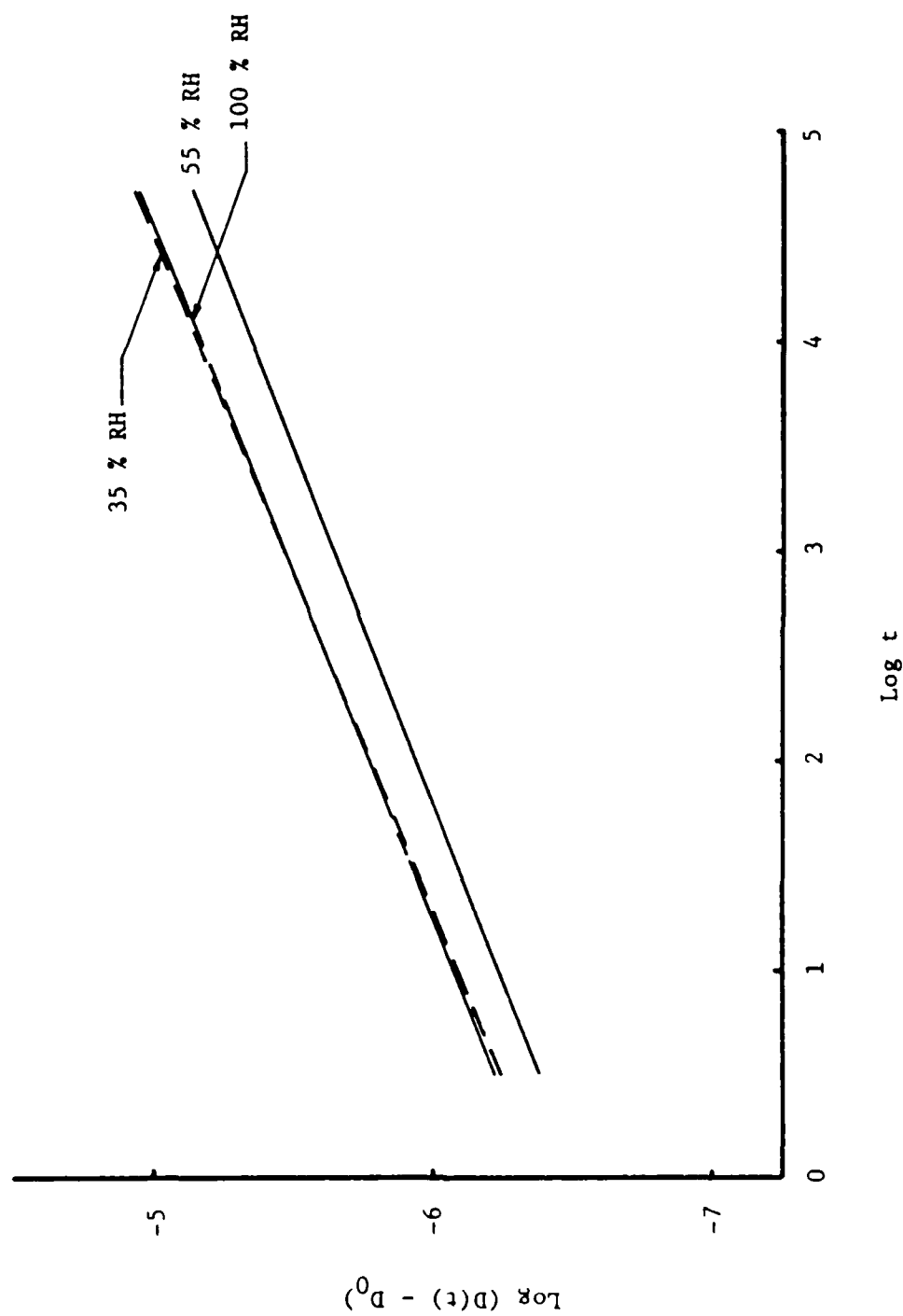


Figure 58.  $\text{Log } (D(t) - D_0)$  vs.  $\text{Log } t$  at different relative humidities.

data and the material properties, the crack growth parameters were calculated and listed in Table 14. Even though the creep responses at 35% and 100% RH's looked almost same, the fatigue behavior would not be the same because of the differences of the fracture energy and the tensile strength terms in the equation (81). For the 35% RH, both the fracture energy and the tensile strength increased and resulted in slower crack growth than at 100% RH. The crack speed index was the largest at 100% RH, and 35% RH and 55% RH gave fairly close crack speed indices.

Temperature. The temperature effects on the creep behavior of cement-stabilized soil are shown in Table 15 and Figures 59 and 60. The investigation of the temperature effects without any interaction with the humidity was extremely difficult. Even though the relative humidity could be kept at 100% in the humidity chamber at different temperatures, the absolute humidity varied with the temperature changes.

Due to the importance of the disjoining pressure at the high humidity on the creep, the absolute amount of water in the air is important. The low creep index and crack speed index at 104° F could be explained by the fact that there might be less water in the same 100% RH than at the lower temperature and smaller disjoining pressure.

The creep at -10° F was very restricted compared to the other temperatures. From the indirect tensile test, the samples stored at -10° F for 6 hours showed high strength but brittle behavior. As can be seen from Table 15, the average tensile strength of samples at

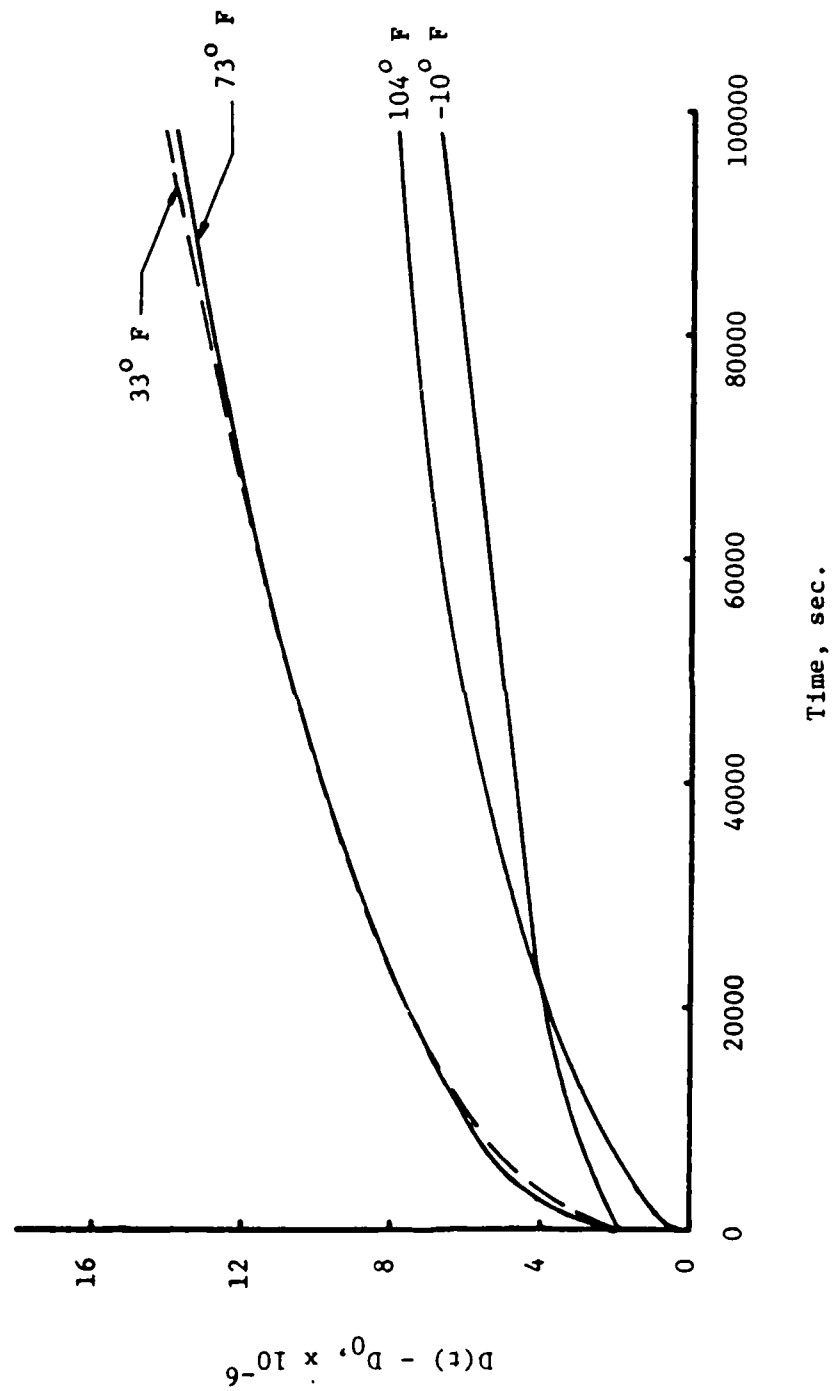


Figure 59. Creep curves at different temperatures.

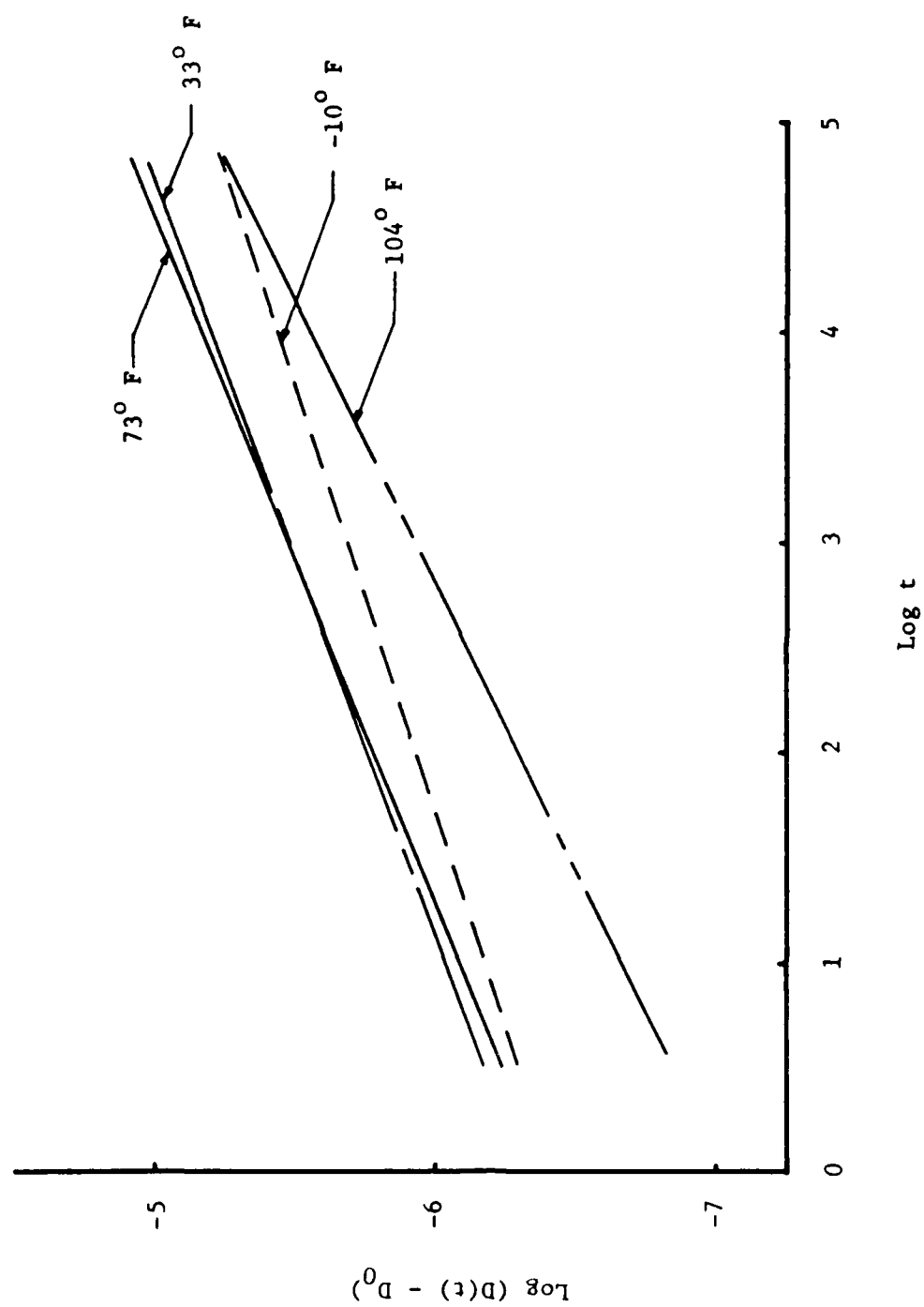


Figure 60.  $\text{Log } (D(t) - D_0)$  vs.  $\text{Log } t$  at different temperatures.

-10° F was almost three times the average from 73° F. This can be explained by the fact that the moisture in the structure is frozen when preconditioned and behaves as a part of the structure. While water in the structure of cement-stabilized soil helps little from the strength viewpoint, ice in the structure increases the tensile strength.

As a result of the creep data, the crack growth was much smaller at -10° F, as shown in Table 15. Therefore, it was concluded that, below the freezing point, the crack growth might be slower without the existence of a critical size flaw. Unfortunately, most cement-stabilized layers have large enough preexisting flaws that the crack propagation at low temperatures is catastrophic due to its brittle nature.

## CHAPTER VI: SUMMARY

A summary of the primary results of the study follows:

(1) Linear elastic fracture mechanics (LEFM) can be used to model cracking behavior of portland cement stabilized fine grained soils which meet appropriate size effect criteria.

(2) The form of an equation which can be used to model a critical toughness parameter as a function of a single variable (composed of a term which is primarily related to the attractive force between material elements times a term which is primarily related to the equilibrium spacing of material elements) was successfully derived from what are essentially "first principles". Further, this model is expected to be useful for any "LEFM material" in which the displacement to failure is relatively constant regardless of toughness and for which terms which are primarily related to separate components of the attractive force model can be identified. The equations appear as equations (33 and 49) in the text.

(3) Some tradeoff between compaction effort and cement content is available for use as a cost minimization measure. However, cement content has the greater effect on toughness.

(4) The "weak link" in the fracture process for this material is at the interface between the soil particle and the matrix made up of hydration products, water, and voids (see Appendix V). It is suspected that changing soil type may also yield significant changes in toughness (by matching soil chemistry more closely with matrix chemistry, a stronger bond may be formed causing the fracture process

to become a combined inter- and intragranular process which may significantly increase toughness).

(5) "Crack speed indices" in two forms from two methods of analysis of crack growth in fatigue were used to describe crack growth under cyclic loading (see Figures 29 and 30, and Table 8). It is suspected that one of these indices is a material property and can be successfully determined even in the presence of systematic lack of fit in regression analyses. Comparison of the various crack speed indices lead to the conclusion that, for the material studied, an increase in fatigue life due to an increase in toughness would not be due primarily to an increased resistance to crack extension but rather would be due primarily to the load generated stress intensity being a lower percentage of the critical stress intensity fluctuation in fatigue.

(6) Systematic lack of fit in the crack length versus cycle behavior in fatigue is apparently related to a process zone which is characterized by a crack branch and rejoin process.

Future research into the factors affecting toughness is expected to lead to more efficient optimization of pavement material mixture design. Future research into analytical approaches to the problem of cracking in two and three dimensions coupled with monotonic and cyclic loading test results is expected to extend consideration of cracked body analyses into existing layered elastic and finite element solutions and computer programs. Improved knowledge of the cracking process will make pavement rehabilitation efforts more effective and economical.

It has been shown that Schapery's crack velocity equation based on the generalized power law can be used to predict the tendency of compacted soil-cement to fatigue. Predicted values of  $\log A$  and  $n$ , based on Schapery's model, are very strong linear functions of  $\frac{1}{m}$ . The regression analysis for the data based on laboratory tensile creep data of soil cement shows that:

$$\log A = -4.956 - 7.463 \times \frac{1}{m} \quad \text{with } R^2 = 0.955, \text{ and}$$

$$n = 1.727 + 3.375 \times \frac{1}{m} \quad \text{with } R^2 = 0.998.$$

Therefore, in order to predict the fatigue life of cement-stabilized soil in terms of Paris' law,  $\frac{1}{m}$  is the most important parameter. The crack growth parameters of the soil-cement,  $A$  and  $n$ , can be predicted from the viscoelastic exponent of the creep test,  $m$ , and the regression equations.

Certainly, there remains doubt concerning how well these predicted  $A$  and  $n$  values can represent the real behavior of soil-cement in a pavement layer. Nevertheless, it has been shown that, at least for the purpose of the comparison under various conditions, the prediction of the fatigue parameters by means of Schapery's theory is very satisfactory. Furthermore, if one considers the cost and the difficulties in fatigue test in soil-cement, there is no doubt that this type of the effort is necessary.

The tensile creep in cement-stabilized soil can be explained extremely well by the microcrack propagation and moisture effect in the system. Specifically, the viscoelastic properties of the soil-cement were controlled by the amount of evaporable water in the

matrix and the moisture-related environmental conditions. The main results from the creep tests are:

1. As the cement content and curing age increase, the fatigue life of a cement-stabilized base layer is enhanced.
2. Relative humidities of 100% and 35% result in higher creep than 55% RH due to the disjoining pressure and the faster drying rate of the evaporable water, respectively.
3. Below the freezing point, the creep is restricted substantially, perhaps by the reinforcing effect of the filled voids.

Based on the above conclusions, several recommendations are presented:

1. Since cement-stabilized soil is heterogeneous and moisture-sensitive, special care should be taken during molding, compaction and curing in the laboratory. Of significant importance is the specification of the curing condition.
2. The generalized power law should be used rather than the power law to fit the time-dependent creep data because of the large immediate strain.
3. In order to predict the moisture effect in the system, internal relative humidity is more meaningful than external relative humidity.
4. The relative humidity should be kept fairly stable, otherwise wetting and drying cause additional creep.
5. In order to observe the temperature effects on the creep, the

absolute humidity should be fixed to one level.

6. Traffic on a cement-stabilized base layer which has only cured for a few days will cause a much shorter fatigue life.

## APPENDIX I.—References

1. AASHTO Standard Test Procedure T99-74, American Association of State Highway and Transportation Officials.
2. AASHTO Standard Test Procedure T180-74, American Association of State Highway and Transportation Officials.
3. Alhashimi, K. and Chaplin, T. K., "An Experimental Study of Deformation and Fracture of Soil-Cement," Geotechnique, Vol. 23, No. 4, December 1973, pp. 541-550.
4. Ashbaugh, N., "Stress Solution for a Crack at an Arbitrary Angle to an Interface", International Journal of Fracture, Vol. 11, No. 2, April, 1975, pp. 205-219.
5. ASTM Standard Test Designation E399-81, American Society for Testing and Materials, July, 1981.
6. ASTM Standard Test Designation E647-83, American Society for Testing and Materials.
7. ASTM Standard Test Designation E813-81, American Society for Testing and Materials, July, 1981.
8. Barenblatt, G.I., "The Mathematical Theory of Equilibrium Cracks in Brittle Fracture", Advances in Applied Mechanics, Vol. 7, 1962, pp. 55-129.
9. Bazant, Z.P., "Size Effect in Blunt Fracture: Concrete, Rock, Metal", Journal of Engineering Mechanics, ASCE, Vol. 110, No. 4, April 1984, pp.518-535.
10. Berg, O. Y., "The Problem of Strength and Plasticity of Concrete," Doklady Akademii Nauk SSSR, Vol. 70, No. 4, 1950, pp. 617.
11. Blakey, F. A. and Beresford, F. D., "A Note on Strain Distribution in Concrete Beams," Civil Engineering and Public Works Review, Vol. 50, No. 586, April 1955, pp. 415-416.
12. Bofinger, H. E., "The Structure of Soil-Cement," Journal of Australian Road Research Board, Vol. 2, No. 1, September 1964, pp. 46-51.
13. Bofinger, H. E., "The Creep of Clay-Cement under Steady Tensile Stress," Journal of Australian Road Research Board, Vol. 4, No. 3, March 1970, pp.80-85.

14. Bradley, W., Course notes, MM607 (Spring 1983), ME623 (Fall 1983), Texas A&M University, 1983.
15. Broek, D., Elementary Engineering Fracture Mechanics, Martinus Nijhof, Boston, 1982.
16. Burmister, D.M., "The Theory of Stresses and Displacements in Layered Systems and Applications to the Design of Airport Runways", Proceedings of the 23rd Annual Meeting, Highway Research Board, 1943, pp. 126-148.
17. Burmister, D.M., "The General Theory of Stresses and Displacements in Layered Systems. I", Journal of Applied Physics, Vol. 16, No. 2, February, 1945, pp. 89-94.
18. Chang, J.B., Engle, R.M., and Szamosi, M., "An Improved Methodology for Predicting Random Spectrum Load Interaction Effects on Fatigue Crack Growth", Advances in Fracture Research (Fracture 81), Francois, D., ed., Pergamon, Volume 5, 1982, pp. 2615-2623.
19. Clark, W.G., and Hudak, S.J., Jr., "Variability in Fatigue Crack Growth Rate Testing", Journal of Testing and Evaluation, Vol. 3, No. 6, Nov. 1975, ASTM, pp. 454-476.
20. Dunlop, R. J., Moss, P. J. and Dodd, T. A. H., "Shrinkage Stresses in Soil-Cement Pavements," Proceeding of Australian Road Research Board Conference, Vol. 6, Part. 5, 1972, pp. 217-234.
21. Evans, A.G., and Fuller, E.R., "Crack Propagation in Ceramic Materials Under Cyclic Loading Conditions", Metallurgical Transactions, Volume 5, Number 1, January 1974, pp. 27-33.
22. Evans, R. H., "Extensibility and Modulus of Rupture of Concrete," The Structural Engineer, Vol. 24, No. 12, December 1946, pp. 636-659.
23. Forman, R.G., Kearny, V.E., and Engles, Journal of Basic Engineering, Vol. 89, 1967, p.459
24. Freiman, S.W., ed., Fracture Mechanics Applied to Brittle Materials, ASTM STP 678, 1979.
25. Freiman, S.W., and Fuller, E.R., Jr., ed., Fracture Mechanics for Ceramics, Rock, and Concrete, ASTM STP 745, 1981.
26. Gartenhaus, S., Physics, Basic Principles, Volume 1, Holt, Rinehart, and Winston, N.Y., 1975.

27. Gdoutos, E.E., Problems of Mixed Mode Crack Propagation, Martinus Nijhoff, Boston, 1984.
28. George, K. P., "Cracking in Pavements Influenced by Viscoelastic Properties of Soil-Cement," Highway Research Record, No. 263, Highway Research Board, 1969, pp. 47-59.
29. George, K.P., "Theory of Brittle Fracture Applied to Soil Cement", Journal of the Soil Mechanics and Foundations Division, ASCE, Vol. 96, No. SM 3, May 1970, pp. 991-1010.
30. George, K. P., "Mechanism of Shrinkage Cracking of Soil-Cement Bases," Highway Research Record, No. 442, Highway Research Board, 1973, pp. 1-10.
31. Germann, F.P. and Lytton, R.L., "Methodology for Predicting the Reflection Cracking Life of Asphalt Concrete Overlays", Research Report 207-5, Texas Transportation Institute, Texas A&M University, College Station, Texas, March 1979.
32. Gillen, M., "Short Term Creep of Concrete at Elevated Temperatures," Construction Technology Labs., Skokie, Illinois, Report NBS-GCR-82-407, September 1982.
33. Glucklich, J. and Ishai, O., "Rheological Behavior of Hardened Cement Paste under Low Stresses," in Proceedings of the Journal of the American Concrete Institute, Vol. 60, No. 7, July 1963, pp. 853-880.
34. Glucklich, J., "The Effect of Microcracking on Time Dependent Deformations and the Long-Term Strength of Concrete," in Proceedings of the International Conference on the Structure of Concrete, London, 1965, pp. 176-189.
35. Gopalaratnam, V.S., and Shah, S.P., "Softening Response of Plain Concrete in Direct Tension", ACI Journal, American Concrete Institute, No. 3, Proceedings Vol. 82, May-Jun 1985, pp. 310-323.
36. Griffith, A.A., "The Phenomena of Rupture and Flow in Solids", Philosophical Transactions of the Royal Society of London, Series A, Vol. 221, March, 1921, pp. 163-198.
37. Griffith, A.A., "The Theory of Rupture", Proceedings of the First International Congress on Applied Mechanics, Biezeno, C.B., and Burgers, J.M., ed., Delft, 1924, pp. 55-63.
38. Hermite, R. G., "What Do We Know about the Plastic Deformation and Creep of Concrete?" RILEM Bulletin, No. 1, March 1959, pp. 21-51.

39. Hertzberg, R.W., Deformation and Fracture Mechanics of Engineering Materials, J. Wiley and Sons, N.Y., 1983.
40. Hewlett-Packard, HP41CX Owner's Manual Volume 2: Operations in Detail, Corvallis, Ore., August 1983.
41. Hondros, G., "The Protection and Manipulation of Electrical-Resistance Strain Gauges of the Bonded-Wire Type for Use in Concrete, Particularly for Internal Strain Measurement," Magazine of Concrete Research, Vol. 9, No. 27, November 1957, pp. 173-180.
42. Hsu, T. T. C., Slate, F. O., Sturman, G. M. and Winter, G., "Microcracking of Plain Concrete and the Slope of the Stress-Strain Curve," in Proceedings of the Journal of the American Concrete Institute, Vol. 60, No. 2, February 1963, pp. 209-224.
43. Illson, J. M., "The Creep of Concrete under Uniaxial Tension," Magazine of Concrete Research, Vol. 17, No. 51, June 1965, pp. 77-84.
44. Irwin, G.R., "Relation of Stresses Near a Crack to the Crack Extension Force", Proceedings, 9th International Congress of Applied Mechanics, University of Brussels, 8, 1957, pp. 245-251.
45. Irwin, G.R., Handbuch der Physik, Vol. VI, Springer, Berlin, 1958
46. Irwin, G.R., "Plastic Zone Near a Crack and Fracture Toughness", Proceedings of the Seventh Sagamore Army Materials Research Conference, 1960, pp. IV-63.
47. Ishai, O. and Glucklich, J., "The Effect of Extreme Hygrometric Changes on the Isotropy and Deformability of Mortar and Concrete Specimens," RILEM Symposium on Moisture in Buildings, Helsinki, August 1965.
48. Jones, A., "Tables of Stresses in Three-Layer Elastic Systems", Highway Research Board Bulletin 342, Stress Distribution in Earth Masses, National Research Council, Washington, D.C., 1962, pp. 176-214.
49. Jones, R., "A Method of Studying the Formulation of Cracks in a Material Subjected to Stresses," British Journal of Applied Physics, Vol. 3, No. 7, July 1952, pp. 229-232.
50. Jones, R., "The Development of Microcracks in Concrete," RILEM Bulletin, No. 9, December 1960, pp. 110-114.

AD-A168 267

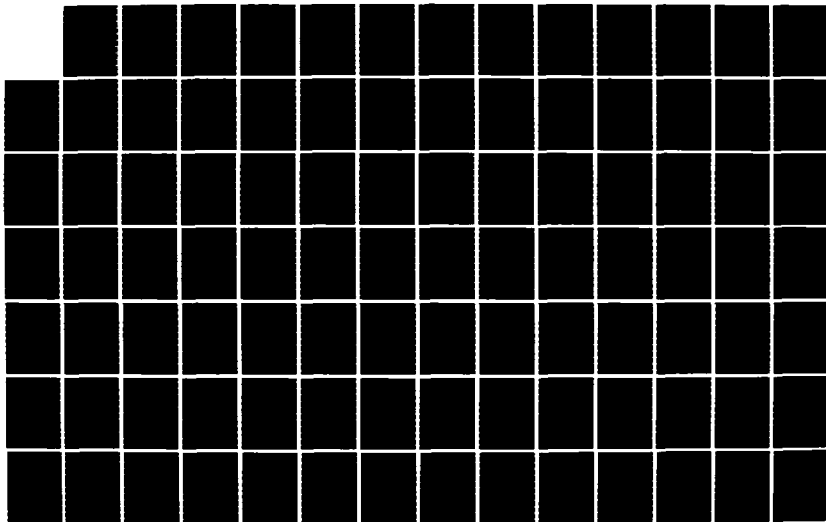
FRACTURE IN STABILIZED SOILS VOLUME 1(U) TEXAS  
TRANSPORTATION INST COLLEGE STATION D N LITTLE ET AL.  
31 DEC 85 AFOSR-TR-86-0242-VOL-1 F49620-82-K-0027

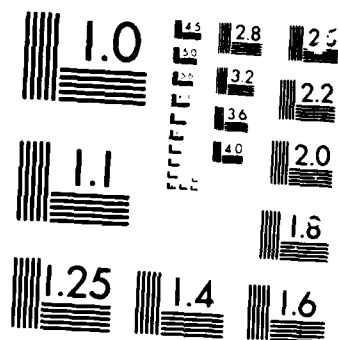
3/4

UNCLASSIFIED

F/G 8/13

NL





MICROCOPY

101 11

51. Jones, R., "Cracking and Failure of Concrete Test Specimens under Uniaxial Quasi-Static Loading," in Proceedings of the International Conference on the Structure of Concrete, London, 1965, pp. 125-129.
52. Kaplan, M. F., "Strains and Stresses of Concrete at Initiation of Cracking and near Failure," in Proceedings of the Journal of the American Concrete Institute, Vol. 60, No. 7, July 1963, pp. 853-880.
53. Kaplan, W., Advanced Calculus, Addison-Wesley, Reading, Mass., 1984.
54. Kassir, M.K., and Sih, G.C., eds., Mechanics of Fracture 2, Three-Dimensional Crack Problems, Noordhoff, Leyden, the Netherlands, 1975.
55. Kaufman, J.G., ed., Progress in Flaw Growth and Fracture Toughness Testing, ASTM STP 536, ASTM, Philadelphia, 1973.
56. Kim, Y., Master of Science Thesis, Texas A&M University, August 1985.
57. Kinra, V.K., Course notes, MM689G, Texas A&M University, Fall 1984.
58. Knott, J.F., Fundamentals of Fracture Mechanics, Butterworths, London, 1973.
59. Latanision, R.M., and Pickens, J.R., eds., Atomistics of Fracture, Plenum Press, N.Y., 1983.
60. Liebowitz, H., ed., Fracture, An Advanced Treatise, Volume II, Mathematical Fundamentals, Academic Press, New York, 1968.
61. Mahboub, K., "Low Temperature Fracture Evaluation of Plasticized Sulfur Paving Mixtures", Master of Science Thesis, Texas A&M University, May 1985.
62. Manson, J.A., Hertzberg, R.W., and Bretz, P.E., "Normalization of Fatigue Crack Propagation Behavior in Polymers", Advances in Fracture Research (Fracture 81), Francois, D., ed., Pergamon, Volume 1, 1982, pp. 443-448.
63. McDonald, J. E., "Creep of Concrete under Various Temperature, Moisture and Loading Conditions," Army Engineer Waterways Experiment Station, Vicksburg, Mississippi Corp Source Codes: 0515000, May 1977.

64. Mencik, J., "Rationalized Load and Lifetime of Brittle Materials", Communications, Journal of the American Ceramic Society, Vol. 67, No. 3, March 1984.
65. Miller, G.A., "The Dependence of Fatigue-Crack Growth Rate on the Stress Intensity Factor and the Mechanical Properties of Some High-Strength Steels", Transactions of the ASM, Vol. 61, 1968, pp. 442-448.
66. Mindess, S., Nadeau, J. S. and Hay, J. M., "Effects of Different Curing Conditions on Slow Crack Growth in Cement Paste," Cement and Concrete Research, 4, 1974, pp. 953-965.
67. Mindess, S. and Young, J.F., Concrete, Prentice-Hall,
68. Mindess, S., "The Application of Fracture Mechanics to Cement and Concrete: A Historical Review," in Fracture Mechanics of Concrete, F. H. Wittmann, Ed., Elsevier Science Publishers B. V., Amsterdam, 1983, pp. 1-30.
69. Molenaar, A. A. A., "Structural Performance and Design of Flexible Road Constructions and Asphalt Concrete Overlays," Ph. D. Dissertation, Delft University of Technology, Holland, May 1983.
70. Muskhelishvili, N.I., Some Basic Problems of the Mathematical Theory of Elasticity, (English translation), Noordhoff, 1953.
71. Newman, K., Lachance, L. and Loveday, R. W., "Strain Measurements on Saturated Concrete Specimens," Magazine of Concrete Research, Vol. 15, No.45, November 1963, pp. 143-150.
72. Nielsen, K. E. C., "Internal Stresses in Concrete," RILEM Bulletin, No. 1, March 1959, pp. 11-20.
73. Owen, M.J., and Cann, R.J., "Fracture Toughness and Crack-Growth Measurements in GRP", Journal of Materials Science, Vol. 14, No.8, August, 1979, pp.1982-1996.
74. Paris, P.C., The Growth of Fatigue Cracks Due to Variations in Load, PhD thesis, LeHigh University, 1962.
75. Paris, P. C. and Erdogan, F., "A Critical Analysis of Crack Propagation Laws," Transactions of the ASME, Journal of Basic Engineering, Series D, 85, No. 3, 1963.
76. Paris, P.C., and Sih, G.C., Stress Analysis of Cracks, ASTM STP 381, 1970, pp. 30-83.

77. Pickett, D.L. and Lytton, R.L., "Laboratory Evaluation of Selected Fabrics for Reinforcement of Asphaltic Concrete Overlays", Research Report 261-1, Texas Transportation Institute, Texas A&M University, College Station, Texas, August 1983.
78. Pihlajavaara, S. E., "Estimation of Drying of Concrete at Different Relative Humidities and Temperatures of Ambient Air with Special Discussion about Fundamental Features of Drying and Shrinkage," in Creep and Shrinkage in Concrete Structures, Chapter IV, John Wiley and Sons Ltd., 1982, 87-128.
79. Porterfield, W.W., Concepts of Chemistry, W.W. Norton, New York, 1972.
80. Pretorius, P. C., "Design Considerations for Pavements Containing Soil-Cement Bases," Ph. D. Dissertation, University of California, Berkeley, 1970.
81. Raad, L., Monismith, C. L. and Mitchell, J. K., "Crack Propagation in Soil-Cement Bases Subjected to Repeated Wheel Loads," Transportation Research Record, No. 690, Transportation Research Board, 1978, pp. 1-5.
82. Reifsnider, K.L., and Lauraitis, K.N., Fatigue of Filamentary Composite Materials, ASTM STP 636, ASTM, Philadelphia, 1977, pp. 47-56.
83. Rice, J.R., "A Path Independent Integral and the Approximate Analysis of Strain Concentration by Notches and Cracks", Journal of Applied Mechanics, Transactions of the ASME, Series E, Vol. 35, No. 2, June 1968, pp. 379-386.
84. Richart, F. E., Brandtzaeg, A. and Brown, L., "A Study of the Failure of Concrete under Combined Compressive Stresses," Urbana, University of Illinois Engineering Experiment Station, Bulletin No. 185, April 1929.
85. Rolfe, S.T., and Barsom, J.M., Fracture and Fatigue Control in Structures, Applications of Fracture Mechanics, Prentice Hall, Inc., N.J., 1977.
86. Rusch, H., "Physical Problems in the Testing of Concrete," Zement-Kalk-Gips, Vol. 12, No. 1, January 1959, pp. 1-9.
87. SAS Institute, Inc., SAS User's Guide, Cary, N.C., 1982.
88. Saxena, A., and Hudak, S.J., Jr., "Review and Extension of Compliance Information for Common Crack Growth Specimens", Scientific Paper 77-9E7-AFCGR-P1, Westinghouse R&D center, Pittsburg, 1977.

89. Saxena, A., and Hudak, S.J., Jr., "Review and Extension of Compliance Information for Common Crack Growth Specimens", International Journal of Fracture, Vol. 14, No. 5, Oct. 1978, pp. 453-468.
90. Schapery, R. A., "A Theory of Crack Growth in Viscoelastic Media," Technical Report No. 2 to Office of Naval Research, Department of the Navy, March 1973.
91. Schapery, R.A., "A Theory of Crack Growth in Viscoelastic Media, I. Theoretical Development", International Journal of Fracture, Vol. 11, No. 1, Noordhoff, Feb 1975, pp. 141-158.
92. Schapery, R.A., "A Theory of Crack Growth in Viscoelastic Media, II. Approximate Methods of Analysis", International Journal of Fracture, Vol. 11, No. 3, Noordhoff, Jun 1975, pp. 369-387.
93. Schapery, R.A., "A Theory of Crack Growth in Viscoelastic Media, III. Analysis of Continuous Growth", International Journal of Fracture, Vol. 11, No. 4, Noordhoff, Aug 1975, pp. 549-562.
94. Secor, K. E. and Monismith, C. L., "Viscoelastic Response of Asphalt Paving Slabs under Creep Loading," Highway Research Record, No. 67, Highway Research Board, 1965, pp. 84-97.
95. Setzer, M. J., "A Method for Description of Mechanical Behaviour of Hardened Cement Paste by Evaluating Adsorption Data," Cement and Concrete Research, 6, 1976, pp. 37-48.
96. Shah, S. P. and Slate, F. O., "Internal Microcracking, Mortar-Aggregate Bond and the Stress-Strain Curve of Concrete," in Proceedings of the International Conference on the Structure of Concrete, London, 1965, pp. 82-92.
97. Sih, G.C., Handbook of Stress Intensity Factors, Lehigh University, Bethlehem, Pa., 1973.
98. Sih, G.C., ed., Mechanics of Fracture 3, Plates and Shells with Cracks, Noordhoff, Leyden, the Netherlands, 1977.
99. Spangler, M.G. and Handy, R.L., Soil Engineering, Harper and Row, N.Y., 1982.
100. Terrel, R.L., Epps, J.A., Barenberg, E.J., Mitchell, J.K., and Thompson, R., Soil Stabilation in Pavement Structures, A User's Manual, Volume 2, Mixture Design Considerations, Federal Highway Administration, Washington, 1979.

101. Thomas, F. G., "Cracking in Reinforced Concrete," The Structural Engineer, Vol. 14, No. 7, 1936, pp. 298-320.
102. Thornton, P.A., "Fatigue Crack Propagation in a Discontinuous Composite", Journal of Composite Materials, Vol. 6, January 1972, pp. 147-151.
103. Tielking, J.T., Course notes, MM601, Theory of Elasticity, Texas A&M University, Fall 1984.
104. Timoshenko, S.P., and Goodier, J.N., Theory of Elasticity, McGraw-Hill, New York, 1970.
105. Wang, M. C. and Lee, K. Y., "Creep Behavior of Cement-Stabilized Soils," Highway Research Record, No. 442, Highway Research Board, 1973, pp. 58-69.
106. Wang, S.S., Chim, E.S.-M., and Zahlan, N.M., "Fatigue Crack Propagation in Random Short-fiber SMC Composite", Journal of Composite Materials, Vol. 17, No. 3, May 1983, pp. 250-266
107. Wei, R.P., Wei, W., and Miller, G.A., "Effect of Measurement Precision and Data Processing Procedures on Variability in Fatigue Crack Growth Rate Data", Journal of Testing and Evaluation, Vol. 7, No. 2, Mar. 1979, ASTM, pp. 90-95.
108. Wittmann, F. H., "Effect of Moisture Content on the Creep of Hardened Cement," Rheologica Acta, Vol. 9, No. 2, 1970, pp. 282-287.
109. Wittmann, F. H., "Structure of Concrete with respect to Crack Formation," in Fracture Mechanics of Concrete, F. H. Wittmann, Ed., Elsevier Science Publishers B. V., Amsterdam, 1983, pp. 43-74.
110. Wittman, F.H., ed., Fracture Mechanics of Concrete, Developments in Civil Engineering, 7, Elsevier, New York, 1983.
111. Yoder, E.J., and Witczak, M.W., Principles of Pavement Design, J. Wiley and Sons, New York, 1975.

## Additional Reading

112. Bazant, Z.P., and Cedolin, L., "Propagation of Crack Bands in Heterogeneous Materials", Advances in Fracture Research (Fracture 81), Francois, D., ed., Pergamon, Vol. 4, 1982, pp. 1523-1529.
113. Beer, F.P., and Johnston, E.R., Jr., Mechanics of Materials, McGraw-Hill, N.Y., 1981.
114. Begley, J.A., and Landes, J.D., "A Comparison of the J-Integral Fracture Criterion with the Equivalent Energy Concept", Progress in Flaw Growth and Fracture Toughness Testing, ASTM STP 536, 1973, pp. 246-263.
115. Boresi, A.P., Sidebottom, O.M., Seely, F.B., and Smith, J.O., Advanced Mechanics of Materials, John Wiley & Sons, New York, 1978.
116. Bowles, J.E., Engineering Properties of Soils and their Measurement, McGraw-Hill, N.Y., 1978.
117. Bueckner, H.F., "The Propagation of Cracks and the Energy of Elastic Deformation", Transactions of the ASME, 80, August, 1958, pp. 1225-1230.
118. Caddell, R.M., Deformation and Fracture of Solids, Prentice-Hall, Englewood Cliffs, New Jersey, 1980.
119. Carpenter, S.H., and Lytton, R.L., "Procedure for Predicting Occurrence and Spacing of Thermal-Susceptibility Cracking in Flexible Pavements", Analysis of Pavement Systems, Transportation Research Record 671, TRB, 1978.
120. Carpinteri, A., "Experimental Determination of Fracture Toughness Parameters  $K_{IC}$  and  $J_{IC}$  for Aggregative Materials", Advances in Fracture Research (Fracture 81), Francois, D., ed., Pergamon, Volume 4, 1982, pp. 1491-1498.
121. Chen, W.F., and Saleeb, A.F., Constitutive Equations for Engineering Materials, Volume I: Elasticity and Modeling, J. Wiley and Sons, N.Y., 1982.
122. Chhuy, S., Benkirane, M.E., Baron, J., and Francois, D., "Crack Propagation in Prestressed Concrete, Interaction with Reinforcement", Advances in Fracture Research, (Fracture 81), Francois, D., ed., Pergamon, Volume 4, 1982, pp. 1507-1514.

123. Cho, K.Z., Kobayashi, A.S., Hawkins, N.M., Barker, D.B., and Jeang, F.L., "Fracture Process Zone of Concrete Cracks", Journal of Engineering Mechanics, ASCE, Volume 110, No. 8, August 1984, pp. 1174-1184.
124. Dabbs, T.P., Lawn, B.R., and Kelly, P.L., "A Dynamic Fatigue Study of Soda-Lime Silicate and Borosilicate Glasses using Small Scale Indentation Flaws", Physics and Chemistry of Glasses, Vol. 23, No. 2, April 1982, pp. 58-66.
125. Davidge, R.W., and Green, T.J., "The Strength of Two-Phase Ceramic/Glass Materials", Journal of Materials Science, Vol. 3, No. 6, November, 1968, pp. 629-634.
126. Dugdale, D.S., "Yielding of Steel Sheets Containing Slits", Journal of the Mechanics and Physics of Solids, Vol. 8, 1960, pp. 100-108.
127. Early, J.G., Shives, T.R., and Smith, J.H., eds., Time-Dependent Failure Mechanisms and Assessment Methodologies, Proceedings of the 35th meeting of the mechanical failures prevention group, National Bureau of Standards, Cambridge University Press, 1983.
128. Evans, A.G., "A Method for Evaluating the Time-Dependent Failure Characteristics of Brittle Materials - and its Application to Polycrystalline Alumina", Journal of Materials Science, Vol. 7, 1972, pp. 1137-1146.
129. Evans, A.G., and Linzer, M., "Failure Prediction in Structural Ceramics using Acoustic Emission", Journal of the American Ceramic Society, Vol. 56, November 1973, pp. 575-580.
130. Evans, A.G., and Faber, K.T., "Crack-Growth Resistance of Microcracking Brittle Materials", Journal of the American Ceramic Society, Vol. 67, No. 4, April 1984, pp. 255-260.
131. Frost, N.E., and Dixon, J.R., "A Theory of Fatigue Crack Growth", International Journal of Fracture Mechanics, Vol. 3, No. 4, December 1967, pp. 301-316.
132. Fuhring, H., "Practical Application of a Model for Fatigue Damage with Irregular Cyclic Loading", Advances in Fracture Research (Fracture 81), Francois, D., ed., Pergamon, Vol. 4, 1982, pp. 1823-1832.
133. Hahn, G.T., "The Influence of Microstructure on Brittle Fracture Toughness", Metallurgical Transactions, Series A, Vol. 15A, June 1984, pp. 947-959.

134. Hillerborg, A., and Petersson, P.E., "Fracture Mechanical Calculations, Test Methods and Results for Concrete and Similar Materials", Advances in Fracture Research (Fracture 81), Francois, D., ed., Pergamon, Vol. 4, 1982, pp. 1515-1522.
135. Irwin, G.R., "Analysis of Stresses and Strains Near the End of a Crack Traversing a Plate", Journal of Applied Mechanics, Vol. 24, No. 3, September 1957, pp. 361-364.
136. Irwin, G.R., "Fracture Mechanics", Structural Mechanics Proceedings of the first Naval Symposium, Pergamon, 1960.
137. Kachanov, M., "Continuum Model of Medium with Cracks", Journal of Engineering Mechanics, ASCE, Vol. 106, No. EM5, October 1980, pp. 1039-1051.
138. Kamal, K., and Durvasula, S., "Bending of a Circular Plate on Elastic Foundation", Journal of Engineering Mechanics, ASCE, Vol. 109, No. EM5, October 1983, pp. 1293-1298.
139. Kaplan, M.F., "Crack Propagation and the Fracture of Concrete", Proceedings, Journal of the American Concrete Institute, Vol. 58, November 1961.
140. Kato, K., "Microcracks, Deformation and Physical Properties of Plain Concrete", Advances in Fracture Research (Fracture 81), Francois, D., ed., Pergamon, Vol. 5, 1982, pp. 2275-2280.
141. Katsikadeli, J.T., and Armenakas, A.E., "Plates on Elastic Foundation by BIE Method", Journal of Engineering Mechanics, ASCE, Vol. 110, No. EM7, July 1984, pp. 1086-1105.
142. Vu, B.Q., and Kinra, V.K., "Brittle Fracture of Plates in Tension - Relative Significance of Boundary Reflected Body and Rayleigh Waves", Technical Note, Engineering Fracture Mechanics, Vol. 18, No. 2, 1983, pp. 479-483.
143. Kobayashi, A.S., Ziv, M., and Hall, L.R., "Approximate Stress Intensity Factor for an Embedded Elliptical Crack Near Two Parallel Free Surfaces", International Journal of Fracture Mechanics, Vol. 1, 1965, pp. 81-95.
144. Mazars, J., "Mechanical Damage and Fracture of Concrete Structures", Advances in Fracture Research, (Fracture 81), Francois, D., ed., Pergamon, Vol. 4, 1982, pp. 1499-1506.
145. Merritt, F.S., ed., Standard Handbook for Civil Engineers, McGraw-Hill, New York, 1983.
146. Ott, L., An Introduction to Statistical Methods and Data Analysis, Second Edition, Duxbury, Boston, 1984.

147. PCA, Soil-Cement Laboratory Handbook, Engineering bulletin, Portland Cement Association, 1971.
148. Ramsamooj, D.V., Majidzadeh, K., and Kauffmann, E.M., "The Analysis and Design of the Flexibility of Pavements", Proceedings, Third International Conference on the Structural Design of Asphalt Pavements, University of Michigan, 1972, pp. 692-703.
149. Rice, J.R., "The Line Spring Model for Surface Flaws", The Surface Crack: Physical Problems and Computational Solutions, Swedlow, J.L., ed., ASME, New York, 1972, pp. 171-185.
150. Sanders, J.L., Jr., "On the Griffith-Irwin Fracture Theory", Journal of Applied Mechanics, Transactions of the ASME, Series E, Volume 27, No. 2, June 1960, pp.352-353.
151. Saouma, V.E., Ingraffea, A.R., and Catalano, D.J., "Fracture Toughness of Concrete:  $K_{IC}$  Revisited", Journal of Engineering Mechanics, ASCE, Volume 108, No. EM6, Dec 1982, pp. 1152-1166.
152. Swartz, S.E., Hu, K.K., Faetash, M., and Huang, C.-M.J., "Stress-Intensity Factor for Plain Concrete in Bending - Prenotched versus Precracked Beams", Experimental Mechanics, Nov. 1982, pp. 412-417.
153. Swedlow, J.L., "On Griffith's Theory of Fracture", International Journal of Fracture Mechanics, Volume 1, No. 3, September 1965, pp.210-216.
154. Ugural, A.C., Stresses in Plates and Shells, McGraw-Hill, N.Y., 1981.
155. VanVlack, L.H., Materials for Engineering: Concepts and Applications, Addison-Wesley, Reading, Ma., 1982.
156. Wecharatan, M., and Shah, S.P., "Predictions of Nonlinear Fracture Process Zone in Concrete", Journal of Engineering Mechanics, ASCE, Vol. 109, No.5, Oct. 1983, pp. 1231-1246.
157. Westergaard, H.M., "Bearing Pressures and Cracks", Journal of Applied Mechanics, ASME, N.Y., June, 1939, pp. A49-A53.
158. Willis, J.R., "A Comparison of the Fracture Criteria of Griffith and Barenblatt", Journal of the Mechanics and Physics of Solids, Vol. 15, No. 3, May 1967, pp. 151-162.

## APPENDIX II.-NOTATION AND CONVERSION FACTORS

SYMBOL	MEANINGS
a	crack length as shown in coordinate system definition
A	regression constant in fatigue equation; area in other cases
b	real constant
B	specimen thickness $x_3$ direction
c	real constant; when used as a subscript critical value
C	piecewise smooth simple closed path of a line integral
$C_i, D_i$	coefficients in power laws used in creep
d	diameter in geometry; total differential in calculus
e	2.71828 . . .
E	Young's modulus of elasticity
f	frequency; function
F	function; statistical distribution
g	function
G	strain energy release rate
h	thickness (depth)
i	$\sqrt{-1}$ in complex variables; row in a matrix; index ( $i=1, 2, 3$ )
$\hat{i}$	unit vector $x_1$ direction
Im	imaginary part of
j	column designator; index (usually 1, 2, 3)
$\hat{j}$	unit vector $x_2$ direction
J	J integral
k, l, m, p	indices (usually 1, 2, 3)
$\hat{k}$	unit vector $x_3$ direction
K	stress intensity factor
m	creep exponent
n	regression constant (exponent) in fatigue equation
$\hat{n}$	unit normal vector
N	number of cycles in fatigue; number of samples in statistics
P	load
r	radius
Re	real part of
S	strain energy density factor
t	time; statistical distribution
T	temperature
T	traction vector normal to integration path
U	potential energy
u	displacement vector
V	volume
W	specimen width in the $x_1$ direction; strain energy density
x, y	$x_1$ and $x_2$ directions respectively
z	depth

$\alpha$	index (1, 2) for plane analyses; angle in geometry; failure zone
$\beta$	index for plane analyses; angle; regression parameter in statistics
$\gamma, \Gamma$	Griffith surface tension parameter= $G/2$
$\Gamma(m)$	gamma function
$\partial$	partial differential
$\delta$	displacement; variation in calculus
$\epsilon$	strain
$\xi$	local coordinate axes
$\theta$	angle
$\kappa$	bulk modulus
$\lambda$	wavelength; Lamé constant; Lagrange multiplier
$\mu$	shear modulus
$\nu$	Poisson's ratio
$\xi$	complex variable
$\pi$	$4\arctan(1)$
$\rho$	density
$\sigma$	stress
$\sigma_1$	principal stress
$\tau$	shear stress
$\phi$	complex function; angle of internal friction
$\chi^2$	statistical distribution
$\omega$	angular rotation
$\Sigma$	summation
$\Phi$	stress function
$\Delta$	difference
$\nabla$	vector differential operator
$\ll$	much less than
$\lim_{x \rightarrow l}$	limit as $x$ approaches $l$
$\therefore$	therefore
$\sqrt{\quad}$	square root
$\int$	the integral of
$  \vec{r}  $	magnitude of
$ c $	absolute value of $c$
$\cdot$	dot or inner product; $d(\quad)/dt$
$\cdot$	used for different values of the same variable, this symbol is not used to indicate differentiation
$\ln$	natural (Napierian) logarithm (base $e$ )
$\approx$	approximately equals
$\infty$	infinity
$\propto$	varies as
$\sin$	trigonometric sine function
$P_{\max}$	maximum load during static test
$\delta P_{\max}$	displacement at $P_{\max}$
$P_{\max}^f(a/W)$	maximum load corrected for crack length

$\sigma_{IDT}$  indirect tensile strength  
 $a_{os}$  crack length at start of static test (after precrack)  
 LL-Krak distance from load line to front of Krak-gage®  
 $P_{min}$  minimum load in cyclic test  
 $a_{of}$  crack length at start of cyclic test  
 $K(a_o)$  K evaluated using original crack length  
 $K(a_{cur})$  K evaluated using instantaneous (current) crack length  
 $V_{max}, V_{min}$  maximum (minimum) load in a cycle in terms of volts  
 CSI crack speed index  
 $K_{QD}$   $K_I$  at failure ( $\approx \Delta K_{IC}$ )

It can be seen that a very few of the symbols have different meanings in different contexts. The contexts in which these symbols are used make the meanings unambiguous.

To convert A from the literature to an equivalent A' in English units:

Given:  $da/dN = A\Delta K^n$

Find: Conversion to units of  $(da/dN)'$  in inches/cycle,  $\Delta K'$  in psi/in.

Assume:  $n = \text{constant}$  (i.e. same in both systems of units)

$$(a \text{ in/L}) * da/dN = aA\Delta K^n = (da/dN)'$$

$$[\beta \text{ psi/in}/(F/L/L^2)] \cdot \Delta K = \Delta K'$$

$$\therefore (da/dN)' = A' \Delta K'^n = A' (\beta \Delta K)^n$$

$$\therefore a \Delta K^n = A' (\beta \Delta K)^n$$

$$\Rightarrow A' = aA/(\beta^n)$$

$$\Rightarrow \log_{10} A' = \log_{10} a + \log_{10} A - \log_{10} (\beta^n) \quad (\text{II-1})$$

To convert from:	To:	In equation (II-1) use:	
da/dN $\Delta K$	in/cy, psi/in	$a$	$\beta$
mm/cy $N/mm^{3/2}$		0.3937	28.7798
in/cy    ksi/in		1.0	1000
mm/cy    MPa/m		0.03937	909.918
$\mu m/cy$ MPa/m		0.00003937	909.918
$\mu in/cy$ ksi/in		$10^{-6}$	1000
in/cy    psi/in		1.0	1.0
m/cy    MPa/m		39.37	909.918

To convert from	To	Multiply by
in	cm	2.54
lb	N	4.448
psi	Pa	6895
psi/in	Pa/m	1099
in-lb/in <sup>2</sup>	N/mm	0.175118
$N/mm^{3/2}$	psi/in	28.7798
$^{\circ}F-32$	$^{\circ}C$	5/9

## APPENDIX III.-DATA

The following raw data is provided for completeness and future research. The format of the data is as follows:

CARD 1 - the specimen identification; M=modified, S=standard; 05, 10, 15=percent cement content; RAW=raw data; 14B=specimen number (B=taken from the bottom of the compacted cylinder, C=center, T=top of cylinder); A107, A114, A128=7, 14, 28 day cure specimens (10% modified).

CARD 2 -  $K_{IC}$ (psi/in),  $J_{IC}$ (lb-in/in<sup>2</sup>),  $dJ/da$ ,  $E_{west}$ (psi),  $P_{max}$ ,  $\delta_{pmax}$ (in),  $P_{max}^f(a/W)$ .

CARD 3 -  $\sigma_{IDT}$ (psi),  $\nu$ , %cement, %moisture, compaction effort(in-lb/in<sup>3</sup>), 0, 0, 0.

CARD 4 -  $a_{OS}$ (mm), LL-Krak(in),  $d\delta/dt$ (in/min),  $P_{min}$ (lb),  $a_{Of}$ (mm), Last cycle

CARD 5 -  $N_S$

CARDS 6 through  $N_S+5$  -  $P$ ,  $a$ ,  $\delta$ ,  $t$  (sec),  $K(a_0)$ ,  $K(a_{cur})$ .

CARD  $N_S+6$  -  $N_f$

CARDS  $N_S+7$  through end -  $V_{max}$  (volts),  $V_{min}$ ,  $a$ ,  $N$

It should be noted that the following specimens were cycled at five seconds per cycle and are not included in the fatigue results in this paper: M05.14T, M05.14B, M15.13T, S05.11T, S05.11B, S15.12C, S15.12B, A107.241T. The following specimens included higher frequency fatigue (>1cps), only the 1 cps portion of which was used: M10.3C, M10.3B, M10.4C, M10.4B.

## M05.RAW14B

90.9	.0159	1.163	182762	12.2	.004715	29.1	
75.0	.15	5.0	16.8	397.9	0	0	0
2.79	.945	.00084	1.0	4.50	54		
14							
7.5	2.79	.002505		0	55.9	55.9	
8.15	2.80	.002745	17.1429		60.7	60.8	
8.75	2.81	.002955	32.1429		65.2	65.3	
10.05	2.84	.00341	64.6429		74.9	75.1	
10.5	2.85	.003565	75.7143		78.2	78.5	
10.9	2.87	.003705	85.7143		81.2	81.6	
11.35	2.91	.003885	98.5714		84.6	85.2	
11.7	3.04	.004025	108.571		87.2	88.6	
11.9	3.24	.004165	118.571		88.7	91.3	
12.0	3.48	.00435	131.786		89.4	93.5	
12.2	3.71	.004715	157.857		90.9	96.5	
12.2	3.92	.005305	200.0		90.9	97.9	
12.1	4.07	.00586	239.643		90.1	98.1	
11.9	4.27	.006495	285.0		88.7	97.8	
10							
0.734	-.109	4.62	17				
0.759	-.079	4.72	23				
0.772	-.064	4.82	26				
0.784	-.049	4.96	30				
0.782	-.047	5.20	36				
0.782	-.047	5.50	39				
0.782	-.047	5.90	43				
0.709	-.046	6.08	47				
0.700	-.044	6.28	50				
0.700	-.044	8.46	54				

## M05.RAW14T

71.7	.0294	.605	153668	9.9	.004345	23.2	
75.0	.15	5.0	16.8	397.9	0	0	0
2.97	.92	.00084	1.0	4.72	604		
10							
4.75	2.97	.00167	0	34.4	34.4		
5.6	2.98	.00209	30.0	40.5	40.6		
6.65	2.99	.002555	63.2143	48.1	48.2		
8.65	3.00	.003335	118.929	62.6	62.7		
9.15	3.02	.00355	134.286	66.2	66.4		
9.5	3.05	.00373	147.143	68.8	69.1		
9.8	3.16	.00396	163.571	70.9	71.8		
9.9	3.32	.004345	191.071	71.7	73.3		
9.85	3.52	.00474	219.286	71.3	73.8		
9.7	3.88	.005075	243.214	70.2	74.4		
21							
0.580	-.009	4.79	14				
0.58	-.009	4.85	28				
0.582	-.008	4.90	43				
0.586	-.009	5.00	65				

0.583	-.010	5.10	91
0.583	-.01	5.25	139
0.580	-.012	5.35	175
0.587	-.003	5.40	188
0.586	-.005	5.45	197
0.586	-.005	5.50	212
0.585	-.009	5.70	263
0.584	-.005	5.80	288
0.583	-.002	5.90	337
0.586	-.005	6.05	390
0.589	-.008	6.15	439
0.586	-.006	6.34	519
0.585	-.005	6.46	557
0.583	-.002	6.50	571
0.637	-.005	6.65	594
0.639	-.006	6.75	599
0.634	-.006	7.24	604

## M05.RAW18C

95.6	.0199	1.251	228648	13.15	.003925	30.9	
75.0	.15	5.0	16.8	397.9	0	0	0
2.82	.929	.00084	1.0	5.41	49554		
12							
8.2	2.82	.002155		0	59.6	59.6	
12.0	2.83	.00315	71.0714	87.3	87.3		
12.35	2.84	.00325	78.2143	89.8	89.9		
12.65	2.87	.00335	85.3517	92.0	92.3		
12.8	2.93	.003445	92.1429	93.1	93.8		
12.85	3.12	.003495	95.7143	93.5	95.3		
13.05	3.33	.003695	110.0	94.9	98.1		
13.15	3.51	.00408	137.5	95.6	100.0		
12.55	3.66	.004745	185.0	91.3	96.4		
12.05	3.86	.00537	229.643	87.6	93.7		
11.65	4.15	.005885	266.429	84.7	92.4		
11.25	4.34	.006295	295.714	81.8	90.4		
20							
0.324	-.001	5.47	252				
0.324	-.001	5.60	1260				
0.324	-.001	5.70	2700				
0.324	-.001	5.80	4590				
0.324	-.001	5.90	6300				
0.324	-.001	6.00	8640				
0.324	-.001	6.10	12240				
0.324	-.001	6.20	16470				
0.324	-.001	6.30	21600				
0.324	-.001	6.40	25200				
0.324	-.001	6.50	28350				
0.324	-.001	6.60	33300				
0.324	-.001	6.70	36000				
0.324	-.001	6.90	39600				
0.325	.004	7.00	41958				

0.330	.003	7.08	44010
0.508	.006	7.10	44154
0.504	.006	7.25	44550
0.513	.006	7.44	49050
0.718	.025	7.45	49554

## M05.RAW18T

114.3	.0534	.321	202008	16.0	.00514	37.2	
75.0	.15	5.0	16.8	397.9	0	0	0
2.66	.924	.00084	1.0	4.95	6690		
10							
7.65	2.66	.002115		0	54.6	54.6	
8.85	2.67	.002495	27.1429	63.2	63.3		
13.1	2.68	.00377	118.214	93.6	93.7		
13.5	2.69	.003885	126.429	96.4	96.6		
14.0	2.70	.004045	137.857	100.0	100.3		
15.4	2.72	.004475	168.571	110.0	110.4		
15.5	3.00	.004565	175.0	110.7	113.1		
15.95	3.41	.004855	195.714	113.9	119.5		
15.8	3.80	.00495	202.5	112.9	121.4		
16.0	4.07	.00514	216.071	114.3	125.2		
14							
.854	-.006	5.40	396				
.857	-.005	5.85	990				
0.855	-.004	6.15	1830				
0.854	-.003	6.51	2550				
0.855	-.003	6.65	3300				
0.857	-.003	6.78	5010				
1.006	-.006	6.85	5234				
1.009	-.005	6.90	5327				
1.009	-.005	6.95	5388				
1.002	-.005	7.05	5550				
1.002	-.005	7.25	5814				
1.005	-.005	7.40	6006				
1.005	-.005	7.65	6342				
1.001	0	8.25	6594				

## M05.RAW6B

94.1	.0431	.169	201047	13.5	.00415	30.9	
75.0	.15	5.0	16.8	397.9	0	0	0
2.12	.930	.0008	1.0	5.30	681		
9							
8.75	2.12	.002425		0	61.0	61.0	
11.45	2.13	.003185	57.0	80.0	79.9		
12.85	2.15	.003615	89.25	89.6	89.8		
13.15	2.30	.00375	99.375	91.7	92.7		
13.25	2.45	.003875	108.75	92.4	94.3		
13.5	2.50	.00405	121.875	94.1	96.4		
13.5	2.76	.00419	132.375	94.1	98.0		
13.45	3.13	.0043	140.625	93.8	100.0		

13.35 3.53 .00438 146.625 93.1 101.8  
24

0.797	.031	5.38	11
0.788	.028	5.44	21
0.781	.025	5.51	30
0.782	.019	5.59	41
0.771	.015	5.75	57
0.779	.012	5.83	73
0.784	.012	5.92	88
0.776	.006	6.04	100
0.785	.015	6.13	113
0.769	.001	6.25	140
0.774	.003	6.35	184
0.778	.016	6.45	218
0.778	.009	6.50	233
0.772	0	6.55	247
0.771	.001	6.60	280
0.776	.013	6.70	335
0.772	.01	6.80	390
0.793	.028	6.90	472
0.791	.026	7.00	548
0.790	.025	7.25	620
0.793	.028	7.40	639
0.787	.026	7.58	650
0.793	.028	8.22	661
0.785	.028	8.80	670

## M05.RAW6C

54.7	.0316	.191	103545	7.9	.00485	18.1	
75.0	.15	5.0	16.8	397.9	0	0	0
2.50	.914	.0008	1.0	4.72	218		

9

5.0	2.50	.00271	0	34.8	34.8
5.8	2.51	.00313	31.5	40.4	40.4
7.7	2.57	.00436	123.75	53.6	53.8
7.8	2.64	.00459	141.0	54.3	54.8
7.85	2.69	.0047	149.25	54.7	55.3
7.85	2.76	.00483	159.0	54.7	55.5
7.85	2.88	.004925	166.125	54.7	56.0
7.8	3.02	.005305	194.625	54.3	56.1
7.65	3.98	.005595	216.375	53.3	58.5

7

0.505	.029	4.80	15
0.494	.025	4.90	36
0.510	.032	4.98	68
0.513	.031	5.00	89
0.523	.037	5.10	146
0.532	.042	5.20	179
0.519	.056	5.35	208

## M05.RAW6T

65.3	.0261	.185	160568	9.1	.00355	21.2	
75.0	.15	5.0	16.8	397.9	0	0	0
2.97	.915	.0008	1.0	5.45	854		
9							
5.35	2.97	.00194	0	38.4	38.4		
7.5	2.98	.00271	57.75	53.8	53.9		
8.4	3.00	.00305	83.25	60.3	60.4		
9.0	3.03	.00342	111.0	64.6	64.9		
9.1	3.15	.00355	120.75	65.3	66.1		
9.1	3.31	.00364	127.5	65.3	66.8		
9.1	3.58	.003755	136.125	65.3	67.9		
9.0	3.84	.003995	154.125	64.6	68.3		
8.85	4.38	.004155	166.125	63.5	69.6		
35							
.551	-.005	5.55	19				
0.539	-.005	5.65	35				
0.533	-.015	5.75	62				
0.542	-.011	5.85	92				
0.533	-.022	5.95	114				
0.543	.001	6.12	143				
0.538	-.011	6.20	164				
0.552	.007	6.35	189				
0.567	.001	6.40	205				
0.539	-.008	6.50	229				
0.563	.004	6.65	253				
0.563	.016	6.75	267				
0.554	.009	6.83	281				
0.557	.012	6.95	306				
0.565	.012	7.05	329				
0.558	.023	7.16	350				
0.548	.003	7.30	374				
0.546	.001	7.40	388				
0.545	.015	7.50	420				
0.548	.015	7.60	446				
0.542	-.003	7.70	467				
0.549	.006	7.85	508				
0.545	.001	7.97	535				
0.554	.006	8.10	571				
0.548	.012	8.27	604				
0.542	.006	8.45	634				
0.548	.004	8.66	683				
0.551	0	8.90	723				
0.535	-.002	9.05	745				
0.541	.003	9.20	761				
0.543	.006	9.35	775				
0.542	.006	9.41	790				
0.536	.007	9.60	808				
0.535	.009	9.75	825				
0.535	.009	10.00	843				

## M10.RAW3B

146.6	.0513	.707	339509	20.6	.0038	47.8	
155.0	.15	10.0	16.8	397.9	0	0	0
2.32	.935	.0008	1.0	4.54			
13							
11.00	2.32	.001820	0.	78.3	78.3		
14.80	2.34	.00253	53.25	105.3	105.5		
17.85	2.36	.00306	93.0	127.0	127.3		
19.75	2.39	.0034	118.5	140.6	141.2		
20.20	2.53	.00355	129.8	143.8	145.7		
20.55	2.70	.00371	141.75	146.2	149.8		
20.60	2.86	.0038	148.5	146.6	151.7		
20.2	2.94	.00389	155.25	143.8	149.5		
20.2	3.09	.004	163.5	143.8	150.9		
20.1	3.22	.004135	173.625	143.0	151.5		
20.0	3.42	.0043	186.0	142.3	152.7		
19.8	3.59	.00446	198.0	140.9	152.8		
19.45	3.74	.004575	206.625	138.4	151.6		
41							
1.198	.01	4.57	13				
1.176	.001	4.61	42				
1.179	0	4.66	67				
1.187	-.005	4.70	101				
1.185	-.009	4.73	123				
1.192	.003	4.75	149				
1.184	.004	4.78	196				
1.181	0.	4.83	237				
1.179	-.008	4.85	278				
1.169	-.003	4.89	315				
1.175	-.014	4.91	332				
1.187	.003	4.95	360				
1.182	-.006	4.98	405				
1.178	.003	5.00	420				
1.168	-.009	5.05	474				
1.163	-.006	5.10	540				
1.168	-.011	5.15	603				
1.168	-.011	5.20	725				
1.166	.022	5.24	777				
1.166	.018	5.30	902				
1.154	.013	5.35	1001				
1.146	.018	5.40	1080				
1.159	.018	5.46	1148				
1.168	.021	5.53	1202				
1.144	.029	5.60	1245				
1.16	.018	5.70	1290				
1.16	.021	5.90	1394				
1.138	.019	5.96	1426				
1.162	.026	6.15	1502				
1.159	.026	6.25	1535				
1.15	.026	6.30	1564				
1.154	.022	6.35	1608				
1.156	.026	6.45	1682				

1.15	.029	6.50	1732
1.156	.028	6.56	1784
1.157	.031	6.62	1819
1.15	.031	6.70	1888
1.153	.031	6.77	1941
1.16	.032	6.88	1978
1.135	.034	6.99	2008
1.135	.034	7.14	2030

## M10.RAW3C

130.4	.0511	.482	302550	18.75	.0038	42.9	
155.0	.15	10	16.8	397.9	0	0	0
2.20	.925	.0008	1.0	4.74			

15

9.5	2.20	.001670	0	66.1	66.1
10.2	2.21	.001825	11.625	70.9	71.0
11.0	2.22	.002	24.75	76.5	76.6
14.35	2.23	.00265	73.5	99.8	100.0
16.5	2.24	.00305	103.5	114.7	115.0
17.75	2.25	.003295	121.875	123.4	123.8
18.0	2.26	.00337	127.5	125.2	125.6
18.35	2.28	.00345	133.5	127.6	128.2
18.5	2.40	.00355	141.0	128.6	130.2
18.65	2.52	.003625	146.625	129.7	132.3
18.75	2.61	.00375	156.0	130.4	133.7
18.75	2.65	.003815	160.875	130.4	134.1
18.7	2.74	.00395	171.0	130.0	134.5
18.25	3.03	.004095	181.875	126.9	133.7
17.55	3.28	.00415	186.0	122.0	130.6

75

1.08	-.053	4.78	17
1.074	-.058	4.83	36
1.084	-.055	4.85	52
1.072	-.061	4.88	80
1.068	-.059	4.91	96
1.077	-.065	4.93	120
1.052	-.063	4.95	142
1.052	-.065	4.97	164
1.04	-.066	5.00	234
1.056	-.063	5.03	268
1.096	-.056	5.09	300
1.086	-.056	5.17	320
1.087	-.058	5.35	351
1.071	-.055	5.49	394
1.093	-.055	5.61	413
1.078	-.058	5.70	436
1.09	-.056	5.85	464
1.086	-.055	5.95	496
1.081	-.056	6.00	534
1.075	-.053	6.04	562
1.091	-.055	6.12	662

1.088	-.056	6.15	705
1.084	-.058	6.21	862
1.081	-.058	6.22	882
1.09	-.056	6.26	945
1.097	-.056	6.28	980
1.088	-.058	6.32	1043
1.077	-.053	6.35	1087
1.086	-.052	6.39	1126
1.088	-.052	6.42	1175
1.087	-.055	6.45	1235
1.099	-.052	6.50	1367
1.083	-.055	6.55	1500
1.083	-.055	6.60	1557
1.091	-.056	6.65	1640
1.09	-.05	6.70	1722
1.072	-.052	6.75	1791
1.08	-.052	6.80	1889
1.096	-.053	6.85	1984
1.087	-.05	6.90	2007
1.084	-.058	6.95	2078
1.078	-.052	7.00	2114
1.083	-.055	7.05	2193
1.069	-.056	7.10	2280
1.084	-.05	7.15	2544
1.081	-.053	7.23	2735
1.068	-.058	7.26	2768
1.08	-.053	7.30	3029
1.059	-.028	7.35	3078
1.056	-.034	7.39	3152
1.086	-.027	7.50	3294
1.086	-.022	7.56	3328
1.069	-.024	7.61	3364
1.074	-.021	7.67	3400
1.084	-.027	7.78	3482
1.086	-.024	7.80	3516
1.081	-.033	7.87	3568
1.072	-.024	7.95	3633
1.074	-.024	8.06	3712
1.074	-.021	8.11	3780
1.08	-.017	8.27	3852
1.084	-.017	8.35	3884
1.078	-.017	8.44	3913
1.078	-.018	8.67	3957
1.078	-.017	8.90	3999
1.074	-.017	9.15	4045
1.072	-.017	9.35	4093
1.08	-.024	9.47	4124
1.075	-.017	9.60	4161
1.065	-.018	9.70	4201
1.069	-.014	9.95	4257
1.072	-.017	10.10	4287
1.072	-.012	10.25	4325

1.065	-.008	10.65	4386
1.065	-.008	11.05	4420

## M10.RAW3T

178.9	.0494	.551	568481	24.1	.00275	57.1	
155.0	.15	10	16.8	397.9	0.	0.	0.
3.18	.925	.0008	1.0	5.2			

9

15.0	3.18	0.0016	0.0	110.9	110.9
19.5	3.19	.00209	36.75	144.2	144.3
22.0	3.20	.002365	57.375	162.7	162.9
23.6	3.38	.0026	75.0	174.5	176.8
24.2	3.48	.002755	86.625	178.9	182.4
23.9	3.66	.002825	91.875	176.7	182.3
23.75	3.8	.002875	95.625	175.6	182.8
24.0	4.05	.00306	109.500	177.5	187.8
23.7	4.29	.00319	119.250	175.2	188.5

24

1.770	0.082	5.25	9
1.77	.081	5.37	23
1.77	.08	5.55	39
1.77	.08	5.71	58
1.77	.08	5.75	66
1.77	.08	5.9	85
1.773	.066	6.0	99
1.773	.066	6.1	120
1.733	.051	6.2	136
1.74	.042	6.25	151
1.755	.034	6.3	164
1.752	.041	6.37	185
1.752	.041	6.43	205
1.749	.048	6.54	227
1.749	.048	6.64	242
1.833	.067	6.75	264
1.822	.069	6.9	289
1.822	.069	6.96	297
1.789	.079	7.07	322
1.79	.066	7.21	346
1.79	.066	7.3	361
1.783	.073	7.45	383
1.796	.07	7.75	412
1.796	.07	8.38	431

## M10.RAW4B

150.6	.0465	.567	357794	21.3	.00375	49.2	
155.0	.15	10.0	16.8	397.9	0	0	0
2.42	.927	.0008	1.0	5.35			

9

11.25	2.42	.00175	0	79.5	79.5
18.05	2.46	.00289	85.5	127.6	127.9

19.85	2.48	.0032	108.75	140.4	140.9
20.45	2.65	.00331	117.0	144.6	146.7
21.05	3.01	.00351	132.0	148.8	154.5
21.30	3.43	.00375	150.0	150.6	160.6
21.25	3.66	.003885	160.125	150.3	162.6
21.15	3.80	.00395	165.0	149.6	163.3
20.70	3.93	.004185	182.625	146.4	161.2

69

1.22	.031	5.44	32
1.216	.035	5.51	42
1.217	.034	5.55	56
1.223	.025	5.60	87
1.225	.031	5.66	105
1.22	.038	5.70	120
1.216	.037	5.75	133
1.223	.031	5.80	150
1.217	.038	5.86	166
1.228	.022	5.92	178
1.212	.035	6.02	195
1.21	.026	6.10	214
1.229	.031	6.20	230
1.212	.028	6.27	244
1.21	.029	6.48	273
1.226	.025	6.51	290
1.217	.031	6.61	310
1.213	.031	6.68	329
1.214	.031	6.76	348
1.214	.028	6.85	373
1.223	.031	6.90	394
1.225	.031	6.99	424
1.212	.029	7.06	438
1.222	.028	7.10	455
1.206	.022	7.15	478
1.21	.028	7.20	511
1.213	.025	7.28	551
1.21	.022	7.35	592
1.231	.035	7.40	626
1.222	.037	7.45	651
1.226	.032	7.58	723
1.235	.034	7.74	811
1.228	.029	7.82	920
1.229	.025	7.90	1071
1.21	.038	7.95	1115
1.22	.03	8.00	1186
1.27	.031	8.01	1224
1.263	.026	8.05	1292
1.257	.032	8.10	1394
1.258	.032	8.25	1502
1.27	.029	8.30	1558
1.263	.04	8.35	1634
1.264	.022	8.43	1708
1.269	.045	8.50	1748

1.27	.026	8.60	1809
1.257	.031	8.70	1890
1.263	.037	8.80	1998
1.261	.038	8.90	2084
1.273	.04	9.00	2155
1.266	.032	9.13	2423
1.275	.034	9.20	2470
1.261	.042	9.25	2543
1.273	.038	9.31	2615
1.261	.042	9.40	2718
1.276	.034	9.50	2821
1.264	.045	9.60	2962
1.267	.035	9.72	3107
1.269	.044	9.80	3152
1.282	.044	9.90	3231
1.27	.037	10.00	3362
1.286	.05	10.12	3478
1.272	.059	10.28	3626
1.276	.048	10.40	3720
1.285	.051	10.53	3805
1.277	.059	10.65	3839
1.288	.066	10.70	3868
1.269	.063	10.80	3901
1.267	.057	10.98	3944
1.266	.072	11.28	3984

## M10.RAW4C

144.5	.0494	.809	392832	21.1	.0033	47.9	
155.0	.15	10.0	16.8	397.9	0	0	0
1.65	.937	.0008	1.0	5.46			
14							
10.85	1.65	.001475	0	74.3	74.3		
14.3	1.67	.002	39.375	98.0	98.1		
18.4	1.69	.002575	82.5	126.1	126.4		
20.5	1.71	.002955	111.0	140.4	141.0		
20.8	1.76	.00305	118.125	142.5	143.5		
21.0	1.98	.0032	129.375	143.9	146.8		
21.1	2.03	.0033	136.875	144.5	147.9		
21.0	2.10	.00344	147.375	143.9	147.9		
20.35	2.23	.00355	155.625	139.4	144.5		
20.25	2.37	.00375	170.625	138.7	145.0		
19.85	2.55	.00395	185.625	136.0	143.8		
19.2	2.72	.004145	200.25	131.5	140.6		
18.65	2.89	.004295	211.5	127.8	138.0		
18.25	3.05	.0044	219.375	125.0	136.5		
39							
0.828	.015	5.53	13				
0.829	.016	5.58	26				
0.835	.013	5.67	52				
0.823	.016	5.70	70				
0.823	.007	5.75	96				

0.832	.01	5.80	120
0.834	.01	5.85	164
0.831	.012	5.90	258
0.836	.01	5.95	378
0.822	.042	6.00	543
0.938	.047	6.10	866
0.938	.044	6.15	941
0.954	.06	6.20	1002
0.955	.054	6.25	1059
0.942	.051	6.30	1107
0.97	.051	6.35	1155
0.955	.057	6.40	1217
0.946	.053	6.45	1274
0.942	.048	6.50	1450
0.967	.067	6.55	1547
0.973	.073	6.60	1605
0.987	.078	6.70	1761
0.98	.07	6.76	1874
0.983	.073	6.81	1953
0.968	.07	6.85	2093
0.968	.07	6.90	2290
0.984	.076	7.02	2744
0.975	.072	7.08	2885
0.968	.07	7.11	2953
0.982	.073	7.15	3173
0.961	.094	7.18	3350
0.98	.095	7.20	3425
0.98	.12	7.23	3532
0.977	.12	7.25	3631
0.962	.11	7.30	3924
0.974	.066	7.36	4024
1.191	.092	7.57	4122
1.192	.094	7.76	4142
1.0	.094	7.96	4165

## M10.RAW4T

127.6	.0483	.543	329272	17.2	.00356	40.9	
155.0	.15	10.0	16.8	397.9	0	0	0
2.82	.943	.0008	0.0	0.0			
16							
10.25	2.82	.0019	0	76.3	76.3		
11.35	2.83	.0021	15	84.4	84.5		
11.90	2.84	.00222	24	88.5	88.7		
14.0	2.85	.0026	52.5	104.2	104.4		
15.5	2.86	.0029	75.0	115.3	115.6		
16.2	2.88	.00305	86.25	120.5	121.0		
16.6	2.89	.00315	93.75	123.5	124.1		
17.15	2.92	.00337	110.25	127.6	128.4		
17.15	3.03	.003565	124.875	127.6	129.3		
16.95	3.25	.003705	135.375	126.1	129.7		
16.4	3.44	.00375	138.75	122.0	127.0		

16.55	3.66	.003935	152.625	123.1	130.1
16.25	3.84	.0041	165.0	120.9	129.3
15.95	4.03	.004285	178.875	118.7	128.5
15.5	4.18	.004425	189.375	115.3	126.2
15.25	4.29	.004595	202.125	113.5	125.1

## M10.RAW7B

127.5	.0560	.337	295465	17.7	.003925	41.3
155.0	.15	10.0	16.8	397.9	0	0
2.82	.923	.0008	1.0	6.20		

11

6.95	2.82	.00125	0	50.1	50.1
8.0	2.83	.0015	18.75	57.6	57.7
16.05	2.85	.0032	146.25	115.6	115.8
17.1	2.86	.003425	163.125	123.2	123.5
17.45	2.88	.003625	178.125	125.7	126.2
17.55	2.99	.00369	183.0	126.4	127.8
17.7	3.04	.003825	193.125	127.5	129.3
17.7	3.31	.003925	200.625	127.5	131.5
17.3	3.41	.0041	213.75	124.6	129.4
17.0	3.67	.004185	220.125	122.5	129.3
16.9	4.28	.00445	240.0	121.7	133.8

32

0.856	-.024	6.40	10
0.861	-.012	6.52	21
0.850	-.021	6.60	33
0.854	-.014	6.76	52
0.860	-.025	6.87	66
0.857	-.033	6.91	79
0.861	-.036	6.98	92
0.856	-.024	7.07	110
0.845	-.021	7.20	134
0.850	-.036	7.30	161
0.844	-.034	7.40	190
0.845	-.046	7.50	230
0.863	-.021	7.60	280
0.847	-.028	7.71	342
0.851	-.025	7.80	393
0.897	.032	7.84	456
0.895	.031	8.00	523
0.904	.016	8.05	615
0.996	.029	8.09	670
0.989	.019	8.15	703
1.078	.034	8.20	752
1.077	.025	8.25	807
1.065	.012	8.30	833
1.072	.015	8.35	862
1.064	.023	8.41	895
1.055	.034	8.52	940
1.064	.044	8.60	977
1.071	.041	8.70	995

1.069	.041	8.75	1008
1.071	.057	8.80	1021
1.08	.064	8.90	1033
1.074	.069	9.10	1049

## M10.RAW7T

102.8	.0365	.281	259225	13.6	.0036	32.7	
155.0	.15	10.0	16.8	397.9	0	0	0
3.52	.925	.0008	1.0	6.72			

9

9.7	3.52	.00235	0	73.3	73.3
10.85	3.53	.00264	21.75	82.0	82.1
12.55	3.56	.003055	52.875	94.8	95.1
13.35	3.85	.00337	76.5	100.9	103.1
13.5	3.93	.003475	84.375	102.0	104.8
13.6	4.01	.003585	92.625	102.8	106.1
13.55	4.20	.0037	101.25	102.4	107.1
13.55	4.37	.003765	106.125	102.4	108.3
13.1	5.03	.004005	124.125	99.0	109.6

17

0.828	.015	6.83	19
0.822	.015	6.89	33
0.832	-.005	6.95	64
0.820	.006	7.10	113
0.832	-.005	7.15	149
0.911	.037	7.20	177
0.904	.028	7.26	196
0.898	.025	7.30	206
0.895	.022	7.35	220
0.899	.04	7.40	243
0.897	.026	7.50	272
0.891	.034	7.65	305
0.897	.042	7.75	326
0.883	.028	7.85	349
0.889	.026	8.00	369
0.878	.031	8.10	385
0.873	.034	8.30	405

## M15.RAW13T

208.0	.0787	.784	618058	29.3	.00295	67.9	
186.0	.15	15.0	16.8	397.9	0	0	0
2.66	.92	.00084	1.0	14.48	41		

12

18.35	2.66	.001725	0	130.3	130.3
19.45	2.67	.00183	7.5	138.1	138.1
22.0	2.68	.00206	23.9286	156.2	156.4
26.05	2.69	.002435	50.7143	184.9	185.3
28.5	2.70	.002715	70.7143	202.3	202.8
29.3	2.72	.002865	81.4286	208.0	208.8
29.05	2.78	.00303	93.2143	206.2	207.8

27.5	3.04	.003335	115.0	195.2	199.9
26.1	3.18	.003615	135.0	195.3	191.4
24.85	3.56	.003785	147.143	176.4	186.8
23.7	3.89	.003975	160.714	168.2	182.0
22.65	4.19	.00417	174.643	160.8	177.4

5

0.444	.01	14.53	16
0.570	.012	14.62	28
0.569	.01	14.75	31
0.568	.009	14.90	35
0.564	.009	15.10	39

## M15.RAW19B

215.5	.0805	1.360	562428	29.9	.003385	69.8	
186.0	.15	15.0	16.8	397.9	0	0	0
2.85	.922	.00084	1.0	7.00	1641		

9

18.45	2.85	.001925		0	133.0	133.0
27.5	2.87	.002885	68.5714		198.2	198.4
28.9	2.89	.00307	81.7857		208.3	208.8
29.55	2.93	.003215	92.1429		212.9	214.0
29.9	2.97	.00337	103.214		215.5	217.1
29.7	3.11	.003525	114.286		214.0	217.6
29.1	3.37	.003875	139.286		210.0	216.7
28.5	3.66	.00422	163.929		205.4	216.3
27.3	3.98	.004545	187.143		196.7	211.6

7

1.286	-.002	7.15	39
1.288	0	7.35	123
1.286	-.002	7.89	390
1.286	-.002	8.29	600
1.286	-.002	8.69	960
1.287	0	9.59	1350
1.287	0	9.79	1500

## M15.RAW19T

167.9	.0665	.625	449392	23.45	.00335	54.6	
186.0	.15	15.0	16.8	397.9	0	0	0
2.25	.943	.00084	1.0	4.81	4740		

10

16.65	2.25	.002175		0	119.5	119.5
22.25	2.29	.002925	53.5714		159.7	160.1
22.9	2.31	.00306	63.2143		164.3	164.9
23.15	2.32	.003125	67.8571		166.1	166.9
23.35	2.34	.003225	75.0		167.6	168.5
23.4	2.37	.00331	81.0714		167.9	169.2
23.4	2.46	.00338	86.0714		167.9	170.2
22.75	2.73	.003715	110.0		163.3	168.3
22.15	3.12	.00397	128.214		158.9	168.0
21.3	3.62	.00421	145.357		152.8	167.0

11

1.219	-.003	4.95	42
1.219	.001	5.05	90
1.219	.006	6.45	834
1.219	.006	6.95	1275
1.217	.004	7.45	2037
1.216	.003	7.95	2592
1.216	.003	8.60	3072
1.219	.001	9.40	4050
1.219	.003	9.75	4425
1.217	0	9.85	4485
1.217	0	10.35	4680

M15.RAW5B

243.8	.0730	.670	744219	34.9	.002975	80.3		
186.0	.15	15.0	16.8	397.9	0	0	0	
2.09	.935	.0008	1.0	5.45	192			

10

15.2	2.09	.001135		0	106.6	106.6		
24.3	2.14	.00185		53.625	170.5	171.0		
28.95	2.16	.0022		79.875	203.1	204.0		
32.5	2.18	.002515		103.5	228.0	229.3		
33.45	2.22	.00263		112.125	234.7	236.6		
34.25	2.31	.00275		121.125	240.3	243.6		
34.75	2.50	.0029		132.375	243.8	250.1		
34.75	2.91	.00306		144.375	243.8	256.7		
33.5	3.03	.003115		148.5	235.0	249.4		
33.6	3.50	.003395		169.5	235.7	257.8		

13

1.979	.018	5.73	11
1.956	0	5.88	21
1.973	.006	6.02	31
1.957	0	6.10	44
1.945	-.008	6.20	62
1.945	-.011	6.25	74
1.969	.004	6.28	91
1.956	-.005	6.35	112
1.948	-.006	6.41	129
1.957	0	6.50	146
1.969	-.002	6.62	161
1.95	.004	6.71	174
1.954	-.002	6.88	184

M15.RAW5C

180.7	.0392	1.099	523266	25.2	.0032	58.8		
186.0	.15	15.0	16.8	397.9	0	0	0	
2.32	.941	.0008	1.0	5.55	775			

12

16.75	2.32	.00187		0	120.3	120.3		
20.25	2.36	.00225		28.5	145.5	145.9		

22.75	2.40	.00255	51.0	163.5	164.3
23.65	2.50	.002675	60.375	169.9	171.9
24.6	2.65	.00285	73.5	176.7	180.5
25.0	2.87	.00298	83.25	179.6	186.0
25.15	2.95	.0031	92.25	180.7	188.1
25.15	3.12	.003205	100.125	180.7	190.2
25.10	3.21	.003315	108.375	180.3	190.9
25.05	3.28	.0034	114.75	180.0	191.4
24.55	3.50	.0037	137.25	176.4	190.3
23.9	3.73	.003945	155.625	171.7	188.1

22

1.572	-.036	5.61	28
1.585	.003	5.65	63
1.582	.019	5.70	102
1.591	.021	5.80	180
1.6	.003	5.85	206
1.582	.016	5.90	237
1.698	.007	6.10	288
1.683	.009	6.21	335
1.666	.001	6.30	373
1.676	0	6.40	393
1.673	-.003	6.50	421
1.718	.028	6.56	475
1.729	.035	6.65	516
1.707	.01	6.77	550
1.686	.018	6.90	579
1.704	.028	7.00	610
1.696	.021	7.10	641
1.705	.015	7.20	670
1.699	.019	7.50	695
1.704	.022	7.65	720
1.688	.013	7.80	739
1.695	.023	7.95	757

## M15.RAW5T

240.0	.0891	.809	688384	33.0	.003175	77.5	
186.0	.15	15	16.8	397.9	0	0	0
2.49	.942	.0008	1.0	4.65	1168		

12

15.7	2.49	.0013	0	114.2	114.2
18.6	2.51	.001585	21.375	135.3	135.5
24.75	2.53	.00215	63.75	180.0	180.5
30.5	2.55	.00265	101.25	221.8	222.7
31.95	2.57	.00284	115.5	232.4	233.6
32.55	2.60	.00298	126.0	236.8	238.4
33.0	2.65	.00315	138.75	240.0	242.5
32.95	2.75	.0033	150.0	239.7	243.7
31.75	3.21	.00354	168.0	230.9	241.9
30.75	3.36	.00365	176.25	223.7	236.6
30.25	3.54	.00377	185.25	220.0	235.5
29.85	3.79	.003965	199.875	217.1	236.3

47

1.808	.057	4.70	31
1.862	.066	4.76	60
1.828	.069	4.86	106
1.825	.062	4.96	126
1.83	.066	5.01	142
1.831	.051	5.05	167
1.847	.06	5.25	224
1.849	.066	5.40	245
1.844	.051	5.46	260
1.855	.051	5.50	272
1.815	.054	5.75	309
1.82	.053	5.85	320
1.812	.051	5.95	341
1.847	.054	6.03	355
1.808	.051	6.11	370
1.82	.057	6.20	385
1.824	.056	6.25	397
1.802	.053	6.30	412
1.827	.057	6.40	451
1.808	.054	6.50	490
1.818	.054	6.60	520
1.824	.048	6.70	565
1.811	.051	6.90	583
1.818	.057	7.06	595
1.830	.057	7.30	613
1.803	.05	7.50	636
1.817	.051	7.65	648
1.802	.048	7.80	662
1.814	.053	7.89	674
1.818	.059	8.00	692
1.811	.054	8.16	709
1.805	.051	8.45	737
1.815	.047	8.55	755
1.787	.053	8.65	776
1.796	.047	8.80	802
1.812	.05	8.90	821
1.817	.051	9.05	871
1.814	.057	9.10	890
1.814	.056	9.20	920
1.811	.056	9.30	965
1.799	.054	9.42	1014
1.8	.05	9.50	1033
1.805	.051	9.70	1080
1.793	.054	9.85	1101
1.805	.056	10.02	1119
1.803	.054	10.22	1140
1.798	.059	10.44	1161

S05.RAW11B

91.1 .0401 .181 186620 12.2 .004525 29.1

40.0	.15	5.0	16.8	87.5	0	0	0
4.1	.895	.00084	1.0	7.18	14		
9							
5.65	4.10	.001755	0	42.2	42.2		
10.05	4.11	.00335	113.925	75.1	75.1		
10.6	4.12	.003535	127.143	79.2	79.3		
11.1	4.16	.003705	139.286	82.9	83.2		
11.9	4.26	.00406	164.643	88.9	89.9		
12.15	4.64	.00426	178.929	90.8	94.0		
12.2	5.26	.004525	197.857	91.1	98.4		
11.8	5.57	.004525	197.857	88.1	97.2		
12.0	5.98	.004705	210.714	89.6	101.7		
4							
1.008	-.025	7.45	4				
1.008	-.025	7.60	8				
1.008	-.025	7.91	11				
1.008	-.025	9.11	14				

## S05.RAW11C

65.8	.0327	.176	147245	9.1	.004145	21.3	
40.0	.15	5.0	16.8	87.5	0	0	0
2.89	.923	.00084	0.0	0.0			
8							
5.6	2.89	.002265	0	40.5	40.5		
8.85	2.90	.00364	98.2143	64.0	64.1		
9.0	2.92	.003815	110.714	65.1	65.2		
9.1	2.95	.004045	127.143	65.8	66.1		
9.05	2.99	.004145	134.286	65.5	65.9		
8.9	3.66	.00445	156.071	64.4	67.7		
8.4	4.09	.004595	166.429	60.8	65.7		
8.25	4.27	.00484	183.929	59.7	65.3		

## S05.RAW11T

68.4	.0331	.202	141087	9.4	.0043	22.1	
40.0	.15	5.0	16.8	87.5	0	0	0
2.29	.950	.00084	1.0	6.00	414		
6							
5.4	2.29	.0023	0	39.3	39.3		
9.35	2.30	.00415	132.143	68.0	68.1		
9.4	2.68	.00439	149.286	68.4	70.1		
9.2	2.88	.00446	154.286	66.9	69.5		
9.2	3.12	.0046875	170.536	66.9	70.6		
9.1	3.59	.00486	182.857	66.2	72.0		
18							
0.330	-.008	6.05	12				
0.330	-.008	6.10	22				
0.330	-.005	6.16	35				
0.328	-.008	6.20	39				
0.330	.005	6.25	47				
0.331	-.005	6.30	59				

0.335	-.006	6.41	97
0.331	-.008	6.45	120
0.330	-.005	6.50	143
0.335	-.006	6.61	191
0.334	-.005	6.70	284
0.333	-.009	6.80	334
0.333	-.005	6.85	372
0.404	-.003	6.90	394
0.482	-.003	7.00	404
0.485	-.006	7.15	409
0.483	-.002	7.80	413
0.483	-.002	8.27	414

## S05.RAW23B

57.6	.0186	.823	110057	8.05	.004745	18.7	
40.0	.15	5.0	16.8	87.5	0	0	0
2.65	.925	.00084	1.0	4.50	3279		

13

5.0	2.65	.002655	0	35.8	35.8
5.65	2.66	.003015	25.7143	40.4	40.4
6.9	2.67	.003665	72.1429	49.3	49.4
7.7	2.68	.004135	105.714	55.1	55.2
8.00	2.69	.00433	119.643	57.2	57.3
8.05	2.72	.00445	128.214	57.6	57.8
8.05	2.85	.00454	134.643	57.6	58.3
8.05	3.14	.004745	149.286	57.6	59.4
7.85	3.41	.004985	166.429	56.1	58.9
7.65	3.52	.00537	193.929	54.7	57.8
7.2	3.62	.006025	240.714	51.5	54.8
6.65	3.74	.00685	299.643	47.5	51.0
6.35	3.90	.007455	342.857	45.4	49.2

15

0.352	.016	4.51	285
0.352	.016	4.52	585
0.349	.013	4.53	885
0.349	.013	4.58	1185
0.349	.013	4.65	1485
0.349	.013	4.77	1785
0.347	.01	5.40	2085
0.347	.01	6.33	2385
0.347	.01	6.52	2565
0.347	.013	6.92	2751
0.347	.013	7.53	2805
0.347	.016	8.50	2961
0.346	.015	8.90	3063
0.344	.018	9.30	3255
0.344	.018	9.57	3279

## S05.RAW23C

64.5	.0292	1.234	128918	9.0	.0048	21.0
------	-------	-------	--------	-----	-------	------

40.0	.15	5.0	16.8	87.5	0	0	0
2.51	.932	.00084	1.0	3.50	4932		
12							
6.05	2.51	.00278	0	43.4	43.4		
8.4	2.52	.00388	78.5714	60.2	60.2		
8.55	2.53	.004	87.1429	61.3	61.4		
8.85	2.55	.004195	101.071	63.4	63.6		
8.95	2.57	.0044	115.714	64.1	64.4		
9.00	2.58	.004665	134.643	64.5	64.8		
9.0	2.61	.0048	144.286	64.5	64.9		
8.9	2.72	.00495	155.0	63.8	64.6		
8.65	2.96	.0054	187.143	62.0	63.8		
8.3	3.13	.00605	233.571	59.5	61.9		
7.8	3.21	.00665	276.429	55.9	58.4		
7.65	3.28	.00701	302.143	54.8	57.6		
9							
0.413	.007	3.58	1080				
0.413	.007	3.67	2160				
0.413	.007	3.95	3096				
0.413	.007	4.00	3168				
0.413	.007	4.10	3420				
0.413	.007	4.20	3780				
0.413	.007	4.40	4248				
0.413	.007	4.60	4536				
0.413	.007	5.10	4932				

## S05.RAW23T

64.3	.0284	.124	140861	8.7	.004005	20.6	
40.0	.15	5.0	16.8	87.5	0	0	0
2.90	.936	.00084	1.0	4.93	21996		
9							
3.3	2.90	.001275	0	24.4	24.4		
6.75	2.91	.002925	117.857	49.9	49.9		
8.2	2.92	.003595	165.714	60.6	60.7		
8.65	2.93	.003905	187.857	64.0	64.1		
8.7	3.02	.004005	194.999	64.3	64.8		
8.65	3.44	.004075	200.0	64.0	66.2		
8.55	3.83	.004265	213.571	63.2	67.2		
8.5	4.28	.004385	222.143	62.8	68.8		
8.35	4.54	.004475	228.571	61.7	68.8		
24							
0.504	.007	4.95	108				
0.505	.009	5.05	184				
0.451	.010	5.10	396				
0.453	.01	5.37	1944				
0.452	.01	5.42	2592				
0.455	.012	5.80	5220				
0.457	.015	6.00	7740				
0.457	.015	6.10	8640				
0.457	.015	6.20	10404				
0.457	.015	6.30	11700				

0.454	.016	6.40	12744
0.454	.016	6.53	14616
0.454	.016	6.60	16200
0.453	.016	6.69	18468
0.447	.012	6.73	19188
0.451	.009	6.75	19512
0.567	.009	6.81	19944
0.573	.01	7.16	20394
0.568	.01	7.30	20520
0.571	.006	7.40	20610
0.567	.009	7.50	20754
0.568	.01	8.05	21510
0.568	.01	8.30	21780
0.568	.01	8.70	21996

## S10.RAW28B

87.5	.0345	.044	219172	12.1	.003505	28.3		
117.0	.15	10.0	16.8	87.5	0	0	0	
2.58	.935	.00084	1.0	5.13	796			
7								
8.3	2.58	.002235	0	60.0	60.0			
11.85	2.59	.003255	72.8571	85.7	85.8			
12.0	2.60	.003365	80.7143	86.8	86.9			
12.1	2.70	.003445	86.4286	87.5	88.2			
12.1	3.32	.003505	90.7143	87.5	91.8			
11.7	3.96	.003525	92.1429	84.6	92.6			
11.6	5.03	.003665	102.143	83.9	98.8			
13								
0.567	.011	5.16	90					
0.567	.011	5.20	180					
0.567	.011	5.25	270					
0.551	-.004	6.01	360					
0.551	-.004	6.21	450					
0.551	-.004	6.41	540					
0.555	.003	6.45	630					
0.541	-.025	6.46	677					
0.659	0.0	6.56	769					
0.801	.007	6.71	785					
0.803	.013	6.78	789					
0.797	.007	6.90	794					
0.797	.007	7.09	796					

## S10.RAW28C

91.2	.0497	.199	159219	12.65	.005315	29.6		
117.0	.15	10.0	16.8	87.5	0	0	0	
2.60	.932	.00084	1.0	5.28	3380			
11								
6.5	2.60	.00241	0	46.9	46.9			
7.5	2.61	.00279	27.1429	54.1	54.1			
10.85	2.64	.004	113.571	78.2	78.4			

11.7	2.67	.004385	141.071	84.3	84.7
11.9	2.69	.004475	147.5	85.8	86.3
12.15	2.73	.0046	156.429	87.6	88.3
12.3	2.76	.0047	163.571	88.7	89.6
12.5	2.93	.00485	174.286	90.1	92.0
12.6	3.28	.005075	190.357	90.8	94.8
12.65	3.43	.005315	207.5	91.2	96.2
11.85	4.12	.00534	209.286	85.4	94.3

34

0.495	-.010	5.35	150
0.495	-.01	5.47	300
0.495	-.01	5.93	450
0.495	-.01	6.14	600
0.495	-.01	6.28	720
0.495	-.01	6.34	750
0.495	-.01	6.66	900
0.495	-.01	6.86	1050
0.495	-.01	7.02	1200
0.495	-.01	7.16	1350
0.495	-.01	7.34	1500
0.495	-.01	7.56	1650
0.489	-.011	7.68	1800
0.489	-.011	7.78	1950
0.489	-.011	7.90	2100
0.489	-.011	7.99	2250
0.489	-.011	8.18	2400
0.489	-.011	8.33	2550
0.489	-.011	8.44	2700
0.486	-.001	8.54	2847
0.491	-.015	8.61	2914
0.493	-.007	8.70	3060
0.495	-.001	8.80	3191
0.492	-.001	8.82	3221
0.608	-.002	8.85	3242
0.599	-.002	8.88	3247
0.608	-.005	8.98	3257
0.601	-.003	9.18	3274
0.605	0.0	9.89	3337
0.608	.001	10.18	3359
0.611	.004	10.68	3361
0.605	.001	11.40	3367
0.608	.006	11.58	3376
0.608	.006	11.80	3380

## S10.RAW8B

101.0	.0370	.589	191761	14.4	.00485	33.1	
117.0	.15	10.0	16.8	87.5	0	0	0
2.49	.919	.0008	1.0	4.70	152		
14							
8.8	2.49	.002585	0	61.7	61.7		
11.65	2.50	.00345	64.875	81.7	81.8		

13.3	2.51	.00397	103.875	93.3	93.4
13.6	2.58	.004085	112.5	95.4	95.9
13.7	2.92	.004175	119.25	96.1	98.7
13.8	2.97	.00425	124.875	96.8	99.7
14.05	3.06	.004375	134.25	98.5	102.1
14.2	3.11	.0045	143.625	99.6	103.5
14.3	3.34	.0046	151.125	100.3	105.8
14.35	3.56	.004665	156.0	100.6	107.7
14.4	3.68	.00478	164.625	101.0	108.9
14.4	3.78	.00485	169.875	101.0	109.6
14.3	3.90	.005225	198.0	100.3	109.7
14.25	3.98	.00558	224.625	99.9	109.9

11

1.028	.054	4.72	2
1.015	.056	4.80	23
1.014	.054	4.94	39
1.028	.05	5.00	51
1.012	.054	5.10	75
1.011	.048	5.25	92
1.008	.047	5.35	103
1.017	.053	5.43	115
1.005	.048	5.55	127
1.008	.045	6.02	136
1.008	.045	7.91	152

## S10.RAW8C

101.8	.0482	.420	219011	14.45	.0041	33.3	
117.0	.15	10.0	16.8	87.5	0	0	0
2.34	.928	.0008	1.0	6.30	763		

14

7.4	2.34	.0019	0	52.1	52.1
8.95	2.36	.002325	31.875	63.1	63.2
11.8	2.37	.00305	86.25	83.2	83.3
12.5	2.38	.00325	101.25	88.1	88.3
13.85	2.40	.00365	131.25	97.6	98.0
14.2	2.42	.00385	146.25	100.1	100.6
14.35	2.46	.00397	155.25	101.1	101.9
14.4	2.55	.00407	162.75	101.5	102.8
14.45	2.65	.00418	171.0	101.8	103.8
14.4	2.72	.004285	178.875	101.5	103.9
14.4	2.83	.00435	183.75	101.5	104.6
13.95	2.99	.00451	195.75	98.3	102.4
13.8	3.32	.0048	217.5	97.3	103.5
13.4	3.62	.004945	228.375	94.4	102.4

35

0.749	.004	6.40	16
0.746	.013	6.50	32
0.749	.015	6.60	53
0.750	.013	6.70	69
0.756	.015	6.80	83
0.756	.013	6.91	94

0.750	.016	7.00	108
0.753	.018	7.10	124
0.752	.012	7.20	139
0.746	.016	7.30	155
0.749	.013	7.40	173
0.741	.009	7.50	194
0.747	.010	7.60	221
0.746	.015	7.70	256
0.749	.012	7.80	284
0.756	.012	7.90	310
0.752	.009	8.00	329
0.759	.013	8.10	358
0.752	.013	8.20	398
0.754	.016	8.30	422
0.753	.018	8.40	453
0.752	.009	8.50	487
0.747	.013	8.60	538
0.752	.018	8.70	570
0.752	.015	8.80	592
0.741	.009	8.90	611
0.752	.009	9.00	633
0.747	.01	9.10	650
0.743	.01	9.20	667
0.750	.01	9.35	689
0.746	.015	9.45	707
0.743	.015	9.55	727
0.743	.018	9.70	745
0.741	.019	9.99	757
0.741	.019	10.12	763

## S10.RAW8T

97.5	.0420	.240	237675	13.55	.00375	31.6		
117.0	.15	10.0	16.8	87.5	0	0	0	
2.11	.95	.0008	1.0	5.42	599			
11								
11.00	2.11	.002735	0	79.1	79.1			
13.1	2.12	.00325	38.625	94.2	94.3			
13.3	2.13	.00348	55.875	95.7	95.8			
13.5	2.14	.00364	67.875	97.1	97.3			
13.55	2.15	.00374	75.375	97.5	97.7			
13.55	2.34	.00384	82.875	97.5	98.9			
13.5	2.54	.003915	88.5	97.1	99.8			
13.5	2.75	.00396	91.875	97.1	101.1			
13.0	3.02	.004015	96.0	93.5	99.1			
12.7	3.24	.004045	98.25	91.4	98.2			
13.0	3.47	.00432	118.875	93.5	102.1			
27								
0.856	-.002	5.59	40					
0.863	.009	5.65	63					
0.872	.007	5.71	75					
0.867	.015	5.75	91					

0.870	.012	5.80	105
0.867	.004	5.93	144
0.866	.015	6.00	165
0.861	.004	6.10	182
0.864	.006	6.20	204
0.866	.004	6.30	230
0.873	.010	6.41	277
0.869	0	6.50	292
0.863	.004	6.60	320
0.861	.013	6.70	347
0.858	-.003	6.80	400
0.856	.001	6.90	418
0.866	.003	7.00	438
0.857	.009	7.10	461
0.863	.006	7.20	484
0.861	.004	7.30	502
0.861	.009	7.40	521
0.856	.004	7.50	538
0.867	.007	7.60	550
0.861	.013	7.71	563
0.866	.007	7.85	575
0.861	.019	7.94	585
0.861	.019	8.24	599

## S15.RAW10T

110.6	.0268	1.128	316005	14.5	.0032	35.0	
145.0	.15	15.0	16.8	87.5	0	0	0
4.30	.900	.0008	1.0	6.79	179		
17							
7.05	4.30	.00139	0	53.8	53.8		
7.55	4.31	.00151	9.0	57.6	57.6		
10.0	4.32	.002035	48.375	76.3	76.4		
13.45	4.33	.00275	102.0	102.6	102.8		
13.95	4.48	.0029	113.25	106.4	107.7		
14.2	4.51	.00299	120.0	108.3	109.8		
14.45	4.60	.00314	131.25	110.2	112.4		
14.5	4.68	.00324	138.75	110.6	113.4		
14.5	4.75	.00335	147.0	110.6	114.0		
14.3	4.86	.003625	167.625	109.1	113.2		
13.9	4.97	.00397	193.5	106.0	110.9		
13.45	5.13	.004125	205.125	102.6	108.4		
13.1	5.29	.00441	226.5	99.9	106.8		
12.7	5.42	.0047	248.25	96.9	104.5		
12.4	5.56	.004975	268.875	94.6	103.0		
12.05	5.67	.005275	291.375	91.9	100.8		
11.65	5.79	.0056	315.75	88.9	98.3		
14							
0.730	.021	6.80	2				
0.724	.029	6.83	12				
0.728	.029	6.90	26				
0.722	.022	7.00	37				

0.716	.018	7.10	53
0.722	.022	7.15	66
0.721	.022	7.20	76
0.722	.021	7.25	99
0.724	.021	7.40	116
0.719	.025	8.08	130
0.713	.021	8.45	146
0.719	.026	8.72	158
0.700	.031	9.20	178
0.700	.031	9.29	179

## S15.RAW12B

172.3	.0727	.601	371654	21.95	.004195	53.9		
145.0	.15	15.0	16.8	87.5	0	0	0	
3.41	.952	.00084	1.0	5.47	15			
9								
13.8	3.41	.002465	0	108.3	108.3			
17.7	3.42	.00317	50.3571	138.9	139.0			
20.05	3.44	.0036	81.0714	157.4	157.7			
20.85	3.60	.00378	93.9286	163.7	165.8			
21.3	3.72	.003895	102.143	167.2	170.7			
21.95	3.95	.004195	123.571	172.3	178.7			
21.8	4.14	.0044	138.214	171.1	179.8			
21.65	4.37	.004655	156.429	169.9	181.4			
21.2	4.84	.00478	165.357	166.4	183.7			
5								
1.359	.029	5.50	3					
1.359	.029	5.52	6					
1.359	.029	5.55	9					
1.359	.029	5.58	12					
1.359	.029	5.67	15					

## S15.RAW12C

150.4	.0532	.603	404162	20.5	.003375	48.4		
145.0	.15	15.0	16.8	87.5	0	0	0	
2.80	.935	.00084	1.0	4.96	339			
13								
10.05	2.80	.0015	0	73.7	73.7			
10.7	2.81	.00161	7.85714	78.5	78.5			
13.2	2.82	.002	35.7143	96.8	96.9			
16.1	2.84	.002415	65.3571	118.1	118.4			
17.9	2.85	.00269	85.0	131.3	131.7			
19.3	2.86	.00291	100.714	141.6	142.1			
19.9	2.88	.00307	112.143	146.0	146.7			
20.25	2.96	.0032	121.429	148.5	150.1			
20.4	3.00	.003275	126.786	149.6	151.6			
20.5	3.13	.003375	133.929	150.4	153.6			
20.15	3.48	.00366	154.286	147.8	154.4			
19.55	3.73	.0038	164.286	143.4	152.3			
18.95	4.03	.004055	182.5	139.0	150.6			

17

1.185	-.005	5.10	26
1.184	-.005	5.25	47
1.184	-.003	5.35	58
1.185	0.	5.45	68
1.181	-.002	5.70	112
1.185	0.	5.80	135
1.185	0.	6.00	172
1.185	0.	6.10	186
1.185	0.	6.20	204
1.185	0.	6.30	219
1.185	0.	6.40	245
1.184	.001	6.50	253
1.188	0.	6.60	265
1.184	-.003	6.90	299
1.182	-.002	7.10	316
1.182	-.002	7.40	330
1.182	-.002	7.97	339

## S15.RAW12T

162.3	.0582	.822	455039	22.75	.00325	52.8	
145.0	.15	15.0	16.8	87.5	0	0	0
1.98	.950	.00084	0.0	0.0			

11

13.4	1.98	.001715	0	95.6	95.6
18.75	1.99	.002405	49.2857	133.8	133.9
20.3	2.00	.002625	65.0	144.8	145.0
21.1	2.02	.002735	72.8571	150.5	150.9
22.1	2.14	.002915	85.7143	157.7	159.3
22.65	2.21	.00311	99.6429	161.6	163.9
22.75	2.30	.00332	114.643	162.3	165.6
22.15	2.51	.003565	132.143	158.0	163.4
21.3	2.68	.00377	146.786	152.0	158.9
20.5	2.92	.00396	160.357	146.3	155.3
19.5	3.20	.004195	177.143	139.1	150.4

## S15.RAW22B

180.6	.0640	.266	543449	23.5	.003	57.0	
145.0	.15	15.0	16.8	87.5	0	0	0
3.29	.944	.00084	1.0	5.81	55584		

9

11.85	3.29	.00139	0	91.0	91.0
20.6	3.30	.00245	75.7143	158.3	158.4
22.8	3.31	.002765	98.2143	175.2	175.4
23.35	3.32	.00289	107.143	179.4	179.8
23.5	3.33	.003	115.0	180.6	181.0
23.25	3.84	.003135	124.643	178.6	185.3
22.7	4.03	.00326	133.571	174.4	183.3
22.35	4.55	.00342	145.0	171.7	187.0
21.5	5.35	.00358	156.429	165.2	190.4

21

0.905	.003	5.83	396
0.901	0.	5.84	1224
0.900	.003	5.87	3600
0.900	.003	5.89	7200
0.900	.003	5.90	12600
0.900	.003	6.26	19800
0.900	.003	6.50	25200
0.900	.003	6.67	32400
0.900	.003	6.73	39600
0.900	.003	6.89	46800
0.899	.007	6.98	52020
1.301	.004	7.05	52380
1.301	.009	7.20	52530
1.307	.003	7.75	53172
1.301	.006	8.03	53700
1.301	.006	8.25	54216
1.301	.006	8.48	54600
1.301	.006	8.70	54900
1.301	.006	9.01	55200
1.301	.006	9.44	55500
1.301	.006	9.67	55584

S15.RAW22T

118.1	.0426	.657	250174	16.75	.004065	38.6	
145.0	.15	15.0	16.8	87.5	0	0	0
2.15	.936	.00084	2.0	5.20	1740		

11

8.95	2.15	.00203	0	63.1	63.1
14.65	2.16	.00337	95.7143	103.3	103.4
16.0	2.17	.00372	120.714	112.8	113.0
16.5	2.18	.003905	133.929	116.4	116.6
16.7	2.21	.00402	142.143	117.8	118.2
16.75	2.27	.00408	146.429	118.1	119.0
16.7	2.85	.00415	151.429	117.8	123.1
16.5	3.06	.00448	175.0	116.4	123.3
16.25	3.23	.004735	193.214	114.6	122.7
15.75	3.44	.004795	197.5	111.1	120.6
15.8	3.65	.005	212.143	111.4	122.7

6

0.798	.003	5.30	147
0.804	.004	6.20	474
0.801	.003	6.89	900
0.801	.003	7.29	1200
0.801	.003	8.01	1500
0.801	.003	9.05	1740

A107.RAW240B

99.6	.0469	.589	218421	14.0	.00403	32.5	
128.0	.15	10.0	16.8	397.9	0	0	0
2.21	.939	.00084	1.0	3.90	16668		
13							
7.85	2.21	.00207	0	55.8	55.8		
8.45	2.22	.00224	12.1429	60.1	60.1		
10.5	2.25	.0028	52.1429	74.7	74.9		
12.0	2.26	.00318	79.2857	85.4	85.6		
13.05	2.27	.00346	99.2857	92.8	93.2		
13.7	2.29	.00375	120.0	97.5	97.9		
13.85	2.30	.00385	127.143	98.5	99.1		
13.95	2.32	.00394	133.571	99.2	99.9		
14.0	2.37	.00403	140.0	99.6	100.6		
14.0	2.52	.00435	162.857	99.6	101.5		
13.85	2.80	.004715	188.929	98.5	102.2		
13.55	3.15	.00507	214.286	96.4	102.3		
13.1	3.42	.00515	220.0	93.2	100.7		
52							
0.615	.006	3.91	162				
0.611	.01	3.92	360				
0.614	.009	3.93	720				
0.614	.009	3.98	1080				
0.614	.009	4.09	1440				
0.614	.009	4.12	1800				
0.614	.009	4.19	2160				
0.614	.009	4.27	2520				
0.614	.009	4.36	2880				
0.614	.009	4.40	3240				
0.614	.009	4.49	3600				
0.614	.009	4.54	3960				
0.614	.006	4.62	4162				
0.615	.009	4.64	4356				
0.615	.009	4.66	4410				
0.614	.01	4.70	4446				
0.618	.009	4.75	4514				
0.614	.009	4.80	4680				
0.614	.009	5.12	5040				
0.614	.009	5.38	5400				
0.614	.009	5.57	5760				
0.614	.009	5.74	6120				
0.614	.009	5.83	6480				
0.614	.009	5.90	6840				
0.614	.009	6.07	7200				
0.614	.009	6.10	7560				
0.614	.009	6.14	7920				
0.614	.009	6.20	8280				
0.614	.009	6.35	8640				
0.614	.009	6.48	9000				
0.614	.009	6.50	9360				
0.614	.009	6.56	9720				
0.614	.009	6.58	10080				
0.614	.009	6.60	10440				

0.614	.009	6.64	10800
0.614	.009	6.68	11160
0.614	.009	6.69	11520
0.614	.009	6.70	11880
0.614	.009	6.75	12240
0.614	.009	6.78	12600
0.614	.009	6.79	12960
0.614	.009	6.80	13320
0.614	.009	6.88	13680
0.614	.009	6.93	14040
0.614	.009	6.97	14400
0.614	.009	7.02	14760
0.614	.009	7.17	15120
0.614	.009	7.30	15480
0.614	.009	7.55	15840
0.614	.009	7.86	16200
0.614	.009	8.48	16560
0.614	.009	9.19	16668

## A107.RAW240C

76.7	.0342	.456	185364	10.7	.003725	24.9	
128.0	.15	10.0	16.8	397.9	0	0	0
2.11	.948	.00084	1.0	5.12	1026		
13							
4.3	2.11	.00121	0	30.8	30.8		
7.7	2.12	.00244	87.8571	55.2	55.2		
8.65	2.13	.00274	109.286	62.0	62.1		
9.5	2.14	.003	127.857	68.1	68.2		
9.9	2.15	.003155	138.929	71.0	71.2		
10.5	2.16	.00341	157.143	75.3	75.5		
10.6	2.17	.003535	166.071	76.0	76.3		
10.65	2.19	.00363	172.857	76.4	76.7		
10.7	2.22	.003705	178.214	76.7	77.3		
10.65	2.36	.00379	184.286	76.4	77.6		
10.6	2.48	.004185	212.5	76.0	77.8		
10.4	2.78	.004605	242.5	74.6	77.8		
10.05	3.50	.00514	280.714	72.1	78.8		
33							
0.571	0	5.17	41				
0.571	0	5.20	84				
0.576	-.002	5.35	122				
0.570	0	5.55	139				
0.571	0	5.65	152				
0.568	.003	5.75	171				
0.571	.0	5.95	191				
0.570	.003	6.10	212				
0.573	.003	6.20	234				
0.564	.00	6.30	260				
0.568	-.003	6.45	296				
0.565	.003	6.50	318				
0.568	0	6.60	389				

0.571	0	6.65	443
0.573	-.005	6.71	525
0.573	0	6.75	555
0.573	0	6.85	623
0.573	.006	6.95	661
0.565	-.002	7.00	682
0.570	.001	7.10	701
0.571	.003	7.20	725
0.567	.001	7.30	743
0.567	0	7.40	762
0.568	.004	7.50	781
0.568	.003	7.60	811
0.573	.003	7.75	839
0.570	0	7.90	903
0.565	.001	8.00	937
0.567	.009	8.10	986
0.565	.004	8.15	1003
0.563	.007	8.30	1018
0.563	.007	8.55	1025
0.563	.007	8.65	1026

## A107.RAW241B

92.9	.0432	.681	202235	12.65	.004245	29.9	
128.0	.15	10.0	16.8	397.9	0	0	0
3.23	.919	.00084	1.0	5.50	1330		
13							
6.85	3.23	.00199	0	50.3	50.3		
8.9	3.24	.00268	49.2857	65.4	65.4		
9.95	3.25	.002985	71.0714	73.1	73.2		
11.15	3.26	.003355	97.5	81.9	82.1		
11.5	3.27	.00345	104.286	84.5	84.7		
12.25	3.28	.003715	123.214	90.0	90.3		
12.65	3.30	.004125	152.5	92.9	93.3		
12.65	3.37	.004245	161.071	92.9	93.8		
12.55	3.58	.004425	173.929	92.2	94.3		
12.5	3.71	.0047	193.571	91.8	94.7		
12.5	4.09	.005015	216.071	91.8	97.1		
12.35	4.25	.0054	243.571	90.7	97.0		
12.1	4.45	.0057	265.0	88.9	96.3		
29							
0.636	.003	5.60	68				
0.636	.006	5.65	97				
0.637	.006	5.70	126				
0.642	.004	5.75	146				
0.636	.004	5.80	191				
0.633	.003	5.85	260				
0.636	.003	5.90	341				
0.643	.007	5.96	443				
0.646	.004	6.00	524				
0.639	.004	6.05	640				
0.639	.009	6.10	819				

0.640	.004	6.16	901
0.753	.007	6.21	1016
0.754	.009	6.25	1049
0.759	.004	6.31	1065
0.757	.009	6.35	1094
0.760	.012	6.40	1112
0.760	.01	6.46	1124
0.757	.009	6.50	1135
0.754	.01	6.55	1149
0.759	.01	6.60	1173
0.759	.012	6.65	1218
0.754	.01	6.70	1237
0.757	.009	6.76	1254
0.759	.013	8.32	1273
0.754	.013	8.48	1290
0.754	.012	8.60	1305
0.754	.013	8.80	1320
0.754	.013	9.60	1330

## A107.RAW241C

99.0	.0332	1.048	256913	12.7	.00359	31.0		
128.0	.15	10.0	16.8	397.9	0	0	0	
3.99	.925	.00084	1.0	5.49	139			
13								
7.6	3.99	.00194	0	59.2	59.2			
10.2	4.00	.00261	47.8571	79.5	79.6			
12.25	4.01	.0032	90.0	95.5	95.6			
12.5	4.03	.00333	99.2857	97.4	97.7			
12.6	4.22	.00342	105.714	98.2	99.7			
12.65	4.23	.003465	108.929	98.6	100.2			
12.7	4.26	.00359	117.857	99.0	100.8			
12.65	4.44	.00397	145.0	98.6	101.6			
12.5	4.55	.00439	175.0	97.4	101.2			
12.15	4.75	.00473	199.286	94.7	99.7			
11.9	4.98	.00515	229.286	92.8	99.2			
11.6	5.13	.0056	261.429	90.4	97.7			
11.2	5.42	.005855	279.643	87.3	96.3			
7								
0.744	.004	5.50	9					
0.867	.001	5.60	110					
0.863	.009	5.70	122					
0.863	.009	5.84	127					
0.850	.009	6.10	135					
0.850	.009	6.40	138					
0.844	.009	6.70	139					

## A107.RAW241T

71.6	.0301	.37	167387	9.45	.004075	22.7		
128.0	0.15	10.	16.8	397.9	0	0	0	
3.87	.913	.00084	1.0	5.69	1916			

14

4.15	3.87	.001475	0	31.5	31.5
6.0	3.88	.00225	55.3571	45.5	45.5
6.65	3.89	.00249	72.5	50.4	50.5
8.4	3.90	.003145	119.286	63.7	63.8
8.6	3.91	.00322	124.643	65.2	65.4
8.9	3.92	.00335	133.929	67.5	67.7
9.0	3.93	.00342	138.929	68.2	68.5
9.2	3.95	.00355	148.214	69.7	70.1
9.35	3.99	.003655	155.714	70.9	71.4
9.40	4.05	.003795	165.714	71.3	72.1
9.45	4.25	.004145	190.714	71.6	73.4
9.3	4.62	.004495	215.714	70.5	74.1
9.0	4.90	.00475	233.929	68.2	73.1
8.8	5.13	.004825	239.286	66.7	72.6

48

0.491	.001	5.73	6
0.488	.003	5.75	19
0.487	.003	5.79	42
0.486	.004	5.80	56
0.486	.0	5.90	87
0.486	.001	6.01	115
0.486	.001	6.09	134
0.486	.004	6.20	204
0.488	.003	6.31	233
0.488	.003	6.35	239
0.483	.003	6.40	271
0.486	.003	6.45	293
0.485	.004	6.50	306
0.485	.004	6.55	335
0.487	.002	6.65	389
0.488	.001	6.75	447
0.486	.001	6.80	477
0.485	.004	6.90	569
0.488	.003	7.10	709
0.485	.003	7.21	827
0.485	-.003	7.30	943
0.486	.003	7.45	1070
0.485	.001	7.50	1117
0.489	.001	7.55	1148
0.489	.0	7.62	1211
0.485	.001	7.71	1249
0.488	.001	7.80	1368
0.488	.003	7.90	1436
0.485	.001	8.21	1587
0.486	.001	8.30	1624
0.488	.003	8.51	1700
0.488	.001	8.60	1729
0.489	.003	8.70	1752
0.486	.003	8.80	1769
0.485	.001	8.90	1781
0.488	.001	9.00	1812

0.486	.001	9.10	1824
0.486	.00	9.20	1841
0.488	.001	9.30	1853
0.486	.003	9.40	1870
0.486	.0	9.50	1880
0.486	.003	9.60	1887
0.486	.001	9.70	1893
0.486	.001	9.80	1899
0.488	.00	9.95	1904
0.488	.0	10.10	1909
0.488	.001	10.40	1914
0.488	.001	11.36	1916

## A114.RAW242B

121.6	.0373	.827	296637	16.65	.00383	33.0	
149.0	.15	10.0	16.8	397.9	0	0	0
2.89	.929	.00084	1.0	4.93	143856		

9

9.85	2.89	.001985	0	72.0	72.0
12.75	2.90	.0026	43.9286	93.1	93.2
14.5	2.91	.002935	67.8534	105.9	106.1
15.45	2.93	.00314	82.5	112.9	113.2
15.9	2.98	.003255	90.7143	116.2	116.8
16.15	3.14	.003345	97.1429	118.0	120.0
16.65	3.54	.00383	131.786	121.6	126.8
16.4	3.79	.004365	170.0	119.8	127.0
15.9	4.25	.00467	191.786	116.2	127.0

33

0.636	.004	4.94	2160
0.708	.006	4.96	61394
0.648	.003	5.50	61646
0.650	.004	6.35	65174
0.646	.003	6.37	65340
0.647	.003	6.63	68112
0.648	.004	6.83	71028
0.649	.004	6.90	72389
0.650	.007	7.05	75024
0.648	.007	7.23	79200
0.653	.01	7.33	82418
0.649	.006	7.47	86443
0.652	.009	7.83	94896
0.652	.009	7.86	96606
0.650	.009	7.93	100206
0.650	.009	8.03	106776
0.650	.009	8.13	112986
0.650	.009	8.23	118206
0.650	.009	8.33	122706
0.650	.009	8.43	127206
0.650	.009	8.53	130086
0.650	.009	8.63	132246
0.650	.009	8.73	134586

0.650	.009	8.83	136296
0.650	.009	8.93	138006
0.650	.009	9.03	139536
0.650	.009	9.13	140076
0.650	.009	9.23	141192
0.650	.009	9.33	142326
0.650	.009	9.43	142938
0.650	.009	9.63	143658
0.650	.009	9.73	143802
0.650	.009	10.03	143856

## A114.RAW242C

124.9	.0570	.568	299252	17.15	.00391	40.3	
149.0	.15	10.0	16.8	397.9	0	0	0
2.97	.924	.00084	1.0	4.99	1193		
11							
14.4	2.97	.002885	0	104.9	104.9		
16.0	2.98	.003225	24.2857	116.5	116.6		
16.8	3.00	.003475	42.1429	122.4	122.6		
17.0	3.01	.00361	51.7857	123.8	124.1		
17.1	3.02	.003755	62.1429	124.6	125.0		
17.15	3.04	.00382	66.7857	124.9	125.5		
17.15	3.12	.00391	73.2143	124.9	126.1		
17.0	3.36	.00412	88.2143	123.8	126.9		
16.7	3.56	.00429	100.357	121.6	126.3		
16.5	3.92	.004535	117.857	120.2	127.8		
16.15	4.15	.0048	136.786	117.6	127.0		
19							
0.999	-.003	5.05	124				
0.999	-.003	5.10	167				
1.002	-.002	5.15	212				
1.00	-.004	5.25	318				
1.0	-.004	5.35	483				
0.999	-.005	5.50	621				
1.0	-.004	5.75	712				
1.000	-.004	5.95	780				
1.0	-.004	6.15	840				
1.0	-.004	6.45	892				
1.0	-.004	6.75	929				
1.0	-.004	7.05	996				
1.0	-.004	7.35	1036				
1.001	-.003	7.75	1077				
1.001	.003	7.90	1097				
1.001	-.003	8.20	1127				
0.999	.001	8.50	1161				
0.999	0	9.00	1184				
0.999	0	9.25	1193				

## A114.RAW242T

187.6	.0700	.861	407910	26.0	.00414	60.8
-------	-------	------	--------	------	--------	------

149.0	.15	10.0	16.8	379.9	0	0	0
2.67	.930	.00084	1.0	5.51	3811		
13							
12.4	2.67	.00174	0	89.5	89.5		
12.9	2.68	.001825	6.07143	93.1	93.2		
13.4	2.69	.001895	11.0714	96.7	96.8		
18.5	2.70	.00269	67.8571	133.5	133.8		
20.65	2.71	.00299	89.2857	149.0	149.4		
23.45	2.72	.0034	118.571	169.2	169.8		
24.1	2.73	.003505	126.071	173.9	174.6		
24.75	2.74	.003635	135.357	178.6	179.4		
25.15	2.90	.003745	143.214	181.5	184.2		
26.0	3.33	.00414	171.429	187.6	195.7		
25.85	3.76	.00448	195.714	186.5	200.1		
25.5	3.96	.00465	207.857	184.0	200.0		
25.1	4.20	.00482	220.0	181.1	200.1		
49							
1.379	.010	5.63	19				
1.377	.006	5.77	74				
1.379	.009	5.80	95				
1.376	.01	6.05	221				
1.383	.009	6.10	258				
1.377	.007	6.35	368				
1.383	.007	6.40	385				
1.374	.004	6.50	445				
1.380	.01	6.60	499				
1.377	.013	6.75	577				
1.377	.007	6.80	702				
1.379	.007	6.92	780				
1.377	.006	7.00	842				
1.376	.012	7.11	888				
1.376	.006	7.20	946				
1.371	.012	7.30	1005				
1.374	.012	7.40	1082				
1.380	.007	7.50	1137				
1.376	.007	7.60	1192				
1.373	.01	7.70	1230				
1.376	.007	7.75	1385				
1.373	.009	7.80	1478				
1.374	.004	7.90	1563				
1.377	.006	8.12	1740				
1.377	.006	8.22	1899				
1.377	.006	8.32	1950				
1.377	.006	8.42	2010				
1.377	.006	8.52	2145				
1.380	.009	8.56	2229				
1.377	.013	8.70	2398				
1.377	.013	8.82	2496				
1.374	.016	9.00	2723				
1.374	.016	9.12	2895				
1.377	.016	9.25	3012				
1.375	.014	9.42	3153				

1.373	.012	9.56	3270
1.374	.012	9.72	3354
1.374	.012	9.92	3456
1.374	.012	10.02	3510
1.374	.012	10.12	3567
1.374	.012	10.22	3615
1.376	.012	10.52	3663
1.376	.012	10.65	3683
1.374	.015	10.75	3703
1.374	.016	10.90	3732
1.374	.016	11.02	3771
1.374	.016	11.32	3786
1.374	.016	11.72	3798
1.374	.016	12.12	3811

## A114.RAW243B

110.8	.0589	.771	190846	15.3	.00518	35.8	
149.0	.15	10.0	16.8	397.9	0	0	0
2.12	.954	.00084	1.0	6.39	6404		
14							
7.0	2.12	.00195	0	50.7	50.7		
7.65	2.13	.002215	18.9286	55.4	55.4		
8.35	2.14	.00248	37.8571	60.5	60.6		
9.85	2.15	.00304	77.8571	71.3	71.5		
10.75	2.16	.00333	98.5714	77.9	78.1		
13.5	2.17	.004185	159.643	97.8	98.1		
14.7	2.18	.004615	190.357	106.5	106.9		
14.9	2.19	.004715	197.5	107.9	108.4		
15.0	2.20	.00481	204.286	108.7	109.2		
15.15	2.27	.004895	210.357	109.7	110.8		
15.3	2.46	.00518	230.714	110.8	113.2		
15.25	2.76	.00573	270.0	110.5	115.1		
15.0	3.11	.00611	297.143	108.7	115.8		
14.8	3.55	.00648	323.571	107.2	117.7		
23							
0.596	-.002	6.41	51				
0.599	.006	6.45	102				
0.599	.004	6.55	285				
0.599	.001	6.65	388				
0.597	.001	6.75	546				
0.597	.001	6.85	828				
0.596	.001	6.90	1050				
0.597	.001	6.95	1170				
0.598	.00	7.36	2502				
0.599	.001	7.45	3168				
0.599	.001	7.65	4380				
0.598	-.002	7.75	5310				
0.598	-.002	7.80	5970				
0.819	.007	7.85	6228				
0.819	.007	7.95	6253				
0.819	.007	8.45	6277				

0.819	.007	8.85	6289
0.605	.007	9.50	6318
0.604	.009	9.85	6340
0.609	.009	10.10	6363
0.606	.013	10.32	6382
0.606	.013	10.55	6391
0.606	.013	11.15	6404

## A114.RAW243C

86.3	.0404	.672	155713	12.05	.004685	28.1	
149.0	.15	10.0	16.8	397.9	0	0	0
2.43	.935	.00084	1.0	4.49	2448		
14							
6.45	2.43	.002345	0	46.2	46.2		
7.30	2.44	.00273	27.5	52.3	52.3		
7.90	2.46	.002985	45.7143	56.6	56.7		
10.35	2.47	.003895	110.714	74.2	74.3		
11.3	2.49	.004255	136.429	81.0	81.3		
11.7	2.52	.00444	149.643	83.8	84.3		
11.95	2.58	.0046	161.071	85.6	86.4		
11.95	2.64	.00463	163.214	85.6	86.8		
12.0	2.70	.004685	167.143	86.0	87.5		
12.05	2.93	.005055	193.571	86.3	89.1		
11.95	3.16	.005525	227.143	85.6	89.7		
11.55	3.45	.00582	248.214	82.8	88.3		
11.4	3.77	.006275	280.714	81.7	89.1		
10.95	3.88	.006365	287.143	78.5	86.2		
23							
0.674	.001	4.53	40				
0.672	.003	4.60	66				
0.674	.002	4.86	150				
0.674	.001	5.00	201				
0.672	0	5.10	226				
0.672	.001	5.35	252				
0.672	.001	5.56	270				
0.672	.001	5.86	288				
0.672	.001	5.90	292				
0.672	.001	8.36	300				
0.423	.004	8.63	357				
0.423	.004	8.66	393				
0.422	.003	8.95	601				
0.425	.003	9.10	758				
0.425	.003	9.20	877				
0.425	0	9.32	1176				
0.423	.003	9.50	1427				
0.426	.0	9.60	1840				
0.425	.001	9.70	2358				
0.500	.005	9.72	2379				
0.574	.009	9.95	2441				
0.574	.009	10.02	2446				
0.574	.009	10.32	2448				

## A128.RAW020B

243.9	.1004	1.020	560861	32.65	.00385	77.9	
155.0	.15	10.0	16.8	397.9	0	0	0
3.01	.938	.00084	3.0	6.14	6506		
15							
15.65	3.01	.00164	0	116.9	116.9		
18.3	3.02	.00198	24.2857	136.7	136.8		
21.05	3.03	.00232	48.5714	157.2	157.5		
24.85	3.04	.00275	79.2857	185.6	186.0		
26.1	3.05	.00289	89.2857	195.0	195.5		
27.55	3.06	.00305	100.714	205.8	206.5		
29.45	3.07	.00325	115.0	220.0	220.9		
30.7	3.08	.0034	125.714	229.3	230.4		
32.0	3.10	.003605	140.357	239.0	240.4		
32.5	3.14	.00375	150.714	242.8	244.8		
32.65	3.24	.00385	157.857	243.9	247.6		
32.3	3.49	.004045	171.786	241.3	248.9		
31.2	3.86	.004345	193.214	233.1	246.4		
30.45	4.02	.00451	205.0	227.5	243.1		
29.85	4.31	.00466	215.714	223.0	243.1		
27							
1.852	.0	6.17	9				
1.302	.007	7.15	63				
1.316	.005	7.25	111				
1.327	.004	7.32	158				
1.327	.003	7.45	177				
1.324	.003	7.66	206				
1.327	.007	7.75	231				
1.330	.007	7.85	267				
1.333	.007	8.03	315				
1.323	.005	8.15	384				
1.323	.005	8.35	456				
1.323	.005	8.65	582				
1.323	.005	9.05	798				
1.323	.005	9.45	1230				
1.323	.005	9.55	1410				
1.327	.005	9.75	1842				
1.327	.005	9.85	2346				
1.327	.005	9.95	2580				
1.327	.005	10.05	2958				
1.327	.005	10.15	3210				
1.331	.006	10.25	3516				
1.331	.006	10.55	3750				
1.331	.006	10.65	3984				
1.331	.006	10.72	4308				
1.330	.010	10.80	4844				
1.332	.004	10.90	5402				
1.525	.010	10.97	6506				

## A128.RAW020C

108.7	.0495	.662	199407	15.05	.00477	35.2
-------	-------	------	--------	-------	--------	------

155.0	.15	10.0	16.8	397.9	0	0	0
3.07	.915	.00084	2.0	4.78	16740		
13							
7.6	3.07	.0021	0	54.9	54.9		
8.0	3.08	.002255	11.0714	57.8	57.8		
11.4	3.09	.00339	92.1429	82.4	82.5		
12.1	3.10	.003595	106.786	87.4	87.6		
12.5	3.11	.003715	115.357	90.3	90.5		
13.45	3.12	.00399	135.0	97.2	97.5		
14.1	3.13	.00419	149.286	101.9	102.3		
14.5	3.15	.004315	158.214	104.8	105.3		
14.7	3.22	.00441	165.0	106.2	107.2		
15.05	3.47	.00477	190.714	108.7	111.5		
14.8	3.86	.005155	218.214	106.9	112.5		
14.05	4.13	.00554	245.714	101.5	108.7		
13.55	4.45	.005775	262.5	97.9	107.1		
23							
0.547	.001	4.80	126				
0.547	.001	4.86	720				
0.547	.001	4.97	2250				
0.547	.001	5.16	2880				
0.547	.001	5.35	3330				
0.547	.001	5.55	3870				
0.547	.001	5.98	5130				
0.547	.001	6.35	6390				
0.547	.001	6.76	7560				
0.547	.001	7.06	8460				
0.547	.001	7.45	9540				
0.547	.001	7.75	10440				
0.547	.001	8.04	11430				
0.547	.001	8.26	12060				
0.547	.001	8.54	12870				
0.547	.001	8.76	13500				
0.547	.001	9.07	14220				
0.547	.001	9.46	14940				
0.547	.001	9.76	15300				
0.547	.001	10.05	15660				
0.547	.001	10.36	16290				
0.547	.001	10.57	16560				
0.547	.001	10.84	16740				

## A128.RAW020T

104.7	.0472	.284	216305	14.75	.00432	34.2	
155.0	.15	10.0	16.8	397.9	0	0	0
1.77	.955	.00084	1.0	3.93	7130		
15							
8.9	1.77	.00234	0	63.2	63.2		
9.1	1.78	.00241	5.0	64.6	64.6		
9.5	1.79	.00251	12.1429	67.4	67.5		
11.2	1.80	.003005	47.5	79.5	79.6		
11.7	1.81	.003125	56.0714	83.0	83.3		

12.3	1.82	.003285	67.5	87.3	87.6
13.0	1.83	.00348	81.4286	92.3	92.6
13.5	1.84	.00361	90.7143	95.8	96.2
14.15	1.87	.0038	104.286	100.4	101.1
14.55	1.89	.00399	117.857	103.3	104.1
14.65	2.00	.00406	122.857	104.0	105.5
14.75	2.36	.00432	141.429	104.7	108.7
14.55	2.75	.00458	160.0	103.3	109.9
14.05	3.11	.004615	162.5	99.7	108.7
14.05	3.30	.00472	170.0	99.7	110.0

57

0.697	.003	3.94	203
0.696	.0	3.95	405
0.696	.0	3.97	600
0.697	-.002	3.99	1320
0.697	-.002	4.01	1680
0.693	-.003	4.09	2040
0.693	-.003	4.13	2265
0.700	-.006	4.15	2326
0.740	-.008	4.18	2468
0.737	-.002	4.20	2500
0.738	-.008	4.25	2593
0.738	-.002	4.30	2733
0.803	-.003	4.35	2855
0.806	-.005	4.41	2949
0.804	-.006	4.50	3062
0.809	-.005	4.60	3130
0.806	-.005	4.71	3219
0.803	-.006	4.80	3288
0.806	-.003	4.90	3356
0.812	-.008	5.00	3424
0.807	-.007	5.17	3600
0.807	-.007	5.31	3720
0.803	-.006	5.55	3886
0.803	-.006	5.87	4080
0.807	-.004	5.97	4188
0.807	-.004	6.17	4323
0.810	-.002	6.41	4482
0.810	-.002	6.47	4560
0.810	-.002	6.57	4650
0.810	-.002	6.67	4755
0.810	-.002	6.77	4902
0.810	-.002	6.87	5025
0.810	-.002	6.97	5130
0.809	-.003	7.05	5204
0.808	-.004	7.27	5406
0.807	-.005	7.35	5533
0.805	-.004	7.47	5730
0.805	-.004	7.57	5859
0.803	-.003	7.75	5988
0.804	-.003	7.91	6138
0.805	-.003	8.17	6360

0.807	-.003	8.40	6580
0.804	-.003	8.50	6653
0.841	-.003	8.57	6795
0.841	-.003	8.67	6849
0.841	-.005	8.80	6905
0.841	-.003	8.90	6949
0.839	-.002	9.00	6987
0.839	-.002	9.27	7017
0.839	-.002	9.57	7038
0.839	-.002	10.07	7051
0.839	-.002	10.27	7062
0.847	-.003	10.37	7077
0.847	-.003	10.40	7098
0.847	-.003	10.57	7110
0.847	-.003	10.70	7122
0.847	-.003	11.14	7130

The format of the following optimum moisture data is the same as for cards 1 through 3 of the previous data.

WM15T						
89.4	.0526	.395	164141	12.3	.00491	28.9
75.0	.15	5.0	11.79	397.9		
WM15C						
73.9	.0441	.294	119999	10.15	.005315	23.9
75.0	.15	5.0	11.79	397.9		
WM16T						
78.8	.0380	.131	155099	9.9	.00465	24.5
75.0	.15	5.0	14.70	397.9		
WM16C						
118.8	.0540	.873	281072	15.8	.00376	37.8
75.0	.15	5.0	14.70	397.9		
WM16B						
85.7	.0479	.340	150227	11.5	.005045	27.4
75.0	.15	5.0	14.70	397.9		
WM17T						
77.8	.0400	.336	140276	10.1	.004995	24.5
75.0	.15	5.0	16.8	397.9		

The following data were used to generate the plots involving  $\log_{10}A$  versus  $n$  and for the CSI plots. For the cement stabilized soil data, the first card is the sample number (SMPL). The second card contains  $K_{IC}$ ,  $K_{QD}$ ,  $\sigma_{IDT}$ , the last cycle number and the calculated size of the "plastic" zone. The third and fourth cards define  $\log_{10}A$  and  $n$  for the total polynomial and modified secant method, respectively. Dots indicate missing values. For the other materials, the type of material is indicated in the first column followed by an equivalent  $\log_{10}A$  calculated from equation (II-1) and  $n$ . If present, the third column of data is an estimate of  $K_{IC}$  in units of psi/in. The last column indicates the source of the original  $A$  and  $n$  values.

#### 5% Modified

```

INPUT SMPL ;
INPUT KC05M KQ05M SIDT LSTCY PLAST;
INPUT L5G N5;
INPUT PFD5 NF5;
006T
65.3 77.2 75 854 0.04021636
-5.83792 1.18178
-7.62366 2.178104
006C
54.7 52.2 75 218 0.02821961
. .
-37.513 19.59141
006B
94.1 100.1 75 681 0.08351329
. .
-52.1137 24.94679
018C
95.6 82.6 75 49554 0.086197
. .
-17.8316 7.459139
018T
114.3 117.4 75 6690 0.1232165
-19.5818 7.4447
-21.9163 8.554816

```

## 10% Modified

```

INPUT SMPL ;
INPUT KC10M KQ10M SIDT LSTCY PLAST;
INPUT L10G N10;
INPUT FFD10 NF10;
003T
178.9 204.7 155 432 0.07067343
. .
-18.9219 6.784452
007T
102.8 104.4 155 415 0.02333575
. .
-28.2829 12.2393
007B
127.5 134.2 155 1057 0.03589681
. .
-69.131 30.96549
003C
130.4 160.2 155 4420 0.03754833
-16.1399 5.626598
-22.2299 8.638283

```

## 15% Modified

```

INPUT SMPL ;
INPUT KC51M KQ51M SIDT LSTCY PLAST;
INPUT L51G N61;
INPUT FFD51 NF61;
005T
240 256.4 186 1168 0.08832741
. .
-6.17707 1.079703
005C
180.7 193.4 186 775 0.05007135
. .
-21.4943 7.866492
019T
167.9 176.8 186 4740 0.04322892
. .
-6.54466 1.015031
005B
243.8 200.6 186 192 0.09114658
. .
-44.1226 17.6802

```

## 5% Standard

```

INPUT SMPL ;
INPUT KC05S KQ05S SIDT LSTCY PLAST;

```

INPUT L5S SN5;  
INPUT FFDS5 NFS5;  
023C  
64.5 43.7 40 4932 0.1379426  
-30.9414 16.18616  
-51.1724 28.78458  
023B  
57.6 53.1 40 3279 0.1100079  
-14.9404 6.828986  
-22.9284 11.46812

#### 10% Standard

INPUT SMPL ;  
INPUT KC10S KQ10S SIDT LSTCY PLAST;  
INPUT L10S SN10;  
INPUT FFDS10 NFS10;  
008C  
101.8 106.6 117 763 0.04016268  
-13.9166 5.138533  
-5.35163 0.8512027  
008T  
97.5 108.2 117 599 0.03684142  
-15.0383 5.687538  
-15.5112 5.954549  
008B  
101 113.7 117 152 0.03953392  
-10.4003 3.50393  
-66.2584 31.90079

#### 15% Standard

INPUT SMPL ;  
INPUT KC15S KQ15S SIDT LSTCY PLAST;  
INPUT L51S SN61;  
INPUT FFDS15 NFS15;  
010T  
110.6 88.4 145 179 0.03086549  
-18.8602 8.168237  
-32.4408 15.31274  
022T  
118.1 117.3 145 1740 0.03519352  
-8.61656 2.280078  
-8.67839 2.305881  
022B  
180.6 176.8 145 55584 0.08229972  
-8.97579 1.658425  
-20.7667 7.418916

## 28 Day Curing Study

INPUT SMPL ;  
 INPUT KC28C KQ28C SIDT LSTCY PLAST;  
 INPUT LCUR8 CURN8;  
 INPUT FFD8 NF8;  
 020C  
 108.7 98.2 155 16740 1.341771 0.02609123  
 -8.745 2.092513  
 -10.4892 3.021132

## 14 Day Curing Study

INPUT SMPL ;  
 INPUT KC14C KQ14C SIDT LSTCY PLAST;  
 INPUT LCUR4 CURN4;  
 INPUT FFD4 NF4;  
 242B  
 121.6 94.5 149 143856 1.323881 0.03533406  
 -34.9014 15.16473  
 -62.3333 29.42854  
 242C  
 124.9 127.6 149 1193 1.288172 0.03727788  
 -16.5168 6.287231  
 -24.5371 10.29098  
 242T  
 187.6 229 149 3811 1.407164 0.08409923  
 -18.8582 6.49338  
 -31.1934 12.00674

## 7 Day Curing Study

INPUT SMPL ;  
 INPUT KC07C KQ07C SIDT LSTCY PLAST;  
 INPUT LCUR7 CURN7;  
 INPUT FFD7 NF7;  
 240B  
 99.6 85.3 128 16668 1.30081 0.03212163  
 -15.6533 5.707298  
 -63.3867 31.4191  
 241B  
 92.9 101.1 128 1330 1.296952 0.0279454  
 -7.95076 1.930708  
 -27.8762 12.63058  
 241C  
 99 89.2 128 139 1.188779 0.03173579  
 -14.1551 5.493632  
 -160.296 81.46883  
 240C  
 76.7 77 128 1026 1.28855 0.01904889

-26.7246 12.39312  
 -29.0484 13.67558

### Gypsum

INPUT GYPA GYPN KQD;  
 Gypsum

-46.848654 24.926173 58.9

### Sulphlex

INPUT SULA SULN;  
 Sulphlex 65°F

-6.18 1.6 [61]

-11.88 3.32

7.34 1.62

-9.39 2.16

AC10 65°F

-9.92 2.4

-9.42 2.22

Sulphlex 58°F

-9.04 2.32

-7.32 1.9

AC10 65°F

-8.02 1.76

-7.57 1.54

### Fabric Reinforced Asphalt Concretes

INPUT ACA ACN;  
 Fabric-Asphalts

-3.60033 4.29 [77]

-1.91721 0.54

-5.44009 6.16

-4.03012 2.97

-3.58336 2.25

-3.38722 2.7

-2.90309 1.66

-2.35853 1.14

-4.6968 4.19

-3.42366 1.8

-3.48545 3.16

-2.46852 1.16

-3.21753 2.23

-3.7986 2.3

-1.48812 0.05

-3.53018 2.83

-3.97062 2.91

-5.68403 6.21

-6.42366 5.52

-5.14874 4.68

-2.92082 2.32

-2.54668 2.67

-6.36151 5.74

-4.35458 4.28

-2.41567	0.95
-1.7122	0.06
-4.5391	5.73
-4.02228	3.38
-2.57349	1.23
-3.67778	2.79

### Steels

INPUT STA STN KQD;

140ksi martensitic steel	-14.9305	2.25	61968 [85]
Ferrite-pearlite	-18.4437	3.0	51381
Austenitic stainless	-19.2729	3.25	43818
Ti	-27.141	5.0	53000
A533 weld	-15.0	2.2	

### Asphalt Concretes (AC5-AC20)

INPUT AC2A AC2N;

Asphalt concretes	-0.91364	0.193	[31]
	-5.82681	2.82	
	-5.92082	2.35	
	-1.53611	0.424	
	-7.55596	4.08	
	-7.85387	4.29	
	-7.81531	3.84	
	-7.66959	4.63	
	-5.07263	2.11	
	-5.56384	4.32	

### Polymers

INPUT PLMA PLMN KQD;

Epoxy	-36.6837	11.94076	[39]
PMMA	-27.2158	8.1948	1200
PS	-12.0711	2.768	870

### Composites

INPUT CMA CMN KQD;

GRP	-84.4858	20.33	9736 [73]
	-29.7551	5.6	34941
SMC-R5	-44.0795	9.65	[106]
Epoxy-Al	-53.9979	11.9	[102]
	-24.4534	4.7	
	-25.4163	4.9	
	-15.9937	2.6	
B-Al	-51.6113	9.83934	49533 [82]

**Bitumens (Asphalt Concrete)**

INPUT ALA AAN;  
Bitumens

-9.81437	2.889
-14.3257	4.026
-16.7728	4.367
-14.2056	3.086
-12.7069	3.787
-11.6469	2.882
-16.1711	4.767
-29.6761	8.696
-11.6452	3.239
-11.0091	2.571
-8.08226	2.994
-6.52326	1.255

[69]

**Data for Figure 40**

INPUT XP YC4;  
0.6 -7.1261  
0.75 -5.433  
0.85 -4.48422  
0.9 -4.05067  
1.00 -3.25151

#### APPENDIX IV.-CALCULATOR AND COMPUTER ANALYSIS OF DATA

Data analysis is based on a one inch (2.54 cm) thick compact tension specimen (CTS) meeting the specifications in reference (5). In some cases, programs allow entries which enable the user to change the CTS thickness.

The first set of programs allow hand analysis of load-displacement records. In general, the programs require information on load in pounds or volts, displacement in inches, and crack length in millimeters. These programs were written for the Hewlett-Packard 41CX with the functions as defined in reference (40).

Program E399 must exist before program PARIS can be run. The fatigue results reported in this dissertation did not come from program PARIS, but came from the SAS program FATIGUE documented later in this appendix. Program PARIS was used early in the data analysis to get a general idea of the value of the parameters in equation (50). Program PARIS uses a form of the secant method shown in reference (6) with a slight difference in how  $\Delta K$  is assigned to  $\Delta a/\Delta N$  as can be seen in the output description for the program. Of course, a regression must be performed on the output data in order to solve equation (50).

Program JINT uses a form of the trapezoidal rule to approximate the area under the load-displacement record.

The following program performs the calculations required in reference (5).

1 LBL <sup>T</sup> E399	20 FS? 01	39 * 59 1
2 0	21 GTO <sup>T</sup> AB	40 ST+ 03
3 STO 03	22 <sup>T</sup> PQ=?	41 RCL 01
4 RDN	23 PROMPT	42 3
5 SF 21	24 GTO <sup>T</sup> AC	43 Y <sup>X</sup>
6 FS? 01	25 LBL <sup>T</sup> AB	44 14.72
7 GTO <sup>T</sup> AO	26 RDN	45 *
8 <sup>T</sup> AO=?	27 X <sup>&gt;</sup> Y	46 ST+ 03
9 PROMPT	28 LBL <sup>T</sup> AC	47 RCL 01
10 LBL <sup>T</sup> AO	29 STO 05	48 4
11 2.0	30 0.886	49 Y <sup>X</sup>
12 STO 06	31 STO 03	50 -5.6
13 ÷	32 RCL 01	51 *
14 STO 01	33 4.64	52 RCL 03
15 2	34 *	53 +
16 +	35 ST+ 03	54 RCL 02
17 STO 02	36 RCL 01	55 *
18 1.0	37 X <sup>2</sup>	56 STO 03
19 STO 04	38 -13.32	57 RCL 01
		58 CHS
		60 +
		61 1.5
		62 Y <sup>X</sup>
		63 RCL 03
		64 X <sup>&gt;</sup> Y
		65 +
		66 STO 07
		67 RCL 05
		68 *
		69 RCL 04
		70 +
		71 RCL 06
		72 √X
		73 ÷
		74 <sup>T</sup> KQ=
		75 ARCL X
		76 AVIEW
		77 END

The input and output for the previous program is described below.

INPUT	STEP
a <sub>0</sub> in inches	8-9
P <sub>q</sub> in pounds	22-23

OUTPUT	STEP
K <sub>q</sub> in psi/in	74-76

The following program performs the calculations required in reference (7).

1	LBL <sup>T</sup> JINT	21	+
2	CLST	22	STO 13
3	000.03301	23	RCL 11
4	CLRGX		+
5	SF 21	25	<sup>T</sup> AO/W=
6	CF 29	26	ARCL X
7	<sup>T</sup> ENTER B IN	27	AVIEW
8	PROMPT	28	STO 14
9	STO 10	29	<sup>T</sup> VLL/VO INTERPOL
10	2	30	AVIEW
11	*	31	<sup>T</sup> LWR AO/W?
12	STO 11	32	PROMPT
13	<sup>T</sup> ENTER LL-KRK IN	33	STO 00
14	PROMPT	34	<sup>T</sup> LWR VLL/VO?
15	STO 12	35	PROMPT
16	<sup>T</sup> AO MM?	36	STO 01
17	PROMPT	37	<sup>T</sup> UPR VLL/VO?
18	STO 18	38	PROMPT
19	0.03937	39	STO 02
20	*	40	X <sup>&gt;</sup> Y

41 -	61 *
42 RCL 14	62 STO 32
43 RCL 00	63 $T_{LB}/IN?$
44 -	64 PROMPT
45 0.05	65 STO 17
46 ÷	66 $T_{Y1} \text{ MAX } IN?$
47 *	67 PROMPT
48 RCL 01	68 *
49 +	69 STO 31
50 STO 15	70 *
51 $T_{VLL}/VO=$	71 2
52 ARCL X	72 ÷
53 AVIEW	73 STO 30
54 $T_{IN}/IN \text{ SCALE?}$	74 RCL 11
55 PROMPT	75 RCL 13
56 STO 16	76 -
57 $T_{TRIANGULAR} \text{ AREA}$	77 STO 20
58 AVIEW	78 1/X
59 $T_{X1} \text{ MAX } IN?$	79 2
60 PROMPT	80 *
81 RCL 13	101 RCL 01
82 *	102 1.0
83 STO 00	103 +
84 $X^2$	104 *
85 RCL 00	105 2.0
86 2.0	106 *
87 *	107 STO 19
88 +	108 $T_{FAO}/W=$
89 2.0	109 ARCL X
90 +	110 AVIEW
91 $\sqrt{X}$	111 $T_{.2-1.5MM} \text{ OK}$
92 RCL 00	112 AVIEW
93 -	113 $T_{NUM} \text{ UNLOADS?}$
94 1.0	114 PROMPT
95 -	115 1000
96 STO 01	116 ÷
97 $X^2$	117 STO 33
98 1.0	118 LBL A
99 +	119 ISG 33
100 1/X	120 GTO 01

121 GTO E	141 -
122 LBL 01	142 STO 02
123 <sup>T</sup> A MM?	143 RDN
124 PROMPT	144 STO 32
125 RCL 18	145 <sup>T</sup> Y IN?
126 -	146 PROMPT
127 0.03937	147 RCL 17
128 *	148 *
129 <sup>T</sup> DELTA A=	149 ENTER ↑
130 ARCL X	150 ENTER ↑
131 AVIEW	151 RCL 31
132 <sup>T</sup> USE COORD IN	152 +
133 AVIEW	153 2.0
134 <sup>T</sup> X IN?	154 +
135 PROMPT	155 STO 01
136 RCL 16	156 RDN
137 *	157 STO 31
138 ENTER ↑	158 RCL 01
139 ENTER ↑	159 RCL 02
140 RCL 32	160 *

161 ST+ 30	169 RCL 15
162 RCL 30	170 *
163 RCL 19	171 T <sub>J</sub> =
164 *	172 ARCL X
165 RCL 10	173 AVIEW
166 +	174 GTO A
167 RCL 20	175 LBL E
168 +	176 END

INPUT	STEP
Specimen thickness, B, inches	7-8
Measurement from load line to front of Krak-gage®, inches	13-14
Initial crack length, a <sub>0</sub> , mm through Krak-gage®	16-17
Interpolate for a <sub>0</sub> /W to get correction factor based on reference (88)	29-38
Smaller value of a <sub>0</sub> /W (88)	31-32
Smaller value of V <sub>11</sub> /V <sub>0</sub> (88)	34-35
Larger value of V <sub>11</sub> /V <sub>0</sub> (88)	37-38
Scale of displacement on plotter (inches LVDT displacement/inch plotter displacement)	54-55
X coordinate (δ) of peak of triangular area defined by linear portion of P-δ record in inches	57-60
Scale of load on plotter (pounds of load per inch of plotter displacement)	63-64
Y coordinate (load) of peak of triangular area in inches	66-67

Number of unloads, or points, at which J will be calculated	113-114
a, mm through Krak-gage®, crack length at $i^{\text{th}}$ data point (or unload) for J	123-124
X ( $\delta$ ) coordinate of $i^{\text{th}}$ data point in inches on plotter	134-135
Y (P) coordinate at $i^{\text{th}}$ point	145-146

OUTPUT	STEP
$a_0/W$	25-27
correction factor, $V_{11}/V_0$ , (88)	51-53
$f(a_0/W)$ reference (7)	108-110
User note as to what general range of crack length is acceptable for regression (varies, see reference (7))	111-112
$\Delta a$ for J versus $\Delta a$ curve	129-131
J for J versus $\Delta a$ curve	171-173

The following program calculates Young's modulus using a compliance relationship found in references (88 and 89).

1 LBL <sup>T</sup> WESTVO	19 CHS	37 LBL 01	55 RCL 01
2 CF 21	20 1.0	38 *	56 4.0
3 <sup>T</sup> ENTER A/W	21 +	39 $\Sigma$ +	57 $Y^X$
4 PROMPT	22 ÷	40 RTN	58 XEQ 01
5 STO 01	23 $X^2$	41 LBL 02	59 -14.4945
6 ENTER B	24 *	42 12.6778	60 RCL 01
7 PROMPT	25 0.25	43 RCL 01	61 5.0
8 <sup>T</sup> ENTER VO	26 RCL 01	44 XEQ 01	62 $Y^X$
9 PROMPT	27 ÷	45 -14.2311	63 XEQ 01
10 *	28 1.0	46 RCL 01	64 RCL 11
11 1/X	29 +	47 $X^2$	65 RCL 02
12 <sup>T</sup> ENTER P	30 *	48 XEQ 01	66 *
13 PROMPT	31 STO 02	49 -16.6102	67 $T_E$ =
14 *	32 $\Sigma$ REG 11	50 RCL 01	68 ARCL X
15 RCL 01	33 CLZ	51 3.0	69 AVIEW
16 1.0	34 1.61369	52 $Y^X$	70 STOP
17 +	35 $\Sigma$ +	53 XEQ 01	71 END
18 RCL 01	36 GTO 02	54 35.0499	

INPUT	STEP
$a_o/W$	3-4
thickness, B	6-7
Front face displacement at top of linear portion of P- $\delta$ curve (inches LVDT displacement)	8-9
Load, P, at $\delta$ in step 8 (pounds)	12-13
OUTPUT	STEP
Young's modulus, E (psi)	67-69

The following program calculates  $da/dN$  using first forward differences and assigns the value to the values of  $\Delta K$  and  $K_{max}$  at the forward end point of the difference.

1 LBL <sup>T</sup> PARIS	21 PROMPT
2 SF 21	22 1.0
3 CF 29	23 X=Y?
4 SF 01	24 SF 02
5 CF 02	25 <sup>T</sup> LD a P MN LB?
6 040.04301	26 PROMPT
7 CLRG X	27 STO 46
8 <sup>T</sup> LL-KRK?	28 LBL <sup>T</sup> DELP
9 PROMPT	29 <sup>T</sup> UPR VP?
10 STO 48	30 PROMPT
11 <sup>T</sup> AO MM=?	31 10
12 PROMPT	32 *
13 0.03937	33 STO 45
14 *	34 RCL 46
15 +	35 +
16 STO 47	36 STO 44
17 <sup>T</sup> AO=	37 RCL 45
18 ARCL X	38 <sup>T</sup> LWR VP?
19 AVIEW	39 PROMPT
20 <sup>T</sup> ALLOW dP 1=Y?	40 10

41 *	61 PROMPT
42 -	62 0.03937
43 STO 39	63 *
44 SF 03	64 RCL 48
45 $T_{DEL} P=$	65 +
46 ARCL X	66 $T_A=$
47 AVIEW	67 ARCL X
48 LBL 01	68 AVIEW
49 FS? 01	69 STO 38
50 GTO 02	70 RCL 47
51 GTO 03	71 -
52 LBL 02	72 $T_{AN}=$
53 FS? 03	73 ARCL X
54 GTO 04	74 AVIEW
55 GTO $T_{DELP}$	75 STO 40
56 LBL 04	76 RCL 41
57 CF 03	77 -
58 GTO 03	78 STO 41
59 LBL 03	79 $T_N=?$
60 $T_A$ MM?	80 PROMPT

81 STO 42	91 STO 41
82 RCL 43	92 RCL 42
83 -	93 STO 43
84 RCL 41	94 RCL 39
85 $X \begin{smallmatrix} > \\ < \end{smallmatrix} Y$	95 RCL 38
86 $\div$	96 $XEQ^{TE}399$
87 $T_{DA/DN}=$	97 RCL 44
88 ARCL X	98 RCL 38
89 AVIEW	99 $XEQ^{TE}399$
90 RCL 40	100 GTO 01

## INPUT

## STEP

Load line to Krak-gage® (inches)

8-9

 $a_0$  (mm into Krak-gage®) at cycle  $N_1=0$ 

11-12

Decision whether to allow load changes or not (yes=1)

20-21

Load at minimum load (pound)	25-26
Voltage at peak load in cycle $i$ (volts)	29-30
(Note: lines 31 and 40 are the number of pounds per volt and will vary with user selected machine settings)	
Voltage at minimum load during cycle $i$	38-39
$a$ (mm) at $i^{\text{th}}$ cycle ( $i \neq 0$ )	60-61
$N$ (cycle number)	79-80

OUTPUT	STEP
$a_0$ (inches)	17-19
change in load in the cycle, $\Delta P$ , (pounds)	45-47
$a_i$ (inches)	66-68
$a_i - a_{i-1} = \Delta N$	72-74
$da/dN = \Delta N / (N_i - N_{i-1})$	87-89
$K_{qi}$ , $\Delta K$	96
$K_{qi}$ , $K_{\text{max}}$	99

The following programs were used on the Amdahl mainframe computer at Texas A&M University. These programs were used to analyze the raw data from load-displacement records, and data from programs E399, JINT, and WESTVO. Unless otherwise noted, all data read into SAS programs uses the blank as a delimiter. The FORTRAN program NTOF uses the comma as a delimiter. Program STATCYC or NOCYCLE were run first for specimens which had fatigue data or did not have fatigue data, respectively (see Appendix III). These programs are listed below. The raw data is input in INDAT1 and the partially processed form is output to the file OUTDAT1. These programs arranged the raw data into an intermediate processed form containing values with appropriate units in the order needed for final processing.

---

```
//STATCYC JOB (B250,004C,2,20,WC), 'CROCKFORD'
//*TAMU PRTY=0
//*FORMAT PR,DDNAME=,DEST=XEROX,FORMS=1101,JDE=JFMT7
//STEP EXEC SAS
//INDAT1 DD DSN=USR.B250.WC.A107.RAW240B,DISP=SHR
//OUTDAT1 DD DCB=(DSORG=PS,LRECL=80),UNIT=SYSDA,SPACE=(TRK,(1,1)),
// DSN=USR.B250.WC.A107.MID240B,DISP=MOD
//OUTDAT2 DD DSN=USR.B250.WC.ASUM107,DISP=MOD
//SYSIN DD *
*****
*****
* NOTE: YOU MUST CHANGE:
* DSN'S ETC. FOR          INDAT1          (LINE 5)
*                          OUTDAT1         (LINE 7)
*                          TITLE1          (LINE72)
*                          OBS=            (LINE77)
*                          FIRSTOBS=      (LINE 97)
* (ALL DATA FILES MUST PREEXIST AS DUMMY FILES ON WYLBUR)
*   FOR EACH RUN ... AND:
* DSN FOR OUTDAT2 FOR EACH TIME YOU CHANGE THE PERCENT
* CEMENT OR COMPACTION.
* YOU MUST ADD A PLOTOUT DD STATEMENT
```

```

* FOR THE ONE PLOT FOR WHICH VECTORS ARE TO BE          *;
* STORED FOR SCRIPT.                                     *;
* VERSION 2 .....12AUG85                                *;
*****;
*****;
      OPTIONS PAGESIZE=60 LINESIZE=90;
*****;
*****;
DATA STATIC;
      INFILE INDAT1 FIRSTOBS=2 OBS=4;
*****;
*COMMENT: INPUT THE STATIC DATA AND LOOPING CONTROLS;
*****;
      INPUT KQ1 JQ1 DJDAL EWEST1 PMAX1 DPMX1 PMFAW;
      INPUT IDT1 NU CMT WOPT CEL POR PERM1 PI;
      INPUT AOSM LLK DDDT1 PMNF1 AOFM LSTCYC;
*****;
*COMMENT: DO UNIT CONVERSION, CALCULATE EJK, TR;
*****;
      EJK1=((KQ1**2)*(1-NU**2))/JQ1;
      TR=((EJK1+EWEST1)/2)*DJDAL/(IDT1**2);
*COMMENT: CONVERT TO MM, MN·M**(-3/2), MPA, N/MM;
      KQSI=KQ1/(.00091);          JQSI=JQ1*4.448*.03937;
      DJDASI=DJDAL/145.;          EJKSI=EJK1/145.;
      EWESTSI=EWEST1/145.;        PMAISI=PMAX1*4.448;
      DPMXSI=DPMX1/.03937;        PMFSI=PMFAW*4.448*.03937;
      IDTSI=IDT1/145.;           CESI=CEL/145.;
      PERMSI=PERM1/.03937;        AOSI=(AOSM*.03937)+LLK;
      AOSSI=AOSI/.03937;          DDDT1=DDDT1/60.;
      DDDTSI=DDDT1/.03937;        PMNFSI=PMNF1*4.448;
      AOFI=(AOFM*.03937)+LLK;     AOFSI=AOF1/.03937;
      CCE=(CMT/100.)*CEL;
*****;
*COMMENT: OUTPUT FILES;
*****;
FILE OUTDAT1;
      FORMAT BEST9.;
      PUT KQ1 JQ1 DJDAL EWEST1 EJK1 PMAISI DPMX1 PMFAW;
      PUT KQSI JQSI DJDASI EWESTSI EJKSI PMAISI DPMXSI PMFSI;
      PUT IDT1 NU CMT WOPT CEL POR PERM1 PI;
      PUT IDTSI NU CMT WOPT CESI POR PERMSI PI;
      PUT AOSI LLK DDDT1 PMNF1 AOFI;
      PUT AOSSI LLK DDDTSI PMNFSI AOFSI;
FILE OUTDAT2;
      FORMAT BEST9.;
      PUT EJK1 EWEST1 KQ1 JQ1 PMFAW CCE DPMX1;
OUTPUT STATIC;
*****;
PROC PRINT DATA=STATIC;
      TITLE1 STATIC DATA SPECIMEN240B;
      TITLE2 SI SUFFIX IS SI UNITS;
*****;

```

```

***COMMENT: CREATE DATA FOR STATIC PLOTS;
DATA STATGROW;
  INFILE INDAT1 FIRSTOBS=5 OBS=18;
  INPUT NS;
  FILE OUTDAT1;
  FORMAT BEST9.;
  DO I=1 TO NS;
  INPUT P1 AMM D T KAO KCUR;
  KCSQ=KCUR**2;
  PUT P1 AMM D T KAO KCUR;
  OUTPUT STATGROW;
  END;
PROC PRINT N DATA=STATGROW;
  TITLE1 GROWTH DURING LOADUP;
  *****;
***COMMENT: CREATE DATA FOR DYNAMIC PLOTS;
DATA DYNGROW;
SET STATIC;
  IF LLK>=0.; IF PMNF1>=0.; IF AOF1>=0.;
  RETAIN LLK PMNF1 AOF1;
  AB4=AOF1;
  RETAIN AB4;          RETAIN NB4 0.;
  INFILE INDAT1 FIRSTOBS=19;
  INPUT NF;
  FILE OUTDAT1;
  FORMAT BEST9.;
  DO J=1 TO NF;
  INPUT VMX VMN AMM N1;
  DELP=(VMX-VMN)*10.;          PMAXF=(VMX*10.)+PMNF1;
  A1=(AMM*.03937)+LLK;          AN=A1-AOF1;
  DANDN1=(A1-AB4)/(N1-NB4);      LDANDN=LOG(DANDN1);
  AB4=A1;                      NB4=N1;
  RETAIN AB4 NB4;
  W1=2.;                      B=1.;
  AOW=A1/W1;                  WMA=W1-A1;
  FAOW=.886+(4.64*AOW)-(13.32*(AOW**2))+(14.72*(AOW**3))-(5.6*(AOW**4));
  FAOW=(FAOW*(2+AOW))/((1-AOW)**1.5);
  DELK=((DELP*FAOW)/B)/SQRT(W1);          LDELK=LOG(DELK);
  KMAX=((PMAXF*FAOW)/B)/SQRT(W1);          LKMAX=LOG(KMAX);
  KEEP DELP PMAXF A1 N1 AN DANDN1 LDANDN DELK LDELK KMAX LKMAX AMM;
  PUT DELP PMAXF A1 N1 AN DANDN1 LDANDN DELK LDELK KMAX LKMAX;
  OUTPUT DYNGROW;
  END;
  *****;
  *****;
PROC PRINT N DATA=DYNGROW;
  TITLE1 FATIGUE;
  *****;
  *****;
  *****;
***COMMENT: START PLOTTING;
  *****;
  *****;

```

```

PROC PLOT DATA=STATGROW;
  TITLE 1 K VS A FOR CURRENT CRACKLENGTH (*) AND KAO;
  PLOT KAO*AMM='O' KCUR*AMM='*' /OVERLAY;
PROC PLOT DATA=DYNGROW;
  TITLE1 CRACKLENGTH (A) VS CYCLE (N);
  PLOT A1*N1='*';
PROC PLOT DATA=DYNGROW;
  TITLE1 MAXIMUM LOAD (PMA XF) VS CYCLE (N);
  PLOT PMA XF*N1='*';

```

---

```

//NOCYCLE JOB (R635,004C,2,20,WC), 'CROCKFORD'
//*TAMU PRTY=3
//*FORMAT PR,DDNAME=,DEST=XEROX,FORMS=1101,JDE=JFMT7
//STEP EXEC SAS
//FT18F001 DD *
  &EPIC DPRESO=150.,DBRUSH=.00333,&END
//IN DAT1 DD DSN=USR.R635.WC.S05.RAW11C,DISP=SHR
//OUT DAT1 DD DCB=(DSORG=PS,LRECL=80),UNIT=SYSDA,SPACE=(TRK,(1,1)),
// DSN=USR.R635.WC.S05.MID11C,DISP=MOD
//OUT DAT2 DD DSN=USR.R635.WC.SUM05S,DISP=MOD
//SYSIN DD *
*****
*****
* NOTE: YOU MUST CHANGE:
* DSN'S ETC. FOR          IN DAT1          (LINE 7)
*                          OUT DAT1         (LINE 9)
*                          TITLE1           (LINE75)
*                          OBS=              (LINE80)
*                          AMM <=           (LINE92)
*                          XXXXXXXXXXXXXXXXXXXX
* (ALL DATA FILES MUST PREEXIST AS DUMMY FILES ON WYLBUR)
*   FOR EACH RUN ... AND:
* DSN FOR OUT DAT2 FOR EACH TIME YOU CHANGE THE PERCENT
* CEMENT OR COMPACTION.
* YOU MUST ADD A PLOTOUT DD STATEMENT
* FOR THE ONE PLOT FOR WHICH VECTORS ARE TO BE
* STORED FOR SCRIPT.
* FIRST VERSION .....22MAR85
*****
*****
  OPTIONS PAGESIZE=60 LINESIZE=90;
*****
*****
DATA STATIC;
  INFILE IN DAT1 FIRSTOBS=2 OBS=4;
*****
*COMMENT: INPUT THE STATIC DATA AND LOOPING CONTROLS;
*****

```

```

      INPUT KQ1 JQ1 DJDA1 EWEST1 PMA1 DPMX1 PMFAW;
      INPUT IDT1 NU CMT WOPT CEL POR PERM1 PI;
      INPUT AOSM LLK DDDT1 PMNF1 AOFM;
      *****;
      *COMMENT: DO UNIT CONVERSION, CALCULATE EJK, TR;
      *****;
      EJK1=((KQ1**2)*(1-NU**2))/JQ1;
      TR=((EJK1+EWEST1)/2)*DJDA1/(IDT1**2);
      *COMMENT: CONVERT TO MM, MN-M**(-3/2), MPA, N/MM;
      KQSI=KQ1/(.00091);          JQSI=JQ1*4.448*.03937;
      DJDASI=DJDA1/145.;          EJKSI=EJK1/145.;
      EWESTSI=EWEST1/145.;        PMA1SI=PMA1*4.448;
      DPMXSI=DPMX1/.03937;        PMFSI=PMFAW*4.448*.03937;
      IDTSI=IDT1/145.;           CESI=CEL/145.;
      PERMSI=PERM1/.03937;        AOS1=(AOSM*.03937)+LLK;
      AOSSI=AOS1/.03937;          DDDT1=DDDT1/60.;
      DDDTSI=DDDT1/.03937;        PMNFSI=PMNF1*4.448;
      AOF1=(AOFM*.03937)+LLK;     AOFSI=AOF1/.03937;
      CCE=(CMT/100.)*CEL;
      *****;
      *COMMENT: OUTPUT FILES;
      *****;
      FILE OUTDAT1;
      FORMAT BEST9.;
      PUT KQ1 JQ1 DJDA1 EWEST1 EJK1 PMA1 DPMX1 PMFAW;
      PUT KQSI JQSI DJDASI EWESTSI EJKSI PMA1SI DPMXSI PMFSI;
      PUT IDT1 NU CMT WOPT CEL POR PERM1 PI;
      PUT IDTSI NU CMT WOPT CESI POR PERMSI PI;
      PUT AOS1 LLK DDDT1 PMNF1 AOF1;
      PUT AOSSI LLK DDDTSI PMNFSI AOFSI;
      FILE OUTDAT2;
      FORMAT BEST9.;
      PUT EJK1 EWEST1 KQ1 JQ1 PMFAW CCE;
      OUTPUT STATIC;
      *****;
      PROC PRINT DATA=STATIC;
      TITLE1 STATIC DATA SPECIMEN11C;
      TITLE2 SI SUFFIX IS SI UNITS;
      *****;
      ***COMMENT: CREATE DATA FOR STATIC PLOTS;
      DATA STATGROW;
      INFILE INDAT1 FIRSTOBS=5 OBS=13;
      INPUT NS;
      FILE OUTDAT1;
      FORMAT BEST9.;
      DO I=1 TO NS;
      INPUT P1 AMM D T KAO KCUR;
      KCSQ=KCUR**2;
      PUT P1 AMM D T KAO KCUR;
      OUTPUT STATGROW;
      END;
      DATA SUBSG;

```

```

      SET STATGROW;
      IF AMM <= 2.95;
PROC PRINT N DATA=STATGROW;
      TITLE1 GROWTH DURING LOADUP;
*****;
*****;
*COMMENT: START PLOTTING;
*****;
*****;
PROC GLM DATA=SUBSG;
      MODEL KCSQ=AMM/P;
      OUTPUT OUT=NEW1 PREDICTED=YHAT1 RESIDUAL=RESID1;
      PROC PLOT;          PLOT RESID1*YHAT1;
PROC GLM DATA=SUBSG;
      MODEL KCUR=AMM AMM*AMM AMM*AMM*AMM/P;
      OUTPUT OUT=NEW2 PREDICTED=YHAT2 RESIDUAL=RESID2;
      PROC PLOT;          PLOT RESID2*YHAT2;
PROC PLOT DATA=STATGROW;
      TITLE1 P VS A;
      PLOT P1*AMM='*';
PROC PLOT DATA=STATGROW;
      TITLE1 A VS K CURRENT;
      PLOT AMM*KCUR='*';
PROC PLOT DATA=STATGROW;
      TITLE1 K CURRENT SQUARED VS A;
      PLOT KCSQ*AMM='*';
PROC PLOT DATA=STATGROW;
      TITLE1 T(SEC) VS A;
      PLOT T*AMM='*';
PROC PLOT DATA=STATGROW;
      TITLE1 A VS CMOD;
      PLOT AMM*D='*';
*****;
GOPTIONS DEVICE=XER9700 COLORS=(C1 C2 C3 C4 C5) NOSYMBOL
      FTITLE=TRIPLEX;
*****;
PROC GPLOT DATA=STATGROW;
      FOOTNOTE .J=LEFT KCUR VS A (SMOOTHED CUBIC SPLINE);
      TITLE1 STATIC;;
      TITLE2 K CURRENT VS A;
      PLOT KCUR*AMM=1;
      SYMBOL1 V=STAR C=C1 I=SPLINE;

```

---

```

STATFAT FROM OLD TRANSFERRED 6 DEC 85
//STATFAT JOB (R635,004C,2,20,WC), 'CROCKFORD'
//*TAMU PRTY=3
//*FORMAT PR,DDNAME=,COPIES=0
//*FORMAT PR,DDNAME=FT12F001,DEST=XEROX,FORMS=1100,JDE=JFMT7,COPIES=1

```

```

//STEP EXEC SAS
//INDAT1 DD DSN=USR.R635.WC.M10.MID7T,DISP=SHR
//OUTDAT1 DD DCB=(DSORG=PS,LRECL=80),UNIT=SYSDA,SPACE=(TRK,(1,1)),
// DSN=USR.R635.WC.STFSUM,DISP=MOD
//SYSIN DD *
*;
*;
*****;
*****;
      OPTIONS PAGESIZE=60 LINESIZE=90;
*****;
*****;
DATA S2;
      INFILE INDAT1 OBS=1;
      INPUT SPL 10.;
OUTPUT S2;
*;
DATA S1;
      MERGE S2;
      INFILE INDAT1 FIRSTOBS=6 OBS=6;
      INPUT A LK1 B C D;
      DROP A B C D;
OUTPUT S1;
*;
DATA S4;
      INFILE INDAT1 FIRSTOBS=8 OBS=16;
      INPUT P1 AMM D T KAO KCUR;
      DROP D T;
OUTPUT S4;
*;
DATA MKUP;
      INFILE INDAT1 FIRSTOBS=17;
      INPUT B P9 A9 C D E F G H I J;
      DROP B C D E F G H I J;
OUTPUT MKUP;
*;
DATA S3;
      MERGE S4 S1;
      IF _N_ = 1 THEN DO; LLK=LK1; SMPL=SPL; DLK=LK1; END;
      RETAIN LLK SMPL DLK;
      AI=(AMM*.03937)+LLK;
      DROP LK1 SPL;
OUTPUT S3;
*;
PROC PRINT N DATA=S3;
      TITLE1 S3;
*;
PROC MEANS MAX NOPRINT DATA=S3;
      BY DLK; VAR P1;
      OUTPUT OUT=ST MAX=MXPO;
DATA TS;
      MERGE ST S3;

```

```

IF _N_ = 1 THEN DO;
  MXP1=MXP0; END;
RETAIN MXP1;
IF P1=MXP1 THEN DO;
  NMO=_N_-1; XMP=P1; W1=AMM;
DROP MXP0 DLK P1 AMM KAO KCUR SMPL LLK AI;
OUTPUT TS; END;
*;
DATA STF1;
MERGE S3 TS;
IF _N_ = 1 THEN DO;
  WA=AMM; PMX=XMP; NM1=NMO; END;
RETAIN PMX WA NM1;
DROP MXP1 NMO XMP W1 DLK;
DPI=4.*ATAN(1.);
RETAIN DPI;
P2=SQRT(1./COS(P1*DPI/2./PMX));
IF _N_ > NM1 THEN DELETE;
OUTPUT STF1;
*;
*;
DATA S8;
SET S3;
DMY=1;
DROP KAO SMPL LLK DLK;
OUTPUT S8;
*;
* USE DPI AS DUMMY VRBL & SAV ONLY OBS AT MAX VALUE OF KCUR ;
PROC MEANS MAX NOPRINT DATA=S8;
BY DMY; VAR KCUR;
OUTPUT OUT=LASTOB MAX=MAXKC;
DATA S6;
MERGE S8 LASTOB;
BY DMY;
IF KCUR=MAXKC THEN DO;
  NM2=_N_; KC6R=KCUR; DROP DMY KCUR P1 AMM AI;
OUTPUT S6; END;
*;
DATA S7;
MERGE S6 STF1;
IF _N_ = 2 THEN STOP;
  AW=((WA*.03937)+LLK)/2.;
  A2W=AW**2; A3W=AW**3; A4W=AW**4;
F1=((2+AW)/((1-AW)**1.5));
FAW=F1*(.886+4.64*AW-13.32*A2W+14.72*A3W-5.6*A4W);
***** CALCULATE PMAX WHICH WOULD GIVE KCURMAX AT A = A AT;
* PMAX (I.E. APPROXIMATE THE 'PHASE ANGLE') *;
  PCX=KC6R*1.*SQRT(2.)/FAW;
DROP LLK P1 AMM KCUR A2W A3W A4W F1 KAO SMPL AI PMX NM1
P2;
OUTPUT S7;
PROC PRINT N DATA=S7;

```

```

    TITLE1 S7;
*;
DATA S9;
    MERGE S8 S7;
    IF _N_ =1 THEN DO;
        WB=WA; AB=AW; FAZ=FAW; PXC=PCX; NMT=NM2; DPJ=DPI;
    END;
    RETAIN WB AB FAZ PXC NMT DPJ PPB4 0.;
    DROP WA AW FAW PCX NM2 DPI;
    IF AMM > WB THEN DO;
        PPHZ=KCUR*1.*SQRT(2.)/FAZ;
        IF PPB4 > PPHZ THEN DO;
            PPHZ=PPB4; END;
        PPB4=PPHZ;
    END;
    IF _N_=NMT THEN STOP;
    END;
    ELSE PPHZ=P1;
OUTPUT S9;
*;
PROC PRINT N DATA=S9;
    TITLE1 S9;
*;
DATA STF2;
    MERGE S9;
    P3=SQRT(1./COS(PPHZ*DPJ/2./PXC));
OUTPUT STF2;
*;
PROC PRINT N DATA=STF1;
    TITLE1 STF1;
    TITLE2 DATA FOR KIC CURVE FIT;
PROC PRINT N DATA=STF2;
    TITLE1 STF2;
    TITLE2 DATA FOR KCURMAX CURVE FIT;
*****;
*   PLOTS AND REGRESSIONS   *;
*****;
PROC REG DATA=STF1 OUTEST=EST1;
    MODEL AI=P2;
    OUTPUT OUT=NEW1 P=AHAT1 R=RESID1;
    TITLE1 STF1;
*;
PROC PLOT DATA=NEW1;
    PLOT AI*P2 AHAT1*P2='*'/OVERLAY;
*;
PROC REG DATA=STF2 OUTEST=EST2;
    MODEL AI=P3;
    OUTPUT OUT=NEW2 P=AHAT2 R=RESID2;
    TITLE1 STF2;
*;
PROC PLOT DATA=NEW2;
    PLOT AI*P3 AHAT2*P3='*'/OVERLAY;
*;

```

```

PROC PLOT DATA=S3;
  PLOT AI*P1;
  TITLE1 PLOT OF APPLIED LOAD VS CRACK LENGTH, INCHES;
  TITLE2 STATIC TEST;
PROC PLOT DATA=MKUP;
  PLOT P9*A9;
  TITLE1 PLOT OF APPLIED LOAD VS CRACK LENGTH, INCHES;
  TITLE2 FATIGUE;
PROC PRINT N DATA=MKUP;
*****;
*   STORE REGRESSION CONSTANTS   *;
*****;
DATA FNL1;
  MERGE S1 EST1 ST;
  FILE OUTDAT1;
  PUT SPL 10.;
  FORMAT BEST14.;
  PUT P2 MXPO INTERCEP;
OUTPUT FNL1;
*;
DATA FNL2;
  MERGE S7 EST2;
  FILE OUTDAT1;
  FORMAT BEST14.;
  PUT P3 PCX INTERCEP;
OUTPUT FNL2;
*****;
*   FIRST VERSION 19 MAY 85   *;
*   LAST UPDATE 30 MAY 85   *;
*****;
* YOU MUST CHANGE LINES 6, 30, 36 EACH RUN *;

```

---

```

//NTOF JOB (R635,004C,4,1,WC), 'CROCKFORD',MSGCLASS=Z
//*TAMU PRTY=1
//*FORMAT PR,DDNAME=,COPIES=0
//*FORMAT PR,DDNAME=FT06F001,DEST=XEROX,FORMS=1100,JDE=JFMT7,COPIES=1
//STEP EXEC WATFIV,REGION=128K
//FT10F001 DD DSN=USR.R635.WC.NFFAT,DISP=MOD
//SYSIN DD DATA
// OPTIONS
  REAL CYS(4,4), OT(4,2)
  CHARACTER *3 SMPL
  DATA ICYCLE, CYS, I,ACUR,W,B,IFLAG,IJ /0,16*0.,0,0.,2.,1.,0,0/
  DPI=4.*ATAN(1.0)
C***** MAIN *****
  NSMPL=50
  1 CALL DINTLZ (IJ,IFLAG,NSMPL,RKFLG,B1,CO,SMPL,FNFOBS)
  IF (IFLAG.EQ. 1) GO TO 999

```

```

      IF (IJ .GT. 1) GO TO 11
      DO 10 JJ=1,4
        OT(JJ,1)=FNFOBS
10    CONTINUE
11    CONTINUE
      CALL FREAD (I,NSMPL,GKMXF,GKLF,ACUR,ICYCLE,PBRKA,IFLAG)
      IF (IFLAG .EQ. 1) GO TO 999
      CALL PROXR(I,GKMXF,GKLF,ACUR,ICYCLE,W,B,PBRKA,DPI,
2B1,C0,RKFLG,CYS,OT)
      IFLAG=0
      GO TO 1
999   CONTINUE
      CALL SUMRY(CYS,I,FNFOBS,SMPL,OT)
      STOP
      END
C*****FUNCTIONS*****
C*****FUNCTIONS*****
C*****F(A/W)*****
      FUNCTION FAW(A,W)
      AOW=A/W
      TEMP=.886+(4.64*AOW)-(13.32*(AOW**2))+(14.72*(AOW**3))-(5.6*
1(AOW**4))
      FAW=TEMP*(2.+AOW)/((1-AOW)**1.5)
      RETURN
      END
C*****KQ*****
      FUNCTION GK1(PQ,AQ,W,B)
      GK1=FAW(AQ,W)*PQ/B/SQRT(W)
      RETURN
      END
C*****P(A)*****
      FUNCTION PO(A,PFA)
      IF (A .LT. PFA ) GO TO 100
      PO= 18.4439-6.94677*A
      GO TO 101
100   PO= 8.59976+.55685*A
101   CONTINUE
      RETURN
      END
C*****P(KQ,A/W)*****
      FUNCTION PKA(QK,A,W,B)
      PKA=B*SQRT(W)*QK/FAW(A,W)
      RETURN
      END
C*****UPR INTEGRATE*****
      FUNCTION PHINT(P1,P0,AC,DPI,C0,B)
      CX=DPI/2./C0
      S3=1/SQRT(COS(P1*CX))
      S2=1/SQRT(COS(P0*CX))
      PHINT= AC+(B*(S3-S2))
      RETURN
      END

```

```

C*****SUBROUTINES*****
C*****SUBROUTINES*****
C*****INITIALIZE*****
      SUBROUTINE DINTLZ(IJ,IFLAG,NSMPL,RKFLG,B1,C0,SMPL,FNFOBS)
        CHARACTER *3 SMPL
        IF (IJ .EQ. NSMPL) GO TO 155
        READ, NSMPL, RKFLG,B1,C0,SMPL,FNFOBS
        PRINT 150,NSMPL,RKFLG,B1,C0,SMPL,FNFOBS
150      FORMAT (' ', $SAMPLES=',I3,2X,F5.3/2(2X,E14.7)
1          /2X,A3,2X,F9.1)
        IJ=IJ+1
        GO TO 156
155      CONTINUE
        IFLAG=1
        RETURN
156      CONTINUE
        RETURN
        END
C*****READ*****
      SUBROUTINE FREAD(I,NSMPL,GKMXF,GKLF,ACUR,ICYCLE,PBRKA,IFLAG)
        IF (I .EQ. NSMPL) GO TO 151
        READ, GKLS,GKMXS,GKMXF,AOF,PBRKA
        PRINT, GKLS,GKMXS,GKMXF,AOF,PBRKA
        RKLS=GKLS/GKMXS
        GKLF=RKLS*GKMXF
        ACUR=AOF
        ICYCLE=0
        I=I+1
        GO TO 152
151      CONTINUE
        IFLAG=1
        RETURN
152      CONTINUE
        RETURN
        END
C*****PROCESS A RECORD*****
      SUBROUTINE PROXR(I,FKX,FKL,AC,IC,W,B,PBRK,DPI,B1,C0,
2RKFLG,CYS,OT)
        REAL CYS(4,4), OT(4,2)
153      CONTINUE
        PMX=P0(AC,PBRK)
        IF ((AC .GE. W) .OR. (PMX .GE. C0)) GO TO 157
158      GO TO 159
157      PRINT, ' **WARNING',AC,W,PMX
        PRINT,PLF,C0,'WARNING*****'
        GO TO 154
159      CONTINUE
        PLF=0.0
        IF ((PLF .GE. C0) .OR. (PLF .GE. PMX) .OR. (PLF .LT. 0.))
2GO TO 157
        C0=PKA(FKX,AC,W,B)
        AC=PHINT(PMX,PLF,AC,DPI,C0,B1)

```

```

        IC=IC+1
        IF (IC .GT. 75000) GO TO 157
        GKCUR=GK1(PMX,AC,W,B)
        RKC=GKCUR/FKX
        IF (RKC .GE. RKFLG) GO TO 154
        GO TO 153
154 CONTINUE
        CYS(I,1)=IC
        OT(I,2)=IC
        CYS(I,2)=RKC
        CYS(I,3)=GKCUR
        CYS(I,4)=AC
        RETURN
    END
C*****SUMMARY
    SUBROUTINE SUMRY(CYS,I,FNFOBS,SMPL,OT)
    CHARACTER *3 SMPL
    REAL CYS(4,4), OT(4,2)
    DO 200 II=1,I
    WRITE (10,249) SMPL,(OT(II,JJ),JJ=1,2),(CYS(II,JK),JK=2,4)
    WRITE (6,250) SMPL,(CYS(II,J),J=1,4)
200 CONTINUE
249 FORMAT (' ',A3,2(2X,F9.1),2X,F8.6,2X,F9.4,2X,F10.8)
250 FORMAT (' ',A3,2X,4(2X,G14.7))
    RETURN
    END
C*****
C*          VERSION 2          30 MAY 85          *
C*****
C**** DATA
C****CARD 1
C ENTRY ORDER:
C TRIALS
C MAX RATIO K/KMAX (USUALLY 1.0)
C B, C, D FROM CUBIC REGRESSION (X THRU X**3 COEFF.) (STFSUM)
C CO=MAX ALLOWABLE LOAD IN THE STATIC TEST
C SAMPLE NUMBER IDENTIFICATION (3 CHARACTERS)
C LAST CYCLE NUMBER OBSERVED
C****CARD 2
C K AT LOWER LIMIT OF CRACK GROWTH
C KIC
C KMAX FATIGUE (OR KIC)
C INITIAL FATIGUE CRACK LENGTH, INCHES
C CRACK LENGTH AT WHICH LOADING FUNCTION CHANGES
C ***** NOTE *****
C YOU MUST CHANGE LINES 50, 52          FOR EACH RUN
C*****
C*****
// DATA
4,1.0,0.002267314,13.6,' 7T',415.
73.3, 102.8, 102.8, 1.18957, 1.20846
4,1.0,0.002267314,13.6,' 7T',415.

```

73.3, 102.8, 104.37, 1.18957, 1.20846  
 4,1.0,0.006178653,14.50191,' 7T',415.  
 73.3, 102.8, 109.6, 1.18957, 1.20846  
 4,1.0,0.006178653,14.50191,' 7T',415.  
 73.3, 102.8, 104.37, 1.18957, 1.20846

---

```
//FATIGUE JOB (B250,004C,2,10,WC),'CROCKFORD',MSGCLASS=Z
//*TAMU PRTY=1
//*FORMAT PR,DDNAME=,DEST=XEROX,FORMS=1100
//STEP EXEC SAS,OPTIONS='MACRO,MACROGEN'
//INDAT1 DD DSN=USR.B250.WC.A128.MID020T,DISP=SHR
//OUTDAT1 DD DSN=USR.B250.WC.FATFOA,DISP=MOD
//FT10F001 DD DSN=USR.B250.WC.NLOUT2,UNIT=SYSDA,
// SPACE=(TRK,(15,2)),DISP=(NEW,CATLG,DELETE)
//SYSIN DD *
  OPTIONS PAGESIZE=60 LINESIZE=90;
                                TITLE;
PROC PRINTTO UNIT=10 NEW;
DATA BILL;
  INFILE INDAT1 FIRSTOBS=47 OBS=108 ; FORMAT BEST9.;
  INPUT DELP PMAXF A1 N1 AN DANDN1 LDANDN DELK LDELK KMAX LK;
    ASQ = A1**2; LNY1=LOG(A1);
    DUMMY = 1; D2=1;
  KIC=104.7; KQD=141.9 ; SIDT=155.0; LSTCY=7130;
  FPI=4*ATAN(1)/(2*(LSTCY+1)); NLNX1=N1*LOG(1/COS(FPI*N1));
  RATIO=KMAX/KQD;
  IF _N_ > 1 THEN DO; LFFD=LOG10((DANDN1+LAG)/2); LKLAG=LKB4; END;
  LAG=DANDN1; RETAIN LAG;
  PLAST=KIC*KIC/(6*4*ATAN(1)*SIDT*SIDT);
  LKMAX=LOG10(KMAX); LKB4=LKMAX; RETAIN LKB4;
  LDK=LOG10(DELK);
  DROP DELP PMAXF AN LDANDN LDELK LK;
OUTPUT BILL;
%LET SMPL='020T';
  LABEL A1 = A
    ASQ = A ** 2
    N1 = N;
*PROC PRINT N DATA=BILL;
  TITLE1 &SMPL;
*PROC REG DATA=BILL OUTEST=EST;
*   MODEL N1=A1 ASQ/P R DW;
*   OUTPUT OUT=NEW P=NHAT R=RESIDL;
*   TITLE2 FIT OF A VS N;
*DATA COEFF;
*   SET EST;
*   DROP N1;* DUMMY=1;
*   RENAME A1 = N A1 ASQ = NASQ;
*OUTPUT COEFF;
```

```

*****
***** REG TO GET B4 AND B5 *****;
PROC REG DATA=BILL OUTEST=SMOOTH;
  MODEL LNY1=NLNX1/P R DW;
  OUTPUT OUT=PRE P=PS R=RS;
  TITLE2 SMOOTH FIRST APPROXIMATION USING 1/COS;
  PROC PRINTTO;
  PROC PLOT DATA=PRE;
    PLOT LNY1*NLNX1 PS*NLNX1=''/OVERLAY;
  PROC PLOT DATA=PRE;
    LABEL LNY1=LN(A);
    PLOT RS*LNY1;
  PROC PRINTTO UNIT=10;
*****
***** RENAME FOR B5 *****;
DATA CO2;
  SET SMOOTH;
  RENAME NLNX1=LNXLN;
  D2=1;
  DROP _TYPE_ _DEPVAR_ _SIGMA_;
  OUTPUT CO2;
*****
***** MEANS TO FIND MAXIMUM A *****;
PROC MEANS DATA=PRE NOPRINT MAX;
  VAR A1; OUTPUT OUT=POST MAX=AMAX;
*****
***** PREPARE TO MERGE *****;
DATA POST1;
  SET POST;
  D2=1;
  OUTPUT POST1;
*****
***** MERGES AND CREATES INITIAL VARIABLE *****;
***** ESTIMATES FOR USE IN NONLINEAR *****;
***** REGRESSION FROM EARLIER REG OUTPUT *****;
***** DATA SET CALLED 'PRE' *****;
DATA DAMPED;
  MERGE PRE POST1 CO2;
  BY D2;
  B04=EXP(INTERCEP);
  RETAIN FLAG 0 FLG2 0 FLG3 0 FLG4 0 CNT 0;
  RETAIN NFST 0 NSND 0 NTHRD 0;
  RETAIN RFST RSND RTHRD NX1 NX2;
  RETAIN NY1 1000000 NY2 1000000;
  SR=A1-(A1/EXP(RS));
  IF _N_ = 1 THEN DO; MXRS=ABS(RS); MXRN=N1; MXSR=SR; END;
  IF _N_ > 1 THEN DO;
    IF FLG4=1 THEN GO TO PERIOD;
    SGL=0; SGC=0;
    IF LAGR>0 THEN SGL=1;
    IF RS>0 THEN SGC=1;
    IF FLG2=1 THEN GO TO SKN1;

```

```

      IF SGL NE SGC THEN DO;
        NX1=(LAGN+N1)/2; FLG2=1; NY1=N1;
      END;
      GO TO PERIOD;
      SKN1:*CONTINUE;
      IF FLG3=1 THEN GO TO PERIOD;
      IF SGL=SGC THEN GO TO PERIOD;
        NX2=(LAGN+N1)/2; FLG3=1; NY2=N1;
      *      WP=2*4*ATAN(1)/((NX2-NX1)*2);
        FLG4=1;
      PERIOD:*CONTINUE;
    END;
    IF N > 1 THEN DO;
      IF FLAG=1 THEN GO TO SKP;
      D1=ABS(RS);
      IF N1 <= NY1 THEN DO;
        IF D1 > MXRS THEN DO;
          MXRS=D1; MXRN=N1; MXSR=SR;
          RETAIN MXRS MXRN MXSR;
        END;
        IF N1=NY1 THEN DO;
          RFST=ABS(MXSR); NFST=MXRN; CNT=1;
        END;
      END;
      IF N1 > NY1 AND N1 <= NY2 THEN DO;
        IF CNT=1 THEN DO; CNT=2; MXRS=ABS(LAGR); MXRN=LAGN;
          MXSR=LGSR; END;
        IF D1 > MXRS THEN DO;
          MXRS=D1; MXRN=N1; MXSR=SR; END;
        IF N1 = NY2 THEN DO;
          RSND=ABS(MXSR); NSND=MXRN; END;
      END;
      IF N1 > NY2 THEN DO;
        DEL1=0;
        IF CNT=2 THEN DO; CNT=3; MXRS=ABS(LAGR); MXRN=LAGN;
          MXSR=LGSR; DEL1=1; END;
        IF D1 > MXRS THEN DO;
          MXRS=D1; MXRN=N1; MXSR=SR; END;
        IF DEL1=1 THEN GO TO SK5P;
        SGL=0; SGC=0;
        IF LAGR > 0 THEN SGL=1;
        IF RS > 0 THEN SGC=1;
        IF SGL=SGC THEN GO TO SK5P;
        RTHRD=ABS(MXSR); NTHRD=MXRN; FLAG=1;
        AVR=(RFST+RSND)/2;
        WP=2*4*ATAN(1)/((NX2-NSND)*4); B01=0;
      *      B01=ABS((RTHRD-RFST)/(NTHRD-NFST));
        SK5P:*CONTINUE;
        IF A1=AMAX THEN DO;
          RTHRD=ABS(MXSR); NTHRD=MXRN; FLAG=1;
          AVR=(RFST+RSND)/2;
          WP=2*4*ATAN(1)/((NX2-NSND)*4); B01=0;

```

```

*          B01=ABS((RTHRD-RFST)/(NTHRD-NFST));
          PHI=(-NX1)*WP;
          END;
        END;
      END;
      SKP:*CONTINUE;
      RETAIN INTERCEP LNX1N B01 B04 AVR WP 0 PHI 0;
      LAG2R=LAGR; RETAIN LAG2R;
      LAGR=RS; RETAIN LAGR;
      LAG2N=LAGN; RETAIN LAG2N;
      LAGN=N1; RETAIN LAGN;
      LGSR=ABS(SR); RETAIN LGSR;
      DROP MODEL DANDN1 DELK KMAX ASQ LNY1 KIC KQD SIDT LSTCY
        PS FPI NLNX1 RATIO LFFD LAG LKLAG LKB4 LKMAX LDK;
      OUTPUT DAMPED;
      *PROC PRINT N DATA=DAMPED;
      DATA RID;
        SET DAMPED;
        IF A1<AMAX THEN DELETE;
        DROP A1 N1 RS;
      OUTPUT RID;
      DATA DMPFNL;
        MERGE BILL RID;
        BY DUMMY;
      OUTPUT DMPFNL;
      PROC NLIN DATA=DMPFNL BEST=3 METHOD=MARQUARDT EFORMAT;
      PARS B0=-.048 B1=.0000313 B2=.00103 B3=-6.283 B4=1.2 B5=.0000047;
        IF ITER=0 THEN IF OBS=1 THEN DO;
          B0=-AVR; B1=B01; B2=WP; B3=PHI;
          B4=B04; B5=LNX1N;
        END;
      EX1=EXP(B1*N1); EX2=SIN(B2*N1+B3); EX3=COS(B2*N1+B3); EX4=1/COS(FPI*N1);
      MODEL A1=(B0*EXP(B1*N1)*SIN(B2*N1+B3))+B4*(EX4**(B5*N1));
        DER.B0=EX1*EX2;
        DER.B1=B0*N1*EX1*EX2;
        DER.B2=B0*N1*EX1*EX3;
        DER.B3=B0*EX1*EX3;
        DER.B4=EX4**(B5*N1);
        DER.B5=B4*(EX4**(B5*N1))*LOG(EX4)*N1;
      OUTPUT OUT=DMP P=DHAT R=RESIDD PARS=B0 B1 B2 B3 B4 B5;
      PROC PRINT N DATA=DMP;
        TITLE2 DATA FROM FIXED PERIOD WAVE (DMP);
      DATA TEMPO;
        SET DMP;
        IF N = 2 THEN STOP;
        FILE OUTDAT1; FORMAT BEST9.;
        CODE1=&SMPL; PUT CODE1 ;
        PUT KIC KQD SIDT LSTCY AMAX PLAST;
        PUT B0 B1 B2 B3 B4 B5;
      OUTPUT TEMPO;
      *****
      *****      PARIS EQUATION      *****

```

```

*****;
*****;
*PROC PRINTTO;
*PROC PLOT DATA=NEW;
*PLOT A1*N1 A1*NHAT = '*' / OVERLAY;
*TITLE PREDICTED AND ACTUAL (NEW); TITLE2 A VS N;
*PROC PLOT DATA=NEW; *PLOT RESIDL*A1;
*PROC PLOT DATA=NEW; * PLOT RESIDL*N1;
*DATA FINAL;
*   MERGE COEFF BILL;
*   BY DUMMY;
*   DADN = 1/SQRT(NA1**2-4*NASQ*(INTERCEP-N1));
*   LDADN = LOG10(DADN);
*   CODE1=&SMPL;
*OUTPUT FINAL;
*PROC PRINTTO UNIT=10;
*PROC REG DATA=FINAL OUTEST=PCO;
*   MODEL LDADN = LKMAX/P R DW;
*OUTPUT OUT=PRED P=LDADHAT R=RESID2;
*   TITLE1 PARIS EQUATION;
*PROC PRINTTO;
*PROC PLOT DATA=PRED;
*   PLOT LDADN*LKMAX LDADHAT*LKMAX='*' /OVERLAY;
*PROC PLOT DATA=PRED;* PLOT RESID2*LDADN;
*DATA PARIS;
*   SET PCO;
*   FILE OUTDAT1;
*   FORMAT BEST9.;
*   PUT INTERCEP LKMAX;
*OUTPUT PARIS;
*****;
***** RUNNING AVERAGE FIRST FORWARD DIFFERENCE *****;
*****;
*****;
*PROC PRINTTO UNIT=10;
PROC REG DATA=BILL OUTEST=PCD;
  MODEL LFFD=LKLAG/P R DW;
  OUTPUT OUT=PRD P=LFP R=RESID3;
  TITLE1 PARIS EQUATION USING THREE POINT RUNNING AVERAGE OF;
  TITLE2 FIRST FORWARD DIFFERENCES (USES KMAX);
PROC PRINTTO;
PROC PLOT DATA=PRD;
  PLOT LFFD*LKLAG LFP*LKLAG='*' /OVERLAY;
PROC PLOT DATA=PRD;
PLOT RESID3*LFFD;
DATA TEMPl;
  SET PCD; FILE OUTDAT1; FORMAT BEST9.;
  PUT INTERCEP LKLAG;
OUTPUT TEMPl;
*****;
***** ANALYSIS TO REMOVE SERIAL *****;
***** CORRELATION *****;

```

```

*****;
PROC PLOT DATA=DMP;
PLOT A1*N1 DHAT*N1=''/ OVERLAY;
TITLE PREDICTED AND ACTUAL (DMP); TITLE2 A VS N;
PROC PLOT DATA=DMP; PLOT RESIDD*A1;
PROC PLOT DATA=DMP; PLOT RESIDD*N1;
DATA F2NAL;
  MERGE DMP BILL;
  BY DUMMY;
B4=B04; B5=LNXLN;
EX1=EXP(B1*N1); EX2=SIN(B2*N1+B3); EX3=COS(B2*N1+B3); EX4=1/COS(FPI*N1);
  DADM=(B0*(B2*EX1*EX3+B1*EX1*EX2))+(B4*(B5*N1*(EX4**(B5*N1-1))*
    (SIN(FPI*N1)*(EX4**2)*FPI)+(LOG(EX4))*(EX4**(B5*N1))*B5));
  IF DADM <= 0 THEN GO TO MS;
  LDADM = LOG10(DADM);
  MS:*CONTINUE;
  CODE1=&SMPL;
OUTPUT F2NAL;
PROC PRINTTO UNIT=10;
PROC REG DATA=F2NAL OUTEST=PC1;
  MODEL LDADM = LKMAX/P R DW;
OUTPUT OUT=PR1D P=LDADMAT R=RESID4;
  TITLE1 PARIS EQUATION [USING DAMPED SINE WAVE (DMP)];
PROC PRINTTO;
DATA TEMP2;
  SET PC1;
  FILE OUTDAT1; FORMAT BEST9.;
  PUT INTERCEP LKMAX;
OUTPUT TEMP2;
PROC PLOT DATA=PR1D;
  PLOT LDADM*LKMAX LDADMAT*LKMAX=''/OVERLAY;
PROC PLOT DATA=PR1D; PLOT RESID4*LDADM;
PROC PLOT DATA=PR1D; PLOT RESID4*LKMAX;
*****;
* VERSION 6                22 SEPTEMBER 1985      *;
* YOU MUST CHANGE LINES 5,14,18,28  EACH RUN*;

```

## NUMERICAL INTEGRATION PROGRAM

```

1.      //KIM JOB (R635.009C,1,10,YK), 'EQN97'
1.1     //*TAMU PRY=3
2.      //*FORMAT PR,DDNAME=,DEST=XEROX,FORMS=1101,JDE=JFMT7
3.      //STEP EXEC FORTXCLG,REGION=512K
7.      //SYSIN DD *
10.     IMPLICIT REAL*8 (A-H,O-Z)
11.     DIMENSION DADN(101)
12.     C
13.     EXTERNAL EQ
14.     C
15.     READ (5,1,END=50) D2,XM,XK1C,GAMMA,SM,DELK
16.     1   FORMAT (D16.8,F11.9,F6.2,F8.6,F6.2,F5.1/)
17.     C
18.     PI = 3.141592653D0
19.     TINTL = 0.
20.     TFINL = 1.
21.     DELT = (TFINL-TINTL)/100.0
22.     T = TINTL
23.     2   IF (DSIN(PI*T).LT.0.) T = 0.
24.     C
25.     DO 10 I=1,101
26.         DADN(I) = EQ(T,D2,XM,XK1C,GAMMA,SM,DELK,PI)
27.         T = T + DELT
28.     10   CONTINUE
29.     C
30.     EVEN = 0.0
31.     C
32.     DO 20 I=2,100,2
33.         EVEN = EVEN + DADN(I)
34.     20   CONTINUE
35.     C
36.     ODD = 0.0
37.     C
38.     DO 30 I=3,99,2
39.         ODD = ODD + DADN(I)
40.     30   CONTINUE
41.     C
42.     C
43.     AREA = DELT/3.0*(DADN(1)+4.0*EVEN+2.0*ODD+DADN(101))
44.     C
45.     WRITE (1,40) DELK,AREA
46.     40   FORMAT (5X,F6.1,3X,D15.8)
47.     C
48.     DELK = DELK + 3.
49.     C
50.     IF (DELK.GE.0.8*XK1C) GO TO 50
51.     GO TO 2
52.     50   STOP
53.     END
54.     C
55.
56.     --- FUNCTION ---
57.     C
58.     DOUBLE PRECISION FUNCTION EQ(T,D2,XM,XK1C,GAMMA,SM,DELK,PI)
59.     C
60.     IMPLICIT REAL*8 (A-H,O-Z)
61.     C
62.     EQ = (0.9775*D2*DELK**2/(2 *GAMMA*(1 -(DELK*DSIN(PI*T)/XK1C)
63.     & **2)))*(1./XM)*PI*(DELK**2)*(DSIN(PI*T))**(2.*(1.+1./XM))/
64.     & (13.5*SM**2)
65.     RETURN
66.     END
67.     //GO FTOIFOO1 DD DSN=USR R635 YK DDTEST,DISP=SHR
68.     //GO SYSIN DD DSN=USR R635 YK INFOTEST,DISP=SHR

```

## APPENDIX V.-SCANNING ELECTRON MICROSCOPY

The following SEM pictures were taken at the SEM center on a JEOL JSM-25SII scanning electron microscope by Richard Drees of Soil and Crop Sciences at Texas A&M University. In the pictures, the long bar is  $10^\psi \mu\text{m}$ , where  $\psi$  is the number of small white squares minus one.

On the first page of pictures the following features are illustrated: Pictures 2033 (upper left) and 2034 (lower left) show side views of the fracture surface and the intergranular nature of the fracture process. Pictures 2099 (upper right) and 2100 (lower right) are pictures of the fracture surface in the plane of the crack and show hydration products (mostly ettringite). Picture 2100 also shows that a particle was apparently pulled out of the material during fracture leaving an empty "nest" made of hydration products and surrounding material. Once again, this last view confirms the weak link at the interface with soil particles or in the matrix material (i.e. water, cement, pores). In addition, the idea of crack closure being at least partly responsible for the loops in Figure 10 is supported by this picture.

The pictures on the second page of this appendix illustrate the following: Pictures 2051 and 2063 show crack branching. It is important to note that the length of the long branch above the number "5" in picture 2051 is 0.44 in (1.11 mm) long. This length is approximately the same as both the plastic zone size and the amplitude of the serial correlation mentioned in the text. Pictures 2071 and 2072 show a crack going "out of its way" to propagate through a void in the material. Note how the crack alters

0160 267

FRACTURE IN STABILIZED SOILS VOLUME 1(U) TEXAS  
TRANSPORTATION INST COLLEGE STATION D N LITTLE ET AL.  
31 DEC 85 AFOSR-TR-86-0242-VOL-1 F49620-02-K-0027

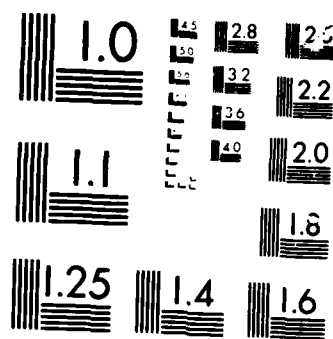
4/4

UNCLASSIFIED

F/G 8/13

NL

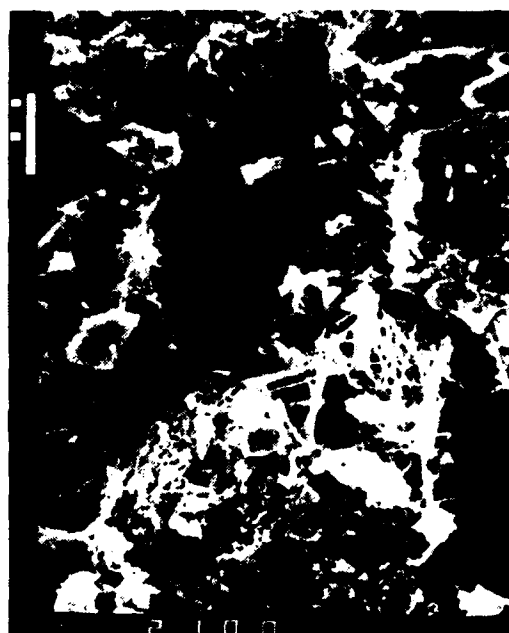
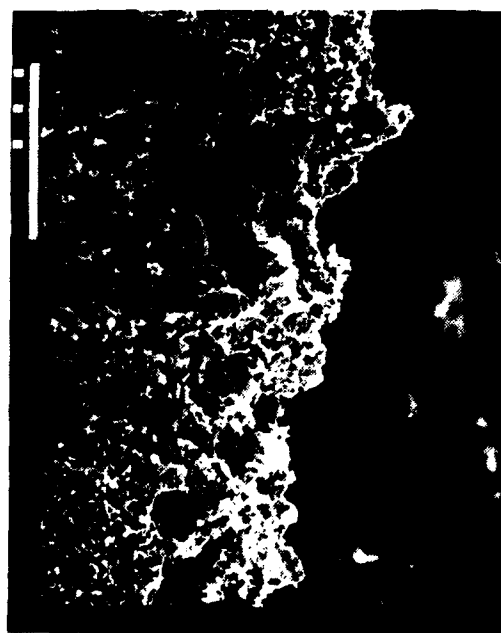
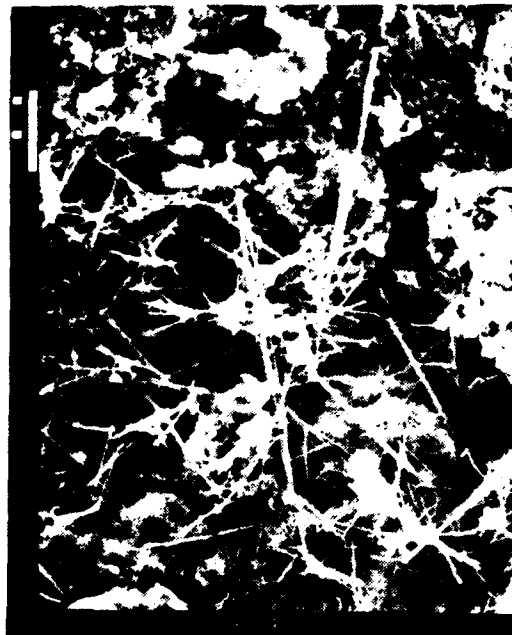


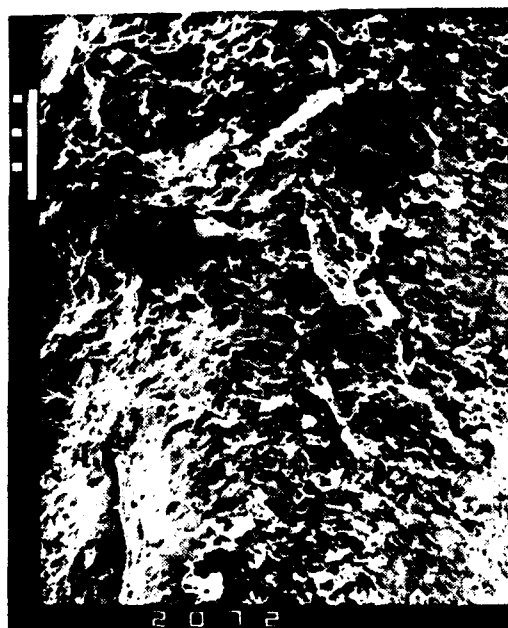


MICROCODS

100M

course to enter the hole and comes out of the hole at an angle back toward its original course line and eventually returns to that line. This illustrates the tendency of the crack to seek out areas of locally higher stress concentration.





## APPENDIX VI.-Individual Creep Test Results

Table VI-1. Individual test results of 7-day-cured samples with  
10% cement at 73° F and 55% relative humidity.  
( Test Designation : A )

	A - 1	A - 2	A - 3
$D_2 ( \times 10^{-7} )$	2.36	3.60	3.03
m	0.320	0.256	0.305
Creep Index ( $\times 10^{-11}$ )	9.05	5.79	9.51
A	$3.50 \times 10^{-29}$	$1.34 \times 10^{-33}$	$2.87 \times 10^{-29}$
n	12.52	14.76	12.63
Crack Speed Index	-3.41	-3.35	-3.29

Table VI-2. Individual test results of 14-day-cured samples with  
10% cement at 73° F and 55% relative humidity.  
( Test Designation : B )

	B - 1	B - 2	B - 3
$D_2 ( \times 10^{-7} )$	2.67	5.88	1.86
m	0.213	0.180	0.224
Creep Index ( $\times 10^{-11}$ )	2.35	3.15	1.90
A	$1.28 \times 10^{-41}$	$2.37 \times 10^{-46}$	$1.26 \times 10^{-40}$
n	17.68	20.63	16.92
Crack Speed Index	-5.54	-4.36	-6.06

Table VI-3. Individual test results of 28-day-cured samples with  
10% cement at 73° F and 55% relative humidity.

( Test Designation : C )

	C - 1	C - 2	C - 3
$D_2 ( \times 10^{-7} )$	2.13	3.87	5.74
m	0.149	0.144	0.136
Creep Index ( $\times 10^{-11}$ )	0.69	1.15	1.50
A	$3.39 \times 10^{-58}$	$2.87 \times 10^{-58}$	$5.50 \times 10^{-60}$
n	24.30	25.11	26.44
Crack Speed Index	-8.87	-7.33	-6.38

Table VI-4. Individual test results of 28-day-cured samples with  
15% cement at 73° F and 55% relative humidity.

( Test Designation : D )

	D - 1	D - 2
$D_2 ( \times 10^{-7} )$	2.50	1.70
m	0.192	0.162
Creep Index ( $\times 10^{-11}$ )	1.60	0.68
A	$4.80 \times 10^{-49}$	$4.40 \times 10^{-58}$
n	19.58	22.90
Crack Speed Index	-9.16	-11.57

Table VI-5. Individual test results of 28-day-cured samples with  
5% cement at 73° F and 55% relative humidity.

( Test Designation : E )

	E - 1	E - 2
$D_2 ( \times 10^{-7} )$	6.95	10.92
m	0.197	0.158
Creep Index ( $\times 10^{-11}$ )	4.79	4.11
A	$2.30 \times 10^{-39}$	$1.28 \times 10^{-46}$
n	18.57	22.77
Crack Speed Index	-1.50	-0.36

Table VI-6. Individual test results of 7-day-cured samples with  
10% cement at 73° F and 100% relative humidity.

( Test Designation : F )

	F - 1	F - 2	F - 3
$D_2 ( \times 10^{-7} )$	6.11	3.49	2.51
m	0.276	0.312	0.334
Creep Index ( $\times 10^{-11}$ )	12.92	11.96	11.45
A	$1.28 \times 10^{-30}$	$1.89 \times 10^{-28}$	$2.32 \times 10^{-27}$
n	13.95	12.52	11.80
Crack Speed Index	-1.99	-2.69	-3.03

Table VI-7. Individual test results of 7-day-cured samples with  
10% cement at 104° F and 100% relative humidity.

( Test Designation : G )

	G - 1	G - 2	G - 3
$D_2 ( \times 10^{-7} )$	1.03	1.17	0.59
m	0.316	0.377	0.415
Creep Index ( $\times 10^{-11}$ )	3.71	9.17	7.41
A	$7.45 \times 10^{-30}$	$9.57 \times 10^{-26}$	$1.33 \times 10^{-24}$
n	12.39	10.65	9.84
Crack Speed Index	-4.35	-3.71	-4.20

Table VI-8. Individual test results of 7-day-cured samples with  
10% cement at  $-10^{\circ}$  F.

( Test Designation : H )

	H - 1	H - 2
$D_2$ ( $\times 10^{-7}$ )	3.95	3.67
m	0.238	0.247
Creep Index ( $\times 10^{-11}$ )	4.95	5.23
A	$2.24 \times 10^{-36}$	$2.16 \times 10^{-35}$
n	15.75	15.23
Crack Speed Index	-4.15	-4.21

Table VI-9. Individual test results of 7-day-cured samples with  
10% cement at 33° F and 100% relative humidity.  
( Test Designation : I )

I - 1	
$D_2 ( \times 10^{-7} )$	4.85
m	0.278
Creep Index ( $\times 10^{-11}$ )	10.62
A	$9.77 \times 10^{-31}$
n	13.83
Crack Speed Index	-2.34

Table VI-10. Individual test results of 7-day-cured samples with  
10% cement at 104° F and 35% relative humidity.

( Test Designation : J )

	J - 1 <sup>a</sup>	J - 2 <sup>b</sup>	J - 3 <sup>b</sup>
D <sub>2</sub> ( $\times 10^{-7}$ )	2.56	3.86	5.18
m	0.339	0.325	0.276
Creep Index ( $\times 10^{-11}$ )	12.46	15.76	11.00
A	$9.77 \times 10^{-28}$	$4.10 \times 10^{-28}$	$1.05 \times 10^{-31}$
n	11.61	12.02	13.88
Crack Speed Index	-3.79	-3.34	-3.21

<sup>a</sup> Test was performed at 77° F and 35% relative humidity by the aid of the dehumidifier.

<sup>b</sup> Tests were performed at 104° F and 35% relative humidity.

END

DTIC

7-86